Report on policy options for AQ and CC

D4.5

February 2019

This project has received funding from the European Union's Horizon 2020 research and innovation programme under grant agreement No 689954.

Project Acronym and Name	iSCAPE - Improving the Smart Control of Air Pollution in Europe	
Grant Agreement Number	689954	
Document Type	Report	
Document version & WP No.	V. 03	WP4
Document Title	Report on policy options for AQ and CC	
Main authors	Silvana Di Sabatino, Erika Brattich, Francesca Di Nicola, Francesco Barbano, Muhammad Adnan, Shiraz Ahmed, Kirsti Jylhä, Kimmo Ruosteenoja, Marco Deserti, Chiara Agostini, Vanes Poluzzi	
Partner in charge	University of Bologna (UNIBO)	
Contributing partners	University of Bologna (UNIBO), University of Hasselt (UH), Finnish Meteorological Institute (FMI), Emilia Romagna Environmental Protection Agency (ARPA-ER)	
Release date	February 2019	

Document Control Page			
Short Description	*This report is the output of the work carried out in Task 4.3 of the iSCAPE project, which addresses the efficacy of policy options to reduce air quality in present and future climate taking into account also possible behavioural change. The evaluation of the efficacy of policy options has been conducted by reconstructing detailed air quality maps in three iSCAPE cities, namely Bologna, Hasselt and Vantaa chosen as representative of south, central and north Europe respectively. Following a thorough validation of all numerical models used in present scenarios, simulations have been conducted using downscaled climate projections for the three cities. Changes in air quality in future climate have been documented for several policy options allowing to extract recommendations for the selected cities and easily extendable to other European cities.*		
Review status	**Action**	**Person**	**Date**
	Quality Check	*Coordination Team*	28-02-2019
	Internal Review	*Giuseppe Forino* *Agnese Riccetti*	14-02-2019 18-02-2019
	Internal Review		
Distribution	Public		

Statement of originality:

This deliverable contains original unpublished work except where clearly indicated otherwise. Acknowledgement of previously published material and of the work of others has been made through appropriate citation, quotation or both.

Revision history			
Version	**Date**	**Modified by**	**Comments**
V0.1	11 Feb 2019	Silvana Di Sabatino, Erika Brattich, Francesca Di Nicola, Francesco Barbano, Muhammad Adnan, Shiraz Ahmed, Kirsti Jylhä, Kimmo Ruosteenoja, Marco Deserti, Chiara Agostini, Vanes Poluzzi	The first draft.
V0.2	18 Feb 2019	Silvana Di Sabatino, Erika Brattich, Francesca Di Nicola	Modifications after receiving the comments from internal reviewers
V0.3	28 Feb 2019	Silvana Di Sabatino, Erika Brattich, Francesca Di Nicola, Kirsti Jylhä, Kimmo Ruosteenoja	Added the Vantaa's part
V0.4			
V0.5			
V0.6			
V0.7			
V0.8			
V0.9			

Table of Contents

Table of Contents ..... - 5 -
List of Tables ..... - 7 -
List of Figures ..... - 9 -
List of Abbreviations ..... - 16 -

1 Executive Summary ..... - 18 -

2 Introduction ..... - 20 -

3 Methodology for AQ simulation in the current scenario ..... - 24 -
3.1 Domain information and description ..... - 25 -
3.1.1 Bologna ..... - 25 -
3.1.2 Hasselt ..... - 28 -
3.1.3 Vantaa ..... - 35 -
Air quality and meteorological measurements ..... - 41 -
3.1.4 Bologna ..... - 41 -
3.1.5 Hasselt ..... - 44 -
3.1.6 Vantaa ..... - 47 -
3.2 Development of the emission inventory ..... - 51 -
3.2.1 Bologna ..... - 53 -
3.2.2 Hasselt ..... - 55 -
3.2.3 Vantaa ..... - 60 -
3.3 Dispersion modeling ..... - 64 -
3.3.1 Bologna ..... - 65 -
3.3.2 Hasselt ..... - 66 -
3.3.3 Vantaa ..... - 66 -
3.4 Validation ..... - 67 -
3.4.1 Bologna ..... - 68 -
3.4.2 Hasselt ..... - 68 -
3.4.3 Vantaa ..... - 68 -
3.5 Choice of policies ..... - 68 -
3.5.1 Bologna ..... - 68 -
3.5.2 Hasselt ..... - 69 -
3.5.3 Vantaa ..... - 70 -

4 AQ simulations in the present scenario ..... - 72 -
4.1 Validation ..... - 72 -
4.1.1 Bologna ..... - 72 -
4.1.2 Hasselt ..... - 76 -
4.1.3 Vantaa ..... - 82 -
4.2 Results ..... - 86 -
4.2.1 Bologna ..... - 86 -

4.2.2 Hasselt ..... - 99 -
4.2.3 Vantaa ..... - 110 -
5 Methodology for AQ simulations in future scenarios ..... - 117 -
5.1 Future climate projections ..... - 117 -
5.1.1 Bologna ..... - 118 -
5.1.2 Hasselt ..... - 122 -
5.1.3 Vantaa ..... - 126 -
5.2 Dispersion modeling ..... - 129 -
5.2.1 Bologna ..... - 130 -
5.2.2 Hasselt ..... - 131 -
5.2.3 Vantaa ..... - 131 -
6 AQ simulation in future scenarios ..... - 131 -
6.1 Results ..... - 131 -
6.1.1 Bologna ..... - 131 -
6.1.2 Hasselt ..... - 142 -
6.1.3 Vantaa ..... - 158 -
7 Conclusions ..... - 164 -
8 References / Bibliography ..... - 167 -

List of Tables

TABLE 1. OVERVIEW AND MAIN PURPOSE OF THE DISPERSION SIMULATIONS PERFORMED IN THE THREE ISCAPE CITIES, WHOSE OUTPUT IS EVALUATED AND PRESENTED IN THIS REPORT. ..... - 23 -
TABLE 2. MONTHLY AVERAGE SPEED AND MOST FREQUENT DIRECTION IN HASSELT DURING THE PERIOD 1981-2010. WIND DATA FROM THE SYNOPTIC METEOROLOGICAL STATION IN SCHAFFEN (SOURCE: ROYAL METEOROLOGICAL INSTITUTE BELGIUM). ..... - 34 -
TABLE 3. MONTHLY AVERAGE SPEED AND MOST FREQUENT DIRECTION IN VANTAA DURING THE PERIOD 1981-2010. WIND DATA FROM THE SYNOPTIC METEOROLOGICAL STATION IN HELSINKI VANTAA (SOURCE: FINNISH METEOROLOGICAL INSTITUTE). ..... - 40 -
TABLE 4. INFORMATION ON REFERENCE MONITORING STATIONS IN BOLOGNA: TYPE, LOCATION (LATITUDE AND LONGITUDE), MEASURED POLLUTANTS WITH ASSOCIATED TIME RESOLUTION. THE EMPTY CELL CORRESPONDING TO ONE POLLUTANT THAT IT IS NOT MEASURED AT THAT STATION OR DATA IS NOT AVAILABLE. ..... - 41 -
TABLE 5. MEASUREMENT INSTRUMENTS AND DETAILS OF MEASUREMENTS OF AIR QUALITY POLLUTANTS IN THE AIR QUALITY MEASUREMENT STATION OF HASSELT (VMM). ..... - 45 -
TABLE 6. PARAMETERS, MEASUREMENT UNITS AND METEOROLOGICAL STATIONS AVAILABLE FOR 2016 YEAR IN HASSELT (SOURCE: ROYAL METEOROLOGICAL INSTITUTE BELGIUM). ..... - 45 -
TABLE 7. MONTHLY AVERAGE SPEED AND MOST FREQUENT DIRECTION IN VANTAA DURING 2016 YEAR. (SOURCE: ROYAL METEOROLOGICAL INSTITUTE BELGIUM). ..... - 47 -
TABLE 8. PARAMETERS, MEASUREMENT UNITS AND METEOROLOGICAL STATIONS AVAILABLE FOR 2017 YEAR IN VANTAA (SOURCE: FINNISH METEOROLOGICAL INSTITUTE). ..... - 49 -
TABLE 9. MONTHLY AVERAGE SPEED AND MOST FREQUENT DIRECTION IN VANTAA DURING 2017 YEAR. (SOURCE: FINNISH METEOROLOGICAL INSTITUTE). ..... - 50 -
TABLE 10. STATISTICAL ANALYSES. REFERENCE STATION: PORTA SAN FELICE (SF), GIARDINI MARGHERITA (GM) AND VIA CHIARINI (CH). ..... - 75 -
TABLE 11. STATISTICS OF DAILY OBSERVED AND MODELLED CONCENTRATIONS OF NO_2, NO_x, PM_{10} AND $PM_{2.5}$ CONCENTRATIONS ($\mu G/M^3$) AND DAILY MAXIMUM O_3 8-HOUR ROLLING MEAN IN HASSELT IN THE MONTH OF JANUARY 2016. ..... - 78 -
TABLE 12. STATISTICS OF DAILY OBSERVED AND MODELLED CONCENTRATIONS OF NO_2, NO_x, PM_{10} AND $PM_{2.5}$ CONCENTRATIONS ($\mu G/M^3$) AND DAILY MAXIMUM O_3 8-HOUR ROLLING MEAN IN HASSELT IN THE MONTH OF AUGUST 2016. ..... - 82 -
TABLE 13. STATISTICS OF DAILY OBSERVED AND MODELLED CONCENTRATIONS OF NO_2 AND $PM_{2.5}$ CONCENTRATIONS ($\mu G/M^3$) IN VANTAA AIR QUALITY STATIONS IN THE MONTH OF JANUARY 2017. ..... - 84 -
TABLE 14. AVERAGE CONCENTRATION VALUES TO RECEPTORS IN WINTER AND SUMMER FOR THE 2017BC SCENARIO IN BOLOGNA. ..... - 91 -
TABLE 15. AVERAGE CONCENTRATION VALUES TO RECEPTORS IN WINTER AND SUMMER FOR 2017P1EC SCENARIO IN BOLOGNA ..... - 92 -
TABLE 16. PERCENTAGES OF REDUCTION/INCREASE IN CONCENTRATION IN THE POLICY 1 SCENARIO COMPARED TO THE BASE CASE (CALCULATED FOR ALL THE RECEPTOR SITES). ..... - 95 -
TABLE 17. AVERAGE CONCENTRATION VALUES TO RECEPTORS IN WINTER AND SUMMER FOR 2017P2EB SCENARIO IN BOLOGNA. ..... - 95 -
TABLE 18. PERCENTAGES OF REDUCTION/INCREASE IN CONCENTRATION COMPARED TO THE BASE CASE (CALCULATED FOR ALL RECEPTOR). ..... - 99 -
TABLE 19. PERCENTAGES OF REDUCTION/INCREASE IN CONCENTRATIONS IN THE CASE OF IMPLEMENTATION OF THE POLICY 1 IN VANTAA COMPARED TO THE BASE CASE (CALCULATED FOR ALL RECEPTOR). ..... - 117 -
TABLE 20. AVERAGE CONCENTRATION VALUES TO RECEPTORS IN WINTER AND SUMMER FOR THE 2055BC SCENARIO IN BOLOGNA. ..... - 135 -
TABLE 21. AVERAGE CONCENTRATION VALUES TO RECEPTORS IN WINTER AND SUMMER FOR 2055P1EC SCENARIO IN BOLOGNA. ..... - 136 -

TABLE 22. PERCENTAGES OF REDUCTION/INCREASE IN CONCENTRATION COMPARED TO THE BASE CASE (CALCULATED FOR ALL RECEPTOR). ..... - 138 -
TABLE 23. AVERAGE CONCENTRATION VALUES TO RECEPTORS IN WINTER AND SUMMER FOR 2055P2EB SCENARIO IN BOLOGNA. ..... - 139 -
TABLE 24. PERCENTAGES OF REDUCTION/INCREASE IN CONCENTRATION COMPARED TO THE BASE CASE (CALCULATED FOR ALL RECEPTOR). ..... - 142 -

List of Figures

FIGURE 1. SCHEMATIC FLOW DIAGRAM BETWEEN THIS DELIVERABLE/TASK AND OTHER TASKS IN THE SAME AND IN OTHER ISCAPE WPS. - 24 -
FIGURE 2. BOLOGNA AND ITS LOCATION IN ITALY. THE LEFT MAP INDICATES THE POSITIONS OF WEATHER STATIONS: NEAR THE CITY CENTRE (BOLOGNA AIRPORT) AND IN THE COUNTRYSIDE (SAN PIETRO CAPOFIUME). SOURCE: OPEN STREET MAP. - 26 -
FIGURE 3. THE MOBILITY POLICIES OF BOLOGNA HAVE ESTABLISHED AREAS WITH A SPEED LIMIT OF 30 KM/H, SHOWN IN THIS MAP (SOURCE: OPEN STREET MAP). - 27 -
FIGURE 4: (LEFT) HASSELT CITY IN RED, WITHIN THE LIMBURG PROVINCE IN BELGIUM. (RIGHT) HASSELT ARRONDISSEMENT IN RED IN A LIMBURG PROVINCE OF BELGIUM. - 29 -
FIGURE 5: LOCATION OF THE CITY OF HASSELT IN BELGIUM. ALSO SHOWN THE LOCATIONS OF THE DIEPENBEEK, SCHAFFEN AND BIERSET SYNOPTIC METEOROLOGICAL STATIONS (SOURCE: GOOGLE MAPS). - 29 -
FIGURE 6: MAP OF THE CITY OF HASSELT WITH THE ROAD NETWORK (THE TWO RING ROADS AND THE MAIN TRAFFIC JUNCTIONS), THE SMALL LOCAL AIRPORT OF KIEWIT AND THE RAILWAY. (SOURCE: OPEN STREET MAPS). - 31 -
FIGURE 7. MEAN, MINIMUM, MAXIMUM TEMPERATURE (°C) AND AVERAGE RAINFALL AMOUNT (MM) IN HASSELT DURING THE REFERENCE PERIOD 1981-2010. (SOURCE: ROYAL METEOROLOGICAL SERVICE BELGIUM). - 33 -
FIGURE 8. ANNUAL MEAN WIND ROSE SHOWING MEAN FREQUENCIES (FREQ, IN PERCENTAGE, BLACK LINE) AND WIND SPEEDS (WS, IN M S^{-1}, RED LINE) IN HASSELT DURING THE PERIOD 1981-2010. WIND DATA FROM THE SYNOPTIC METEOROLOGICAL STATION IN SCHAFFEN (SOURCE: ROYAL METEOROLOGICAL INSTITUTE BELGIUM). - 34 -
FIGURE 9. MEAN SOLAR RADIATION (RED COLUMN) AND INSOLATION DURATION (BLUE LINE) FOR THE BASELINE CLIMATOLOGICAL PERIOD 1981-2010 IN HASSELT (SOURCE: ROYAL METEOROLOGICAL INSTITUTE BELGIUM)... - 35 -
FIGURE 10. VANTAA AND ITS LOCATION IN FINLAND AND IN THE REGION OF UUSIMA (SOURCE: GOOGLEEARTH AND OPENSTREETMAPS). - 36 -
FIGURE 11: MAP OF THE CITY OF VANTAA WITH THE ROAD NETWORK, THE AIRPORT AND THE RAILWAY (THE SYMBOL LOCATES THE RAILWAY STATION IN TIKKURILA). (SOURCE: OPEN STREET MAPS). - 37 -
FIGURE 12. MEAN, MINIMUM, MAXIMUM TEMPERATURE (°C) AND AVERAGE RAINFALL AMOUNT (MM) IN VANTAA DURING THE REFERENCE PERIOD 1981-2010. (SOURCE: FINNISH METEOROLOGICAL INSTITUTE). - 39 -
FIGURE 13. ANNUAL MEAN WIND ROSE SHOWING MEAN FREQUENCIES (FREQ, IN PERCENTAGE, BLACK LINE) AND WIND SPEEDS (WS, IN M S^{-1}, RED LINE) IN VANTAA DURING THE PERIOD 1981-2010. WIND DATA FROM THE SYNOPTIC METEOROLOGICAL STATION IN HELSINKI VANTAA (SOURCE: FINNISH METEOROLOGICAL INSTITUTE). - 39 -
FIGURE 14. MEAN SOLAR RADIATION (RED COLUMN) AND INSOLATION DURATION (BLUE LINE) FOR THE BASELINE CLIMATOLOGICAL PERIOD 1981-2010 IN VANTAA (SOURCE: FINNISH METEOROLOGICAL INSTITUTE). - 40 -
FIGURE 15. WIND ROSE SHOWING OCCURRENCES OF HOURLY AVERAGE WIND DIRECTION AND SPEED FOR THE CITY OF BOLOGNA IN 2017, AS RECORDED AT THE BOLOGNA URBANA METEOROLOGICAL STATION. - 42 -
FIGURE 16. MONTHLY AIR TEMPERATURE FOR 2017 AT BOLOGNA URBANA (BLUE LINE) AND SAN PIETRO IN CAPOFIUME (RED LINE) MONITORING STATIONS. - 43 -
FIGURE 17. DIFFERENCES IN TEMPERATURE BETWEEN CITY (BOLOGNA URBANA) AND COUNTRYSIDE (SAN PIETRO IN CAPOFIUME). - 43 -
FIGURE 18. MONTHLY AVERAGE PRECIPITATION FOR 2017 AT BOLOGNA URBANA (BLUE) AND SAN PIETRO IN CAPOFIUME (RED) MONITORING STATIONS - 44 -
FIGURE 19. MEAN MONTHLY AND ACCUMULATED PRECIPITATION OVER THE 2016 YEAR IN HASSELT (SOURCE: ROYAL METEOROLOGICAL INSTITUTE BELGIUM) - 46 -
FIGURE 20. WIND ROSE FOR 2016 METEOROLOGICAL DATA IN HASSELT (SOURCE: ROYAL METEOROLOGICAL INSTITUTE BELGIUM). - 47 -
FIGURE 21. MAP OF PERMANENT AND MOBILE AIR QUALITY STATIONS IN VANTAA (2017). - 48 -
FIGURE 22. MEAN MONTHLY AND ACCUMULATED PRECIPITATION OVER THE 2017 YEAR IN VANTAA (SOURCE: FINNISH METEOROLOGICAL INSTITUTE). - 49 -

FIGURE 23. WIND ROSE FOR 2017 METEOROLOGICAL DATA IN VANTAA (SOURCE: FINNISH METEOROLOGICAL INSTITUTE). ..... - 50 -
FIGURE 24. SCHEMATIC REPRESENTATION OF THE CONSTRUCTION OF THE EMISSION INVENTORY WITH THE EMIT SOFTWARE FOR ITS USE IN THE ADMS-URBAN DISPERSION MODEL. ..... - 51 -
FIGURE 25. MAP OF NO_x EMISSIONS FROM ROAD SOURCES ("MAJOR ROADS") IN BOLOGNA, GOOGLE SATELLITE BASE MAP PROVIDED BY QGIS. ..... - 54 -
FIGURE 26. MAP OF PM_{10} EMISSIONS FROM "DOMESTIC" SOURCES IN BOLOGNA. ..... - 55 -
FIGURE 27. NO_x EMISSIONS (IN G/KM/S) FOR ROAD SOURCES CONSIDERED AS MAJOR ROADS IN HASSELT IN THE BASE CASE (PRESENT) SCENARIO. ..... - 58 -
FIGURE 28. PM_{10} EMISSIONS (IN G/KM/S) FOR ROAD SOURCES CONSIDERED AS MAJOR ROADS IN HASSELT IN THE BASE CASE (PRESENT) SCENARIO. ..... - 59 -
FIGURE 29. NO_x EMISSIONS ($G/M^2/S$) FROM RESIDENTIAL HEATING IN HASSELT IN THE BASE CASE (PRESENT) SCENARIO. .- 60 -
FIGURE 30. NO_x EMISSIONS (IN G/KM/S) FOR ROAD SOURCES CONSIDERED AS MAJOR ROADS IN VANTAA IN THE BASE CASE (PRESENT) SCENARIO. ..... - 62 -
FIGURE 31. $PM_{2.5}$ EMISSIONS (IN G/KM/S) FOR ROAD SOURCES CONSIDERED AS MAJOR ROADS IN VANTAA IN THE BASE CASE (PRESENT) SCENARIO. ..... - 63 -
FIGURE 32. PM_{10} EMISSIONS ($G/M^2/S$) FROM RESIDENTIAL HEATING IN HELSINKI METROPOLITAN AREA IN THE BASE CASE (PRESENT) SCENARIO. ..... - 63 -
FIGURE 33. AREA OF THE INTERVENTION (CLOSURE OF THE AREA TO THE TRAFFIC) TESTED IN THE POLICY 1 SCENARIO FOR VANTAA. ..... - 71 -
FIGURE 34. WINTER TIME SERIES OF NO_x HOURLY CONCENTRATION. MODELED DATA (MOD) AND OBSERVED DATA (OBS) AT THE AIR QUALITY ARPAE PORTA SAN FELICE STATION. ..... - 73 -
FIGURE 35. SUMMER TIME SERIES OF NO_x HOURLY CONCENTRATION. MODELED DATA (MOD) AND OBSERVED DATA (OBS) AT THE AIR QUALITY ARPAE PORTA SAN FELICE STATION. ..... - 73 -
FIGURE 36. TIME SERIES OF DAILY NO_x CONCENTRATION FOR 2017. MODELED DATA (MOD) AND OBSERVED DATA (OBS) AT THE AIR QUALITY ARPAE PORTA SAN FELICE STATION. ..... - 74 -
FIGURE 37. TIME SERIES OF DAILY PM_{10} CONCENTRATION FOR 2017. MODELED DATA (MOD) AND OBSERVED DATA (OBS) AT THE AIR QUALITY ARPAE PORTA SAN FELICE STATION. ..... - 74 -
FIGURE 38. TIME VARIATION ANALYSIS FOR NO_x, PERIOD:1/01/2017 – 1/01/2018 REPRESENTING DIURNAL PATTERN, WEEKLY PATTERN AND MONTHLY PATTERN FOR THE BASE CASE SIMULATION FOR PORTA SAN FELICE STATION AS COMPARED TO THE MEASUREMENTS. ..... - 75 -
FIGURE 39. COMPARISON OF NO_x, NO_2, O_3, PM_{10}, AND $PM_{2.5}$ HOURLY MEASURED AND ADMS-URBAN SIMULATED CONCENTRATIONS AT THE HASSELT AIR QUALITY STATION IN THE MONTH OF JANUARY 2016. ..... - 77 -
FIGURE 40. SCATTER PLOT OF OBSERVED AND SIMULATED DAILY MEAN NO_2, NO_x, PM_{10} AND $PM_{2.5}$ CONCENTRATIONS AND DAILY MAXIMUM O_3 8-HOUR ROLLING MEAN IN HASSELT IN THE MONTH OF JANUARY 2016. THE STRAIGHT REPRESENTS THE 1:1 REGRESSION LINE, WHILE THE DOTTED LINES REPRESENT THE 95% CONFIDENCE INTERVAL AROUND THE MEAN. ..... - 79 -
FIGURE 41. MEAN MEASURED AND SIMULATED DIURNAL PATTERN FOR NO_x, NO_2, O_3, PM_{10}, AND $PM_{2.5}$ CONCENTRATIONS IN THE MONTH OF JANUARY 2016 IN HASSELT. ..... - 80 -
FIGURE 42. MEAN OBSERVED AND SIMULATED WEEKLY PATTERN FOR NO_2, NO_x, O_3, PM_{10} AND $PM_{2.5}$ CONCENTRATIONS IN JANUARY 2016 IN HASSELT. ..... - 81 -
FIGURE 43. COMPARISON OF NO_2, AND $PM_{2.5}$ HOURLY MEASURED AND ADMS-URBAN SIMULATED CONCENTRATIONS AT THE VANTAA AIR QUALITY STATIONS OF TIKKURILA, AIRPORT AND REKOLA IN THE MONTH OF JANUARY 2017. ..... - 83 -
FIGURE 44. MEAN MEASURED AND SIMULATED WEEKLY DIURNAL PATTERNS FOR NO_2, AND $PM_{2.5}$ CONCENTRATIONS IN THE MONTH OF JANUARY 2017 IN VANTAA AT THE THREE AIR QUALITY STATIONS. ..... - 86 -
FIGURE 45. CONCENTRATION MAPS FOR NO_x (TOP: WINTER, BOTTOM: SUMMER) IN THE 2017BC SCENARIO FOR BOLOGNA. THE MAPS REPRESENT CONCENTRATION VALUES AVERAGED OVER THE PERIOD CONSIDERED. ..... - 88 -
FIGURE 46. CONCENTRATION MAPS FOR PM_{10} (TOP: WINTER, BOTTOM: SUMMER) IN THE 2017BC SCENARIO FOR BOLOGNA. THE MAPS REPRESENT CONCENTRATION VALUES AVERAGED OVER THE PERIOD CONSIDERED. ..... - 89 -

FIGURE 47. CONCENTRATION MAPS FOR O_3 (TOP: WINTER, BOTTOM: SUMMER) IN THE 2017BC SCENARIO FOR BOLOGNA. THE MAPS REPRESENT CONCENTRATION VALUES AVERAGED OVER THE PERIOD CONSIDERED. ..... - 90 -
FIGURE 48. WIND ROSE FOR BASE REFERENCE CASE IN BOLOGNA, WINTER (LEFT) AND SUMMER (RIGHT) 2017. DATA FROM LIPE METEOROLOGICAL STATION. ..... - 91 -
FIGURE 49. CONCENTRATION MAPS FOR NO_x IN THE 2017P1EC SCENARIO FOR BOLOGNA. THE MAPS REPRESENT CONCENTRATION VALUES AVERAGED OVER WINTER 2017. ..... - 93 -
FIGURE 50. CONCENTRATION MAPS FOR PM_{10} IN THE 2017P1EC SCENARIO FOR BOLOGNA. THE MAPS REPRESENT CONCENTRATION VALUES AVERAGED OVER WINTER 2017. ..... - 93 -
FIGURE 51. MAPS OF CONCENTRATION DIFFERENCES FOR NO_x FOR WINTER 2017. THE DIFFERENCES ARE CALCULATED BETWEEN 2017P1EC SCENARIO AND 2017BC SCENARIO. ..... - 94 -
FIGURE 52. MAPS OF CONCENTRATION DIFFERENCES FOR PM_{10} FOR WINTER 2017. THE DIFFERENCES ARE CALCULATED BETWEEN 2017P1EC SCENARIO AND 2017BC SCENARIO. ..... - 94 -
FIGURE 53. CONCENTRATION MAPS OF NO_x IN THE 2017P2EB FOR BOLOGNA. THE MAPS REPRESENT CONCENTRATION VALUES AVERAGED OVER WINTER 2017. ..... - 96 -
FIGURE 54. CONCENTRATION MAPS OF PM_{10} IN THE 2017P2EB FOR BOLOGNA. THE MAPS REPRESENT CONCENTRATION VALUES AVERAGED OVER WINTER 2017. ..... - 97 -
FIGURE 55. MAPS OF CONCENTRATION DIFFERENCES FOR NO_x FOR WINTER 2017. THE DIFFERENCES ARE CALCULATED BETWEEN 2017P2EB SCENARIO AND 2017BC SCENARIO. ..... - 98 -
FIGURE 56. MAPS OF CONCENTRATION DIFFERENCES FOR PM_{10} FOR WINTER 2017. THE DIFFERENCES ARE CALCULATED BETWEEN 2017P2EB SCENARIO AND 2017BC SCENARIO. ..... - 98 -
FIGURE 57. NO_2 CONCENTRATION MAP FOR THE HASSELT PRESENT SCENARIO (JANUARY 2016 MEAN). ALSO SHOWN ARE THE MAJOR ROADS CONSIDERED IN THE SIMULATIONS. THE MAP REPRESENTS THE AVERAGE CONCENTRATION FOR JANUARY 2016. ..... - 100 -
FIGURE 58. PM_{10} CONCENTRATION MAP FOR THE HASSELT PRESENT SCENARIO (JANUARY 2016 MEAN). ALSO SHOWN ARE THE MAJOR ROADS CONSIDERED IN THE SIMULATIONS. THE MAP REPRESENTS THE AVERAGE CONCENTRATION FOR JANUARY 2016. ..... - 100 -
FIGURE 59. WIND ROSE FOR THE JANUARY 2016 BASE REFERENCE CASE IN HASSELT. ..... - 101 -
FIGURE 60. NO_2 CONCENTRATION MAP FOR THE IMPLEMENTATION OF THE POLICY 1 FOR HASSELT CASE IN THE PRESENT (JANUARY 2016) SCENARIO. ..... - 102 -
FIGURE 61. PM_{10} CONCENTRATION MAP FOR THE IMPLEMENTATION OF THE POLICY 1 FOR HASSELT CASE IN THE PRESENT (JANUARY 2016) SCENARIO. ..... - 102 -
FIGURE 62. MAP OF DIFFERENCES IN NO_2 CONCENTRATION BETWEEN THE POLICY 1 SCENARIO AND THE BASE CASE IN HASSELT. ..... - 103 -
FIGURE 63. MAP OF DIFFERENCES IN PM_{10} CONCENTRATION BETWEEN THE POLICY 1 SCENARIO AND THE BASE CASE IN HASSELT. ..... - 104 -
FIGURE 64. NO_2 REDUCTION IN THE POLICY 1 SCENARIO IN HASSELT, EVALUATED AS CONCENTRATION RATIO BETWEEN THE CONCENTRATION DIFFERENCE PREVIOUSLY EVALUATED (FIGURE 62) AND THE CONCENTRATION OBSERVED IN THE BASE CASE (FIGURE 57). ..... - 105 -
FIGURE 65. PM_{10} REDUCTION IN THE POLICY 1 SCENARIO IN HASSELT, EVALUATED AS CONCENTRATION RATIO BETWEEN THE CONCENTRATION DIFFERENCE PREVIOUSLY EVALUATED (FIGURE 63) AND THE CONCENTRATION OBSERVED IN THE BASE CASE (FIGURE 58). ..... - 105 -
FIGURE 66. NO_2 CONCENTRATION MAP FOR THE IMPLEMENTATION OF THE POLICY 2 FOR HASSELT CASE IN THE PRESENT (JANUARY 2016) SCENARIO. ..... - 106 -
FIGURE 67. PM_{10} CONCENTRATION MAP FOR THE IMPLEMENTATION OF THE POLICY 2 FOR HASSELT CASE IN THE PRESENT (JANUARY 2016) SCENARIO. ..... - 107 -
FIGURE 68. MAP OF DIFFERENCE IN NO_2 CONCENTRATION BETWEEN THE BASE CASE AND THE POLICY 2 CASE IN HASSELT. ..... - 108 -
FIGURE 69. MAP OF DIFFERENCE IN PM_{10} CONCENTRATION BETWEEN THE BASE CASE AND THE POLICY 2 CASE IN HASSELT. ..... - 108 -

FIGURE 70. NO_2 REDUCTION IN THE POLICY 2 SCENARIO IN HASSELT, EVALUATED AS CONCENTRATION RATIO BETWEEN THE CONCENTRATION DIFFERENCE PREVIOUSLY EVALUATED (FIGURE 68) AND THE CONCENTRATION OBSERVED IN THE BASE CASE (FIGURE 57). ..... - 109 -
FIGURE 71. PM_{10} REDUCTION IN THE POLICY 2 SCENARIO IN HASSELT, EVALUATED AS CONCENTRATION RATIO BETWEEN THE CONCENTRATION DIFFERENCE PREVIOUSLY EVALUATED (FIGURE 69) AND THE CONCENTRATION OBSERVED IN THE BASE CASE (FIGURE 58). ..... - 110 -
FIGURE 72. NO_2 CONCENTRATION MAP FOR THE VANTAA PRESENT SCENARIO (JANUARY 2017 MEAN). ALSO SHOWN ARE THE MAJOR ROADS CONSIDERED IN THE SIMULATIONS. THE MAP REPRESENTS THE AVERAGE CONCENTRATION FOR JANUARY 2017. ..... - 111 -
FIGURE 73. $PM_{2.5}$ CONCENTRATION MAP FOR THE VANTAA PRESENT SCENARIO (JANUARY 2017 MEAN). ALSO SHOWN ARE THE MAJOR ROADS CONSIDERED IN THE SIMULATIONS. THE MAP REPRESENTS THE AVERAGE CONCENTRATION FOR JANUARY 2017. ..... - 111 -
FIGURE 74. WIND ROSE FOR THE JANUARY 2017 BASE REFERENCE CASE IN VANTAA. ..... - 112 -
FIGURE 75. NO_2 CONCENTRATION MAP FOR THE IMPLEMENTATION OF THE POLICY 1 FOR VANTAA CASE IN THE PRESENT (JANUARY 2017) SCENARIO. ..... - 113 -
FIGURE 76. $PM_{2.5}$ CONCENTRATION MAP FOR THE IMPLEMENTATION OF THE POLICY 1 FOR VANTAA CASE IN THE PRESENT (JANUARY 2017) SCENARIO. ..... - 113 -
FIGURE 77. MAP OF DIFFERENCES IN NO_2 CONCENTRATION BETWEEN THE POLICY 1 SCENARIO AND THE BASE CASE IN VANTAA. ..... - 114 -
FIGURE 78. MAP OF DIFFERENCES IN $PM_{2.5}$ CONCENTRATION BETWEEN THE POLICY 1 SCENARIO AND THE BASE CASE IN VANTAA. ..... - 115 -
FIGURE 79. NO_2 REDUCTION IN THE POLICY 1 SCENARIO IN VANTAA, EVALUATED AS CONCENTRATION RATIO BETWEEN THE CONCENTRATION DIFFERENCE PREVIOUSLY EVALUATED (FIGURE 77) AND THE CONCENTRATION OBSERVED IN THE BASE CASE (FIGURE 72). ..... - 116 -
FIGURE 80. $PM_{2.5}$ REDUCTION IN THE POLICY 1 SCENARIO IN VANTAA, EVALUATED AS CONCENTRATION RATIO BETWEEN THE CONCENTRATION DIFFERENCE PREVIOUSLY EVALUATED (FIGURE 78) AND THE CONCENTRATION OBSERVED IN THE BASE CASE (FIGURE 73). ..... - 116 -
FIGURE 81. PROJECTED TRENDS IN (A) MONTHLY MEAN AIR TEMPERATURE, (B) MONTHLY PRECIPITATION TOTAL, (C) MONTHLY MEAN OF DAILY MINIMUM TEMPERATURE, AND (D) MONTHLY MEAN OF DAILY MAXIMUM TEMPERATURE BETWEEN THE PERIODS 1981-2010 AND 2040-2069 IN BOLOGNA (GRID POINT 1) UNDER THE RCP8.5 SCENARIO. THE MULTI-MODEL MEAN PROJECTIONS FOR EACH CALENDAR MONTH (1 = JANUARY, 12 = DECEMBER) ARE DENOTED BY SYMBOLS. SHADING SHOWS THE 90% UNCERTAINTY INTERVALS FOR THE CHANGE. ..... - 119 -
FIGURE 82. PROJECTED TRENDS IN (A) MONTHLY MEAN DIURNAL TEMPERATURE RANGE, (B) MONTHLY MEAN INCIDENT SOLAR RADIATION AND (C) MONTHLY STANDARD DEVIATION OF DAILY MEAN TEMPERATURE (IN % PER DECADE, BOTTOM) BY THE PERIOD 2040–2069 IN BOLOGNA UNDER THE RCP8.5 SCENARIO. THE BASELINE PERIOD IS 1981-2010 (TOP) OR 1971-2000 (BOTTOM). FOR FURTHER INFORMATION, SEE CAPTION OF FIGURE 81. ..... - 120 -
FIGURE 83. PROJECTED TRENDS IN (A) MONTHLY MEAN SURFACE AIR PRESSURE AND (B) WIND SPEED BETWEEN THE PERIODS 1981-2010 AND 2040-2069 IN BOLOGNA UNDER THE RCP8.5 SCENARIO. FOR FURTHER INFORMATION, SEE CAPTION OF FIGURE 81. ..... - 121 -
FIGURE 84. PROJECTED CHANGES IN FREQUENCY DISTRIBUTIONS OF SIMULATED WIND DIRECTIONS IN WINTER (DJF), SPRING (MAM), SUMMER (JJA) AND AUTUMN BETWEEN THE PERIODS 1971-2000 AND 2040-2069 IN BOLOGNA BASED ON SIMULATIONS WITH 21 GCMS UNDER THE RCP8.5 SCENARIO. THE UNIT IS PERCENTAGE POINTS, WITH RED BARS DEPICTING AN INCREASE AND BLUE BARS A DECREASE. THE CIRCLES INDICATE THE CHANGES FOR EACH CARDINAL AND INTERCARDINAL DIRECTION WITH AN INTERVAL OF 0.5%. ..... - 122 -
FIGURE 85. PROJECTED TRENDS IN (A) MONTHLY MEAN AIR TEMPERATURE, (B) MONTHLY PRECIPITATION TOTAL, (C) MONTHLY MEAN OF DAILY MINIMUM TEMPERATURE, AND (D) MONTHLY MEAN OF DAILY MAXIMUM TEMPERATURE BETWEEN THE PERIODS 1981-2010 AND 2040-2069 IN HASSELT UNDER THE RCP8.5 SCENARIO. THE MULTI-MODEL MEAN PROJECTIONS FOR EACH CALENDAR MONTH (1 = JANUARY, 12 = DECEMBER) ARE DENOTED BY SQUARES. SHADING SHOWS THE 90 % UNCERTAINTY INTERVALS FOR THE CHANGE. ..... - 123 -

FIGURE 86. PROJECTED TRENDS IN (A) MONTHLY MEAN INCIDENT SOLAR RADIATION, (B) MONTHLY MEAN DIURNAL TEMPERATURE RANGE, AND (C) MONTHLY STANDARD DEVIATION OF DAILY MEAN TEMPERATURE BY THE PERIOD 2040–2069 IN HASSELT UNDER THE RCP8.5 SCENARIO. THE BASELINE PERIOD IS 1981-2010 (TOP) OR 1971-2000 (BOTTOM). FOR FURTHER INFORMATION, SEE THE CAPTION OF FIGURE 85. ..... - 124 -
FIGURE 87. PROJECTED TRENDS IN MONTHLY MEAN SURFACE AIR PRESSURE (IN HPA PER DECADE, LEFT) AND WIND SPEED (IN % PER DECADE, RIGHT) BETWEEN THE PERIODS 1981-2010 AND 2040-2069 IN HASSELT UNDER THE RCP8.5 SCENARIO. FOR FURTHER INFORMATION, SEE CAPTION OF FIGURE 85. ..... - 125 -
FIGURE 88. PROJECTED CHANGES IN THE FREQUENCY DISTRIBUTIONS OF SIMULATED CURRENT (BASELINE) WIND DIRECTIONS IN WINTER (DJF), SPRING (MAM), SUMMER (JJA) AND AUTUMN BETWEEN THE PERIODS 1971-2000 AND 2040-2069 IN HASSELT BASED ON SIMULATIONS WITH 21 GCMS UNDER THE RCP8.5 SCENARIO. THE CHANGES ARE GIVEN IN PERCENTAGE POINTS, WITH RED BARS DEPICTING AN INCREASE AND BLUE BARS A DECREASE IN THE FREQUENCY. THE CIRCLES INDICATE THE CHANGES FOR EACH CARDINAL AND INTERCARDINAL DIRECTION WITH AN INTERVAL OF 0.5%. ..... - 125 -
FIGURE 89. PROJECTED TRENDS IN (A) MONTHLY MEAN AIR TEMPERATURE, (B) MONTHLY PRECIPITATION TOTAL, (C) MONTHLY MEAN OF DAILY MINIMUM TEMPERATURE, AND (D) MONTHLY MEAN OF DAILY MAXIMUM TEMPERATURE BETWEEN THE PERIODS 1981-2010 AND 2040-2069 IN VANTAA UNDER THE RCP8.5 SCENARIO. THE MULTI-MODEL MEAN PROJECTIONS FOR EACH CALENDAR MONTH (1 = JANUARY, 12 = DECEMBER) ARE DENOTED BY SQUARES. SHADING SHOWS THE 90 % UNCERTAINTY INTERVALS FOR THE CHANGE. ..... - 126 -
FIGURE 90. PROJECTED TRENDS IN (A) MONTHLY MEAN DIURNAL TEMPERATURE RANGE, (B) MONTHLY MEAN INCIDENT SOLAR RADIATION, AND (C) MONTHLY STANDARD DEVIATION OF THE TEMPORAL VARIABILITY OF DAILY MEAN TEMPERATURE BY THE PERIOD 2040–2069 IN VANTAA UNDER THE RCP8.5 SCENARIO. THE BASELINE PERIOD IS 1981-2010 (TOP) OR 1971-2000 (BOTTOM). FOR FURTHER INFORMATION, SEE THE CAPTION FOR FIGURE 89.- 127 -
FIGURE 91. PROJECTED TRENDS IN A) MONTHLY MEAN SURFACE AIR PRESSURE AND B) WIND SPEED BETWEEN THE PERIODS 1981-2010 AND 2040-2069 IN VANTAA UNDER THE RCP8.5 SCENARIO. FOR FURTHER INFORMATION, SEE CAPTION FOR FIGURE 89..... - 128 -
FIGURE 92. PROJECTED CHANGES IN THE FREQUENCY DISTRIBUTIONS OF SIMULATED WIND DIRECTIONS IN WINTER (DJF), SPRING (MAM), SUMMER (JJA) AND AUTUMN BETWEEN THE PERIODS 1971-2000 AND 2040-2069 IN VANTAA BASED ON SIMULATIONS WITH 21 GCMS UNDER THE RCP8.5 SCENARIO. THE CHANGES ARE GIVEN IN PERCENTAGE POINTS, WITH RED BARS DEPICTING AN INCREASE AND BLUE BARS A DECREASE IN THE FREQUENCY. THE CIRCLES INDICATE THE CHANGES FOR EACH CARDINAL AND INTERCARDINAL DIRECTION WITH AN INTERVAL OF 0.5%..... - 128 -
FIGURE 93. MONTHLY MEAN TEMPERATURE AS ESTIMATED BY THE CC PROJECTIONS (RCP8.5) FOR BOLOGNA. .... - 132 -
FIGURE 94. MONTHLY ACCUMULATED RAINFALL AS ESTIMATED BY THE CC PROJECTIONS (RCP8.5) FOR BOLOGNA.. - 132 -
FIGURE 95. WIND ROSE OF YEARLY WIND FREQUENCIES AS ESTIMATED BY CC PROJECTIONS FOR BOLOGNA. ..... - 133 -
FIGURE 96. CONCENTRATION MAPS FOR NO_X IN THE 2055BC SCENARIO FOR BOLOGNA. THE MAPS REPRESENT CONCENTRATION VALUES AVERAGED OVER WINTER 2055. ..... - 134 -
FIGURE 97. CONCENTRATION MAPS FOR PM_{10} IN THE 2055BC SCENARIO FOR BOLOGNA. THE MAPS REPRESENT CONCENTRATION VALUES AVERAGED OVER WINTER 2055. ..... - 134 -
FIGURE 98. CONCENTRATION MAPS OF NO_X IN THE 2055P1EC FOR BOLOGNA. THE MAPS REPRESENT CONCENTRATION VALUES AVERAGED OVER WINTER 2055. ..... - 136 -
FIGURE 99. CONCENTRATION MAPS OF PM_{10} IN THE 2055P1EC FOR BOLOGNA. THE MAPS REPRESENT CONCENTRATION VALUES AVERAGED OVER WINTER 2055. ..... - 137 -
FIGURE 100. MAPS OF CONCENTRATION DIFFERENCES FOR NO_X FOR WINTER 2055. THE DIFFERENCES ARE CALCULATED BETWEEN 2055P1EC SCENARIO AND 2055BC SCENARIO..... - 137 -
FIGURE 101. MAPS OF CONCENTRATION DIFFERENCES FOR PM_{10} FOR WINTER 2055. THE DIFFERENCES ARE CALCULATED BETWEEN 2055P1EC SCENARIO AND 2055BC SCENARIO. ..... - 138 -
FIGURE 102. CONCENTRATION MAPS OF NO_X IN THE 2055P2EB FOR BOLOGNA. THE MAPS REPRESENT CONCENTRATION VALUES AVERAGED OVER WINTER 2055. ..... - 140 -
FIGURE 103. CONCENTRATION MAPS OF PM_{10} IN THE 2055P2EB FOR BOLOGNA. THE MAPS REPRESENT CONCENTRATION VALUES AVERAGED OVER WINTER 2055. ..... - 140 -

FIGURE 104. MAPS OF CONCENTRATION DIFFERENCES FOR NO_x FOR WINTER 2055. THE DIFFERENCES ARE CALCULATED BETWEEN 2055P2EB SCENARIO AND 2055BC SCENARIO. ..... - 141 -
FIGURE 105. MAPS OF CONCENTRATION DIFFERENCES FOR PM_{10} FOR WINTER 2055. THE DIFFERENCES ARE CALCULATED BETWEEN 2055P2EB SCENARIO AND 2055BC SCENARIO. ..... - 141 -
FIGURE 106. MONTHLY MEAN TEMPERATURE AND ACCUMULATED RAINFALL AS ESTIMATED BY THE CC PROJECTIONS FOR HASSELT. ..... - 143 -
FIGURE 107. WIND ROSE OF YEARLY WIND FREQUENCIES AS ESTIMATED BY CC PROJECTIONS FOR HASSELT. ..... - 143 -
FIGURE 108. NO_2 CONCENTRATION MAP IN HASSELT IN JANUARY 2055, AS RESULTING FROM CHANGES IN METEOROLOGY ONLY. ..... - 144 -
FIGURE 109. PM_{10} CONCENTRATION MAP IN HASSELT IN JANUARY 2055, AS RESULTING FROM CHANGES IN METEOROLOGY ONLY. ..... - 145 -
FIGURE 110. NO_x EMISSIONS (IN G/KM/S) FOR ROAD SOURCES CONSIDERED AS MAJOR ROADS IN HASSELT IN 2030 AS ESTIMATED FROM THE ADOPTION OF CLEANER TECHNOLOGIES AND CHANGES IN FLEET COMPOSITION IN THE FUTURE. ..... - 146 -
FIGURE 111. PM_{10} EMISSIONS (IN G/KM/S) FOR ROAD SOURCES CONSIDERED AS MAJOR ROADS IN HASSELT IN 2030 AS ESTIMATED FROM THE ADOPTION OF CLEANER TECHNOLOGIES AND CHANGES IN FLEET COMPOSITION IN THE FUTURE. ..... - 147 -
FIGURE 112. NO_x EMISSIONS ($G/M^2/S$) FROM RESIDENTIAL HEATING IN HASSELT IN 2050 AS ESTIMATED FROM THE ADOPTION OF CLEANER TECHNOLOGIES. ..... - 147 -
FIGURE 113. NO_2 CONCENTRATION MAP IN HASSELT IN JANUARY 2055, AS RESULTING FROM CHANGES IN METEOROLOGY AND REDUCTION EMISSIONS DUE TO THE EFFECT OF CLEANER TECHNOLOGIES. ..... - 148 -
FIGURE 114. PM_{10} CONCENTRATION MAP IN HASSELT IN JANUARY 2055, AS RESULTING FROM CHANGES IN METEOROLOGY AND REDUCTION EMISSIONS DUE TO THE EFFECT OF CLEANER TECHNOLOGIES. ..... - 149 -
FIGURE 115. NO_2 CONCENTRATION MAP IN HASSELT IN JANUARY 2055, AS RESULTING FROM CLIMATE CHANGES IN METEOROLOGY AND WITH THE IMPLEMENTATION OF THE POLICY 1, I.E. CLOSING THE INNER RING ROAD TO THE TRAFFIC. ..... - 149 -
FIGURE 116. PM_{10} CONCENTRATION MAP IN HASSELT IN JANUARY 2055, AS RESULTING FROM CLIMATE CHANGES IN METEOROLOGY AND WITH THE IMPLEMENTATION OF THE POLICY 1, I.E. CLOSING THE INNER RING ROAD TO THE TRAFFIC. ..... - 150 -
FIGURE 117. MAP OF DIFFERENCES IN NO_2 CONCENTRATION BETWEEN THE CLIMATE CHANGE SCENARIO WITH REDUCTION IN EMISSIONS AND THE SAME SCENARIO BUT IN CASE OF IMPLEMENTATION OF POLICY 1 IN HASSELT. .....- 151 -
FIGURE 118. MAP OF DIFFERENCES IN PM_{10} CONCENTRATION BETWEEN THE CLIMATE CHANGE SCENARIO WITH REDUCTION IN EMISSIONS AND THE SAME SCENARIO BUT IN CASE OF IMPLEMENTATION OF POLICY 1 IN HASSELT. .....- 152 -
FIGURE 119. NO_2 REDUCTION IN CASE OF IMPLEMENTATION OF POLICY 1 IN CC SCENARIO IN HASSELT, EVALUATED AS CONCENTRATION RATIO BETWEEN THE CONCENTRATION DIFFERENCE PREVIOUSLY EVALUATED (FIGURE 117) AND THE CONCENTRATION OBSERVED IN THE CC SCENARIO (FIGURE 113). ..... - 152 -
FIGURE 120. PM_{10} REDUCTION IN CASE OF IMPLEMENTATION OF POLICY 1 IN CC SCENARIO IN HASSELT, EVALUATED AS CONCENTRATION RATIO BETWEEN THE CONCENTRATION DIFFERENCE PREVIOUSLY EVALUATED (FIGURE 118) AND THE CONCENTRATION OBSERVED IN THE CC SCENARIO (FIGURE 114). ..... - 153 -
FIGURE 121. NO_2 CONCENTRATION MAP IN HASSELT IN JANUARY 2055, AS RESULTING FROM CHANGES IN METEOROLOGY AND WITH THE IMPLEMENTATION OF THE POLICY 2 I.E. WITH AN INCREASE IN THE BUS FREQUENCIES. ..... - 154 -
FIGURE 122. PM_{10} CONCENTRATION MAP IN HASSELT IN JANUARY 2055, AS RESULTING FROM CHANGES IN METEOROLOGY AND WITH THE IMPLEMENTATION OF THE POLICY 2 I.E. WITH AN INCREASE IN THE BUS FREQUENCIES. - 154 -
FIGURE 123. MAP OF DIFFERENCES IN NO_2 CONCENTRATION BETWEEN THE CLIMATE CHANGE SCENARIO WITH REDUCTION IN EMISSIONS AND THE SAME SCENARIO BUT IN CASE OF IMPLEMENTATION OF POLICY 2 IN HASSELT. .....- 155 -

FIGURE 124. MAP OF DIFFERENCES IN PM_{10} CONCENTRATION BETWEEN THE CLIMATE CHANGE SCENARIO WITH REDUCTION IN EMISSIONS AND THE SAME SCENARIO BUT IN CASE OF IMPLEMENTATION OF POLICY 2 IN HASSELT. .....- 156 -
FIGURE 125. NO_2 REDUCTION IN CASE OF IMPLEMENTATION OF POLICY 2 IN CC SCENARIO IN HASSELT, EVALUATED AS CONCENTRATION RATIO BETWEEN THE CONCENTRATION DIFFERENCE PREVIOUSLY EVALUATED (FIGURE 123) AND THE CONCENTRATION OBSERVED IN THE CC SCENARIO (FIGURE 113). ..... - 157 -
FIGURE 126. PM_{10} REDUCTION IN CASE OF IMPLEMENTATION OF POLICY 2 IN CC SCENARIO IN HASSELT, EVALUATED AS CONCENTRATION RATIO BETWEEN THE CONCENTRATION DIFFERENCE PREVIOUSLY EVALUATED (FIGURE 124) AND THE CONCENTRATION OBSERVED IN THE CC SCENARIO (FIGURE 114). ..... - 157 -
FIGURE 127. MONTHLY MEAN TEMPERATURE AND ACCUMULATE RAINFALL AS ESTIMATED BY THE CC PROJECTIONS FOR VANTAA. ..... - 158 -
FIGURE 128. WIND ROSE OF YEARLY WIND FREQUENCIES AS ESTIMATED BY CC PROJECTIONS FOR VANTAA. ..... - 159 -
FIGURE 129. NO_2 CONCENTRATION MAP IN VANTAA IN JANUARY 2055, AS RESULTING FROM CHANGES IN METEOROLOGY ONLY. ..... - 160 -
FIGURE 130. $PM_{2.5}$ CONCENTRATION MAP IN VANTAA IN JANUARY 2055, AS RESULTING FROM CHANGES IN METEOROLOGY ONLY. ..... - 160 -
FIGURE 131. NO_2 CONCENTRATION MAP IN VANTAA IN JANUARY 2055, AS RESULTING FROM CLIMATE CHANGES IN METEOROLOGY AND WITH THE IMPLEMENTATION OF THE POLICY 1, I.E. CLOSING AN AREA IN THE EAST OF VANTAA TO THE TRAFFIC. ..... - 161 -
FIGURE 132. $PM_{2.5}$ CONCENTRATION MAP IN VANTAA IN JANUARY 2055, AS RESULTING FROM CLIMATE CHANGES IN METEOROLOGY AND WITH THE IMPLEMENTATION OF THE POLICY 1, I.E. CLOSING AN AREA IN THE EAST OF VANTAA TO THE TRAFFIC. ..... - 162 -
FIGURE 133. MAP OF DIFFERENCES IN NO_2 CONCENTRATION BETWEEN THE CLIMATE CHANGE SCENARIO WITH REDUCTION IN EMISSIONS AND THE SAME SCENARIO BUT IN CASE OF IMPLEMENTATION OF POLICY 1 IN VANTAA. - 163 -
FIGURE 135. NO_2 REDUCTION IN CASE OF IMPLEMENTATION OF POLICY 1 IN CC SCENARIO IN VANTAA, EVALUATED AS CONCENTRATION RATIO BETWEEN THE CONCENTRATION DIFFERENCE PREVIOUSLY EVALUATED (FIGURE 133) AND THE CONCENTRATION OBSERVED IN THE CC SCENARIO (FIGURE 129). ..... - 164 -

List of Abbreviations

AADT: Annual Average Daily Traffic count

ADMS: Atmospheric Dispersion Modelling System

AKT: Annual Kilometres Total

AQ: Air Quality

ARPAE: Emilia Romagna Environmental Protection Agency (new acronym replacing ARPA-ER)

A.S.L.: Above Sea Level

BC: Base Case

BE: Belgium

CC: Climate Change

CERC: Cambridge Environmental Research Consultants

CLINO: Climate NOrmals

CMIP5: Coupled Model Intercomparison Project Phase 5

CO: Carbon Monoxide

D: Deliverable

FA2: Factor of 2

FB: Fractional Bias

FEBIAC: Fédération Belge et luxembourgeoise de l'Automobile et du Cycle

FMI: Finnish Meteorological Institute

GCM: Global Circulation Model

GTFS: General Transit Feed Specification

GHG: Greenhouse Gases

GIS: Geographic Information System

HSL/HRT: Helsinki Regional Transport Authority

HSY: Waste Management's Seututieto

IMOB: Transportation Research Institute of the Hasselt University

LTZ: Low Traffic Zone

NMSE: Normalized Mean Square Error

NO: Nitric Oxide

NO_2: Nitrogen Dioxide

NO_x:	Nitrogen Oxides
O_3:	Ozone
PCS:	Passive Control Systems
P1EC:	Policy 1 Electric Centre
P2EB:	Policy 2 Electric Buses
PM:	Particulate Matter
PM_1:	Particulate Matter with aerodynamic diameter less or equal to 1 μm
$PM_{2.5}$:	Particulate Matter with aerodynamic diameter less or equal to 2.5 μm
PM_{10}:	Particulate Matter with aerodynamic diameter less or equal to 10 μm
r:	Pearson's correlation coefficient
R^2:	coefficient of determination
RCP:	Representative Concentration Pathway
SO_2:	Sulphur Dioxide
SSP:	Socioeconomic Pathway
UH:	University of Hasselt
UNFCCC:	United Nations Framework Convention on Climate Change
VMM:	Flanders Environment Protection Agency
VOC:	Volatile Organic Compounds
WHO:	World Health Organization
WMO:	World Meteorological Organization
WP:	Work Package

1 Executive Summary

This report addresses the efficacy of policy options to improve air quality in present and future climate projections considering also possible behavioural change. The evaluation of the efficacy of policy options has been conducted by reconstructing detailed air quality maps using a well-validated dispersion model in three iSCAPE cities namely Bologna, Hasselt and Vantaa, representative of south, central and north Europe, respectively. The choice of the three cities derived to represent different climatic bands and from previous results obtained with GPS-loggers campaigns, part of an iSCAPE task evaluating the environmental effect of some behavioral actions such as telecommuting, start time to work and number of cold and warm starts. These results were used to fine-tune the inputs of model simulations. In particular, as reported in the '*Demonstrator of a cost/utility function*'[1] (D4.2), an activity-based model (FEATHERS) was developed at UH to conduct traffic simulations for Hasselt (BE); results from traffic simulations were used as input to develop the emission inventory for the current scenario. At other iSCAPE cities, instead, because of the unavailability of information as detailed as in Hasselt, a light activity-based model was developed to perform behavioral simulations (see D4.2 and '*Behavioral Simulations Design Aspects Report*'[2], D4.3). In the case of Bologna, the complete emission inventory was developed using data available from the Municipality, which was used to compare and validate the results obtained from the traffic simulations. Finally, the source emission inventory was used as input to the dispersion modeling simulations carried on under the present scenario conditions, i.e., under present meteorology and without considering the effect of traffic policies management, or behavioral changes. In both cases, results of dispersion models carried out in present scenario were used to validate the developed emission inventory and dispersion models. The emission inventory and dispersion models are meant to be further used to evaluate the effectiveness of policies to reduce air quality in both present-day conditions as well as under the effect of changes in meteorology as evaluated by future climate projections.

Data used for the validation of the model simulations in Bologna derive partially from the monitoring campaign conducted as part of the planning and evaluation of the iSCAPE Passive Control System solutions WP3. The results obtained analyzing data gathered in the campaign were reported in the '*Air pollution and meteorology monitoring report*[3]' (D5.2). Other air quality data in Bologna are provided from the Emilia-Romagna Environmental Protection Agency (ARPAE). In the case of Hasselt, where no specific monitoring campaign was conducted and information on available air quality and meteorological measurements is scarce (see the '*Report on climate change and air quality interactions*'[4], D1.4), air quality and meteorological data for the current scenario were provided from the Flanders Environmental Protection Agency and from the Royal Meteorological Institute of Belgium. Finally, in the case of Vantaa, air quality and meteorological data were obtained from the Finnish Meteorological Institute (FMI).

Here, the methodology used to carry out traffic simulations with the activity-based model, already presented in D4.2, is summarized, whereas the methodologies adopted to use those simulations to develop the emission inventory to feed the dispersion model in the present scenario are described in great detail. In addition, a synthesis of the methodology adopted to extract meteorological variables in

[1] Demonstrator of a cost/utility function taking activity-based information into account

[2] The Report will be available on the iSCAPE reports webpage

[3] The Report will be available on the iSCAPE reports webpage

[4] Report on climate change and air quality

future climate scenarios, which will be thoroughly described in the upcoming '*Detailed report on local meteorological conditions*' (D6.4), is also provided.

The development and build-up of the emission inventories involve the identification of all the major pollutant emission sources specific for each site, which is of paramount importance in the correct and adequate planning of traffic management policies effective in mitigating air pollution. In fact, the results of the simulations conducted in the current scenario highlighted the presence of different air pollution hotspots in the two cities. In both cities, indeed, policies adequately setup in view of the major hotspots identified were revealed to be effective in improving air quality both in present as well as in future climate scenarios. This fulfills the objective of assessing the effectiveness of behavioral changes both in current (baseline) as well as in future climate.

2 Introduction

Air pollution and climate change represent two of the main environmental problems we are facing and, as known, the two are linked. In particular, both problems are a result of the same context, i.e. the current energy model. In fact, air pollution and climate change are worsened and linked to the burning of fossil fuels, which increases CO_2 emissions causing global warming. At the same time, the burning of fossil fuels produces other pollutants, such as nitrogen oxides, sulfur oxides and particulate matter, therefore worsening of air quality. Many of the air pollutants are not only harmful to human health and ecosystems but also contribute to climate change, affecting the amount of radiation that is reflected or absorbed by the atmosphere. In particular, some of them (for instance sulfate aerosol particles) reflect the radiation contributing to a cooling of the climate, while others (for instance black carbon) absorb radiation and thus contribute to a warming of the climate. Both of these problems may have a serious impact on society. In particular, air pollution represents the current leading environmental cause of premature deaths, with the WMO (World Meteorological Organization) estimating it to cause about 7 million premature deaths annually (WHO, 2014). By contrast, climate change contributes to worsen drought, flooding, deforestation (IPCC, 2014), resulting in famine and diseases (e.g. Robine et al., 2008; Zhou et al., 2008). Recent researches also showed that climate change resulted in a change of allergenic patterns while air pollution may potentially modify the allergenic potential of pollen grains especially in the event of particular weather conditions (D'Amato et al., 2014).

Although all plans to minimize climate change depend critically on swift action to reduce CO_2 emissions, internationally agreed climate targets may not be achievable without additional activities to mitigate short-lived climate-forcing pollutants. In particular, the development of such plans depends strongly on the identification of the understanding and identification of the sources of short-lived climate-forcing pollutants. Although at present policies to mitigate climate change and air pollution are often tackled in separate policy arenas and at different levels, due to their various links, the potential of developing joint policies for contrasting and mitigating both climate change and air pollution has to be investigated. In general terms, transport policies are dealt from the global general level to the smaller city council level (e.g., United Nations Environment Programme -UNEP-, Task Force on Hemispheric Transport of Air Pollution -HTAP-). At intermediate level, also the European Commission sets up actions for transport plans issues including environmental aspects, while the national governments, besides transposing European Union guidelines into the national legislation, also develop their own transport policies. Regional and local governments make land-use decisions with a potential impact on transport choices. It is therefore of paramount importance to establish a link and collaboration between science and stakeholders from the local to the global point of view to develop and test the effect of policies for mitigating climate change and air pollution.

Transport policies may have significant impacts on the environment. This deliverable aims to analyse the extent to which some policies and future trends in meteorological variables may impact on local levels of air pollution concentrations in three selected iSCAPE cities, namely Bologna, Hasselt and Vantaa. The choice of the two cities derived from the previous results obtained with GPS-loggers campaigns that were used to fine-tune the inputs of traffic model simulations ran at UH. In addition, the thee cities share other similarities for instance in terms of emitting sources mostly impacted by traffic and residential heating; while Bologna and Hasselt are also similarly located in a valley, Vantaa is instead representative of a coastal landscape. Finally, the three cities also are representative of three latitudinal bands differently impacted by climate change, i.e., northern, central and southern Europe. In

fact, the impact of climate change will not be the same all over Europe; for example, heat waves will impact nearly twice as likely over southern Europe and the Mediterranean (Jacob et a., 2018).

The analysis is based on the development of specific emission inventories for the iSCAPE cities test cases, whose results are used as input to a well-validated air dispersion model. Simulations have been carried out using a reference year and validated against measurements from available air quality stations. The simulations in current (baseline) case have been carried out in the presence of transport policies with or without the presence of climate change impacting on meteorological variables. In particular, for each city, two transport policies were implemented to evaluate their impact in both current (baseline) and future case scenarios.

The following Table presents an overview of all the cases for which air dispersion simulations were performed in the three cities, and that will be thoroughly presented and discussed in this report.

City	Scenario	Policy	Purpose
Bologna	Current (baseline) (2017)	None	Verification of the simulations; analysis of concentration maps and air pollution hotspots in the current (baseline) case
Bologna	Current (baseline) (2017)	Electric centre	Estimation of the air pollution reduction through the implementation of the policy in the current (baseline) scenario
Bologna	Current (baseline) (2017)	Electric buses	Estimation of the air pollution reduction through the implementation of the policy in the current (baseline) scenario
Bologna	CC scenario (2055)	None	Estimation of concentration maps and air pollution hotspots in the future scenario
Bologna	CC scenario (2055)	Electric centre	Estimation of the air pollution reduction through the implementation of the policy in the future scenario
Bologna	CC scenario (2055)	Electric buses	Estimation of the air pollution reduction through the implementation of the policy in the future scenario
Hasselt	Current (baseline) (2016)	None	Verification of the simulations; analysis of concentration maps and air pollution hotspots in the current (baseline) case
Hasselt	Current (baseline) (2016)	Closure of the inner ring	Estimation of the air pollution reduction through the implementation of the policy in the current (baseline) scenario
Hasselt	Current (baseline) (2016)	Increase in the frequency of buses	Estimation of the air pollution reduction through the implementation of the policy in the current (baseline) scenario
Hasselt	CC scenario (2055)	None	Analysis of concentration maps and air pollution hotspots in the future scenario
Hasselt	CC scenario (2055) with emissions reduction	None	Analysis of concentration maps and air pollution hotspots in the future scenario with emissions reductions due to the use of cleaner technologies in the future
Hasselt	CC scenario (2055)	Closure of the inner ring	Estimation of the air pollution reduction through the implementation of the policy in the future scenario
Hasselt	CC scenario (2055)	Increase the frequency of buses	Estimation of the air pollution reduction through the implementation of the policy in the future scenario
Vantaa	Current (baseline) (2017)	None	Verification of the simulations; analysis of concentration maps and air pollution hotspots in the current (baseline) case
Vantaa	Current (baseline) (2017)	Closure of the inner ring	Estimation of the air pollution reduction through the implementation of the policy in the current (baseline) scenario
Vantaa	Current (baseline) (2016)	Increase in the frequency of buses	Estimation of the air pollution reduction through the implementation of the policy in the current (baseline) scenario
Vantaa	CC scenario (2055)	None	Analysis of concentration maps and air pollution hotspots in the future scenario
Vantaa	CC scenario (2055)	Closure of the inner ring	Estimation of the air pollution reduction through the implementation of the policy in the future scenario
Vantaa	CC scenario (2055)	Increase the frequency of buses	Estimation of the air pollution reduction through the implementation of the policy in the future scenario

Table 1. Overview and main purpose of the dispersion simulations performed in the three iSCAPE cities, whose output is evaluated and presented in this report.

As such, the report summarizes the effect of behavioral changes related to mobility on air quality both in the present and in the future scenarios in selected cities. The output of this task will provide the basis for the links between AQ and CC and for establishing behavioral recommendations, exploiting the iSCAPE results (Tasks T7.3 and T7.4). The following Figure presents in a schematic form the major connections and links of this task within the iSCAPE project.

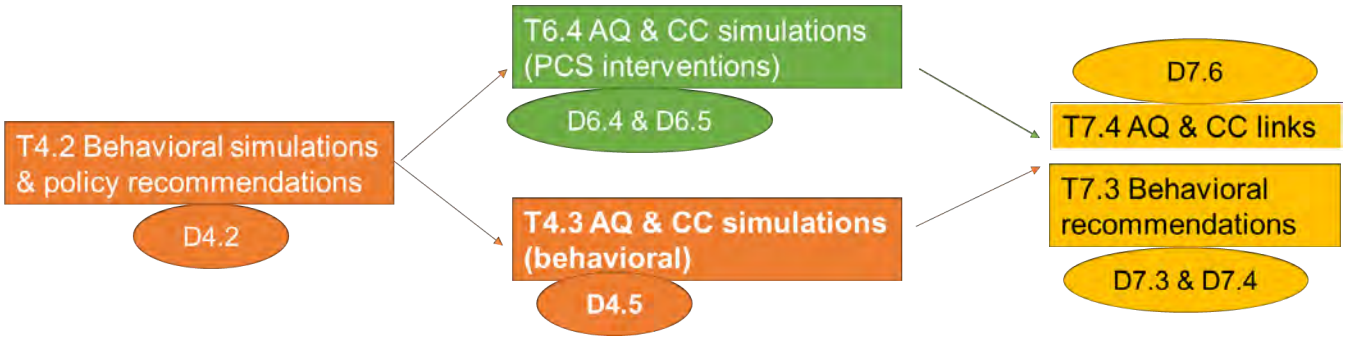

Figure 1. Schematic flow diagram between this Deliverable/Task and other tasks in the same and in other iSCAPE WPs.

3 Methodology for AQ simulation in the current scenario

Due to their position in a valley region, Bologna and Hasselt cities are located in hotspots in terms of air pollution and climate change. Although according to data released by World Health Organization (WHO, 2016), air quality in Finland is the best in the world, a recent research (Lehtomäki et al., 2018) suggests that it is one of the leading health risks, representing about 2% of the total national burden of disease and including 2000 premature deaths. In addition, although the average temperature in Europe has been observed to increase with regionally and seasonally different rates depending on the latitude (Kovats et al., 2014), with the greatest increases in Northern Europe (Larsen et al., 2014). Global model simulations of future climate show significant agreement in warming, with strongest warming projected in Southern Europe in summer, and in Northern Europe in winter (Goodess et al., 2009; Kjellström et al., 2011). Behavioral changes and urban policies management are fundamental tools to mitigate the impact of both air quality and climate change risks. Seeking this goal, behavioral changes and urban policies management were tested by means of pollutant dispersion simulation in various scenarios in the three cities. Though being different in terms of population and common behaviours, the three cities share similarities in terms of major emitting sources, position in low topography regions, and in the case of Bologna and Hasselt also significant potential of changing with relatively small behavioural changes in attitudes (Ahmed et al., 2018).

In order to accurately model the dispersion characteristics over a study area, the meteorology, the topography, the background concentrations, the parameters of the emission sources, and the variability over time of the emissions must be known and set. In the three cities the current scenario is modelled through the construction of a complete emission inventory describing all major emitting sources.

Once the complete emission inventory had been compiled for each city, emissions were used as input to the dispersion model in order to calculate the spatial distribution of major pollutant concentrations in the current meteorological conditions. All simulations run for the current (baseline) case are compared with measured data. Model performance is evaluated using statistical analyses. After validation the model is used to assess the effectiveness of policies to reduce air pollution in both present as well as future climate projections.

In the following sections we describe the three sites, the network for meteorological and air quality measurements, and the methodology adopted sites to construct the emission inventory and then the dispersion model. In addition, the methodologies used to evaluate the performance of the model, and the effectiveness of the policies are also described in this section.

3.1 Domain information and description

3.1.1 Bologna

The urban area of Bologna, the main city of the Emilia-Romagna region of Italy, is located at the foot of the Apennines in the vast flat area the Po Plain in the north of Italy (44°29' N, 11°20' E), with a mean altitude about of 54 m a.s.l (Figure 2). A detailed description of the city geography and morphology was previously reported in the '*Detailed report for the assessment of air quality and UHI in EU selected cities pre-infrastructural solutions*'[5] (D6.1).

[5] Report on the Assessment of air quality and microclimate in EU selected cities pre-infrastructural solutions

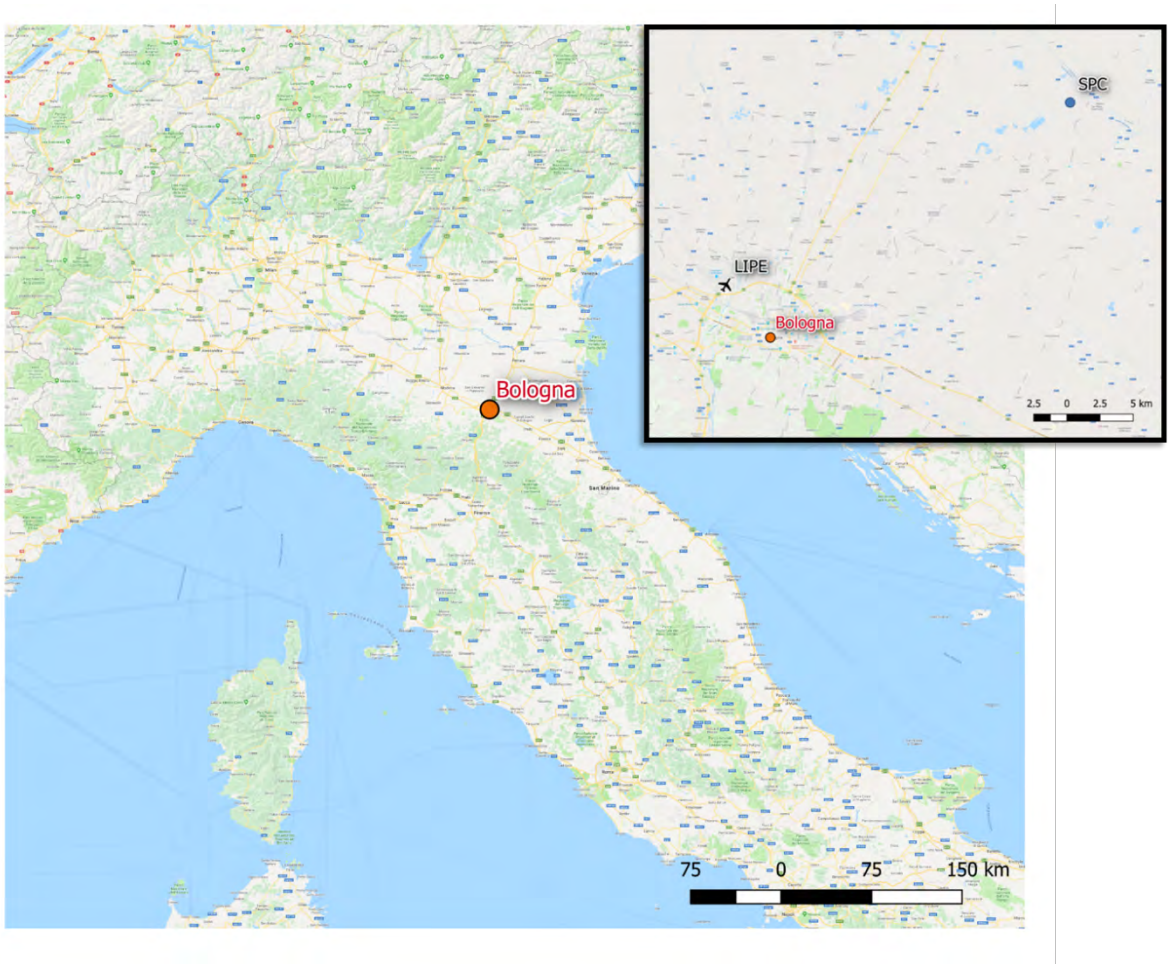

Figure 2. Bologna and its location in Italy. The left map indicates the positions of weather stations: near the city centre (Bologna Airport) and in the countryside (San Pietro Capofiume). Source: Open Street Map.

The city covers about 141 km^2 of which 105 are included in the area of high and medium plains and 36 in the hills. The hilly area represents about 25% of the municipal territory, extending in the south-west area. The position exposes the provincial territory of Bologna to the winds that arrive from the Alps, characterizing its climate. Indeed, within the Province of Bologna three altimetric and consequently climatic bands can be distinguished, i.e. the mountain belt, hilly and plain. The urban population of Bologna is 389,261 inhabitants (ISTAT, 2018), reaching one million people if the metropolitan area is included. Bologna is also known as a university town as it has an old university with around 85,500 students.

Bologna is one of the main Italian road nodes, heavily interested by large-scale transportation (railway and aviation) (Figure 2**Error! Reference source not found.**). The main transport infrastructures and arterial roads of regional and national importance cross the entire area while the provincial road network surrounds Bologna developping mainly in the flat territory. The transport infrastructure, and mobility in general, represents a considerable environmental pressure on the entire metropolitan area. In fact, the air quality in the city of Bologna is critical. For example, PM_{10} (Particulate Matter with an aerodynamic diameter of 10 µm or less) shows a very problematic situation, especially in the winter months, with

numerous exceedances of the thresholds (ARPAE, 2018). In order to mitigate the impact and improve air quality, the municipality has implemented policies and actions in the field of mobility (Urban Plan for Sustainable Mobility–PUMS, Comune di Bologna, 2018), paying particular attention to issues such as: metropolitan public transport, the cycle network, bike and car sharing, the transition to electric vehicles, pedestrian areas and intermodality (Figure 3 and **Error! Reference source not found.**). The territory is not directly affected by large-scale industrial facilities, however in the whole area both mechanical and food manufacturers are densely present; moreover a municipal waste incinerator is active in the town outskirts (a detailed description of air pollution was previously reported in D6.1).

The road network is characterized by an internal ring road that delimits the historical centre of Bologna, and a road arch located to the north that surrounds Bologna from East to West (Figure 2). The internal ring road is characterized by high volumes of urban traffic, while the arch (external ring road) is traveled by traffic mainly coming from the hinterland and the motorway.

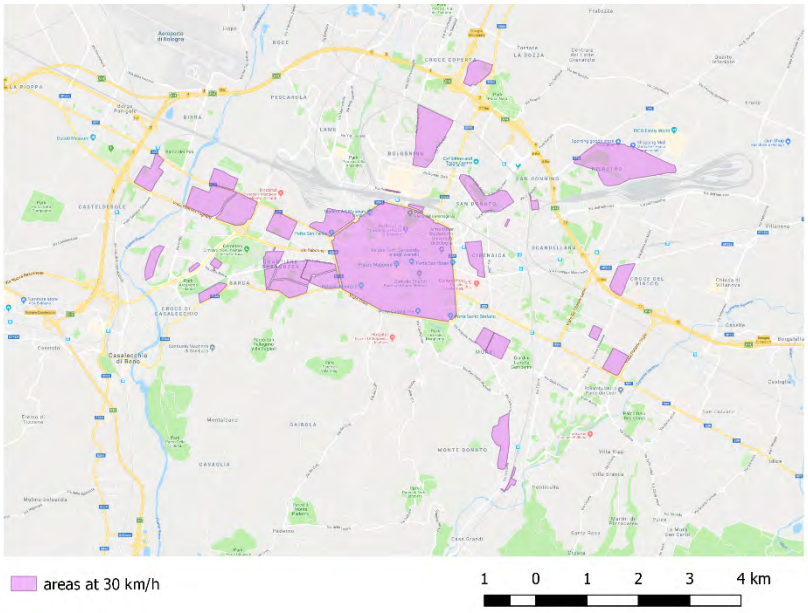

Figure 3. The mobility policies of Bologna have established areas with a speed limit of 30 km/h, shown in this map (Source: Open Street Map).

The climate in Bologna is strongly dominated by its geographical position within the Po Valley. It is characterized by a warm and humid summer and long, cold winter with little rainfall occurring in spring and autumn. Fog is a recurrent condition that occurs in the presence of a strong inversion, a typical condition in the basin at night and early morning. The geographic conformation also influences the winds that blow on the basin that are not very intense, due to the presence of both the mountain chains and the Adriatic Sea which favor a breeze regime.

A detailed description of recent climatology was previously reported in D6.1, with a statistical elaboration on a 10 years basis (2006-2016) of meteorological parameters. Here, we summarize the main peculiarities to compare the records of the last few years and determine the worst case in terms of weather conditions impacting on air quality.

Wind speed and directions data used for this purpose are taken from the measurement station Bologna Urbana, inside the city of Bologna. For air temperature and precipitation analysis, data coming from two different sites are compared: a representative measurement station in the city centre (Bologna Urbana) and a countryside station (San Pietro Capofiume) for rural background data (Figure 2). The wind rose of winds blowing over the 10 years taken into consideration shows that the major occurrences point to south-west. The winds impinging on the city are mainly characterized by low speeds (<4 m s^{-1}) that are generally ineffective for air recirculation and cleaning.

The time series of air temperature (over 10 years taken into consideration) shows an annual period oscillation in a range between 0°C and 30°C, with urban temperatures being typically larger than those in the countryside (except for 2006). Major differences are evident during winter, when heating systems increase the environmental temperature until 3-4°C in urban area, while during the rest of the year differences are between 1 and 2°C.

Annual precipitation (over the 10 years taken into consideration) is higher in urban than in rural areas (except for 2016). This trend is present in every month of the year, with the exception of the hot months, when the rainfall in the two sites is comparable. The annual values for the period 2006-2016 range are between 500 and 900 kg m^{-2} in Bologna and between 200 and 800 kg m^{-2} in the countryside, with average values of 718 kg m^{-2} and 537 kg m^{-2} respectively.

3.1.2 Hasselt

The city of Hasselt (50°55'48"N, 05°20'15"E) is a Flemish city and municipality, one of the urbanized Arrondissement in the Limburg province of Belgium. It is located in the middle of a very populated and industrialized area, characterized by many diverse anthropogenic emissions of air pollution.

Hasselt Arrondissement is a combination of 17 municipalities including Hasselt City. With a population of about 77,651 inhabitants and a density of 759.8 inhabitants/km^2, Hasselt is the 8th biggest city in Flanders. Hasselt city is also a capital of Limburg, and therefore for a variety of administrative issues individuals living in a surrounding region may frequently visit this city. The total area of the Arrondissement is 906 square km, while Hasselt city has an area of around 102 square km with a population density of 750 inhabitants per square km. Figure 4 represents Hasselt Arrondissement and Hasselt city as part of the Limburg province of Belgium.

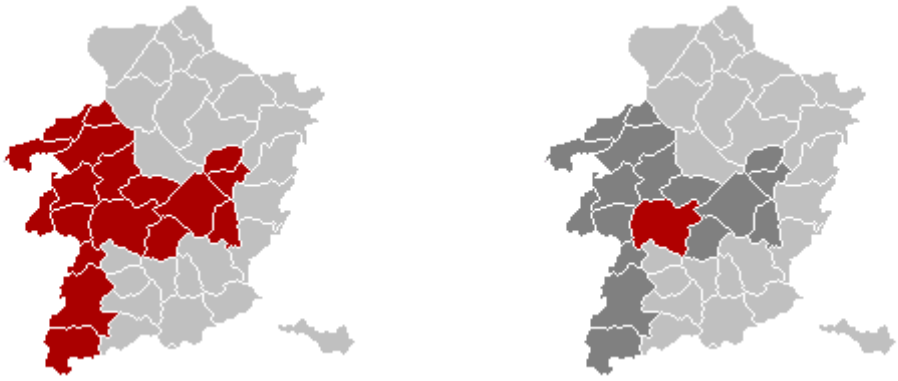

Figure 4: (left) Hasselt city in red, within the Limburg province in Belgium. (right) Hasselt Arrondissement in red in a Limburg province of Belgium.

In particular, Hasselt (Figure 5) is located in between the Campine region, north of the Demer river, and the Hesbaye region, to the south. On a larger scale, it is situated in the Meuse-Rhine region. The city is crossed by two main rivers, the Demer and the Albert Canal.

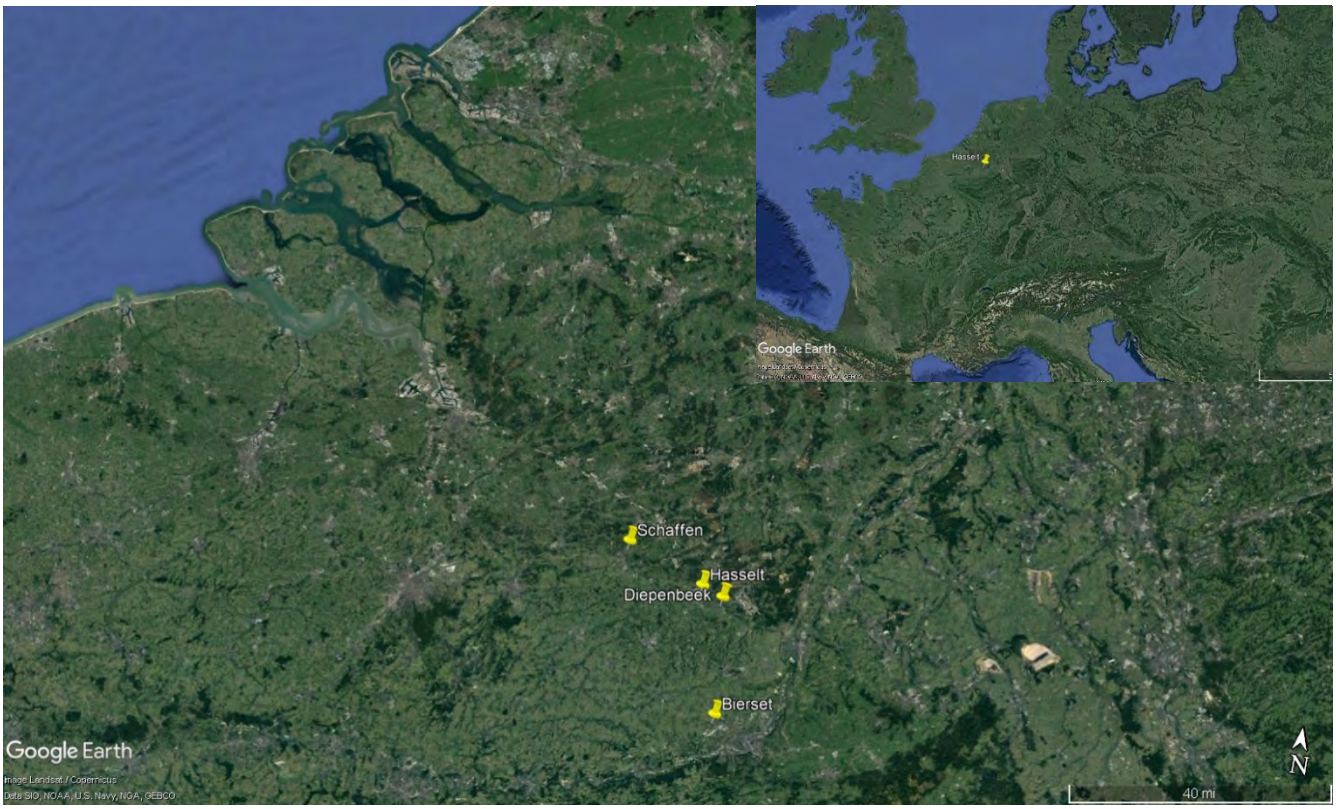

Figure 5: Location of the city of Hasselt in Belgium. Also shown the locations of the Diepenbeek, Schaffen and Bierset synoptic meteorological stations (source: Google Maps).

The major economic activities in the Limburg province are tourism, agriculture, and industry. After being a major coal mining centre, the region is trying to constantly promote innovation and sustainability. Manufacturing is the major economic activity in the provinces of East Flanders, and Limburg. In particular, pollutant emissions from the industry sector showed a decline in the whole Flanders region in the last decades (VMM, 2017). However, no major industry is located in Hasselt surroundings. The energy sector also showed a downward trend in Flanders, mainly due to the switch to alternative fuels with fewer solid and liquid fuels and more natural gas consumption, and as a result of the introduction of technical measures (VMM, 2017). In Flanders, emissions from building heating include emissions from households and emissions from the tertiary sector. While the switch from coal and fuel oil to natural gas had a positive influence on emissions from heating, on the contrary the rising of the use of wood as primary heating source had a negative impact on emissions.

Traffic contributes most of exhaust emissions (61% of total NO_2 emissions in 2016) and almost three quarters of particulate matter emissions through non-exhaust (wear and tear of the road surface, tyres and brakes). In fact, car traffic and related problems such as traffic congestion and air pollution are major problems in Flanders where the number of passenger cars and of kilometres driven continue to grow. In Hasselt, car ownership has significantly increased in the last 2 decades (Ahmed et al., 2018). In particular, Hasselt city is at the junction of important traffic arteries from several directions. The most important motorways are the European route E313 (Antwerp-Liège) and the European route E314 (Brussels-Aachen). The old town of Hasselt is enclosed by 2 ring roads. The outer ring road serves to keep traffic out of the city centre and main residential areas. The inner ring road, the 'Green Boulevard', serves to keep traffic out of the commercial centre, which is almost entirely a pedestrian area. There are also important traffic arteries to Tongeren, Sint-Truiden, Genk, and Diest. The road network of the Hasselt is illustrated through Figure 6. In the last two decades, car ownership has significantly increased in the area generating problems like traffic congestion and air pollution. In Hasselt, 73% of the total trips are performed using a car. For a trip distance of around 8 to 10 km, after car the bicycle has the 2nd largest share, which is the result of adopting a bicycle-oriented policy by the City administration such as development of relevant infrastructure (i.e. segregated bicycle lanes, bicycle priority streets, bicycle parking facilities), availability of bike sharing schemes and increase in car parking cost in the inner core areas. However, in the inner core region, there are streets still allowing car movements despite some of the shopping streets are completely pedestrianized. There are more than 8 large car parking areas (having a capacity of more than 100 cars) surrounding the inner ring. Car parking areas facilitate citizens to park their cars and then walk around the inner region for shopping or other activities. Public transport is available and a major transport hub is located near the Hasselt train station. There is only one operator (*dlijn*) providing the bus-based public transport services within the Hasselt Arrondissement. However, bus service is not very frequent except a few routes that cover Hasselt train station and Hasselt University campus located in Diepenbeek, a small town near Hasselt city.

There is also a small airport for small private aircrafts in Hasselt (Kiewit). Finally, the city has also a major railway station with high speed trains connecting it to Liège and Leuven (Figure 6).

Figure 6: Map of the city of Hasselt with the road network (the two ring roads and the main traffic junctions), the small local airport of Kiewit and the railway. (source: Open Street Maps).

Due to the problems of traffic congestion and air pollution, the local government is careful about public transport and parking spaces; however, notwithstanding the efforts of the local government in Hasselt, 73% of total trips are still performed by car as compared to public and active transport ('*Report on challenges and opportunities in iSCAPE cities*')[6]. Altogether, it is clear that traffic and residential heating are the dominant air pollution sources in the Hasselt domain.

The most recent annual air report for Flanders reports that in the region the European air quality targets are met for a large number of substances (VMM, 2017). However, for some substances, the targets are not yet met; in particular, model calculations and local measurement campaigns show that nitrogen dioxide concentrations are still too high at locations with high traffic. Even though the percentage of the population exposed to high NO_2 concentration has consistently declined over the past four years, about one-third of the population was exposed to excessive concentrations in 2017 when taking the 20 $\mu g\ m^{-3}$ target from the draft 2030 Air Policy Plan of the Flemish Government as reference framework. As for particulate matter, model simulations show that, while less than 0.01 of the population was living in an area where the annual or daily European PM_{10} limit value (40 $\mu g\ m^{-3}$) was exceeded, 20% of population was living in areas with excessively high annual PM_{10} average and 96% with too many excess days for PM_{10}, when considering WHO guideline values (20 $\mu g\ m^{-3}$ and maximum 3 days exceedances). Similarly, the European limit value for $PM_{2.5}$ (25 $\mu g\ m^{-3}$) was broadly complied with, whereas 95% of population was exposed to concentrations over the WHO guideline value of 10 $\mu g\ m^{-3}$ and to more than 3 days with concentrations exceeding 25 $\mu g\ m^{-3}$. As for O_3, model simulations show that the European target was met

[6] Report on challenges and opportunities in iSCAPE cities

everywhere, but the entire Flemish population was living in areas with concentrations exceeding the WHO guideline value and to too many days with high O_3 concentrations.

The Flanders Environment Agency (VMM) also estimated that the number of premature deaths caused by $PM_{2.5}$ and O_3 in Flanders in 2015 was about 4,100 and 100, respectively, while those caused by NO_2 amounted to 1,800 or 3,600 depending on the adopted dose-response function and threshold (VMM, 2017).

The climate of Hasselt is classified as Cfb (where C indicates temperate midlatitudes climate, the subgroup f indicates humid climate with abundant precipitations all year-long, and finally the third letter b indicates the presence of warm summers) according to the Köppen-Geiger classification[7]. Indeed, the climate in Hasselt is warm and temperate, with significant rainfall throughout the year. In the following, in order to characterize Hasselt climatology, we adopt the concept of CLINO (CLImate NOrmals), a statistical elaboration on a 30 years basis (here 1981-2010) of meteorological parameters. CLINO is widely used to characterize climatological values of meteorological variables at a specific location, and it serves as a basis to calculate anomalies, i.e. differences of parameters between the considered period and the 30 years reference period[8].

[7] The Köppen climate classification, proposed for the first time by Wladimir Köppen in 1918, is the most used for geographical purposes and defines climate boundaries to correspond to vegetation zones. The first capital letter indicates the main group, defined by temperature criteria and/or dryness, whereas the second and third letter indicate the subtypes within the major groupings (for instance indicating seasonality of precipitation, warmth of the summer or coldness of the winter).

[8] Climatological means for Hasselt are available from the Royal Meteorological Institute Belgium through their website (https://www.meteo.be/meteo/view/fr/27484519-Climat+dans+votre+commune.html).

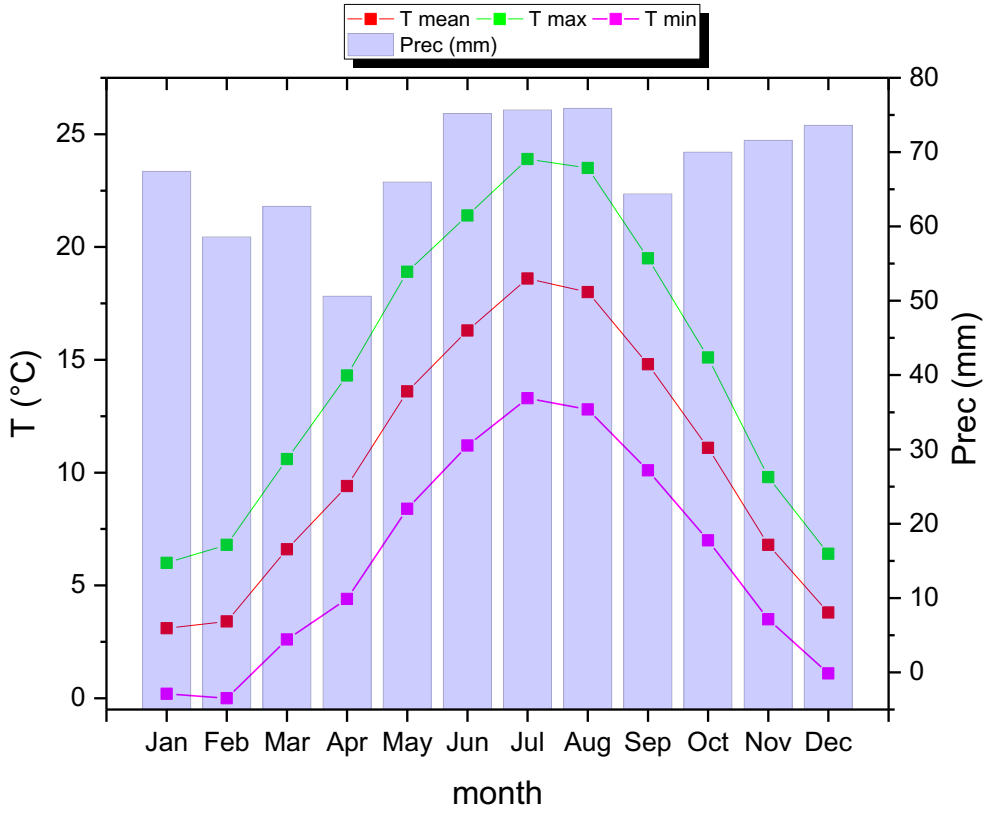

Figure 7. Mean, minimum, maximum temperature (°C) and average rainfall amount (mm) in Hasselt during the reference period 1981-2010. (source: Royal Meteorological Service Belgium).

As observed from Figure 7, precipitations are widely distributed all year round, with maximum precipitations recorded during the summer months. The mean yearly temperature during the 1981-2010 period was 10.5°C, indicating a warm temperate climate as previously anticipated; the few temperature extremes are linked to the mid-latitude westerlies and passage of frontal cyclones (D6.1). On average, February is the coldest month and July is the hottest.

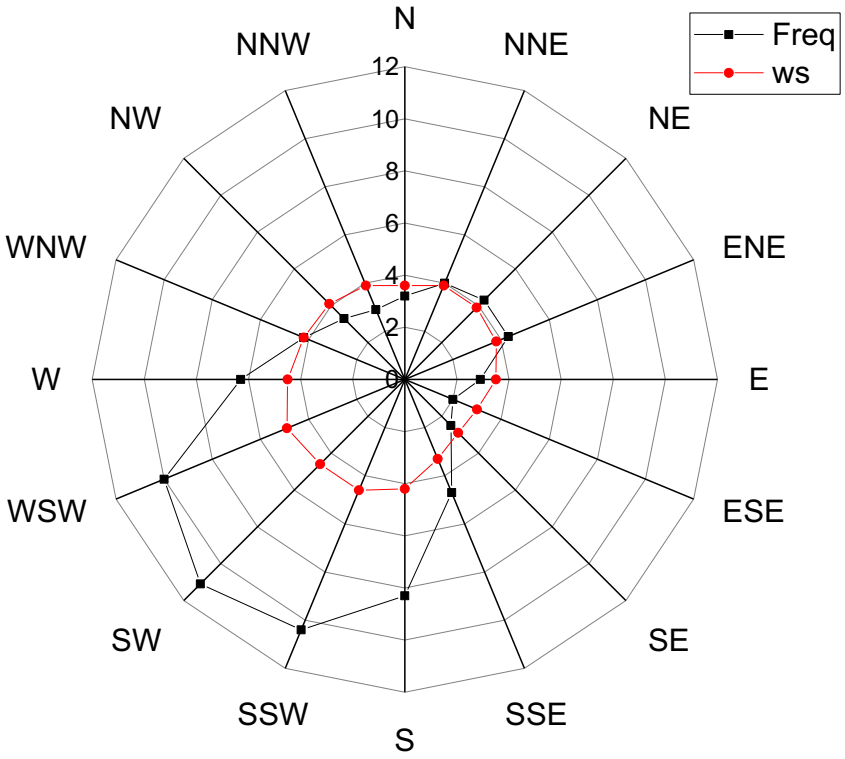

Figure 8. Annual mean wind rose showing mean frequencies (Freq, in percentage, black line) and wind speeds (ws, in m s^{-1}, red line) in Hasselt during the period 1981-2010. Wind data from the synoptic meteorological station in Schaffen (source: Royal Meteorological Institute Belgium).

As from Figure 8, prevailing surface winds are from SW, WSW, SSW and S directions. In general, winds are slow (about 4 m/s on average) from all directions; as reported in D6.1, prevailing wind directions are connected to the topography and the presence of a depression 20 m below the adjacent areas southward of Hasselt, which tends to channel the wind in longitudinal direction. In addition, stagnation conditions and very intense wind speeds are not very frequent in Hasselt.

Following Table 2 provides average wind speeds and the most frequent directions according to each calendar month.

	Jan	Feb	Mar	Apr	May	Jun	Jul	Aug	Sep	Oct	Nov	Dec
Average wind speed (m s^{-1})	4.5	4.2	4.2	3.8	3.5	3.3	3.3	3.2	3.3	3.6	3.8	4.1
Most frequent direction	SSW	SW	SW	S	SW	WSW	SW	SW	SW	SSW	SSW	SSW

Table 2. Monthly average speed and most frequent direction in Hasselt during the period 1981-2010. Wind data from the synoptic meteorological station in Schaffen (source: Royal Meteorological Institute Belgium).

As from Table 2, on average wind speeds are higher during winter months, with January as the windiest month, while in summer and fall winds are generally weaker (about 3 m s^{-1}). Most frequent directions are from SSW, SW during winter and autumn, while summer and spring winds are more variable and including S and WSW provenances.

According to Figure 9 and to the mid-latitude position, solar radiation and insolation duration are maximum during the summer months from May to July (about 150 kW m^{-2} $month^{-1}$ solar radiation and 200 hours insolation per month), while minima are observed during winter and especially in December (less than 20 kW m^{-2} $month^{-1}$ solar radiation and about 50 hours insolation over the month).

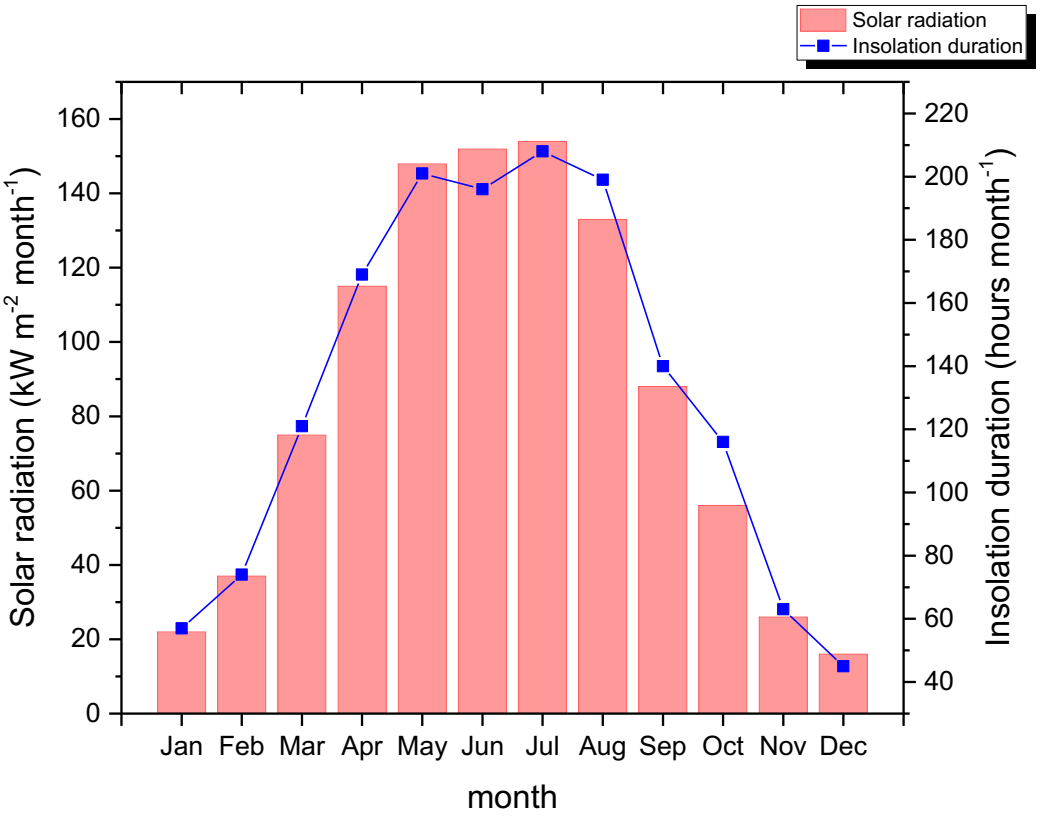

Figure 9. Mean solar radiation (red column) and insolation duration (blue line) for the baseline climatological period 1981-2010 in Hasselt (source: Royal Meteorological Institute Belgium).

3.1.3 Vantaa

Vantaa is a Finnish city and municipality, located in southern Finland in the region of Uusima (Figure 10). It is part of the inner core of the Finnish Capital Region together with Helsinki, Espoo and Kauniainen. With a population of 226,160 inhabitants[9], it is the fourth most populated city in Finland. The city encompasses 240.35km of which 1.97km^2 is water, with an average population density of 948.78/km^2. The city is mostly suburban and urban area with some rural landscape.

[9] "Ennakkoväkiluku kuukausittain sukupuolen mukaan alueittain, elokuu 2018" *(in Finnish). Statistics Finland*. Last accessed 22 Feb 2019.

The river Vantaa (99km) runs through western Vantaa and extends for 27km over Vantaa, while its tributary Keravanjoki runs through eastern Vantaa. The city encompasses two natural lakes and one artificial lake.

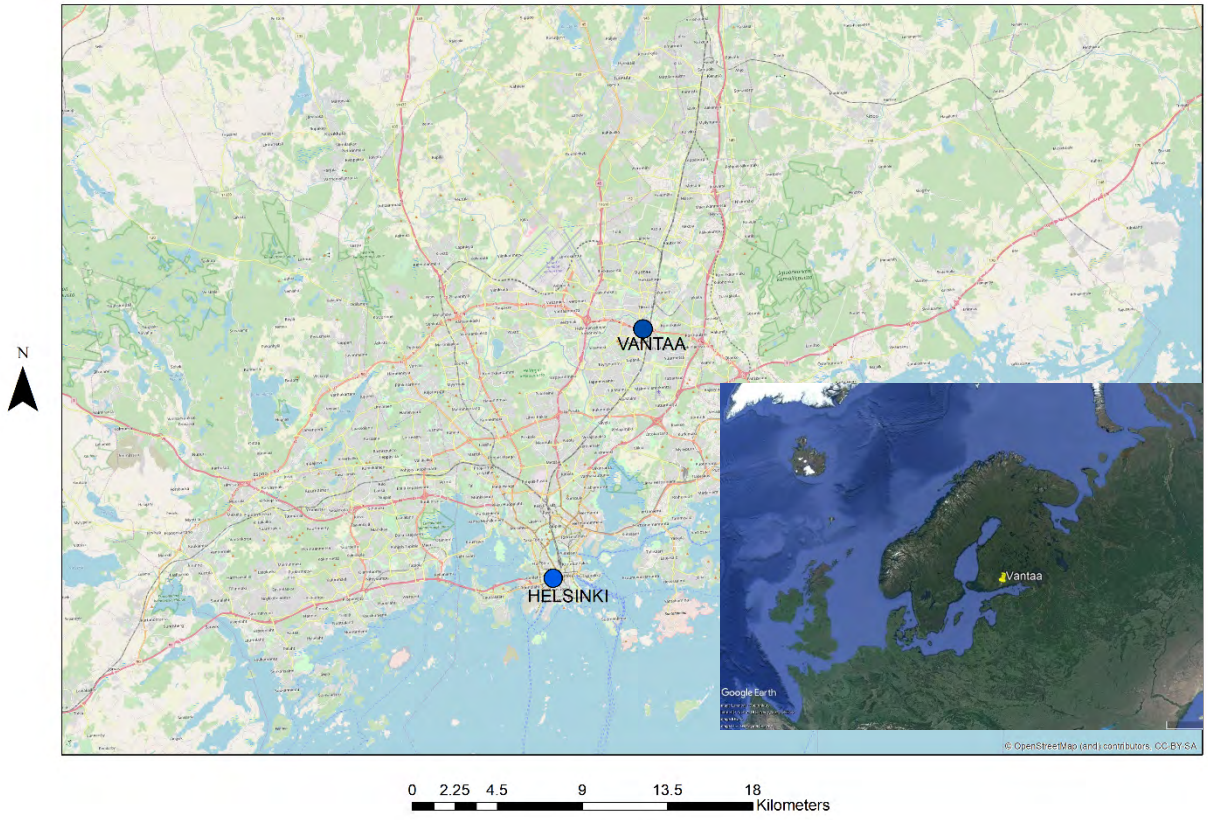

Figure 10. Vantaa and its location in Finland and in the region of Uusima (source: GoogleEarth and OpenStreetMaps).

Vantaa is divided into seven major regions: Tikkurila, Hakunila, Koivukylä, Korso, Aviapolis, Myyrmäki, and Kivistö. These major regions are then divided into a total of 60 major city districts.

The Helsinki airport, the largest airport in Finland, is located in Vantaa. The most common industries in Vantaa include the food, architectural engineering, and machine industries. Companies with their headquarters in Vantaa, at the Helsinki airport, include Finnair, Finavia and Nordic Regional Airlines.

Vantaa infrastructurally serves as the transport hub of the Helsinki metropolitan area. Several key freeways and highways, such as Ring III and Porvoonväylä, originate in or pass through the municipality. Additionally, two of the three railway lines exiting Helsinki pass through Vantaa, connecting the city's 14 stations. All long-distance trains exiting Helsinki stop at Tikkurila railway station in Vantaa, with the exception of train D. Tikkurila station is one of the busiest railway stations in Finland. Most of the trains leaving from Helsinki Central Railway Station go through Tikkurila, including one train connecting Helsinki with St. Petersburg in Russia.

Most of the main roads (Ring Road III, Tuusulanvaylä, Hämeenlinna motorway), run through Vantaa. In particular, four freeways out of Helsinki go to Vantaa and the main east-western road is the third ring road (Kehä III). In Finland, in general, highways radiate from the capital Helsinki or from Turku in the south-western coast of Finland. Out of the seven highways radiating from Helsinki, one highway connects Vantaa with Tampere and Ylöjärvi.

As such, Vantaa contains 162.3km of state-managed roads, 13.4km of railways and 1,264km of municipal roads, with a total length of about 1440km (Vantaan kaupunki, 2012).

Public transport in Vantaa consists of a bus network and commuter rail, provided by HSL/HRT (Helsinki Regional Transport Authority) and VR (a government-owned railway company). Since the introduction of the Ring Rail Line in 2015, Vantaa has had a total of 14 stations. Key railway stations also act as central bus stations. The Ring Rail Line is speeding up the development in Western parts of Vantaa.

Figure 11 shows the main roads of Vantaa together with the location of the airport and of the Tikkurila railway station.

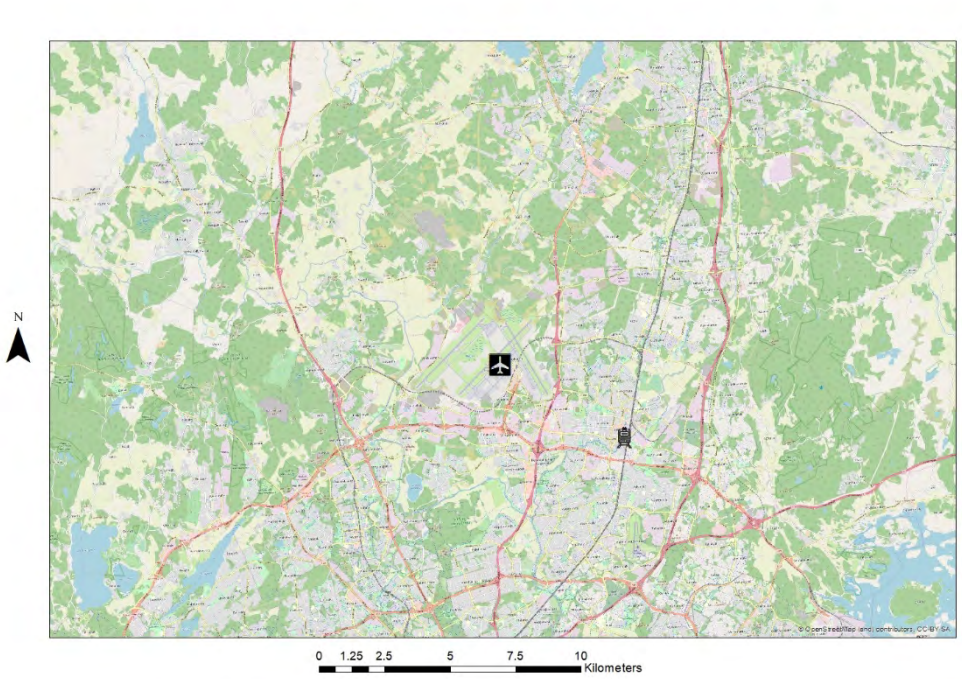

Figure 11: Map of the city of Vantaa with the road network, the airport and the railway (the symbol locates the railway station in Tikkurila). (source: Open Street Maps).

In general, the emissions from aviation are local and small compared to emissions from roads and streets (Karppinen et al., 2000). In the morning and afternoon rush hours traffic can get quite busy and in the winter traffic can be completely blocked because of heavy snowfalls or larger accidents due to the often over-frozen road surface.

In the Helsinki metropolitan area, the most significant air pollutants consist of particles, nitric oxides, ozone, sulphur oxide, carbon monoxide, and volatile organic compounds. The biggest emissions of air pollutants in Vantaa and in the whole Helsinki Metropolitan Area are generated by traffic and energy production, in particular by power plants and fireplaces used in residential areas (City of Vantaa, 2012; Soares et al., 2014; D6.1).

Guideline values for nitric oxide are often overpassed in Vantaa as well as in the rest of Finland during spring, especially along busy roads and streets (City of Vantaa, 2012), even though model simulations (Soares et al., 2014) showed that the $PM_{2.5}$ WHO reference guideline value is not exceeded all over the Helsinki Metropolitan area, whereas a few spots of PM_{10} exceedances are located along major trafficked roads. As such, the city of Vantaa has devised air quality action programs in the past to prevent for the exceedances of the maximum values for nitric oxides and particle contents, consisting of long-term measures related to land-use planning, traffic, street dust, combustion, information and education (City of Vantaa, 2012).

Vantaa has a humid continental climate (Köppen Dfb classification), slightly above the threshold for subarctic classification. Although since 2009 the city has no longer a coastline along the Baltic Sea, its location is close enough to be under the mitigating influence of the sea and the Gulf Stream.

As previously done for Hasselt, also for Vantaa we characterize the climate through the concept of CLINO over the 1981-2010 period. Statistical elaborations for the main meteorological parameters over the period for Vantaa and for other sites in Finland are available through FMI[10]. As reported in D6.1, the weather is typically cold and temperate in Vantaa, with significant amount of rainfall also during the driest months (Figure 12).

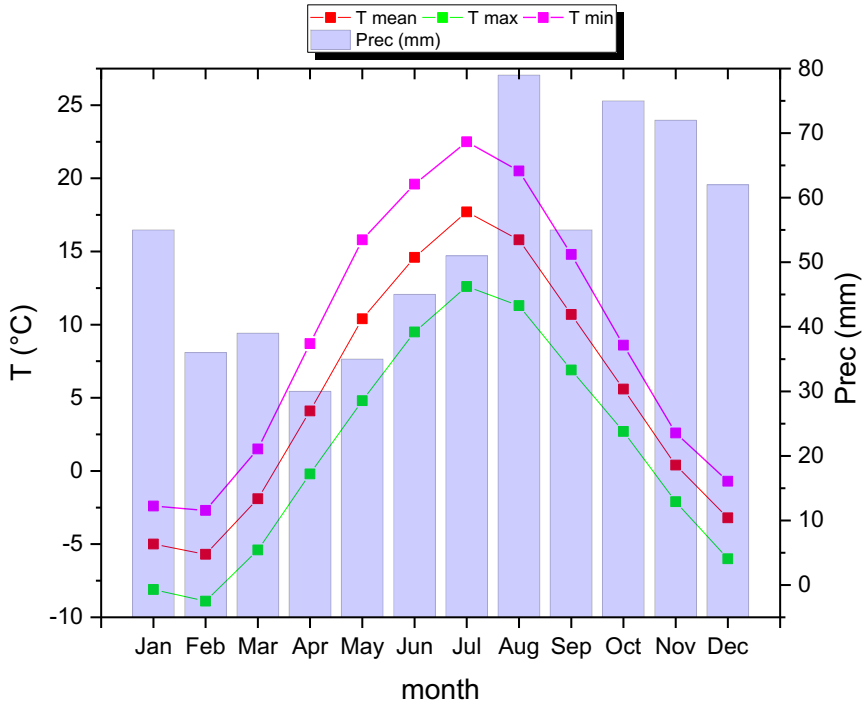

[10] Tilastoja Suomen Ilmastosta 1981-2010

Figure 12. Mean, minimum, maximum temperature (°C) and average rainfall amount (mm) in Vantaa during the reference period 1981-2010. (source: Finnish Meteorological Institute).

The mean yearly temperature during the 1981-2010 period was 5.3°C, indicating a cold temperate climate as previously anticipated. Winters in Vantaa are notably warmer than in other countries at the same latitude (D6.1). On average, February is the coldest month and July is the hottest.

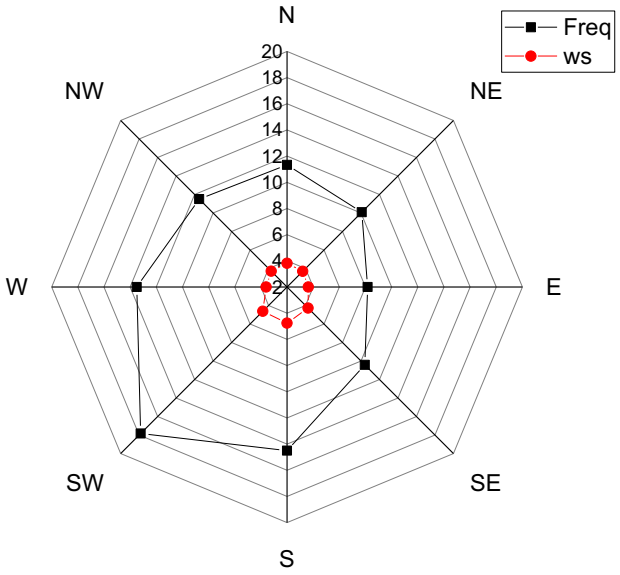

Figure 13. Annual mean wind rose showing mean frequencies (Freq, in percentage, black line) and wind speeds (ws, in m s^{-1}, red line) in Vantaa during the period 1981-2010. Wind data from the synoptic meteorological station in Helsinki Vantaa (source: Finnish Meteorological Institute).

Wind direction distribution is quite homogeneous all over the cardinal rose, with a slight prevalence of SW direction (Figure 13**Error! Reference source not found.**), accounting for winds flowing along the coast or coming from the western part of the Baltic Sea which provide the main contribution to the ventilation of the Helsinki Metropolitan Area (D6.1). Secondary wind components account for westerly winds coming from inland, sea breezes, easterly along-coast winds and southward inland flows. Wind speeds are generally included between 2 m s^{-1} and 10m s^{-1} in every sector, accounting prevalently in the range 2-7 m s^{-1}. Higher values of speed occur only for wind coming from the western sector, with maximum velocities arriving from south-west and south-south-west. The intensity of all the components of the rose is an efficient mechanism to air pollutants cleaning and recirculation and provides an important mitigation effect, appreciable not only on the coast, but also in the inland. In fact, Finland, being part of the Scandinavia's peninsula, is warmed by the so called north Atlantic Drift, an airflow following the northern path of the Gulf Stream, which itself bring warm water into the Baltic Sea. So, thanks to wind and sea influence, Finland experiences less rigid winter than countries at the same latitude (D.)

Following Table 3 provides average wind speeds and the most frequent directions according to each calendar month.

	Jan	Feb	Mar	Apr	May	Jun	Jul	Aug	Sep	Oct	Nov	Dec
Average wind speed (m s^{-1})	4.4	4.1	4.0	3.9	3.9	3.8	3.6	3.5	3.7	4.1	4.3	4.4
Most frequent direction	SW	SW	SW	SW	SW	SW	SW	SW	SW	SW	SW	SW

Table 3. Monthly average speed and most frequent direction in Vantaa during the period 1981-2010. Wind data from the synoptic meteorological station in Helsinki Vantaa (source: Finnish Meteorological Institute).

On average wind speeds are in the 2-5 m s^{-1} with slightly higher values during winter months, with January and December as the windiest months, while in summer winds are generally weaker (. Most frequent directions are from SW all year-long.

Because of the latitude, days last less than 6 hours around the winter solstice with very low Sun (at noon Sun is little bit over 6 degrees in the sky), and the cloudy weather at this time of year accentuates the darkness (). Conversely, Vantaa enjoys long daylight in summer; during the summer solstice days last slightly less than 19 hours (Tukiainen, 2011).

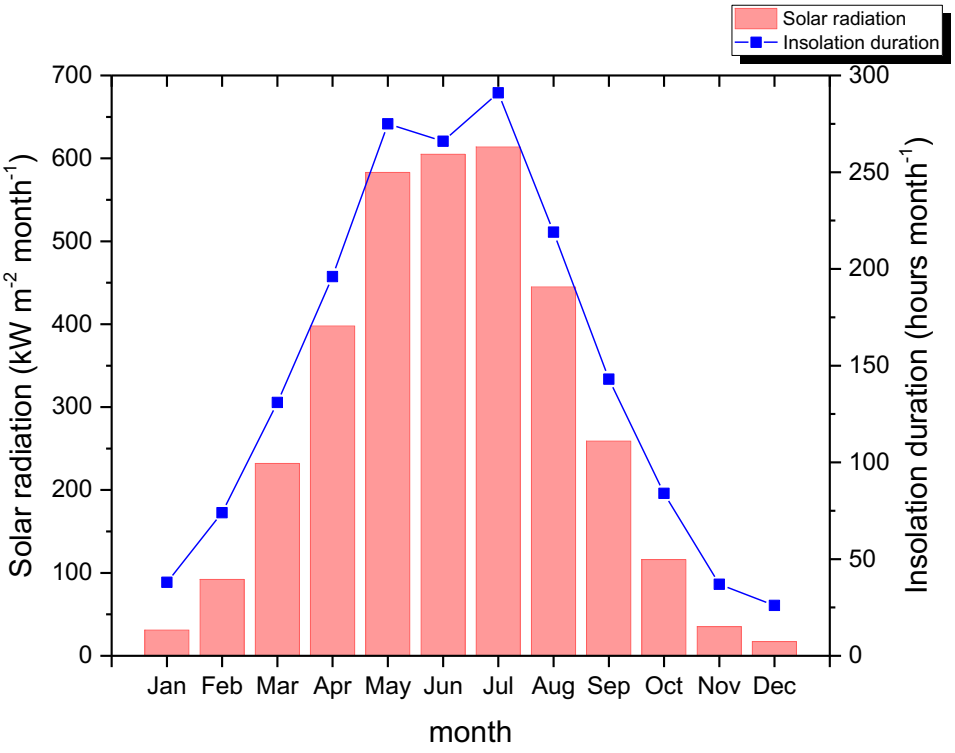

Figure 14. Mean solar radiation (red column) and insolation duration (blue line) for the baseline climatological period 1981-2010 in Vantaa (source: Finnish Meteorological Institute).

Air quality and meteorological measurements

3.1.4 Bologna

The regional air quality monitoring network of Emilia Romagna region (ARPA-ER, now ARPAE) consists of 47 monitoring stations, with a total of 171 automatic analyzers for the main pollutants: particulate Matter (in form of PM_{10} and $PM_{2.5}$), nitrogen oxides (NO_x, NO_2 and NO), carbon monoxide (CO), benzene (C_6H_6), sulfur dioxide (SO_2), and ozone (O_3). The network is completed by other sensors of micro-pollutants, as well as by 10 mobile laboratories and numerous mobile units for the implementation of evaluation campaigns. Out of the 47 stations belonging to the regional network, 4 are located in the agglomeration of Bologna, 18 are located in the West Plain area, 20 in the Eastern Plain area, while the remaining 5 are located in the Apennines area.

Among the automatic air quality monitoring stations located in the agglomeration of Bologna, 3 are located within its urban agglomeration: Table 4 provides information on the position (Figure 2), the type of station and the pollutants measured at the three air quality stations.

Station	Type	Lat	Lon	NO_x	NO_2	CO	O_3	PM_{10}	$PM_{2.5}$
Porta San Felice (SF)	Traffic	44.5000	11.3285	Hourly data	Hourly data	Hourly data		Daily data	Daily data
Via Chiarini (Ch)	Suburban background	44.5001	11.2861	Hourly data	Hourly data		Hourly data	Daily data	
Giardini Margherita (GM)	Urban background	44.4836	11.3550		Hourly data		Hourly data	Daily data	Daily data

Table 4. Information on reference monitoring stations in Bologna: type, location (latitude and longitude), measured pollutants with associated time resolution. The empty cell corresponding to one pollutant that it is not measured at that station or data is not available.

In addition, data collected during two intensive field campaigns in Bologna (one summer campaign in August-September 2017, one winter campaign in January-February 2018, thoroughly described in '*Report on footprint of PCSs*'[11] (D3.3) and D5.2) were used in the analysis and in the evaluation of the simulations. In fact, as described in those reports, during the two summer and winter experimental campaigns, two ARPA-ER mobile laboratories for the measurement of atmospheric pollutants (NO_x, CO, SO_2, O_3, PM_{10} and $PM_{2.5}$) were located in addition to other instrumentation for the measurement of meteorological and turbulence variables along two parallel street canyons in the city of Bologna, namely Marconi St. and Laura Bassi Veratti St.

The IdroMeteoClima Service of ARPAE Emilia-Romagna (Arpae-Simc) carries out operational observational and forecasting activities, supporting planning and research and development, in meteorology, climatology, hydrology, agro-meteorology, radar-meteorology and environmental

[11] Report on footprint of passive control systems

meteorology (https://www.arpae.it/sim/). The network includes almost a thousand sensors of various types located in over three hundred regional survey sites. The instruments are connected in real time and feed different databases[12].

Below, a brief analysis comparing meteorological and air quality data for the year 2017 and the statistical elaboration on 10 years basis (summarized in section 3.1.1 and described in detail in D6.1), is presented and discussed.

During 2017, the wind direction and wind speed pattern is the same as the one observed during the decade previously considered (Figure 15).

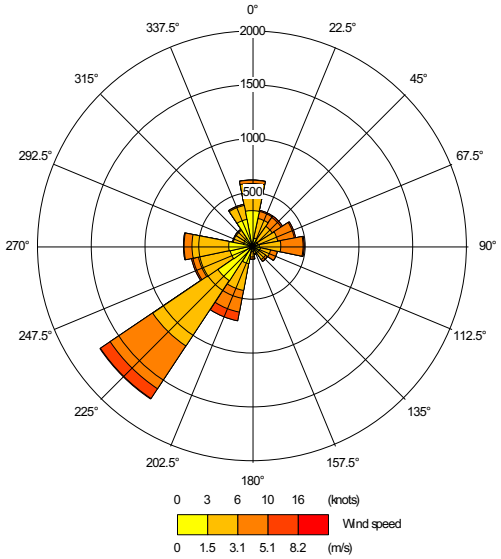

Figure 15. Wind rose showing occurrences of hourly average wind direction and speed for the city of Bologna in 2017, as recorded at the Bologna Urbana meteorological station.

During 2017, the time series of air temperature shows the same annual period oscillation (Figure 16) with the differences in temperature between city and countryside less marked than in the decade previously considered. Specifically, the maximum difference is about 2°C and occurs in January, March, July and December (Figure 17).

[12] Data are stored in a computerized archive and can be consulted in various ways on the website (https://www.arpae.it/dettaglio_generale.asp?id=2897&idlivello=1625). For instance, observational meteorological network data are available for free through the Dexter system (https://simc.arpae.it/dext3r).

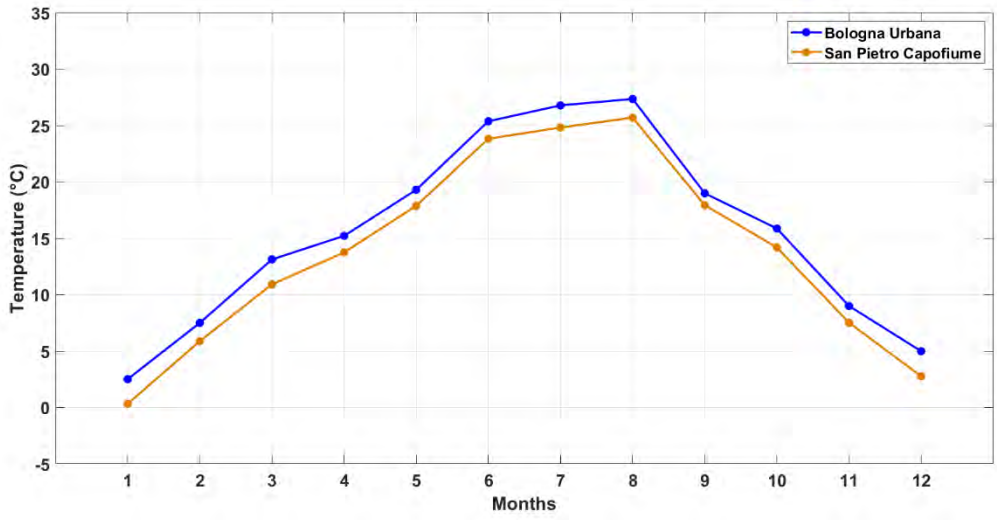

Figure 16. Monthly air temperature for 2017 at Bologna Urbana (blue line) and San Pietro in Capofiume (red line) monitoring stations.

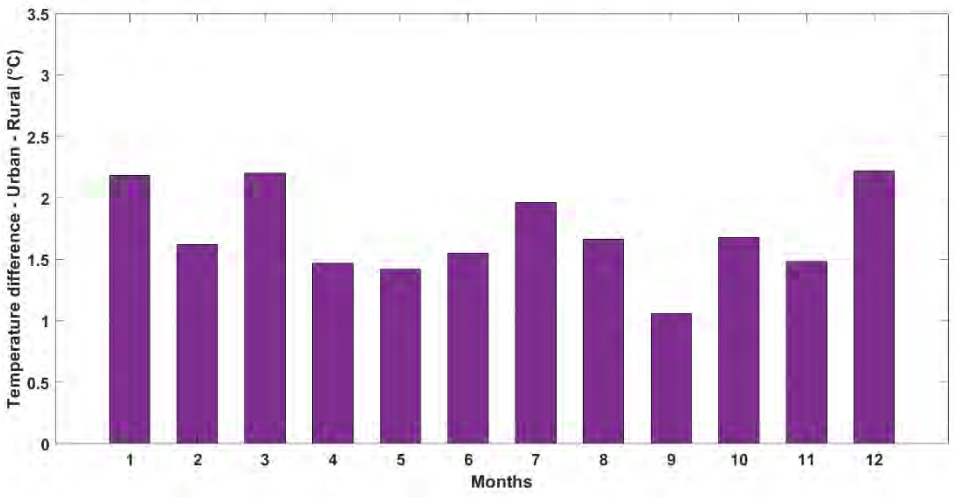

Figure 17. Differences in temperature between city (Bologna Urbana) and countryside (San Pietro in Capofiume).

As for precipitation, the monthly trend observed in the ten years (2006-2016) does not match that of year 2017 (Figure 18), where the precipitation data in the city are similar to the values measured in the countryside. In 2017, the annual average values are respectively 575.4 kg m^{-2} and 560.4 kg m^{-2}, showing a marked decrease in rainfall in the city.

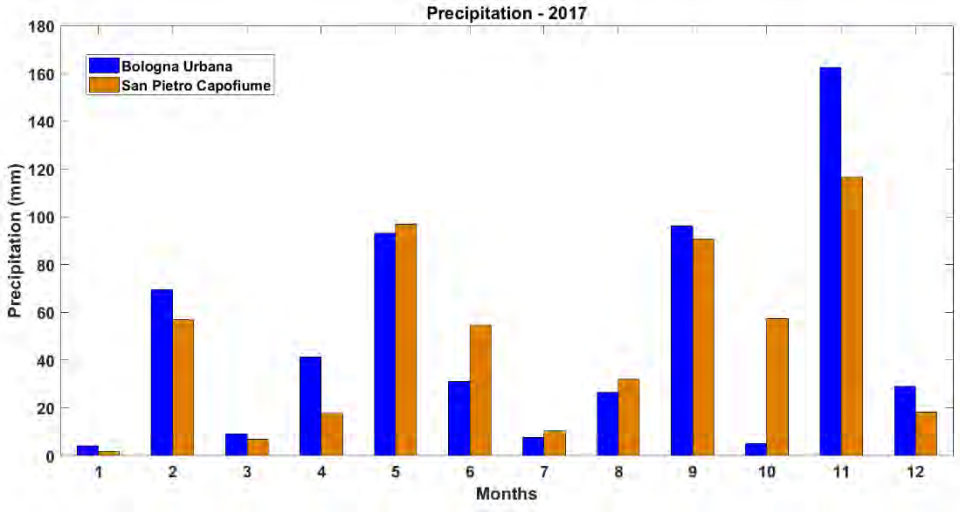

Figure 18. Monthly average precipitation for 2017 at Bologna Urbana (blue) and San Pietro in Capofiume (red) monitoring stations

Finally, 2017 was a very peculiar year in Emilia-Romagna from the hydro, weather and climate point of view. The most significant phenomenon was the prolonged drought in the region, which began in October 2016 and ended only in September 2017 with the highest temperatures recorded since June. The annual regional average temperature in 2017 was 19.0°C, the highest since 1961; while the annual regional average of rainy days (with rainfall> 1 mm) in 2017 was 92 days, the lowest since 1961 (ARPAE, 2018). In the year 2017 there were numerous relevant events:

- intense late frosts (April);
- thunderstorms with very strong winds;
- hailstorm;
- flooding during the summer;
- hot record in the first week of August (with maximum temperatures even above 40°C);
- snowfall in November.

This information contributes to describe broadly the type of meteorological year considered as current (baseline case) for the city of Bologna.

3.1.5 Hasselt

In the past and until 31st December 2016, the Flanders Environment Agency had an air quality urban traffic measuring station in Hasselt (Boksbeemdenstraat), providing hourly average concentrations for NO, NO_2, SO_2, O_3, PM_{10} and $PM_{2.5}$. Due to infrastructure works in this location, VMM was forced to stop the measurements at the end 2016.

As such, in order to setup and validate the dispersion modeling simulations for the present scenario that will be described in the following, we chose the latest available year for which air quality data from VMM were available for the city of Hasselt, i.e. 2016. In particular, the following table reports the main methodology and instrumentation adopted in the measurements of air quality pollutants.

Parameter	Measurement unit	Measurement instrument	Measurement principle	Measurement uncertainty
NO	$\mu g/m^3$	TS 42i	chemiluminescence	-
NO_2	$\mu g/m^3$	TS 42i	chemiluminescence	12 % of hourly mean up to 200 $\mu g/m^3$; 12 % of daily mean up to 40 $\mu g/m^3$
O_3	$\mu g/m^3$	API T400	UV-photometry	11 % of hourly mean up to 240 $\mu g/m^3$; 10 % of 8-hour mean up to 120 $\mu g/m^3$
SO_2	$\mu g/m^3$	TS 43i	UV-fluorescence	12 % of hourly mean up to 350 $\mu g/m^3$; 12 % of daily mean up to 125 $\mu g/m^3$
PM_{10}	$\mu g/m^3$	FIDAS200	optical particle counter + conversion to mass concentration	12 % of daily mean up to 50 $\mu g/m^3$
$PM_{2,5}$	$\mu g/m^3$	FIDAS200	optical particle counter + conversion to mass concentration	13 % of daily mean up to 30 $\mu g/m^3$

Table 5. Measurement instruments and details of measurements of air quality pollutants in the air quality measurement station of Hasselt (VMM).

The following Table provides information and metadata for the available hourly 2016 meteorological parameters.

Parameter	Measurement unit	Meteorological station	Number of observations
Air temperature	°C	Diepenbek	8785
Wind speed	m/s	Diepenbek	8785
Wind direction	°	Diepenbek	8778
Rainfall amount	mm	Diepenbek	8785
Global solar radiation	Wh/m^2	Diepenbek	8784
Insolation duration	min and 10^{th}	Diepenbek	8785
Cloud cover	oktas	Bierset	8779

Table 6. Parameters, measurement units and meteorological stations available for 2016 year in Hasselt (source: Royal Meteorological Institute Belgium).

With respect to the baseline climatological period 1981-2010, mean monthly temperatures (Figure 19) were only slightly higher. Precipitation amounts in 2016 were similar but slightly higher than the

observed baseline climatology, with the exception of the summer months and especially June and July 2016, recording very intense precipitation amounts (103 and 232 mm month^{-1}, respectively).

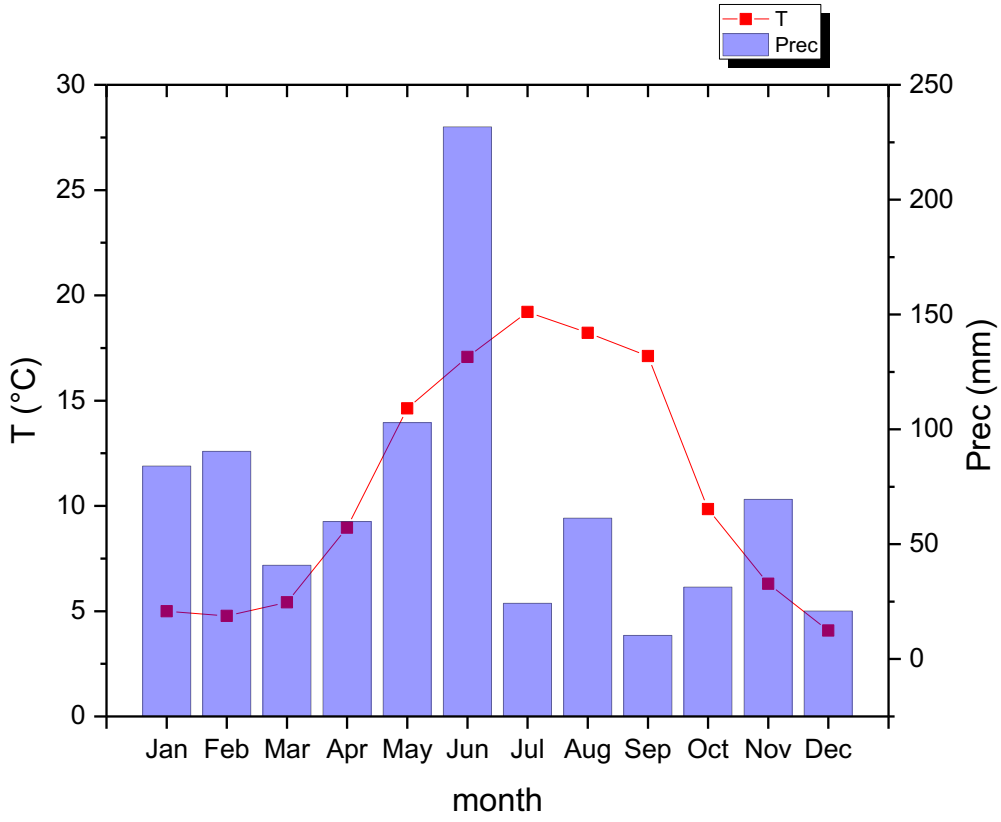

Figure 19. Mean monthly and accumulated precipitation over the 2016 year in Hasselt (source: Royal Meteorological Institute Belgium).

Wind rose for the 2016 period (Figure 20) shows prevailing wind directions from SW and SSW similar to the baseline climatology and due to the effect of topography. However, WSW and S directions appear slightly reduced in 2016, while WNW direction appears more frequent. In addition, in 2016 wind speeds were mostly in the 2-6 m s^{-1} range, with rare calm very intense wind conditions.

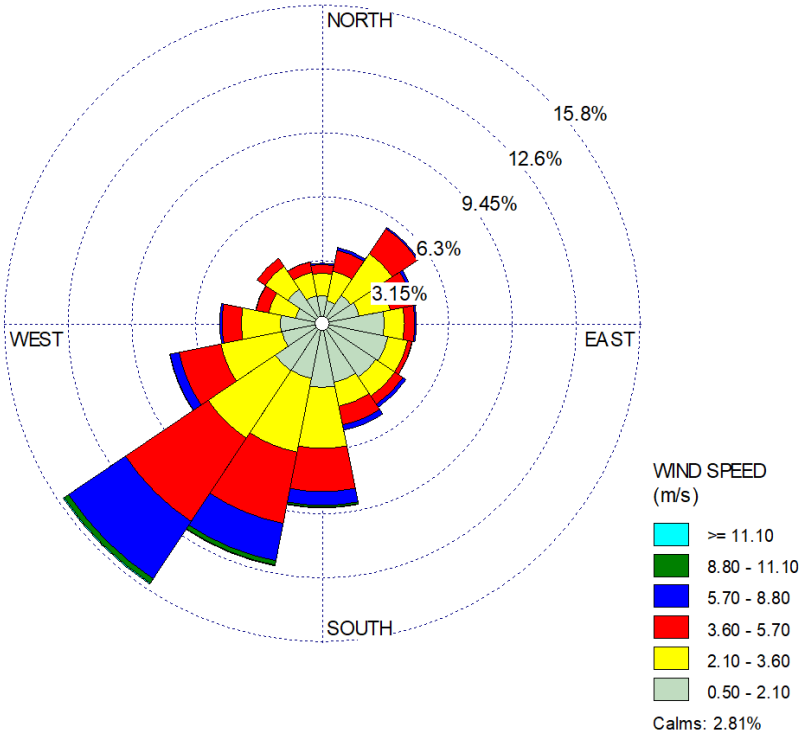

Figure 20. Wind rose for 2016 meteorological data in Hasselt (Source: Royal Meteorological Institute Belgium).

However, comparing the monthly mean wind speed and most frequent direction in 2016 with that observed over the climatological baseline (1980-2010), it appears that average monthly wind speeds were slightly lower in 2016 and prevailing wind directions were different especially concerning May and October, which shows a prevailing wind direction from WNW not observed in the baseline climatology.

	Jan	Feb	Mar	Apr	May	Jun	Jul	Aug	Sep	Oct	Nov	Dec
Average wind speed (m s^{-1})	3.8	4.2	3.3	3.1	2.7	2.4	2.6	2.5	1.9	2.3	3.1	2.2
Most frequent direction	SSW	SW	SW	SW	WNW	SSW	SW	SW	SW	WNW	SW	SW

Table 7. Monthly average speed and most frequent direction in Vantaa during 2016 year. (source: Royal Meteorological Institute Belgium).

3.1.6 Vantaa

Air quality in Vantaa and in Helsinki Metropolitan Area has long been measured by HSY (Waste Management's Seututieto) by means of continuous and indicative measurements, models and bioindicators. HSY monitors air quality in the metropolitan area with continuous measurements and

mobile measuring stations monitoring hourly concentrations for the most important air pollutants, such as particles, nitric oxides, ozone, sulphur dioxide, carbon monoxide, and benzene.

HSY monitors air quality at 11 monitoring stations in the Helsinki Metropolitan Area, out of which one is located in the busy district centre of Tikkurila in Vantaa. A regional background centre is instead situated in Luuki, Eespo, to the west of Vantaa.

In 2017, two additional mobile air quality stations, measuring hourly concentrations of carbon monoxide, nitrogen dioxide, ozone, PM_{10} and $PM_{2.5}$, were located in Vantaa, in Rekola and in the Helsinki airport.

Figure 21 provides the location of the HSY permanent and mobile air quality stations in Vantaa for 2017.

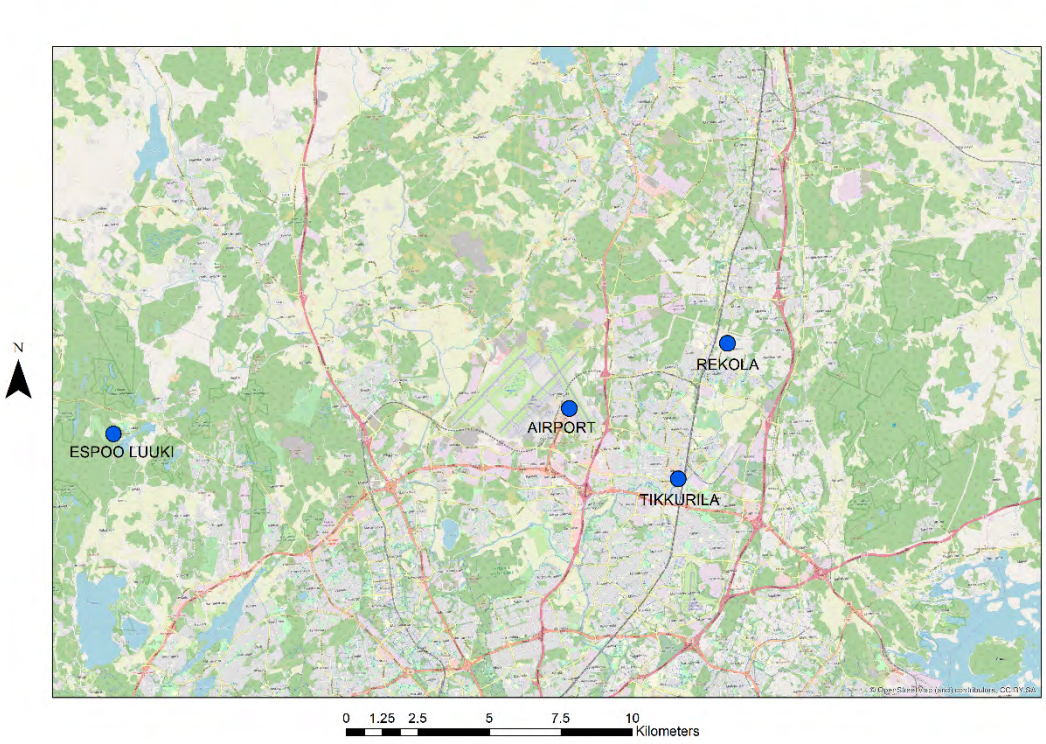

Figure 21. Map of permanent and mobile air quality stations in Vantaa (2017).

Meteorological and air quality observations for measuring sites in Finland are available free of charge through an online service from FMI[13].

The following Table provides information and metadata for the available hourly 2017 meteorological parameters from the Helsinki airport synoptic meteorological station.

[13] https://ilmatieteenlaitos.fi/avoin-data

Parameter	Measurement unit	Meteorological station	Number of observations
Air temperature	°C	Helsinki-Vantaa airport	8761
Wind speed	m/s	Helsinki-Vantaa airport	8759
Wind direction	°	Helsinki-Vantaa airport	8759
Rainfall amount	mm/h	Helsinki-Vantaa airport	8757
Global solar radiation	W/m^2	Helsinki-Vantaa airport	8761
Cloud cover	oktas	Helsinki-Vantaa airport	8761

Table 8. Parameters, measurement units and meteorological stations available for 2017 year in Vantaa (source: Finnish Meteorological Institute).

With respect to the baseline climatological period 1981-2010, 2017 mean monthly temperatures in Vantaa (Figure 22) were very similar. Precipitation amounts in 2017 were higher than during the observed baseline climatology especially during the fall period (150 mm month-1 over October 2017 compared to the average 75 mm month^{-1} of 1981-2010).

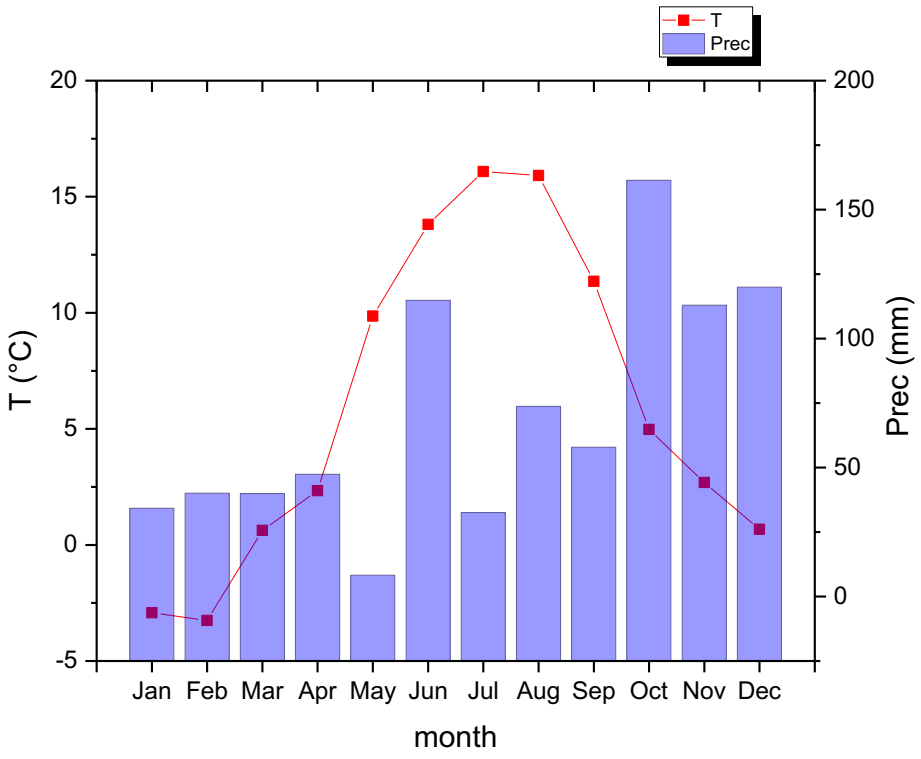

Figure 22. Mean monthly and accumulated precipitation over the 2017 year in Vantaa (source: Finnish Meteorological Institute).

Wind rose for the 2017 period (Figure 20) shows winds distributed all over the cardinal points, with prevailing wind directions from SW and SSW similar to the baseline but with slightly lower frequencies of the easterly directions. Wind speeds were mostly in the 2-11 m s^{-1} range, with rare calm wind conditions (0.18%), a situation which is also similar to the baseline climatology (D6.1).

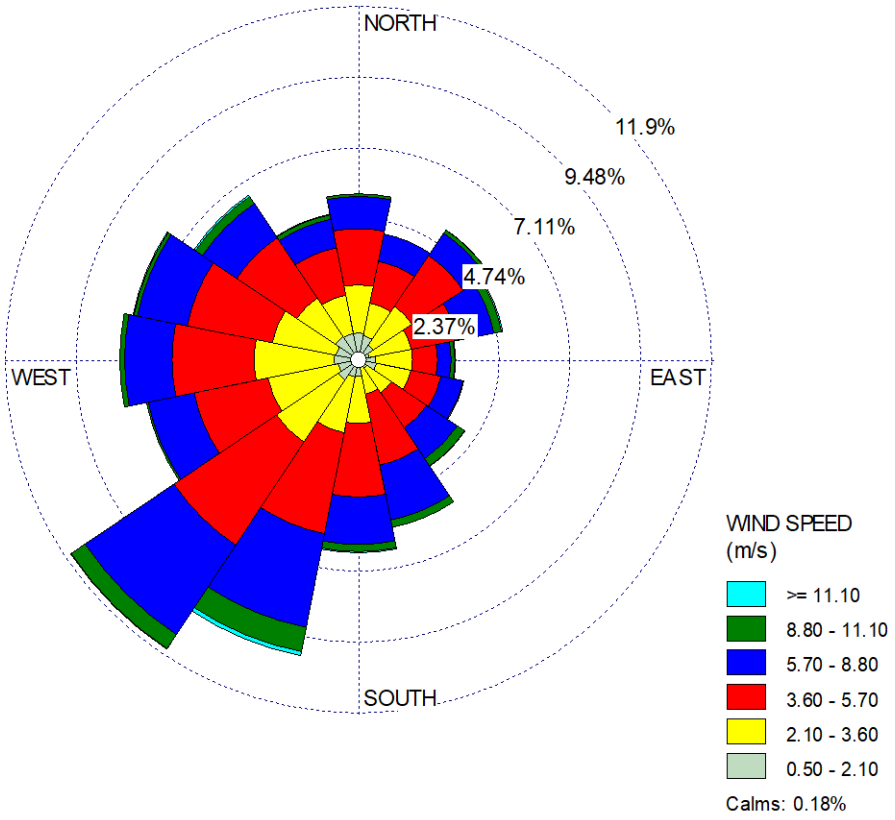

Figure 23. Wind rose for 2017 meteorological data in Vantaa (Source: Finnish Meteorological Institute).

Comparing the monthly mean wind speed and most frequent direction in 2017 (Table 9) with that observed over the climatological baseline (1980-2010), it appears that average 2017 monthly wind speeds were higher and prevailing wind directions were different with the appearance of prevailing wind directions other than the SW generally observed in the baseline reference period.

	Jan	Feb	Mar	Apr	May	Jun	Jul	Aug	Sep	Oct	Nov	Dec
Average wind speed (m s^{-1})	5.0	4.1	5.1	4.6	4.1	4.6	3.9	4.2	4.0	4.6	4.7	5.1
Most frequent direction	SW	W	SW	SW	W	W	NW	SW	E	N	S	S

Table 9. Monthly average speed and most frequent direction in Vantaa during 2017 year. (source: Finnish Meteorological Institute).

3.2 Development of the emission inventory

Air emission inventory is a structured collection of information about emissions and technological, economical and territorial data. In general, to develop such an inventory it is necessary to quantify all emissions of the different sources in the appointed area of the inventory during the selected time frame.

The compilation and build-up of the emission inventory was built through the EMIT tool available from CERC (CERC, 2015), which has the potential to calculate emissions across large urban areas for dispersion modeling with the ADMS-Urban model.

EMIT is a database tool for storing, manipulating and assessing emissions data from several sources (major roads, rail and industrial sources, minor road, commercial and domestic sources). EMIT allows to store emissions data that have been directly imported, or to calculate emissions from source activity data using emission factors. Alternately, EMIT can calculate emissions using a scaling of national or regional emissions by a local statistic such as population, as will be described later on.

The EMIT tool was also developed to estimate the consequences of traffic management schemes such as Clean Air Zones and Local Emission Zones with regards to emissions. In fact, EMIT allows to consider the effect on emissions of the following aspects, stand-alone or in combination:

- Projected changes in traffic flows due to national trends;
- Projected changes in national fleet composition through the introduction of cleaner technology in the course of time;
- Changes in local fleet composition, traffic flows, and speeds due to local interventions.

The following figure provides a scheme to better comprehend the steps taken in this study to build up the emission inventory to be used for air dispersion modelling.

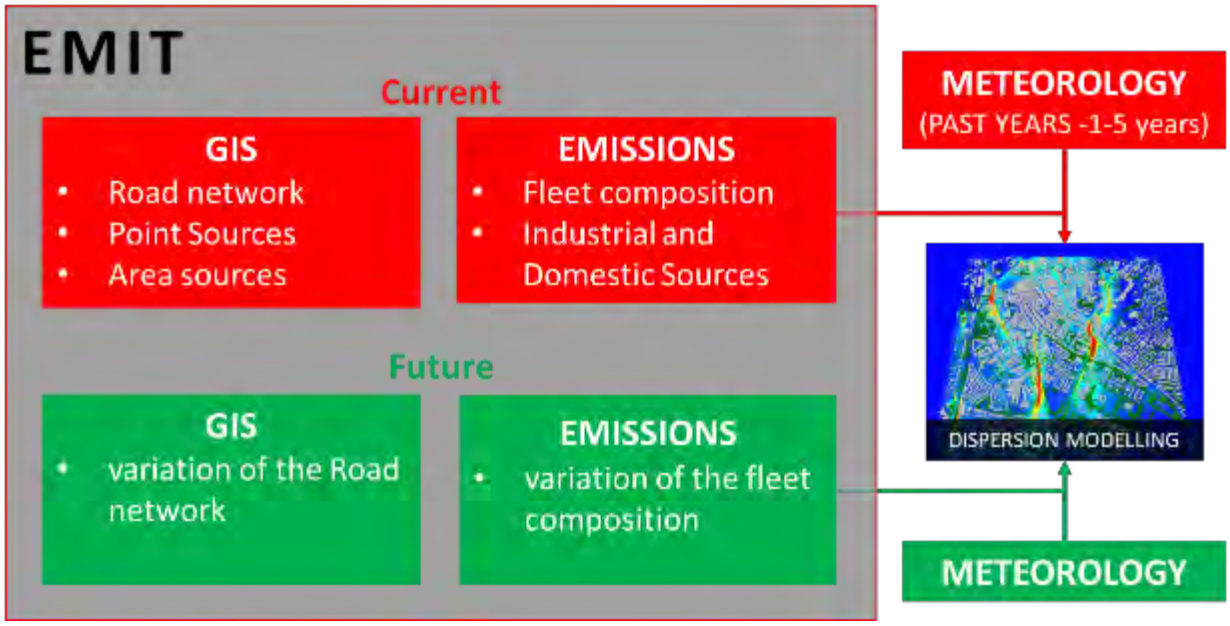

Figure 24. Schematic representation of the construction of the emission inventory with the EMIT software for its use in the ADMS-Urban dispersion model.

In the case of road traffic, emission factors estimate the rate at which a vehicle emits pollutants while its engine is running. These emissions depend on many parameters, such as the engine size, engine technology (legislative standard in the year of manufacturing of the vehicle), fuel type (petrol, diesel), age of the engine and standard of maintenance, total weight, speed, recent history of activity (cold starts, hot soaks).

In general, to develop an emission inventory for road sources, it is necessary to know traffic counts on a link-by-link basis or at least to have fuel consumption data.

EMIT calculates the emissions of local pollutants starting from traffic flows in the roads, considering the emission factors, the fleet components and the route type. The emission factors are a set of data obtained from experimental results that relate emission rates for different pollutants to vehicle sub-categories. There are several different sets of emission factors available for road and rail traffic sources in the EMIT database, with the number of vehicle sub-categories ranging from 2 to 124. For each of these vehicle sub-categories there is a set of pollutant emission rates in g/vehicle/km. They vary with speed, and with year. EMIT calculates the emissions using its own database containing UK emission factors. Comparing Italian and English fleet composition (fuel type and technology), it was estimated that the fleet for UK are quite likely the Italian one. In the case of Bologna, emission factor data are derived from NAEI 2014 datasets. In this dataset the emission factor data are taken from the COPERT 4 model version 10.0 (Katsis et al., 2012) compiled as part of the UK National Atmospheric Emissions Inventory (UK NAEI 2014). NAEI 2014 datasets include factors for:

- The regulated pollutants: NO_x, VOC, CO and CO_2; PM_{10}; $PM_{2.5}$; NO_2; SO_2.
- The unregulated pollutants: Benzene; 1,3 Butadiene; Methane; N_2O; Benzo[a]Pyrene; Ammonia.

Emission factors of PM_{10}, $PM_{2.5}$, NOx, NO_2 and VOC (volatile organic compounds) have been released in June 2014, as part of the UK National Atmospheric Emissions Inventory (UK NAEI 2014) and include the effect of mileage and new fuels. In addition, CERC (CERC, 2015) suggests to use this dataset among the available ones to investigate the emission-reduction scenarios, as they include a number of vehicle subcategories that represent new vehicle technologies.

Emission factors must take into account non-exhaust emissions, i.e. road traffic particulate emissions emitted due to mechanical abrasion and corrosion, and the re-suspension of material deposited on the road surface by tyre shear, vehicle-induced turbulence and wind. These emissions are very important because while the improvements in vehicle technologies are constantly decreasing the exhaust emissions, non-exhaust emissions are not controlled and increase with the increase in traffic volumes. A recent research (Soret et al., 2014) suggests that the electrification of the fleet though having potential for NO_x and CO abatement, has limited impact on PM_{10} reductions because of the high contribution of non-exhaust that is not reduced by fleet electrification. Here, non-exhaust emission factors derived using the Tier 2 methodology in the 2009 EMEP/EEA emission inventory guidebook (EMEP, 2009) were considered.

The fleet components are a classification of traffic according to a relatively small number of broad categories used to describe the traffic composition. This classification is likely to be similar to that output from a traffic model or from traffic count observations. For road traffic, EMIT supports either standard fleet components with 3 categories (heavy traffic/light traffic/motorcycles) as well as the 11 components

categorization (cars, taxis, large good vehicles, rigid heavy goods vehicles, articulated heavy good vehicles, buses, coaches, mopeds, motorcycles 2 strokes, motorcycles 4 strokes). The route type describes the relative composition of each fleet component, in terms of the percentage of that component in each vehicle sub-category. Route types can be year-dependent. EMIT calculates the emission rate (the mass flux of a particular pollutant from a specified source, g/s or kg/year) for all sources and allows to directly create the input files for ADMS-Urban.

In the case of road traffic, source specific data needed are as follows:

- Annual Average Daily Traffic count (AADT), i.e. the sum of the number of vehicles/day for each fleet component, which might be obtained by current (baseline) observations or from a traffic model.
- Fleet components, the breakdown of the AADT into the different fleet components, e.g. heavy vehicles, light vehicles and motorcycles, again available from traffic count data or from traffic simulations. EMIT supports 3 or 11 fleet components for road traffic.
- Length of road, as the emission factors are defined per unit length of road.
- Drive cycle, as driving behavior in 'urban', 'rural', and 'motorway' environment leads to differing rates of engine deterioration and thus of emissions.

The breakdown of the total traffic into the fleet components into the vehicle sub-categories used by the emission factors is specified through the route type, which is a bridge between the emission factors (vehicle subcategories) and the source AADT data (fleet components).

The emissions from residential heating sources instead are modelled as area sources, because it is difficult to obtain specific emission data for each household. In general, there are two ways to assign an emission rate to each grid cell:

1) calculate emissions for sources using activity data and fuel consumption, together with emission factors;

2) scaling groups of sources using a known statistic (e.g., population, licensed vehicles, number of sites, …). In this case, the emission for each source can be calculated applying the following simple relation:

$$E = \frac{STAT_{local}}{STAT_{country}} * E_{country}$$

For the specific case of residential heating, the statistic can be for example the number of local inhabitants and the total inhabitants of the country, for which emissions data are known.

3.2.1 Bologna

The study area includes all sources of urban pollutants, meteorological stations and the air quality monitoring network, over a domain of 12 x 19 km. A number of cartography data used was downloaded from the geo-portale of the Emilia Romagna Region (http://geoportale.regione.emilia-romagna.it/it), while road network and buildings data were provided by the municipality of Bologna. The emission sources, which can be modeled in EMIT and ADMS-Urban, can be road (major and minor roads), industrial (punctual, aeriform, volumetric and linear), domestic (like domestic heating). In the case of Bologna, the most important sources of emissions are traffic and domestic heating.

Traffic

For road emission sources, the municipality of Bologna has provided traffic flows divided into light, heavy vehicles and buses, in a geo-referenced format and displayed as roads. The road sources of Bologna correspond to the roads shown in the graph. Each road of the graph consists of several arcs, that is, road segments in which the traffic flow was counted. Given the presence of a large number of links (about 9000) that make up the graph, the road network of Bologna has been divided into major and minor roads. Major road is a source type, providing emissions from traffic on a road that is represented explicitly as a line source. Minor road is a source type, providing emissions from traffic on small roads these are not represented explicitly but their emissions are combined (aggregated) over one or more grid squares. In order to split the whole graph into major and minor roads, it has been assumed that all the arches inside the internal ring road are major roads, while the arches outside the ring road are considered major roads in case the traffic flow was more than 500 vehicles. The remaining arches are treated as minor roads. The main roads are extrapolated from the spatial analysis carried out in the geographic information system (GIS) using QGis Desktop 3.2.3 with Grass 7.4.1 (*QGIS Project, 2017)*. The final number of major roads considered in the emission inventory turns out to be 1593 (Figure 25).

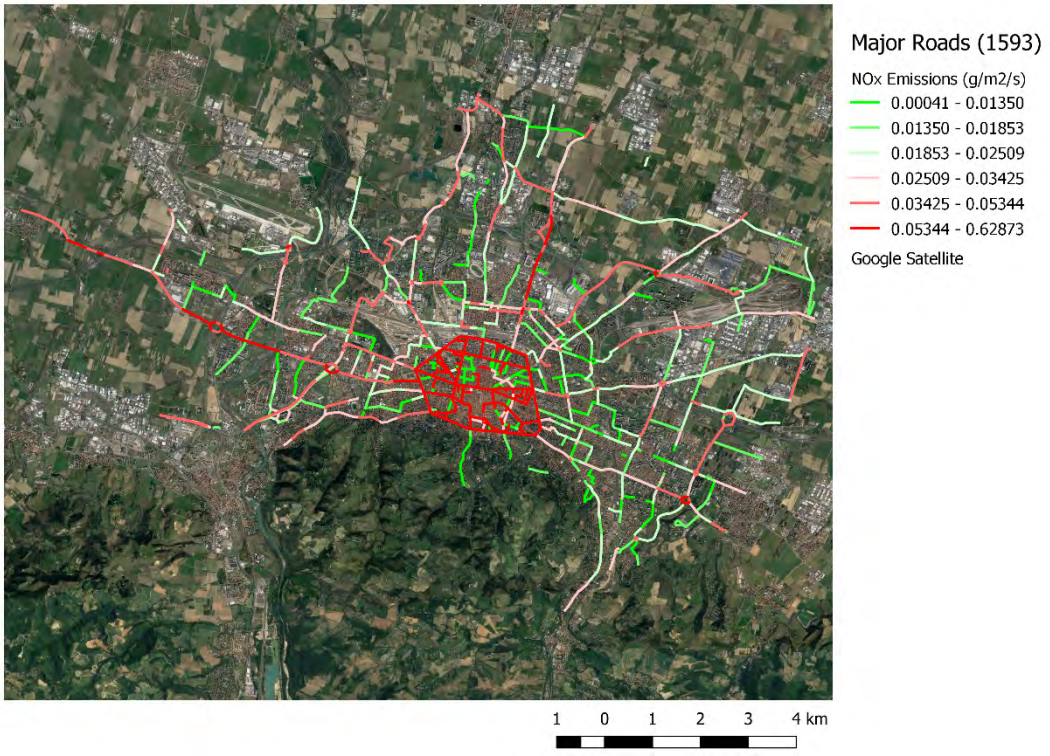

Figure 25. Map of NO_x emissions from road sources ("Major Roads") in Bologna, Google satellite base map provided by QGis.

The roads outside the ring road, with a traffic flow less than 500 vehicles, have been considered as minor roads, i.e. small roads which are not represented explicitly but whose emissions are combined (aggregated) over one or more grid squares (as opposed to a major road source which is modelled as

a line source). This typology of source is modelled as an area: from the shapefile[14] of roads, the lines are converted in square areas of 1000x1000 meters, so that the road sources become grid sources. EMIT calculates the emission rates using its own database for minor roads in the same way as for major roads. The count of vehicles in the roads falling within each grid cell is used to calculate the emissions and create the input files for ADMS-Urban.

Domestic

As stated above, the emissions from residential heating sources were modelled as grid sources, because it is very difficult to obtain the emission data of each household. The emissions due to domestic heating can be approximated, within the EMIT database, by scaling national emissions using a local statistic (such as population). The population at the municipal level is spread over the territory based on the resident population spread over cells of 1 km (Figure 26).

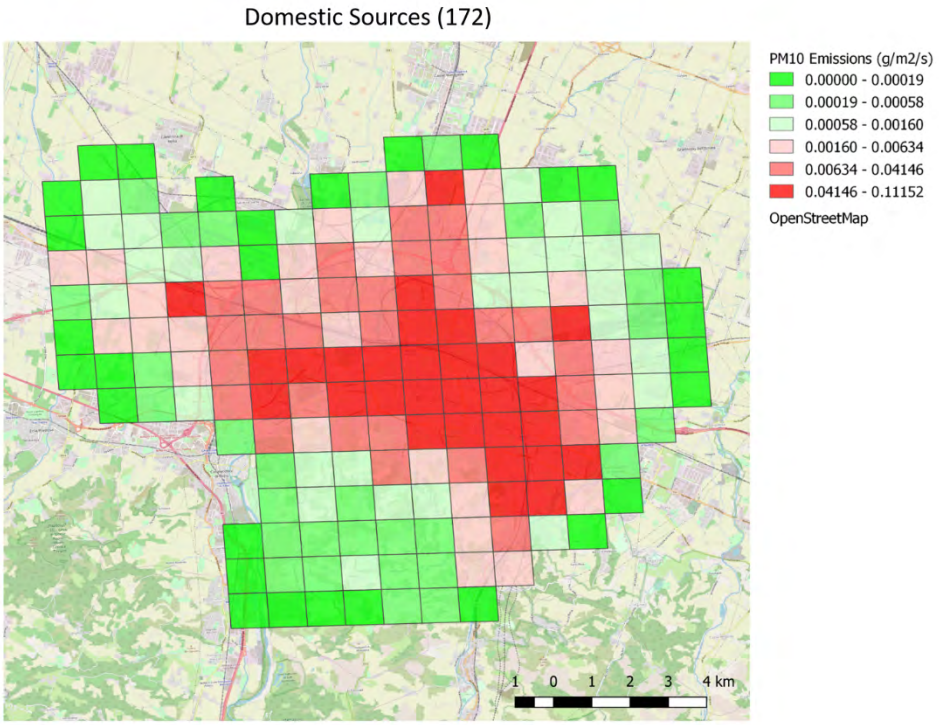

Figure 26. Map of PM_{10} emissions from "Domestic" sources in Bologna.

3.2.2 Hasselt

As previously mentioned no major industrial sources are present in Hasselt. The construction of the emission inventory needs therefore to take into account emissions of air pollutants deriving from the two

[14] The shapefile is a vector data storage format developed by Esri which stores the location, shape, and attribute of geographic features as a set of related files

major emission sources, i.e. road traffic and residential heating. The study area covers a domain of 27x31km.

D4.2 and following upcoming deliverables '*Behavioral simulations design aspects report*' (D4.3) and '*Prototype of a fully integrated behavioural (data-driven) simulator*'[15] (D4.4) present and discuss a comprehensive methodology for simulating mobility patterns of individuals, type of data used, calibration and also traffic patterns effects in relation to tested policy scenarios. In order to provide a context, here we provide a synthesis of traffic simulations used for estimating emission and resulting pollution concentrations.

In the case of Hasselt, FEATHERS (an Activity-based demand model) is used to predict the activity-travel schedules of individuals residing in whole Flanders regions of Belgium. The FEATHERS model requires a synthetic population of a region, which is generated using iterative proportion updating algorithm in relation with satisfying socio-economic characteristics such as the distribution of gender, income, education status, the presence of children in the household and vehicle ownership for all spatial units. FEATHERS uses this population along with land use and network level of service data, such as travel time and cost for different modes of transport, to predict the activity-travel schedule. The various sub-models within FEATHERS are based on the decision tree approach and are trained with a personalized travel survey data (OVG data) of the region. The prediction from FEATHERS provides a complete plan for an individual containing information on activities, their location, duration, activity start times along with a related trip between the activity locations with an indication of chosen transport mode. The FEATHERS outputs are then integrated with MATSIM, an open-based mobility microsimulation platform, to predict the traffic flow on the network. MATSIM requires an initial activity-travel schedule of individuals, and then simulate those plans in a co-evolutionary algorithm to equilibrate traffic on the given road network. Apart from schedules, other datasets required by MATSIM are taken from open source platforms such as road network from Open Street maps, while public transport supply data are available as general transit feed specification (GTFS) data. An algorithm developed within IMOB (Transportation Research Institute, Hasselt University) has been utilised to match the bus stop locations on the Open Street maps and also to prepare the data into the format required by MATSIM. Various parameters of MATSIM simulation platform are adjusted so that the output matches with the base traffic counts available at various traffic count locations at major arterial roads. The reason to simulate the entire Flanders region is to obtain decent results in terms of traffic, as not only Hasselt citizens but also the population in the surrounding regions use the traffic network of Hasselt for reaching their activity locations. Based on some previously available estimates, freight traffic is also loaded on the network, so that the base case calibration provides more than satisfactory results. In fact, we obtain a root mean square error of 0.23, which is considered reasonable. Furthermore, the outputs provide shares of transport modes that are replicating the shares mentioned in OVG data. More details about the results are available in D4.4. In order to limit the efforts to Hasselt city, a reduced form of a road network is used for further processes such as emission estimation and dispersion modelling. The road network contains 7627 links and includes all important roads such as the inner ring and outer ring along with minor roads as well.

The output from traffic simulations, containing information on traffic volumes for each vehicle fleet component (light, heavy, and buses) for each road link for both directions, was matched with OpenStreet Map to derive road width, speed limit and road category (living street, residential, motorway, motorway-

[15] Reports will be available on the iSCAPE reports webpage

link, primary, primary-link, secondary, secondary-link, trunk, trunk-link, tertiary, tertiary-link, service, unclassified) for each link through GIS modeling. The information on speed limit was used to estimate the average speed on each road link, while the information on road category was used to estimate average traffic counts for each road type. It was then calculated that the average highest traffic volumes were associated with the motorway, motorway-link, primary, primary-link, secondary, secondary-link, trunk, and trunk-link categories, which were then considered as major roads, i.e. explicitly modelled sources with detailed time-varying profiles. The other road categories were instead considered as minor roads i.e. diffuse sources with simpler time variation and defined for a given area, instead of road length, and using annual vehicle kilometres (AVK) as the basic unit of traffic flow. Road length was instead derived directly through GIS modelling.

In order to assign pollutant emissions to each road link, it is necessary to assign emission factors to each vehicle category. In this case, emission factors used to calculate emission rates for major and minor roads are based on UK NAEI 2014, which includes emissions data from the COPERT 4 version 10 software tool (Katsis et al., 2012). In particular, since in the case of Hasselt we considered a domain centred over the city, urban road type emission factors, available from 2008 until 2030 were considered.

As stated above, the use of the NAEI emission factors requires the number of light vehicles, heavy vehicles, and motorcycles for each road link; in this case, while the volume of heavy vehicles was estimated as the sum of buses and heavy vehicles obtained as output of traffic simulations, the share of motorcycles over the number of light vehicles output of traffic simulations was estimated from the average in Belgium available from FEBIAC (Fédération Belge et luxembourgeoise de l'Automobile et du Cycle) (FEBIAC, 2018).

However, the comparison of the fleet composition for NAEI 2014 (http://naei.beis.gov.uk/data/ef-transport) with that of Belgium (FEBIAC, 2018) suggested to consider the emission factors of the year previous the one to be modelled for Hasselt.

Besides traffic counts for the different source categories during the rush hour, traffic simulations also estimated the diurnal (weekday, Saturday and Sunday) and monthly variation of road sources.

The following Figures represent NO_x and PM_{10} emissions for the 850 road sources (major roads) considered in Hasselt.

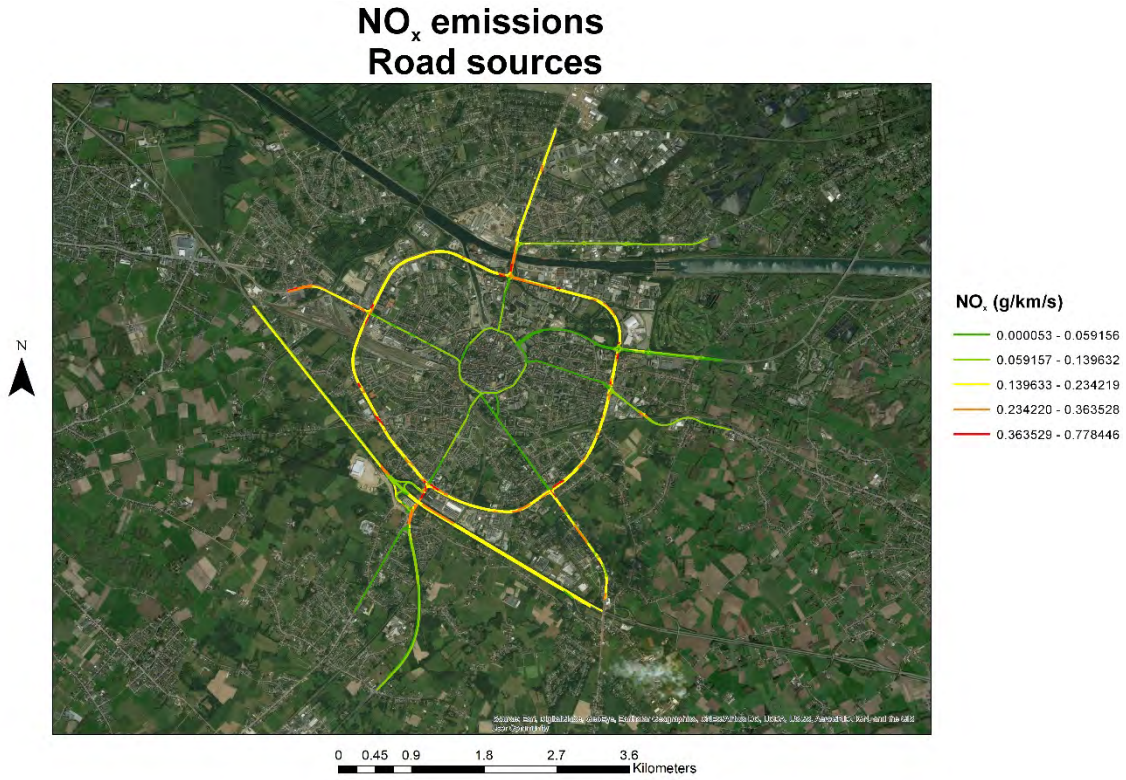

Figure 27. NO_x emissions (in g/km/s) for road sources considered as major roads in Hasselt in the base case (present) scenario.

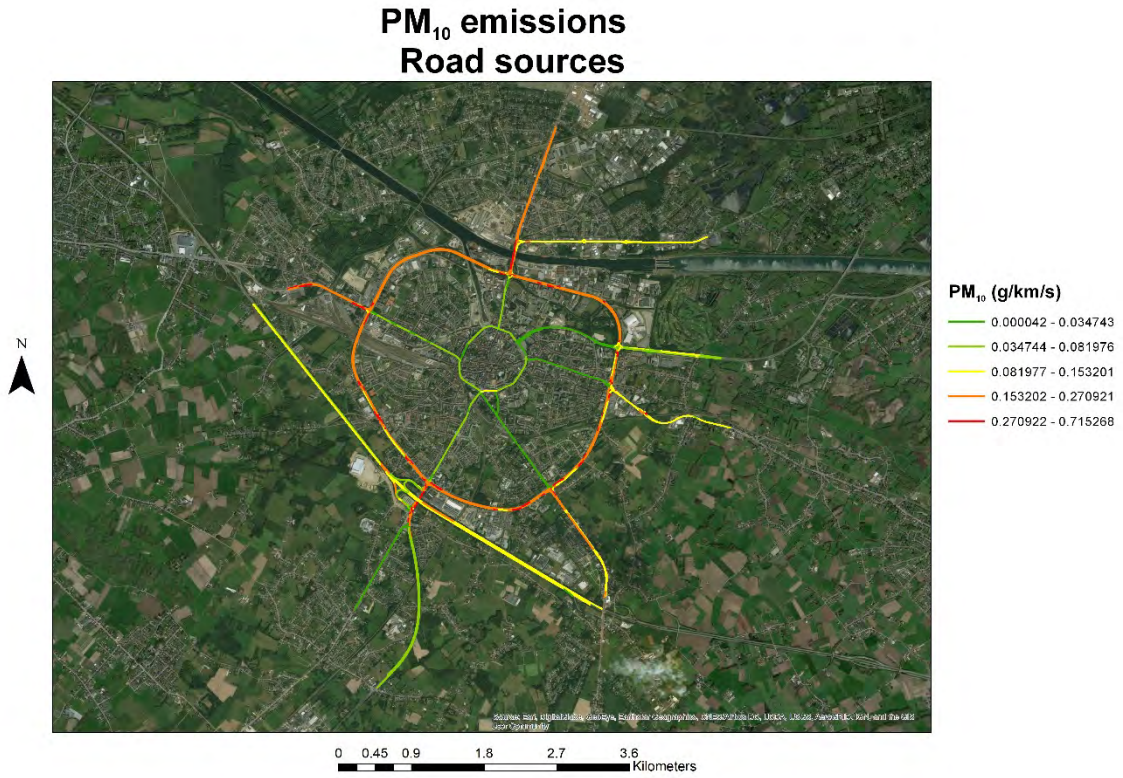

Figure 28. PM_{10} emissions (in g/km/s) for road sources considered as major roads in Hasselt in the base case (present) scenario.

Both Figures show that the major emissions of air quality pollutants derive from the outer ring and the motorways, whereas inside the outer ring and in the inner ring emissions are relatively lower.

In the case of Hasselt, information on emissions for the whole city was derived from VMM (https://www.vmm.be/lucht/luchtverontreiniging/huishoudens/huishoudens), while population data in the city and in the surroundings was obtained from https://www.citypopulation.de/php/belgium-limburg.php

Monthly and diurnal variation of residential heating sources were estimated considering the normal operating hours and operating periods (Mid-October to March) of residential heating sources in households in Limburg from the 3E consulting company (http://www.3e.eu/).

The following Figure represents NO_x emissions from residential heating in Hasselt and its surroundings.

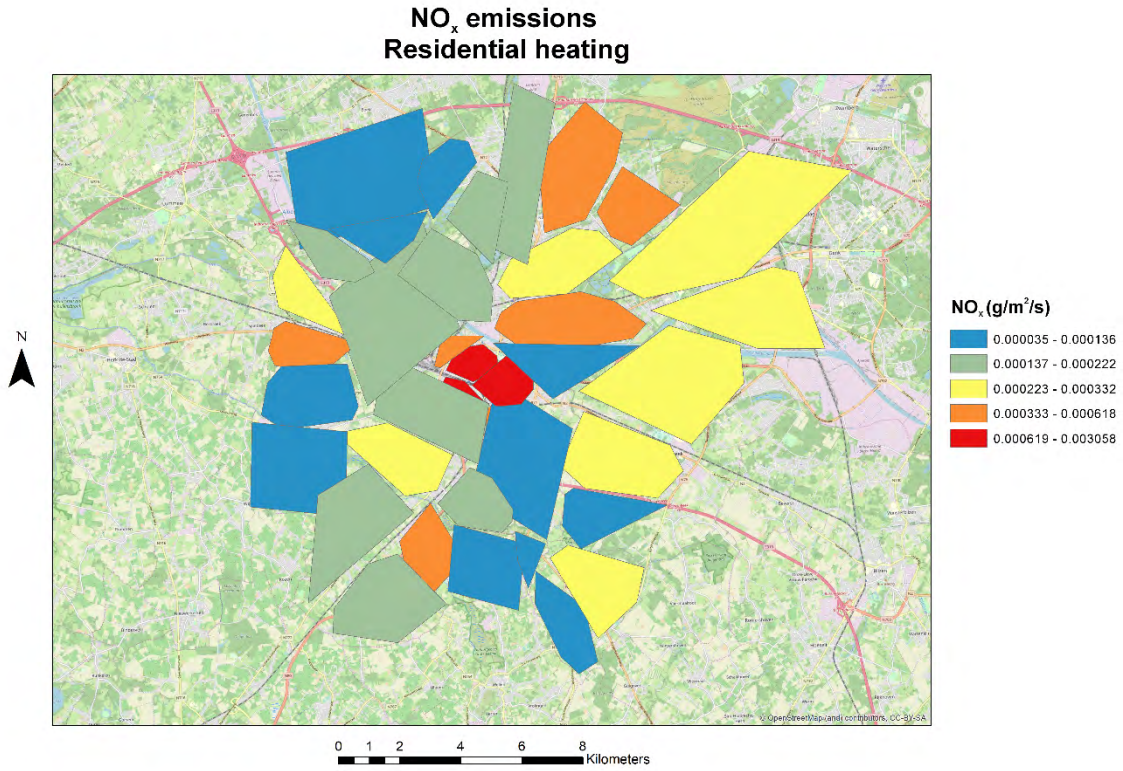

Figure 29. NO_x emissions ($g/m^2/s$) from residential heating in Hasselt in the base case (present) scenario.

Similar to what previously observed for road emissions, higher emissions are in the Hasselt city centre (more populated), while in the Hasselt outskirts and in surrounding areas emissions are generally more reduced.

3.2.3 Vantaa

As previously mentioned, the major emission sources of air pollution in Vantaa are road traffic and residential heating, although industrial sources, aviation, and small-scale combustion represents smaller contributions (Soares et al., 2014). The emission inventory developed for Vantaa takes into account the two major emission sources, road traffic and residential heating, with a study area covering a domain of 34x18km.

D4.2 and following upcoming D4.3 and D4.4 present and discuss the approach adopted to determine traffic volumes on each road link from a light activity-based model in the absence of detailed activity-travel diary for the iSCAPE cities other than Hasselt. The Deliverables present and discuss all the methodologies and the approach for simulating mobility patterns of individuals, type of data used, calibration and also traffic patterns effects in relation to tested policy scenarios. As done for Hasselt, here we provide a synthesis of traffic simulations used for estimating emission and resulting pollution concentrations.

In the case of Vantaa, a light activity-based model based on certain rules for estimating schedules for the population was used. The model requires a synthetic population of a region, which is generated

using census and other population statistics and socio-economic information. The model uses this population along with land use and network level of service data, available from recent research studies and from open-source platforms, to predict the activity-travel schedule, which is calibrated comparing with measurements of network travel times. The schedules obtained for Flanders with the FEATHERS are used as schedules for Vantaa with some adjustments to consider the peculiarities of this city. The schedules are then finalized with some checks considering for instance the length of bicycle and walk trips and on the activity duration of the last activity.

As done for Hasselt, the output from the light activity-based model contains information on traffic volumes for light vehicles, heavy vehicles for each road link for both directions was matched with OpenStreet Map to derive road width, speed limit and road category (living street, residential, motorway, motorway-link, primary, primary-link, secondary, secondary-link, trunk, trunk-link, tertiary, tertiary-link, service, unclassified) for each link through GIS modeling. The information on speed limit was used to estimate the average speed on each road link.

Given the presence of a large number of links (about 43000) that make up the graph, the road network of Vantaa has been divided into major and minor roads. The split between major and minor roads was carried out considering as major all road links with traffic counts larger than 400 and longer than 100 m. The remaining arches are treated as minor roads. The final number of major roads considered in the emission inventory for Vantaa turns out to be 3000.

Similar to what done for Hasselt, we considered urban NAEI 2014 emission factors for each vehicle road category. The share of motorcycles over the number of light vehicles provided as output from traffic simulations was estimated from the average in Finland available from Statistics Finland[16].

The comparison of the fleet composition for NAEI 2014 with that of Belgium suggested to consider the emission factors of the same year to be modelled for Vantaa.

Besides traffic counts for the different source categories during the rush hour, traffic simulations also estimated the diurnal (weekday, Saturday and Sunday) and monthly variation of road sources.

The following Figures represent estimated NO_x and $PM_{2.5}$ emissions for the 3000 road sources (major roads) considered in Vantaa.

[16] http://tilastokeskus.fi/til/mkan/index_en.html

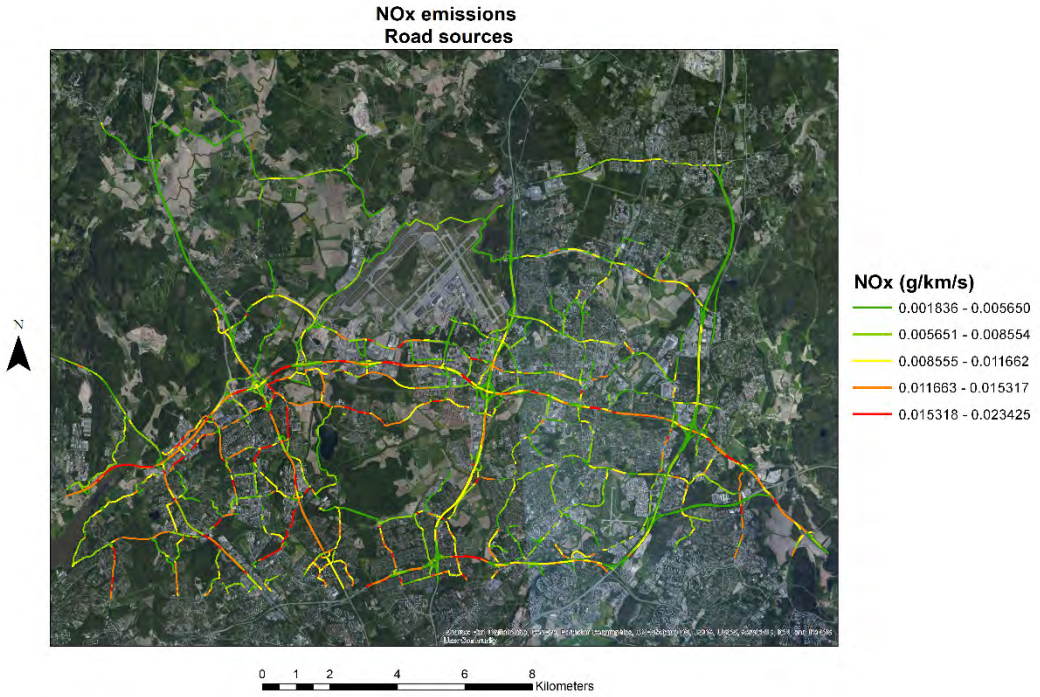

Figure 30. NO_x emissions (in g/km/s) for road sources considered as major roads in Vantaa in the base case (present) scenario.

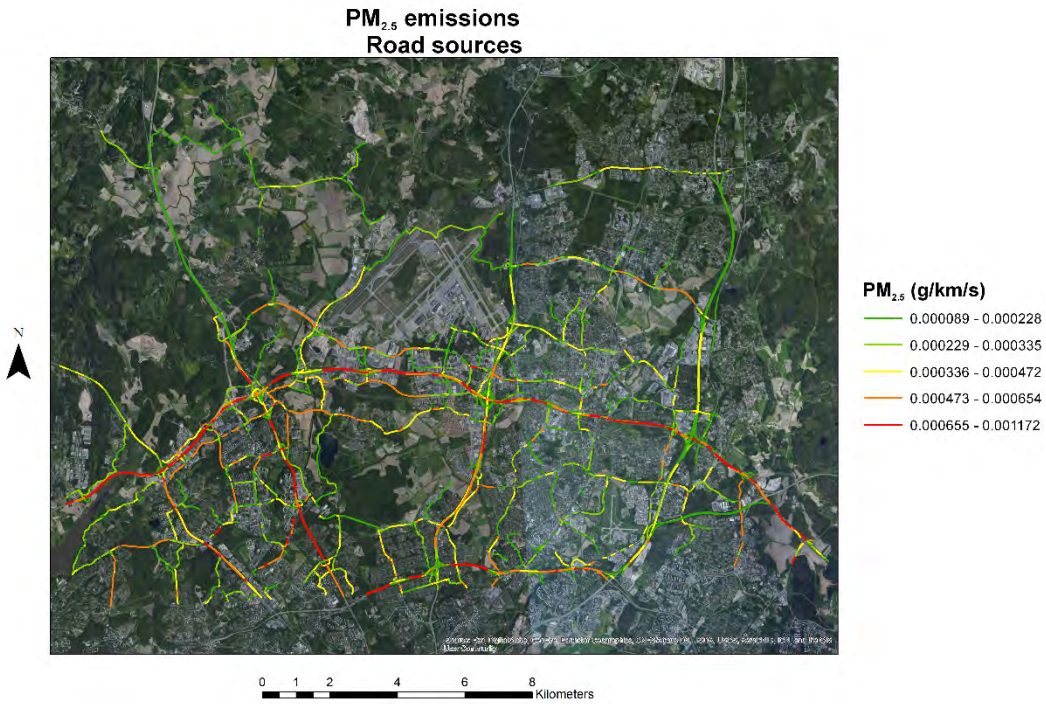

Figure 31. $PM_{2.5}$ emissions (in g/km/s) for road sources considered as major roads in Vantaa in the base case (present) scenario.

Both Figures show that the major emissions of air quality pollutants are located in proximity of major arteries such as highways or ring roads but with respect to Bologna and Hasselt emissions are relatively more spread.

In the case of Vantaa, information on emissions for the whole Finland was derived from Statistics Finland[17], while Helsinki population data are available as open-source data from avoindata.fi

Monthly and diurnal variation of residential heating sources were estimated considering the normal operating hours and operating periods (October to April) of residential heating sources in households in Finland from the Finnish Energy company[18].

Figure 32 shows estimated NO_x emissions from residential heating over the Helsinki Metropolitan Area.

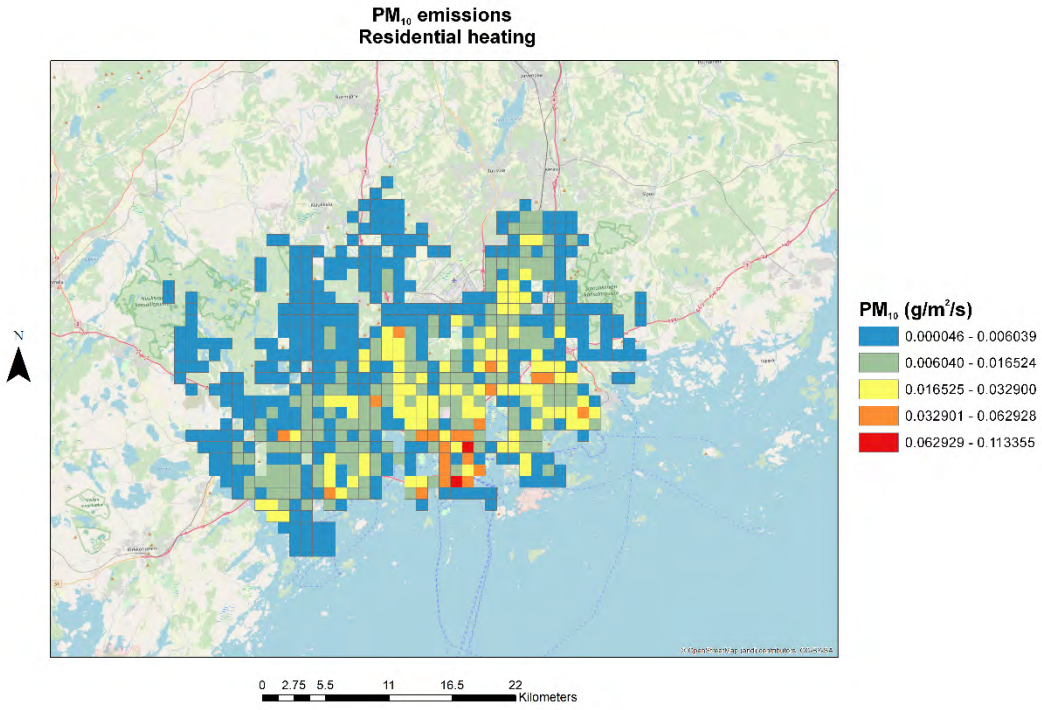

Figure 32. PM_{10} emissions ($g/m^2/s$) from residential heating in Helsinki Metropolitan Area in the base case (present) scenario.

Similar to what previously observed for road emissions, as compared to Bologna and Hasselt, in Vantaa emissions from residential heating are generally more spread and not concentrated only over the city centre.

[17] https://www.stat.fi/til/tilma/index_en.html

[18] https://energia.fi/en/news_and_publications/statistics/district_heating_statistics

3.3 Dispersion modeling

The source emission inventory was used as input to the dispersion modeling simulations carried on under the present scenario conditions. In this work, the ADMS-Urban model (version 4.1.1.0) developed by Cambridge Environmental Research Consultants (CERC) was used (CERC, 2011) to calculate the concentration of pollutants emitted from the sources considered in the emission inventory. The ADMS-Urban model is a quasi-Gaussian plume air dispersion model able to simulate a wide range of passive and buoyant releases to the atmosphere. The dispersion of pollutants has been simulated with the Atmospheric Dispersion Modelling System (ADMS; CERC, 2017). This model has been already extensively verified within a large number of studies and its performance has been compared with other EU and US EPA models, such as CALPUFF, AERMOD for instance (e.g., Carruthers et al., 2000; Di Sabatino et al., 2008; Stocker et al., 2012).

Being a local dispersion model, ADMS is able to resolve concentration gradients occurring close to various emission source types, including point, jet, line, area and volume sources. Minimum input data for the modeling setup and for the representation of the modeled domain consists in the emission sources including emission rates and time varying emission factors, meteorological data (at least: air temperature, wind speed, wind direction, and either cloud cover either sensible heat flux either Monin-Obukhov length for estimating boundary layer height), and background concentrations. Within the model, the dispersion calculations are driven by hourly meteorological profiles of wind speed and direction, characterized through Monin-Obukhov length similarity theory. As such, input meteorological data are among the most important input parameters for modeling air pollution dispersion.

The simulations were conducted in two different ways:

- Short term - any gridded concentration output files contain output for the first 24 lines of meteorological data only. If specified point output is selected, it contains a set of concentrations for every line of meteorological data. This simulation type in particular was used for the verification and comparison of model outputs with measured values.
- Long term - the concentration output files contain a single set of concentration data, averaged over all the lines of meteorological data. However, a file containing data at all output points for each meteorological line can be created for the long-term output. This simulation type in particular was used for evaluating the dispersion producing concentration maps in the current (baseline) scenario (base reference case) and in the simulations to be compared to it (policies, and climate change to be presented in the next section).

Output concentrations of short-term simulation are post-processed to calculate long-term averages as required for the validation. Output concentrations of long-term simulation are used to obtain the concentration maps for each pollutant in the various scenarios.

Additional options for the simulations include gaseous and particle dry and wet deposition; in case these options are selected, the user needs to include information on dry deposition velocity and washout coefficients for each pollutant for including dry and wet deposition in the dispersion simulations. Further, in case the wet deposition is also considered in the simulations, precipitation needs to be included in the meteorological dataset. The dry deposition velocity contains a diffusive part, the deposition velocity itself, and the terminal velocity of a particle, which is due to gravitational settling in the plume. Both are

required in ADMS-Urban for dry deposition modelling. If the values are unknown, they can be estimated by the model. Wet deposition occurs when there is precipitation (rain, sleet, snow, etc.) and it is modelled through a washout coefficient which is dependent on the nature of the pollutant, the rainfall rate and droplet size. This washout coefficient can be taken as constant value (in which case the wet deposition is independent of the rainfall rate) or it can depend on the rainfall rate. Finally, the model includes the option to include the NOx photolytic chemistry module, which accounts for fast, near-road oxidation of NO by O_3 to form NO_2 (Smith et al., 2017). In order to consider the NO_2-NO-O_3 chemical reactions in the simulations, meteorological data need to include solar radiation and time and hour of the day. The modelling also uses the ADMS-Urban NOx photolytic chemistry module, which incorporates both reactions for the photochemical reaction between nitric oxide (NO), nitrogen dioxide (NO_2), volatile organic compounds (VOC) and ozone (O_3), and reactions that govern the oxidation of sulfur dioxide (SO_2) leading to the formation of ammonium sulfate particles, i.e. particulate matter (PM). To use this scheme, solar radiation information and background concentration data for the critical pollutants NO_X, NO_2, O_3 and SO_2 are required.

Here, it is important also to note that ADMS treats all NO_x data as "NO_x as NO_2", i.e., assuming that 100% of the NO_x is NO_2, which generally means to overestimate the true situation (CERC, 2011), since the molecular mass of NO_2 (46 g mol^{-1}) is greater than the molecular mass of NO (30 g mol^{-1}). Typical applications of the model include the following: developing and testing policy on air quality; the development of air quality action plans; air quality and health impact assessments of proposed developments and use of the model for the provision of detailed street-level air quality forecasts (e.g., Hood et al., 2018; Zeng et al., 2017; Dėdelė and Miškinytė, 2015).

3.3.1 Bologna

Emissions covering the Bologna area were considered. The runs use hourly measured meteorological data from Marconi airport for the whole domain, with data available over 95% of hours in 2017.

In order to assess the baseline air quality in the modelled area for 2017, data of background pollution concentrations were included in the modelling. Background concentrations of air pollutants were obtained from the ARPAE monitoring network: Via Chiarini (in the western part of Bologna, measuring hourly data for NO_x, NO_2, O_3 and daily data for PM_{10}); Giardini Margherita (in the southern part of Bologna, measuring hourly data for NO_2). No monitoring data are available for CO because the annual average is smaller than the legal limit (0.6 mg/m^3). According to the work of Righi et al. (2009), to correctly model also the CO concentrations, it is necessary to insert its background value, in particular considering that this pollutant is affected by a "memory effect" that can be corrected taking into account the concentrations of CO present in the hours immediately preceding the specific time considered in the model. For these reasons, here the background concentration for CO was inserted as that measured at the ARPAE urban traffic Porta San Felice station the hour previous to that of the simulations.

The emissions from air pollution sources are time dependent, so time varying emission factors for road and grid sources need to be considered. The ADMS-Urban model has an ability to take into account hourly factors for weekdays, Saturdays, and Sundays and monthly factors. In this study, detailed data of hourly factors for weekdays (24 hours), Saturdays (24 hours) and Sundays (24 hours) (i.e. diurnal profiles) and monthly profiles are defined.

The parameters of wind speed, wind direction, surface temperature, precipitation, solar radiation and cloud cover were used. The dispersion of pollutants on Bologna has been modeled considering the year

2017 as a base case, as discussed in sections 3.1 and 3.2. The meteorological data is a very important parameter in air pollution dispersion. The meteorological dataset contained hourly sequential data measured by the Bologna airport weather station, considered the reference meteorological station for the city of Bologna not influenced by the presence of buildings in the city itself:

- Name: Bologna/Borgo Panigale (Bologna airport);
- WMO number: 16140 and WMO code: LIPE;
- Latitude: 44.5308 and Longitude: 11.2969.

3.3.2 Hasselt

Dispersion and chemistry modelling are independent of the output grid resolution. The model estimates the dispersion of air quality pollutants included in the emission inventory and emitted by the sources therein included. The model considers emissions of all sources within the domain, either explicitly with detailed with detailed time-varying profiles, such as major roads and industrial sources, or as grid-averaged emissions with simpler time variations, normally representing diffuse sources (for instance, heating and minor roads). In this case, emissions covering the whole Hasselt area were taken into account. Time varying emission factors (i.e., weekday-Saturday-Sunday and monthly) were derived from the traffic simulations and knowing the operating hours of households for residential heating in Limburg in the winter season (from mid-October to March). In the case of Hasselt, the hourly meteorological dataset previously described (Sect. 3.2.2), consisting of 2016 hourly observations of wind speed, wind direction, surface temperature, solar radiation, precipitation, and cloud cover, was used.

Background hourly concentrations, i.e. pollutant values deriving from sources outside the domain but that because of meteorological conditions and wind directions are transported to the domain, for NO_x, NO_2, O_3, PM_{10} and $PM_{2.5}$ were provided from VMM as estimates for a virtual rural station in Flanders (average of all rural stations in the region).

3.3.3 Vantaa

Similar to what previously mentioned for Hasselt, the dispersion model considers emissions of all sources within the domain, either explicitly with detailed with detailed time-varying profiles, such as major roads and industrial sources, or as grid-averaged emissions with simpler time variations, normally representing diffuse sources (for instance, heating and minor roads). In this case, road traffic and residential heating emissions covering the whole Vantaa area were taken into account, with time varying emission factors (i.e., weekday-Saturday-Sunday and monthly) derived from the traffic simulations and from the operating hours of households for residential heating in Finland in the winter-spring season (from October to April). In the case of Vantaa, the hourly meteorological dataset previously described (Sect. 3.2.2), consisting of 2017 hourly observations of wind speed, wind direction, surface temperature, solar radiation, precipitation, and cloud cover at the Vantaa Helsinki airport (WMO number 02974; 60.33 N, 24.96 E), was used.

Background hourly concentrations for NO_x, NO_2, O_3, PM_{10} and $PM_{2.5}$ were obtained from the rural background air quality station of Espoo Luuki through the previously mentioned open data service offered by FMI[19].

3.4 Validation

In order to evaluate the ADMS-Urban model, comparisons of measured and predicted concentrations were carried out by using hourly data. Data analysis and comparison of modelling results with observations were carried out using the Model Evaluation Toolkit (CERC, 2015).

In particular, the performance of the ADMS-Urban model was evaluated by calculating some basic statistical parameters, (mean and standard deviation (SD)), and other indicators with a methodology developed by Hanna (1993) and summarized by Chang and Hanna (2004). The following indicators set, proposed by Carruthers et al. (2003) were considered for the evaluation of the performance of the dispersion model:

- the fractional bias (FB), a measure of the mean difference between the modelled and observed concentrations
- the normalized mean square error (NMSE), a measure of the mean difference between matched pairs of modelled and observed concentrations
- the factor of two (FA2), i.e. the fraction of modelled concentrations within a factor of 2 of observations
- the Pearson's correlation coefficient (r), a measure of the extent of a linear relationship between the modelled and observed concentrations,
- and the coefficient of determination (R^2), the proportion of the variance in the dependent variable that is predictable from the independent variable(s).

Following equations describe the calculations of those statistical parameters:

$$FB = \frac{(\overline{C_o} - \overline{C_m})}{0.5(\overline{C_o} + \overline{C_m})}$$

$$NMSE = \frac{\overline{(M - O)^2}}{\overline{MO}}$$

FA2 = the fraction of data for which $0.5 < C_m/C_o < 2$

$$r = \frac{\sum_{i=1}^{n}(C_{o.i} - \overline{C_o})(C_{m.i} - \overline{C_m})}{\sqrt{\sum_{i=1}^{n}(C_{o,i} - \overline{C_o})^2 \sum_{i=1}^{n}(C_{m,i} - \overline{C_m})^2}}$$

$$R^2 = \frac{[\sum_{i=1}^{n}(C_{o.i} - \overline{C_o})(C_{m.i} - \overline{C_m})]^2}{\sum_{i=1}^{n}(C_{o,i} - \overline{C_o})^2 \sum_{i=1}^{n}(C_{m,i} - \overline{C_m})^2}$$

[19] https://ilmatieteenlaitos.fi/avoin-data

Where C_o denotes observations, C_m denotes model simulations, and the overbar denotes the average over the dataset.

Ideally, a perfect model would have FB and NMSE tending to zero, while FA2, r and R^2 should be equal to 1.

3.4.1Bologna

Validation of dispersion modeling simulations carried out for Bologna was performed comparing hourly concentrations of air quality pollutants (NO_x, NO_2, O_3, CO, and PM_{10}) observed at the air quality measuring stations with those simulated with the ADMS-Urban model during the 2017 year.

3.4.2 Hasselt

Validation of dispersion modeling simulations carried out for Hasselt was performed comparing hourly concentrations of air quality pollutants (NO_x, NO_2, O_3, PM_{10}, and $PM_{2.5}$) observed at the Hasselt air quality measuring station with those simulated with the ADMS-Urban model during one winter and one summer 2016 month.

3.4.3 Vantaa

Validation of dispersion modeling simulations carried out for Vantaa was performed comparing hourly concentrations of air quality pollutants (NO_2 and $PM_{2.5}$ which were the only available for the period of interest) observed at the three Vantaa air quality measuring stations (Tikkurila, Rekola and Vantaa airport) with those simulated with the ADMS-Urban model during one winter 2017 month.

3.5 Choice of policies

In this work, the evaluation of the policies implemented has been carried out considering the current scenario, i.e., implementing only the policies but with no change in the rest of the setup of the dispersion model (as for meteorology, background concentrations, and emission sources other than traffic). The estimation of the effectiveness of the policies is then evaluated comparing the results obtained for long-term averages with those obtained in the reference current case (baseline scenario).

3.5.1 Bologna

The main traffic area in Bologna is the centre (inside the inner ring road) which also corresponds to the main commercial area. In order to improve the air quality in Bologna, any traffic management policy should take into account this criticality. The policies chosen to implement and simulate in Bologna act specifically on the composition of the fleet and on certain traffic limitations, and as such also indirectly affect the behavior of citizens.

In particular, the policies investigated are:

- Policy 1 "electric centre": light and heavy vehicles are banned from the internal ring road, and only electric vehicles are allowed in this area.
- Policy 2 "electric buses": conversion of the bus fleet in Bologna to electric with increase in bus frequency in the centre, and all non-electric vehicles are banned from the internal ring road.

3.5.2 Hasselt

Different policy scenarios were implemented for Hasselt with the integrated behavioral simulation model, and a few of them were discussed in D4.2, with the purpose to demonstrate the ability of the simulator to simulate the policies.

Here, two particular policies were chosen to evaluate their impact on air pollution in the city of Hasselt. These policies are in line with the Hasselt City plans for future mobility in the city.

In particular, the two policies chosen were:

1. The complete closure of the Hasselt inner ring and of roads within it, thus implementing a fully pedestrianized area within it;
2. The increase in the frequency of buses, most of them doubling in a hour, while the frequencies of the other buses are only slightly increased.

Although the first policy may seem not justified from the emission maps resulted and presented above, and since the area is already largely pedestrian, the reason to test this policy is to take care of local inhabitants (the centre is a very populated one, as presented previously) and of commercial shops in the city centre (where the inner ring serves to keep off from the traffic). In addition, the restriction of car use in core city areas has been proven very effective in reducing air pollution and congestion from the core city areas to make such places more livable (e.g., Khreis & Nieuwenhuijsen, 2016). Regarding the first policy, we must say that in order to raise awareness, Hasselt city organized an event in the city where for a single day inner ring and all roads encompassing the inner ring were completely banned for cars. Similarly, here, car access was completely banned for 319 links in the traffic simulation model. This intervention has been implemented in the behavioural simulator by restricting car access to these roads introducing a very high penalty to car drivers in the MATSIM simulation platform. There are multiple mobility effects noted for this intervention which are as follows:

a) Several drivers have detoured their routes as they are now using longer routes in comparison with the base case where car drivers were using more direct routes. It is noted that the travel time of the car drivers on an average has been increased by 9%.

b) Due to the introduction of very high penalty for using the inner ring, most of the trips where the destination is the inner core zone of the city, 21% of the car drivers have changed their travel modes. This 21% of car trips have been distributed as 11% to PT, 7% to bicycle and 4% to walking. Furthermore, around 6-7% of individuals have changed their location of activities from inner city area to other areas in Hasselt city.

c) In relation to the distribution of traffic on the road network, the radial roads leading to the inner core ring are having low traffic density in comparison to the base case, which indicates that traffic has moved towards the outer ring region. However, there was no notable difference on motorways and other primary arterial roads. More detailed results on this policy with graphical

illustration are provided in D4.4. As previously detailed, here the aim of this report is to document the effect of this policy on the pollutant concentrations in the inner core region of Hasselt city.

In relation to Policy 2, there is a relatively less concentration of Hasselt city on investments and subsidies for bus-based public transport in the city. As a result, operators have reduced their bus fleet to a significant extent and recently most of the bus routes were re-designed. More than 80% of the households have car ownership and public transport is mainly used by low-income individuals, students and senior citizens. All these categories of citizens also have to pay less fare in comparison with other classes. Only 10-11% of the trips are based on public transport, and this depends mainly on the reduced frequency (higher waiting times) of the buses. Based on this context, a scenario was implemented in the microsimulation platform by increasing the frequency of buses. In fact, the increase of the attractiveness of the public transport might cause a reduction in the use of private cars because of the decrease in waiting time for passengers (D4.2), and the impact of such change on air quality might be interesting. To test this, the frequency of around 50% of the current bus routes is doubled, while for other 50% bus routes the frequency is increased by 25%. Within the mode choice model, the public transport utility contains a waiting time variable, whose values are changed during the execution of this policy scenario. The results indicate that this change increased the public transport mode share by only 5% (i.e. the overall share of public transport for this scenario is 15%). Because of this scenario, car use has been reduced but not significantly as the majority of the bicycle users rather than car users have shifted their mode to public transport. This policy has not obtained results as expected. Therefore, to encourage the use of public transport it is also necessary that some other car-based interventions are implemented, such as an increase in car use tax and increase in parking cost, etc. More details and discussion on these aspects are available in D4.4.

3.5.3 Vantaa

As previously mentioned, in Vantaa emissions from road traffic sources appear quite spread and for this reason it is more difficult to correctly identify traffic management policies that can adequately and efficiently impact on observed air pollution. We therefore decided to evaluate the impact of the same policies evaluated in Hasselt, i.e. the complete closure of an area (almost corresponding to a sort of city centre) to the traffic and the increase in bus frequency all over the road network. The aim is to evaluate the efficacy of the two policies in a city with a totally different spatial distribution of pollutants' emissions.

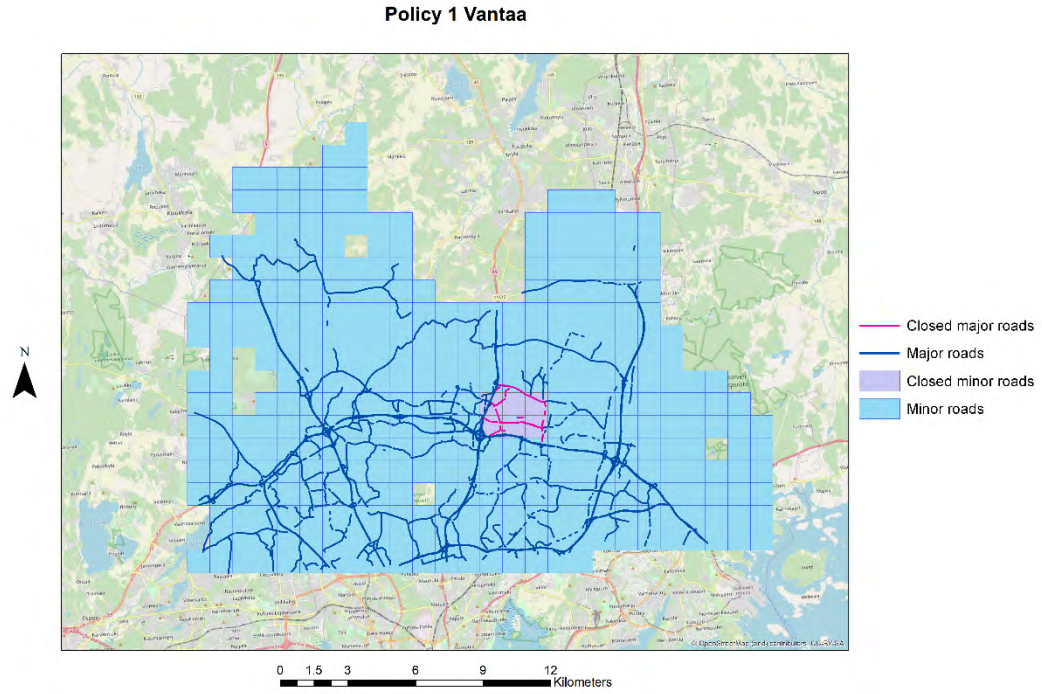

Figure 33. Area of the intervention (closure of the area to the traffic) tested in the policy 1 scenario for Vantaa.

Similar to what previously explained for Hasselt, we can note the main differences of this scenario compared with the base case for Vantaa:

a) The fact that several drivers in the policy scenario use longer routes in comparison with the base case where car drivers were using more direct routes leads to an increase in the travel time of the car drivers.

b) Because of the introduction of very high penalty for using the area banned to the traffic, most of the drivers needing to reach the area changed either the transportation mode either the location of their activities.

In relation to Policy 2, we have to consider that the transport system of Finland is well-developed, because of the sparse population, the long distance between towns and cities, and the cold climate with waterways freezing and land covered with snow in winter. As such, Finland is characterized by a well-developed road network with total 78,162km of main roads, of which 779km are constituted by motorways with additional 124km reserved only for motor traffic. Coaches are mainly operated by private companies and provide services widely across the country. Also, there is a large network of ExpressBus services connecting all major cities and the most important rural areas. Local bus services inside cities and towns are often regulated by the councils, many of which have also their own bus operators.

Helsinki, Espoo, Kauniainen, Vantaa, Kerava, Sipoo, Kikkonummi, Siuntio and Tuusula form an integrated public transport area with an integrated ticketing system. Besides buses, metros, local railways and ferry services, Helsinki is currently the only city in Finland to have a tram system. 50% of commuting trips in Helsinki within the city limits of Helsinki are made using public transport and only

28% using a private car (European Commission Directorate-General for Regional Policy, 2010)., even though 48% of households have access to a private car. Many of the buses operating in eastern Helsinki act as feeder lines for the Helsinki Metro. Nearly all other routes have the other end of their lines in the downtown near the Helsinki Central railway station. The regional bus lines today are managed by HSL similarly to the internal lines in Helsinki, with the aim to connect important points of the metropolitan area. While the operating hours of regional lines are similar to those of internal lines, the departures are often not as frequent. In this framework, the light activity-based model was used to simulate a scenario where the frequency of buses was increased. Similar to what previously simulated in Hasselt, the frequency of around 50% of the current bus routes is doubled, while for other 50% bus routes the frequency is increased by 25%. Within the mode choice model, the public transport utility contains a waiting time variable, whose values are changed during the execution of this policy scenario.

4 AQ simulations in the present scenario

4.1 Validation

As described in Section 3, we present here the evaluation of the dispersion modeling simulations conducted in the three cities, comparing the simulated air pollution values with observed concentration values and calculating statistical parameters, to objectively determine the performance of the simulations.

4.1.1 Bologna

The statistical evaluation of the performance of the ADMS-Urban model was carried out comparing simulations for 2016 with measured values in the air quality stations of Bologna and calculating the statistical parameters reported in Section 3. In particular, the assessment was made considering NO_x, NO_2, CO, O_3 and PM_{10} measurements over the whole 2017.

Figure 34 and Figure 35 represent the comparison of hourly simulated and observed NOx concentrations for the winter and summer (January - February – March and June - July – August, respectively) related to Porta San Felice.

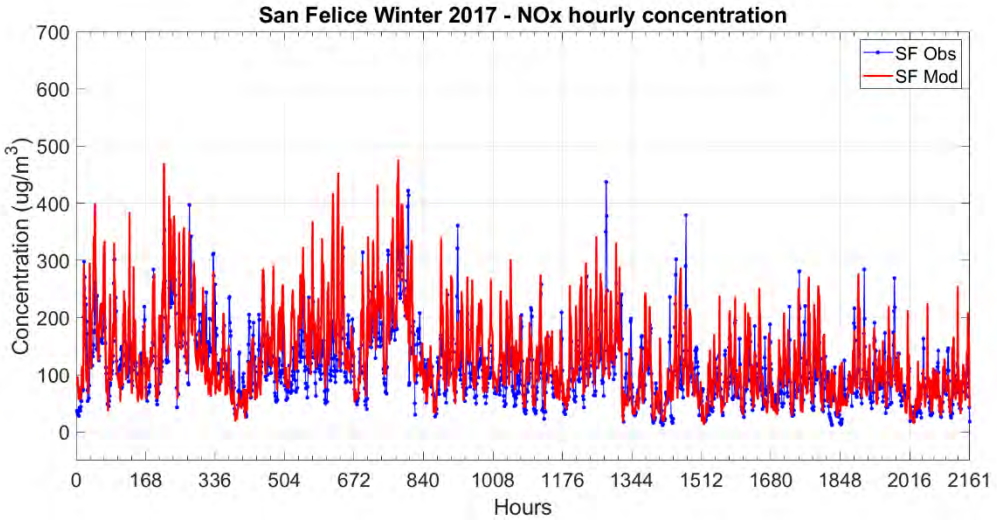

Figure 34. Winter time series of NO_x hourly concentration. Modeled data (Mod) and observed data (Obs) at the air quality ARPAE Porta San Felice station.

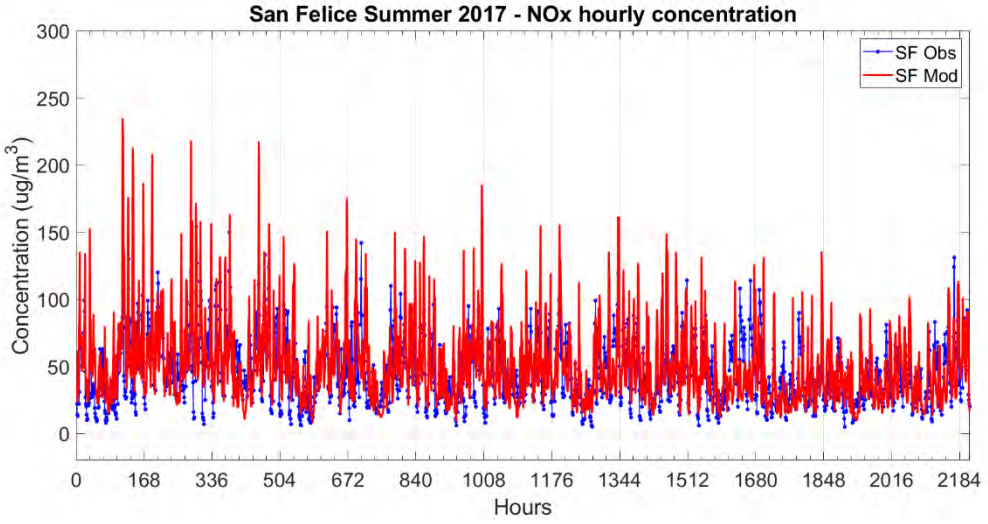

Figure 35. Summer time series of NO_x hourly concentration. Modeled data (Mod) and observed data (Obs) at the air quality ARPAE Porta San Felice station.

The modeled data are comparable with those observed, even though at high temporal resolution the model simulated concentrations show a slight overestimation that is still visible, even if less pronounced in the daily data. Figure 36 and Figure 37 report the daily simulated and observed concentrations related to Porta San Felice for the whole 2017 year for the NO_x and PM_{10} pollutants, respectively.

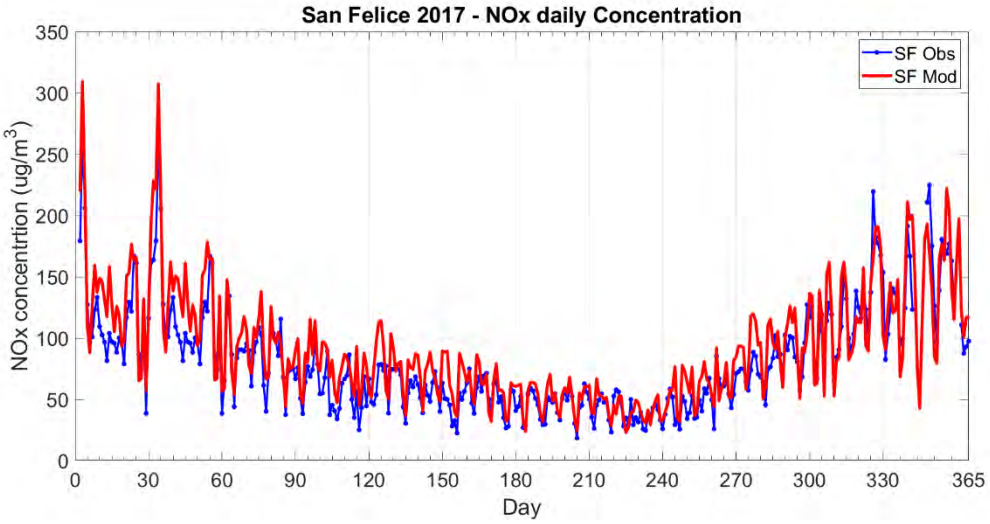

Figure 36. Time series of daily NO_x concentration for 2017. Modeled data (Mod) and observed data (Obs) at the air quality ARPAE Porta San Felice station.

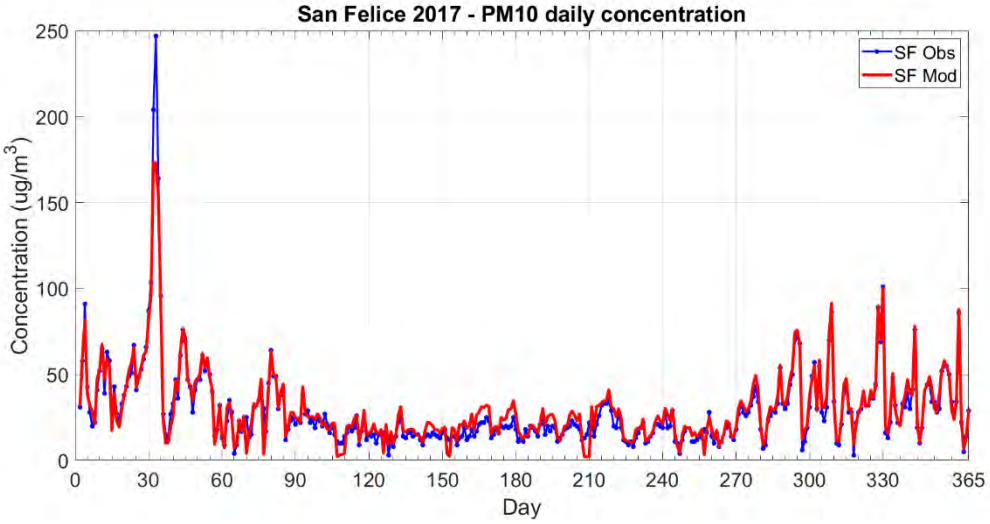

Figure 37. Time series of daily PM_{10} concentration for 2017. Modeled data (Mod) and observed data (Obs) at the air quality ARPAE Porta San Felice station.

The overestimation of the model is also highlighted in Figure 38, which shows the NO_x weekly time concentration cycle in San Felice.

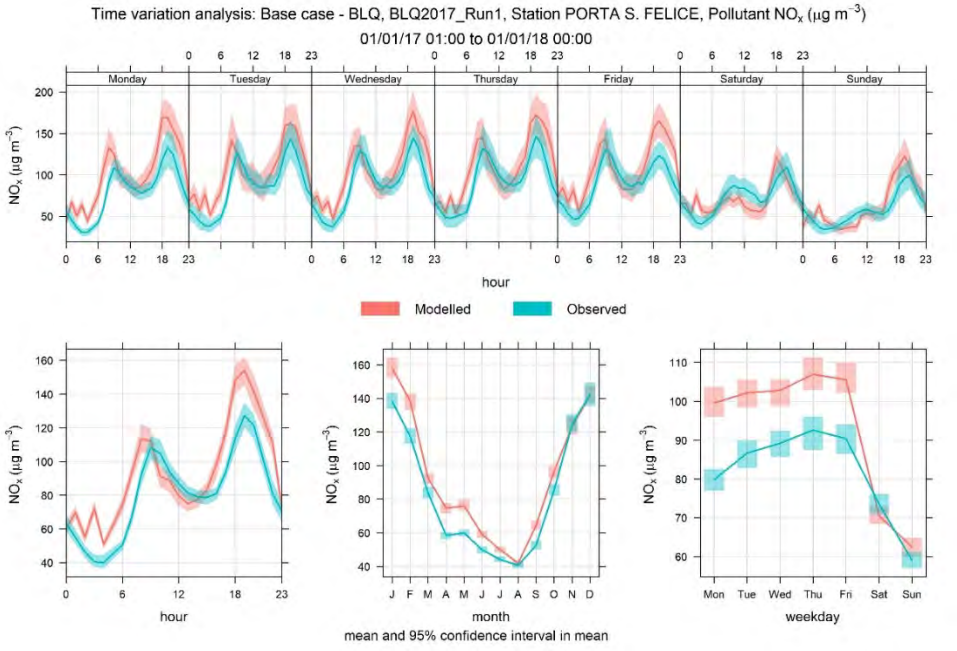

Figure 38. Time variation analysis for NO_x, period:1/01/2017 – 1/01/2018 representing diurnal pattern, weekly pattern and monthly pattern for the base case simulation for Porta San Felice station as compared to the measurements.

Figure 38 shows that the model represents correctly the overall pattern of air quality pollutants, even though it tends to overestimate NO_x concentrations. However, as from Table 10, statistical parameters for the ADMS simulations are reasonably good.

Station	Pollutant	type	Obs Mean ± SD	Mod Mean ± SD	MB	NMSE	Fb	R	R^2	FA2
SF	NO_x	traffic	81.8 ± 43.7	91.9 ± 47.4	10.18	0.07	0.12	0.91	0.82	1.00
SF	NO_2	traffic	46.1 ± 14.9	43.9 ± 16.7	-2.17	0.05	-0.05	0.82	0.68	0.97
SF	CO	traffic	0.7 ± 0.2	0.7 ± 0.2	-0.01	0.00	-0.01	1.00	0.47	1.00
SF	PM_{10}	traffic	28.9 ± 24.2	30.3 ± 21.7	1.37	0.05	0.05	0.97	0.94	0.96
GM	NO_2	urban background	25.0 ± 16.8	25.6 ± 15.0	0.61	0.02	0.02	0.99	0.96	0.97
GM	O_3	urban background	48.0 ± 35.4	44.2 ± 32.2	-3.81	0.02	-0.08	1.00	0.95	0.98
GM	PM_{10}	urban background	25.0 ± 23.0	26.4 ± 20.8	1.42	0.06	0.06	0.96	0.93	0.94
Ch	NO_x	suburban background	33.2 ± 28.6	33.3 ± 24.7	0.17	0.04	0.01	0.98	0.99	0.99
Ch	NO_2	suburban background	20.4 ± 10.6	24.9 ± 15.1	4.50	0.11	0.20	0.94	0.89	0.98
Ch	O_3	suburban background	41.2 ± 32.9	42.9 ± 32.9	1.70	0.09	0.04	0.92	0.83	0.88
Ch	PM_{10}	suburban background	27.7 ± 20.4	27.7 ± 20.4	0.01	0.00	0.00	1.00	1.00	1.00

Table 10. Statistical analyses. Reference station: Porta San Felice (SF), Giardini Margherita (GM) and Via Chiarini (Ch).

Considering SF station (traffic reference station), FA2 results show good agreement between observed and modelled concentrations, R^2 correlation coefficients are in the range 0.47 -0.94 (for CO and PM_{10}, respectively). The normalized mean square error is low for all pollutants. The values of the fractional bias are very low (0.01 for CO), where the low positive values indicate a slight overestimation and the low negative values indicate a slight underestimation.

4.1.2 Hasselt

As reported in Section 3, the statistical evaluation of the performance of the ADMS-Urban model was carried out comparing graphically simulations for 2016 with measured values in the air quality station of Hasselt (VMM) and calculating some statistical parameters. In particular, the assessment was made considering NO_x, NO_2, O_3, PM_{10}, and $PM_{2.5}$ measurements over one winter and one summer month in 2016, January and August, respectively.

The following Figure represents the comparison of hourly simulated and observed concentrations for the month of January. The Figure shows that the model represents correctly the overall pattern of air quality pollutants, even though it tends to overestimate NO_x, NO_2, PM_{10} and $PM_{2.5}$ concentrations, while O_3 concentrations tend to be underestimated. This can be attributed to having neglected dry and wet deposition from the simulations, whose effect would be to lower gaseous NO_x and NO_2 and particulate concentrations. The underestimation of O_3 is instead strictly connected to the overestimation of NOx and NO_2 concentrations, and from the NO_x-NO_2-O_3 equilibrium reaction[20]. However, observing that the overestimation of NO_2 and especially of NO_x is higher than that of PM_{10} and $PM_{2.5}$, a slight overestimation of input NO_x and NO_2 emissions must be also considered, which could depend on an overestimation of diesel vehicles, which emit more NO_x than equivalent petrol engine vehicles (e.g., Beevers et al., 2015; Degraeuwe et al., 2017), or from wrong NO_2/NO_x ratios in the emissions. As known, in fact, estimating the on-road concentrations of NO_2 from near-road monitors is complicated by atmospheric chemistry: the majority of tailpipe NO_x is NO, with a small NO_2 fraction becoming quickly larger after emissions because of the fast reaction of NO with ambient O_3 (Kota et al., 2013; Wang et al., 2011). The correct estimation of the fraction of NO_x directly emitted as NO_2 (f-NO_2) is of particular interest for air quality modeling and in particular for ADMS-Urban which as stated above treats all NO_x data as "NO_x as NO_2", i.e., assuming that 100% of the NO_x is NO_2, which generally means to overestimate the true situation (CERC, 2011). Finally, the NO_x overestimation/O_3 underestimation could also depend on the chemistry ADMS module incorrectly representing the NO_2-NO-O_3 equilibrium reaction.

[20] In the troposphere, during day, sunlight splits nitrogen dioxide into nitric oxide and an oxygen atom

$$NO_2 + \text{sunlight} \rightarrow NO + O$$

A single oxygen atom then combines with an oxygen molecule to produce ozone

$$O + O_2 \rightarrow O_3$$

Ozone then reacts readily with nitric oxide to yield nitrogen dioxide and oxygen

$$NO + O_3 \rightarrow NO_2 + O_2$$

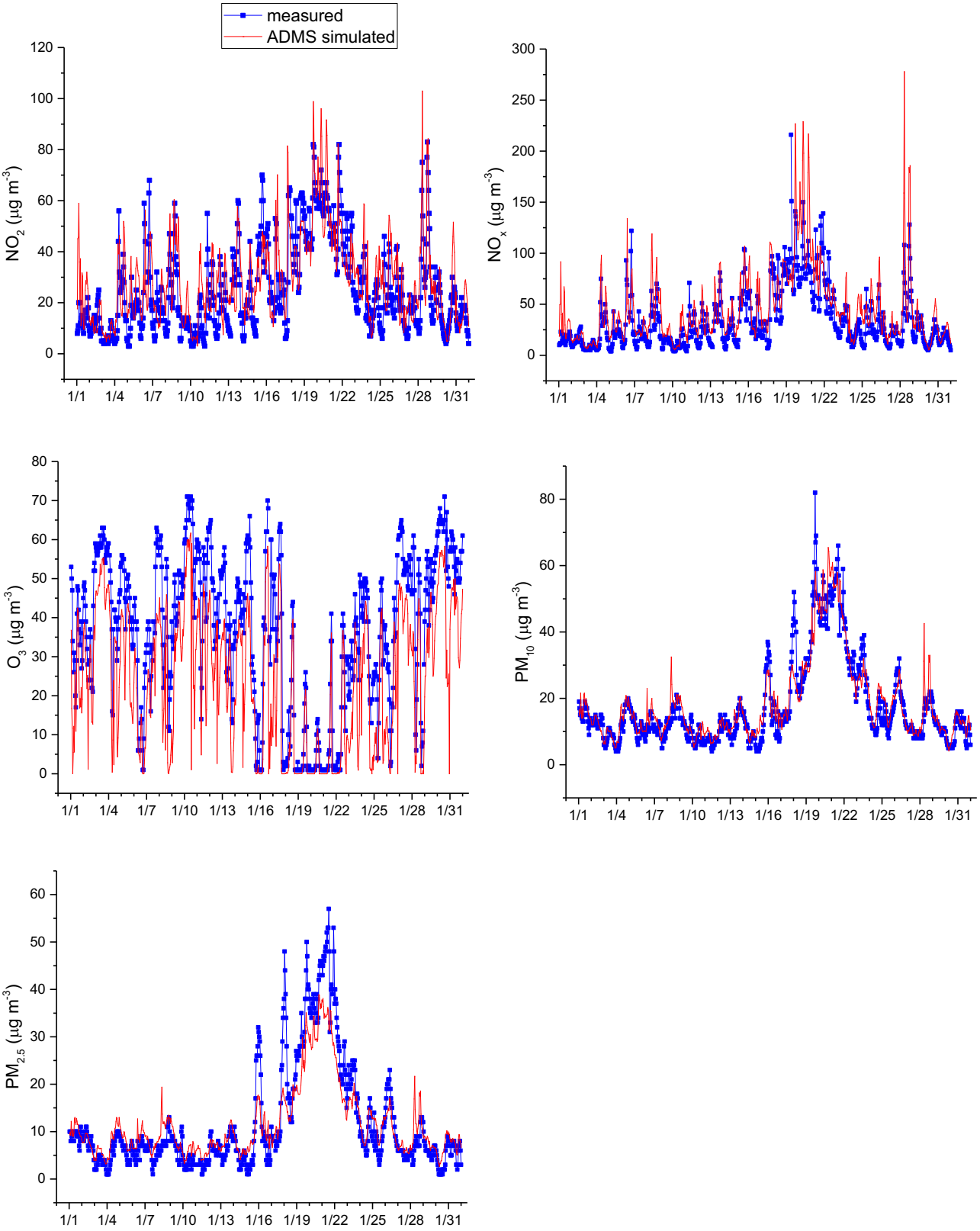

Figure 39. Comparison of NO_x, NO_2, O_3, PM_{10}, and $PM_{2.5}$ hourly measured and ADMS-Urban simulated concentrations at the Hasselt air quality station in the month of January 2016.

However, as from Table 11, statistical parameters for the ADMS simulations are reasonably good: FA2 results show good agreement between observed and modelled concentrations, R correlation coefficients are in the range 0.59 -0.88 (for NO_2 and $PM_{2.5}$, respectively), the normalized mean square error is low in particular for NO_2 and PM_{10}, while the values of the fractional bias indicate the previously observed overestimation of NO_2 and in particular of NO_x and the underestimation of O_3.

Parameter	Mean ± SD		NMSE	R	R^2	FA2	Fb
	Observed	Modelled					
NO_2	25.6 ± 13.7	29.0 ± 11.9	0.04	0.95	0.90	1.00	0.13
NO_x	33.9 ± 22.7	45.2 ± 26.8	0.14	0.94	0.89	0.97	0.29
O_3	47.9 ± 14.2	36.1 ± 12.1	0.09	0.95	0.91	0.97	-0.28
PM_{10}	17.6 ± 11.8	18.4 ± 11.1	0.02	0.98	0.96	1.00	0.04
$PM_{2.5}$	11.8 ± 10.5	11.5 ± 7.0	0.11	0.98	0.97	1.00	-0.02

Table 11. Statistics of daily observed and modelled concentrations of NO_2, NO_x, PM_{10} and $PM_{2.5}$ concentrations ($\mu g/m^3$) and daily maximum O_3 8-hour rolling mean in Hasselt in the month of January 2016.

Similar observations hold considering the following Figure representing the scatterplots between simulated and observed NO_x, NO_2, O_3, PM_{10}, and $PM_{2.5}$ daily concentrations.

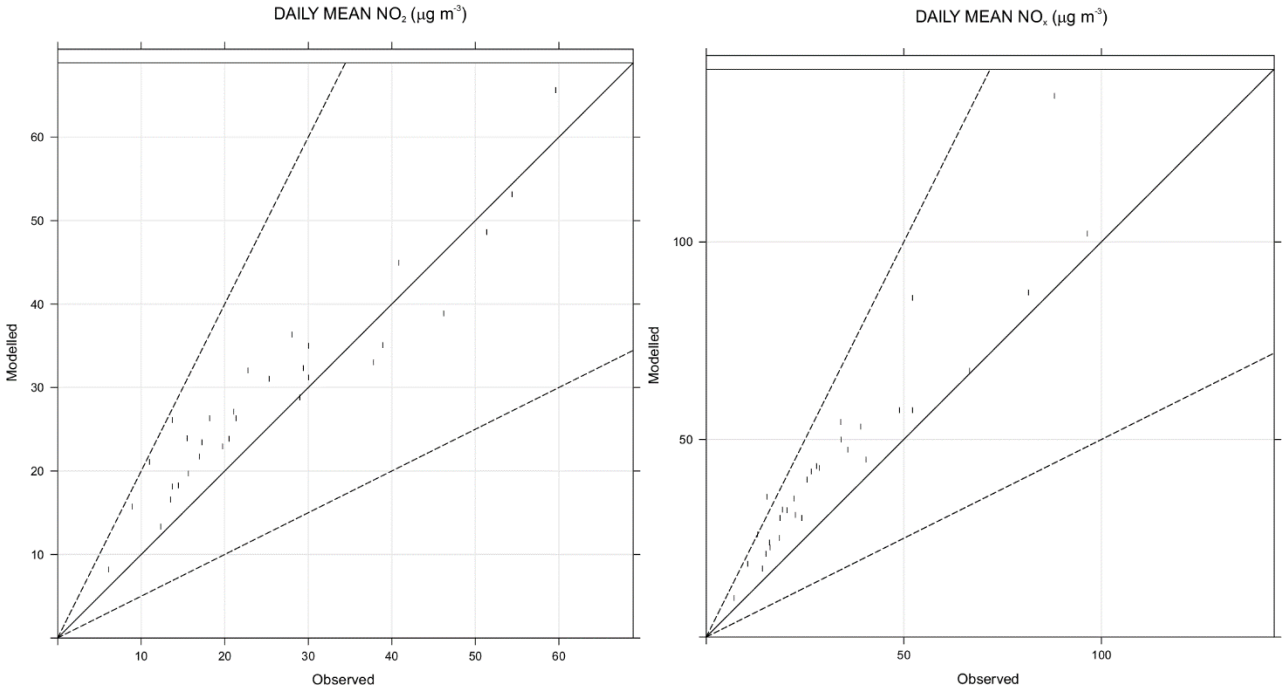

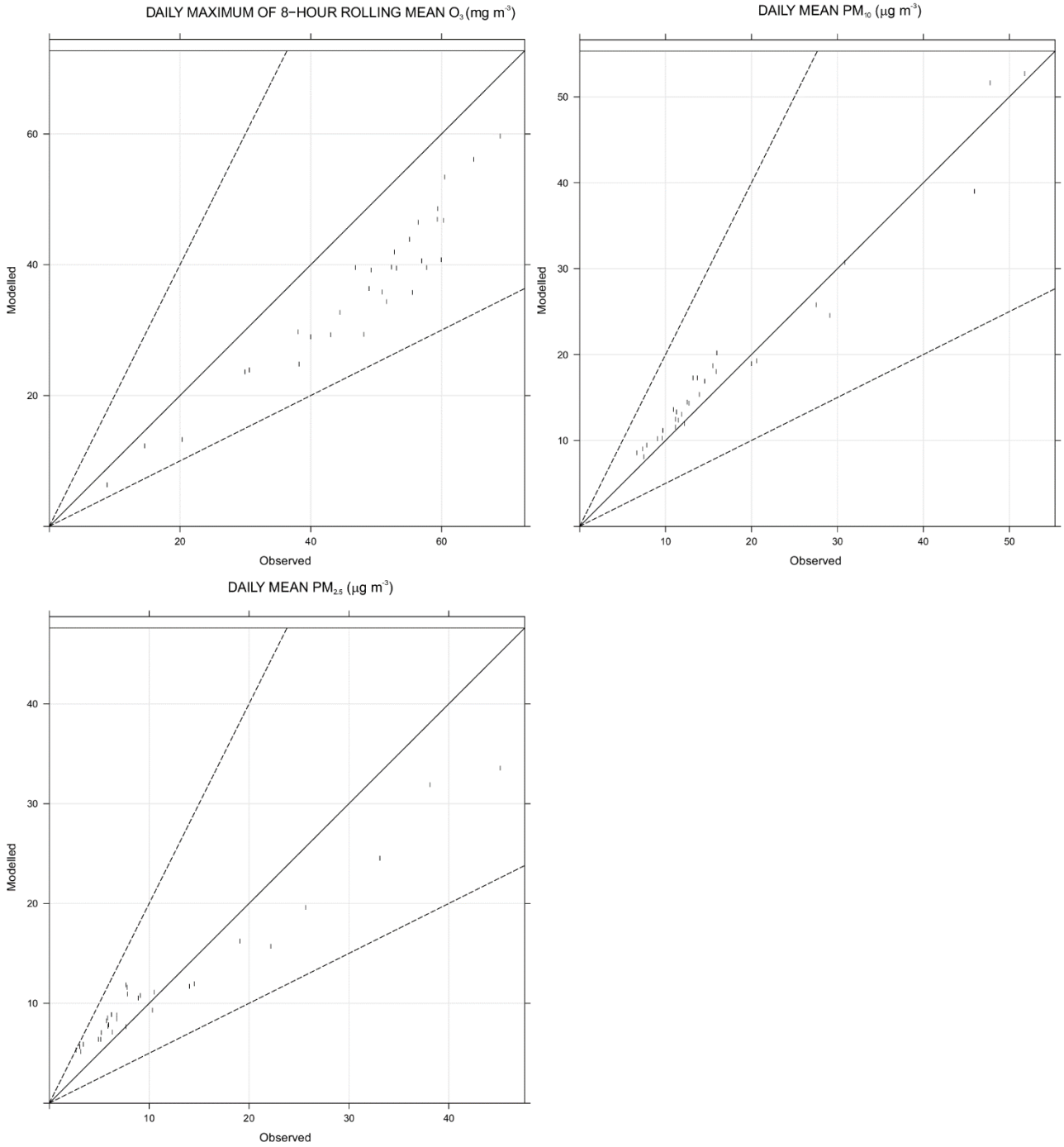

Figure 40. Scatter plot of observed and simulated daily mean NO_2, NO_x, PM_{10} and $PM_{2.5}$ concentrations and daily maximum O_3 8-hour rolling mean in Hasselt in the month of January 2016. The straight represents the 1:1 regression line, while the dotted lines represent the 95% confidence interval around the mean.

Finally, the following Figures represent the comparisons of the weekly and diurnal pattern of observed and simulated concentrations. The Figures clearly show that even though the model tends to overestimate the NO_2, PM_{10}, $PM_{2.5}$ and particularly NO_x concentrations, and to underestimate O_3 concentrations, the overall weekly and diurnal pattern is captured in the simulations, meaning that the

time modulation of the sources included in the emission inventory for Hasselt was correct. In addition, apart from NO_x and O_3 weekly patterns and O_3 diurnal pattern, all the other patterns fall in the 95% confidence interval around the mean, indicating that the tendency to overestimate is generally not too large and within the standard deviation of measured values.

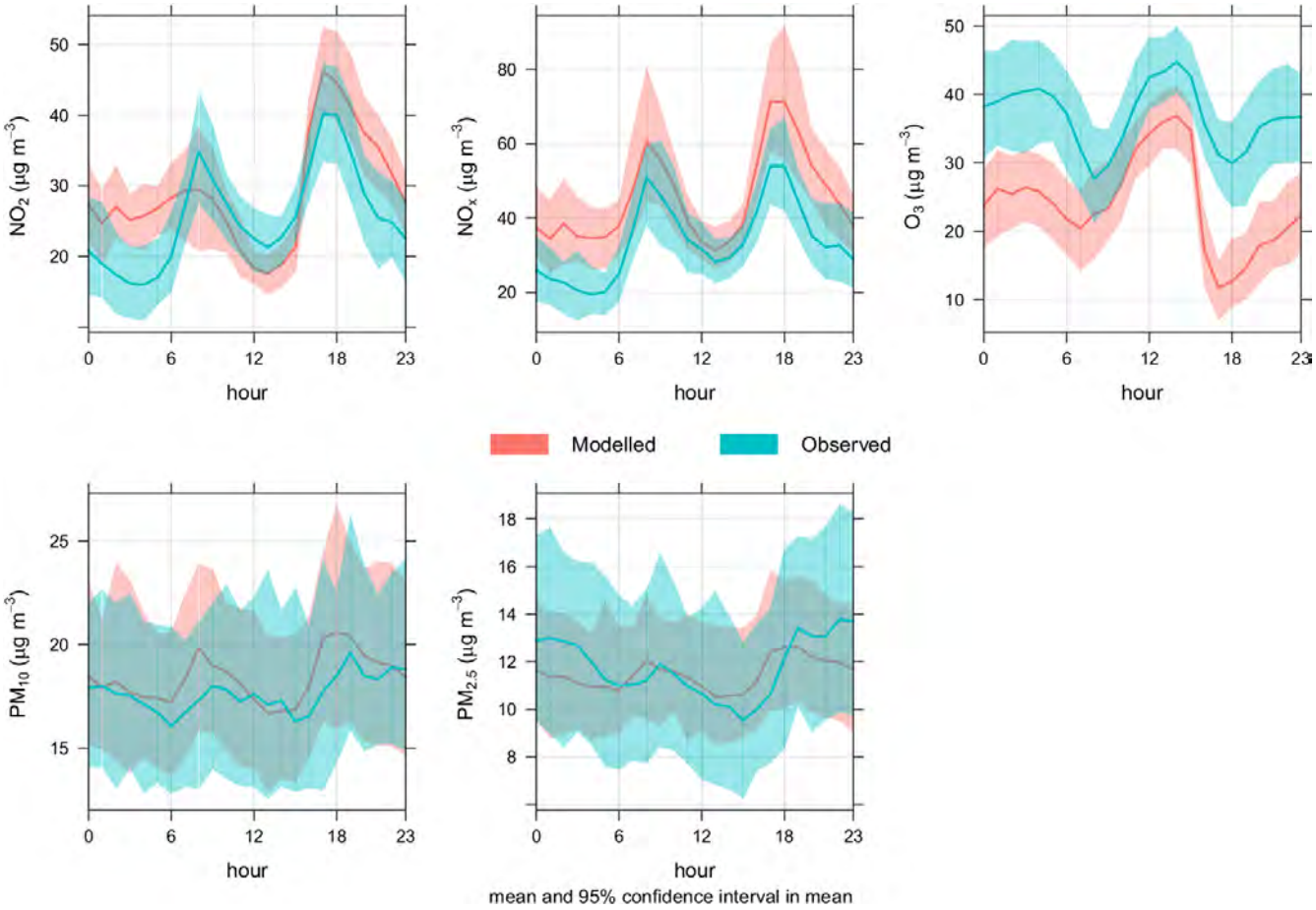

Figure 41. Mean measured and simulated diurnal pattern for NO_x, NO_2, O_3, PM_{10}, and $PM_{2.5}$ concentrations in the month of January 2016 in Hasselt.

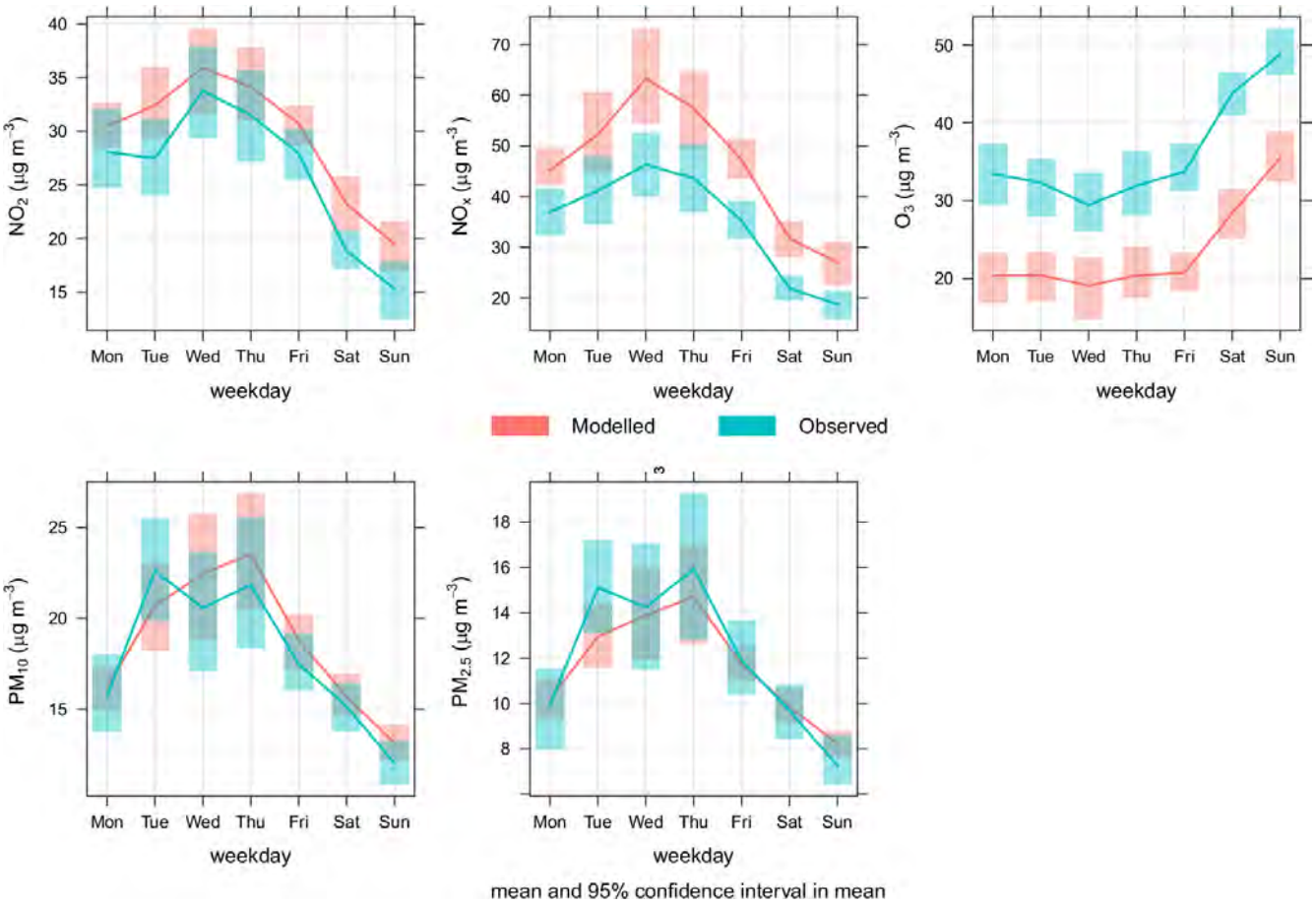

Figure 42. Mean observed and simulated weekly pattern for NO_2, NO_x, O_3, PM_{10} and $PM_{2.5}$ concentrations in January 2016 in Hasselt.

Similar results, i.e. a tendency to overestimate NO_x and underestimate O_3 concentrations, but with an overall good (though worse than in the winter month) statistical performance as justified by the calculated statistical parameters (Table 12) and by similar diurnal and weekly pattern (not shown), are obtained when considering the August 2016 summer month. We thus may consider the dispersion simulations for Hasselt as generally validated.

Parameter	Mean ± SD		NMSE	R	R^2	FA2	Fb
	Observed	Modelled					
NO_2	19.6 ± 8.6	25.1 ±7.9	0.09	0.89	0.810	0.94	0.24
NO_x	24.9 ± 11.2	40.5 ± 12.3	0.29	0.82	0.67	0.68	0.47
O_3	81.6 ± 32.5	64.0 ± 27.5	0.07	0.98	0.97	1.00	-0.24
PM_{10}	17.5 ± 5.2	20.3 ± 7.2	0.05	0.90	0.82	1.00	0.15
$PM_{2.5}$	8.6 ± 3.6	12.7 ± 4.7	0.22	0.84	0.71	0.90	0.39

Table 12. Statistics of daily observed and modelled concentrations of NO_2, NO_x, PM_{10} and $PM_{2.5}$ concentrations ($\mu g/m^3$) and daily maximum O_3 8-hour rolling mean in Hasselt in the month of August 2016.

4.1.3 Vantaa

As reported in Section 3, the statistical evaluation of the performance of the ADMS-Urban model was carried out comparing graphically simulations for 2017 with measured values in the air quality stations of Vantaa (HSY) and calculating some statistical parameters. In particular, the assessment was made considering NO_2 and $PM_{2.5}$ measurements over the January 2017 winter month.

Figure 43 represents the comparison of hourly simulated and observed concentrations at the Vantaa air quality stations for the month of January 2017.

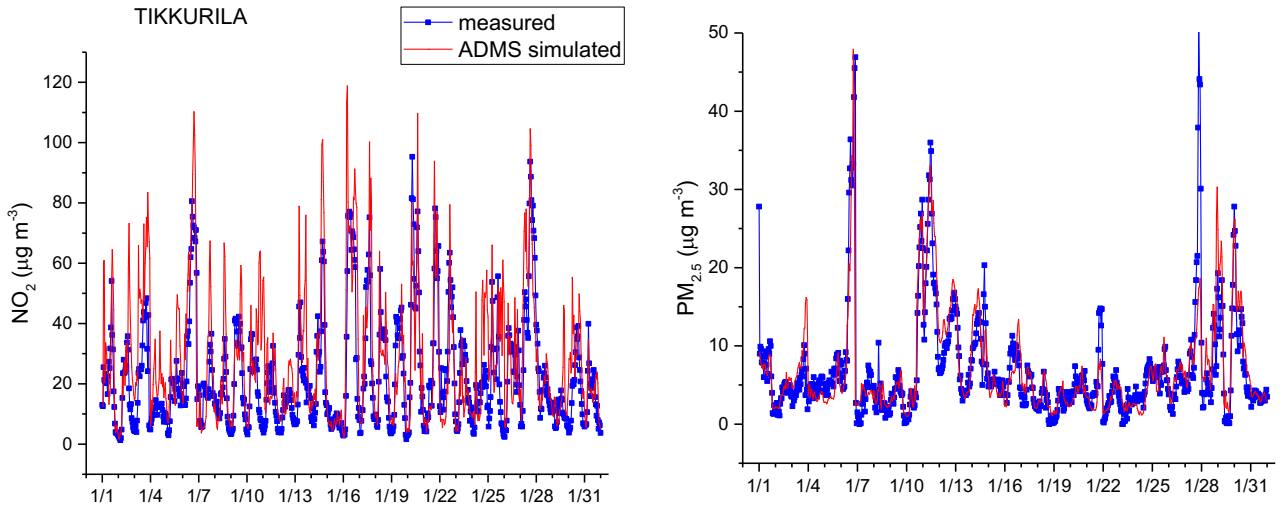

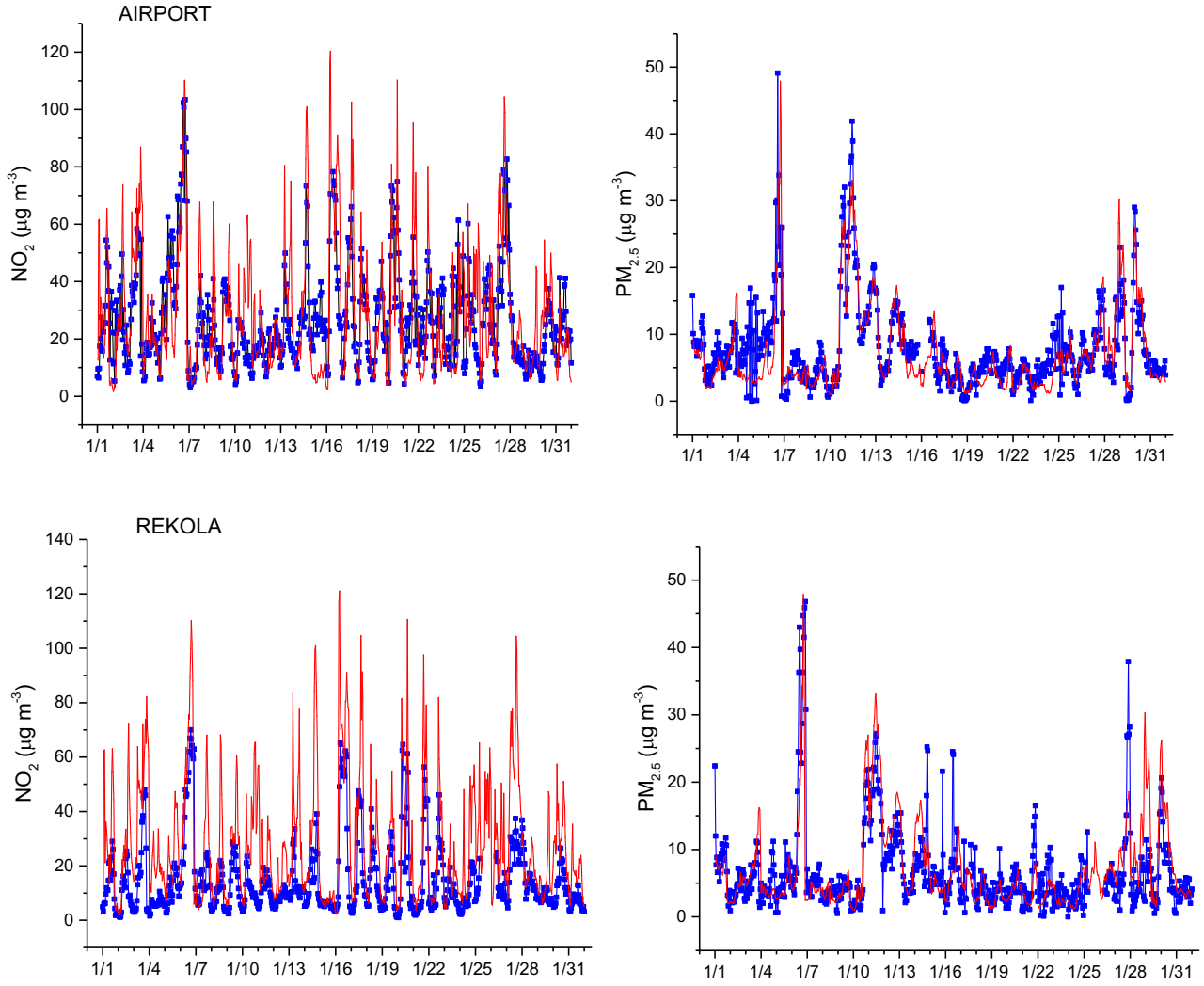

Figure 43. Comparison of NO_2, and $PM_{2.5}$ hourly measured and ADMS-Urban simulated concentrations at the Vantaa air quality stations of Tikkurila, Airport and Rekola in the month of January 2017.

The Figure shows that the model represents correctly the overall pattern of $PM_{2.5}$ concentrations, while for NO_2 the model simulates correctly concentrations especially at the Tikkurila and secondarily at the airport air quality stations, while simulated concentrations tend to be overestimated in Rekola. This may result from incorrect and too high local NO_2 emissions

However, statistical parameters for the ADMS simulations are reasonably good (Table 13**Error! Reference source not found.**): FA2 results show good agreement between observed and modelled concentrations apart from NO_2 at Rekola, R correlation coefficients are in the range 0.75 -0.94 (for NO_2 and $PM_{2.5}$ at the airport air quality station, respectively), the normalized mean square error is low at all stations apart from NO_2 in Rekola, while the values of the fractional bias indicate again the previously observed overestimation of NO_2 in Rekola and a slight underestimation of $PM_{2.5}$ at the airport, possibly depending from local aviation emissions.

Station	Parameter	Mean ± SD		NMSE	R	R^2	FA2	Fb
		Observed	Modelled					
Tikkurila	NO_2	22.6 ± 10.2	28.5 ± 12.3	0.12	0.84	0.73	1.00	0.23
Tikkurila	$PM_{2.5}$	6.9 ± 4.5	7.1 ± 4.6	0.08	0.90	0.80	1.00	0.03
Airport	NO_2	26.8 ± 10.2	28.5 ± 12.3	0.09	0.75	0.58	0.97	0.06
Airport	$PM_{2.5}$	7.8 ± 4.4	7.1 ± 4.7	0.06	0.94	0.89	0.93	-0.09
Rekola	NO_2	14.8 ± 8.0	28.5 ± 12.3	0.56	0.86	0.71	0.55	0.63
Rekola	$PM_{2.5}$	6.7 ± 4.3	7.2 ± 4.8	0.15	0.83	0.70	0.97	0.06

Table 13. Statistics of daily observed and modelled concentrations of NO_2 and $PM_{2.5}$ concentrations ($\mu g/m^3$) in Vantaa air quality stations in the month of January 2017.

Finally, Figure 44 represents the comparisons of the weekly and diurnal pattern of observed and simulated concentrations in Tikkurila, airport and Rekola air quality station. The Figure clearly shows that even though the model tends to overestimate the NO_2 concentrations in Rekola, the overall weekly and diurnal patterns observed at the three stations are captured in the simulations, indicating that the time modulation of the sources included in the emission inventory for Hasselt was correct. In addition, the NO_2 and $PM_{2.5}$ patterns fall in most cases in the 95% confidence interval around the mean, indicating that the tendency to overestimate is generally not too large and within the standard deviation of measured values.

TIKKURILA

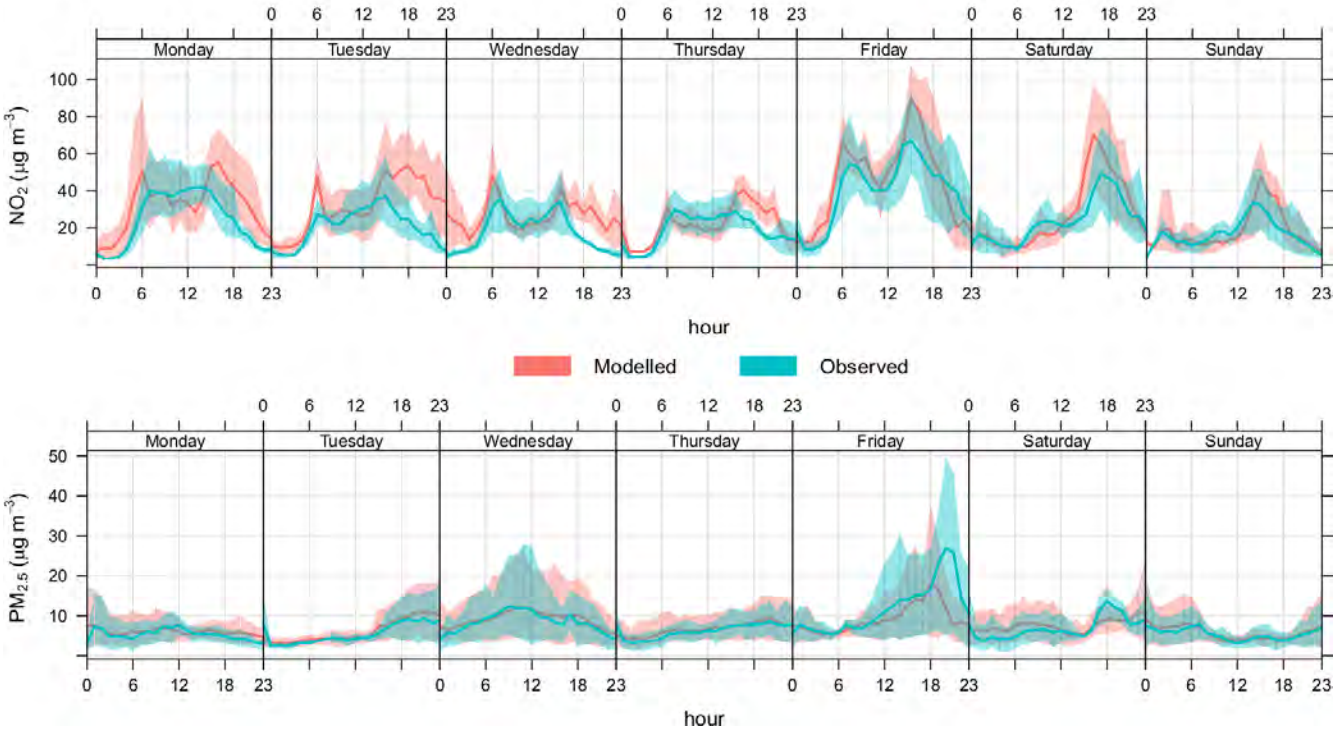

AIRPORT

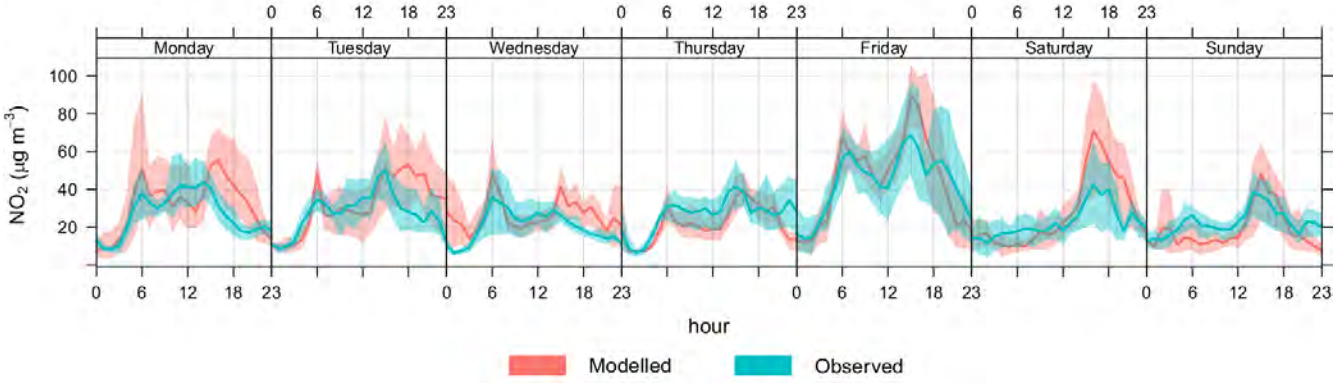

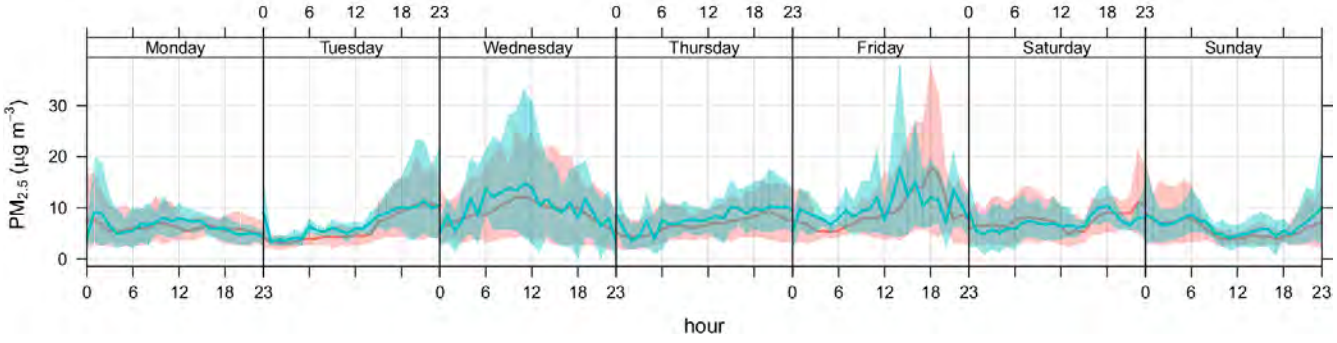

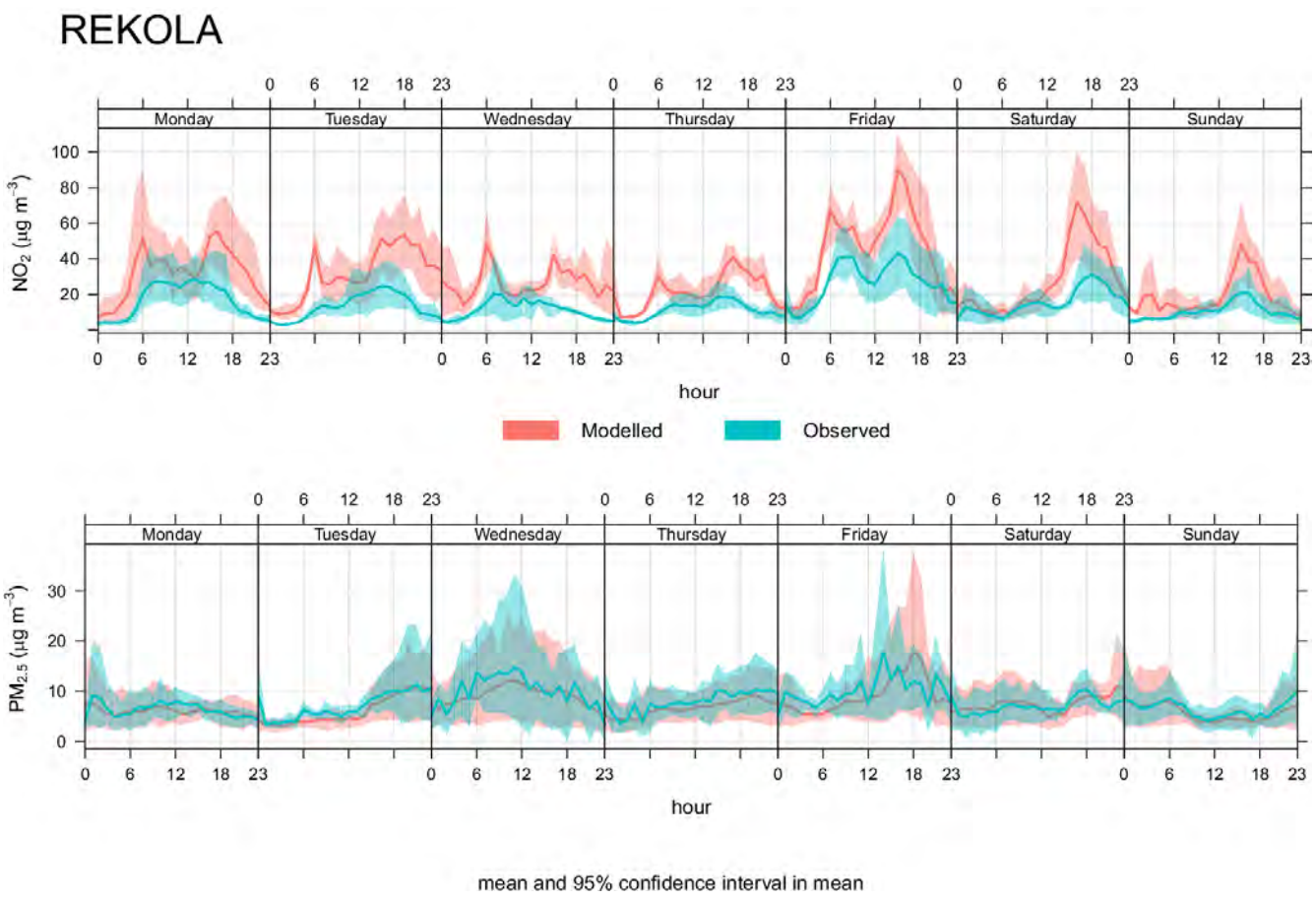

Figure 44. Mean measured and simulated weekly diurnal patterns for NO_2, and $PM_{2.5}$ concentrations in the month of January 2017 in Vantaa at the three air quality stations.

4.2 Results

As described in the methodology section, in the following we will present the results of the dispersion simulations conducted in the current scenario in the three cities, previously validated in Section 4.1., both in the current (baseline) case, as well in the cases of implementing the policies previously presented. Results are presented in the form of concentration maps for considered pollutants, obtained as output of long-term simulations of the ADMS-Urban 4 dispersion model. In addition, the policies scenarios are presented with maps of concentration differences between the scenario when the policy is implemented and the current (baseline) case. Finally, reductions are evaluated in terms of concentration ratios between these concentration differences and the concentrations observed in the base case.

4.2.1Bologna

Since the concentrations of pollutants present significant variations during the seasons, and these variations are especially significant between summer and winter, only two periods are shown, i.e. winter (January, February and March 2017) and summer (June July and August 2017) to present the current

(baseline) scenario (base case) and the application of the two selected policies (policy1 and policy2). The methodology used, described in section 3.4.1, is the long-term simulation whose outputs are spatial concentration maps for each pollutant.

4.2.1.1 Present scenario

The following Figures show the spatial distribution of the concentration of pollutants in the base case for 2017 (2017BC scenario), averaged over the period considered. The NO_x and PM_{10} concentration maps in Figure 45 and Figure 46 appear similar in the two seasons with regard to the spatial distribution, while the simulated concentration ranges are very different in the two seasons, as expected. The same observations apply for NO_2 and CO (not shown), while for O_3 (Figure 47) there is a completely different dynamics in winter and summer, governed by atmospheric chemistry. The spatial distribution of the concentration of O_3 shows a pattern different from other pollutants and opposite to that of NO_2, with low concentrations in trafficked areas and in urban areas.

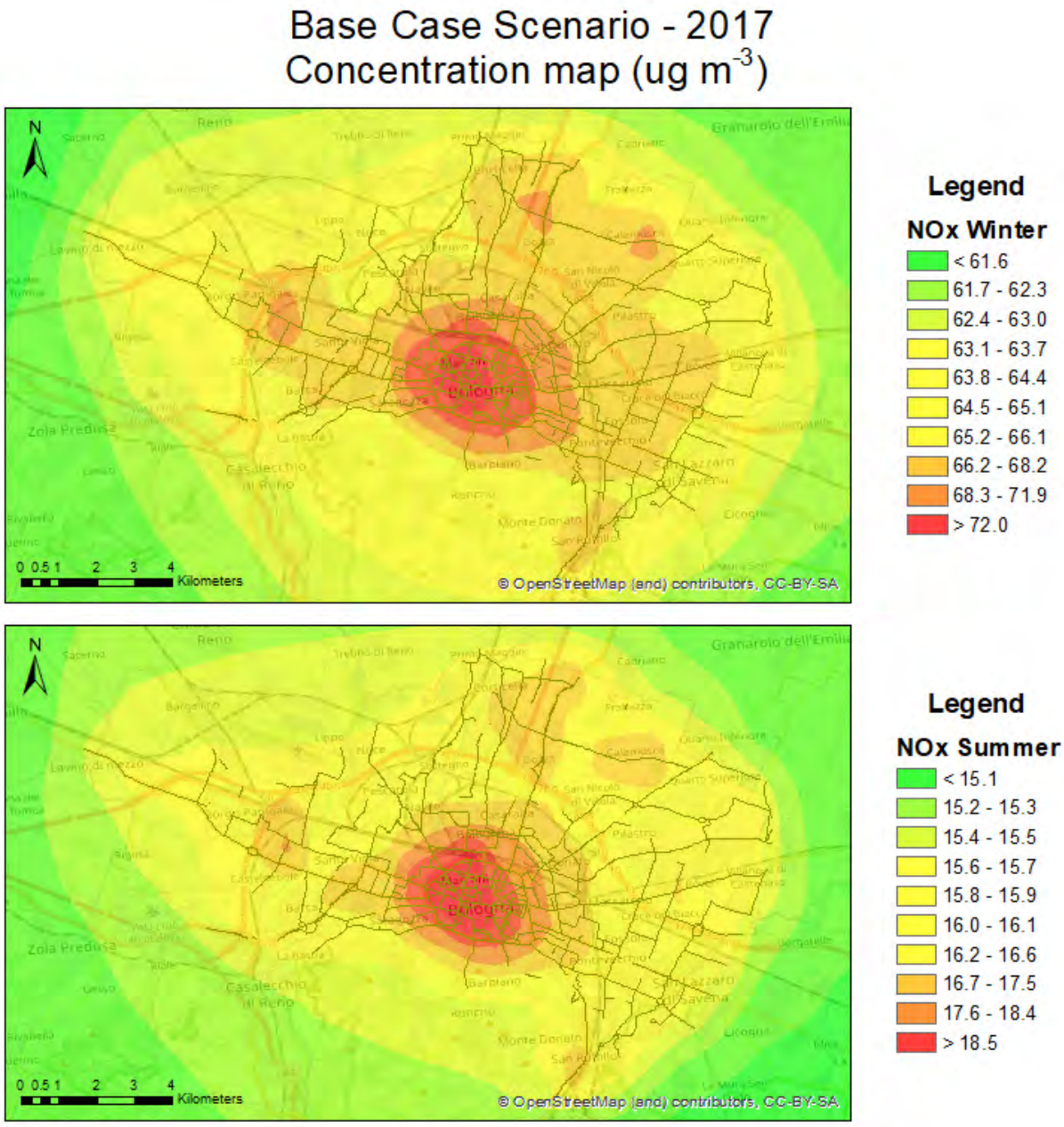

Figure 45. Concentration maps for NO_x (top: winter, bottom: summer) in the 2017BC scenario for Bologna. The maps represent concentration values averaged over the period considered.

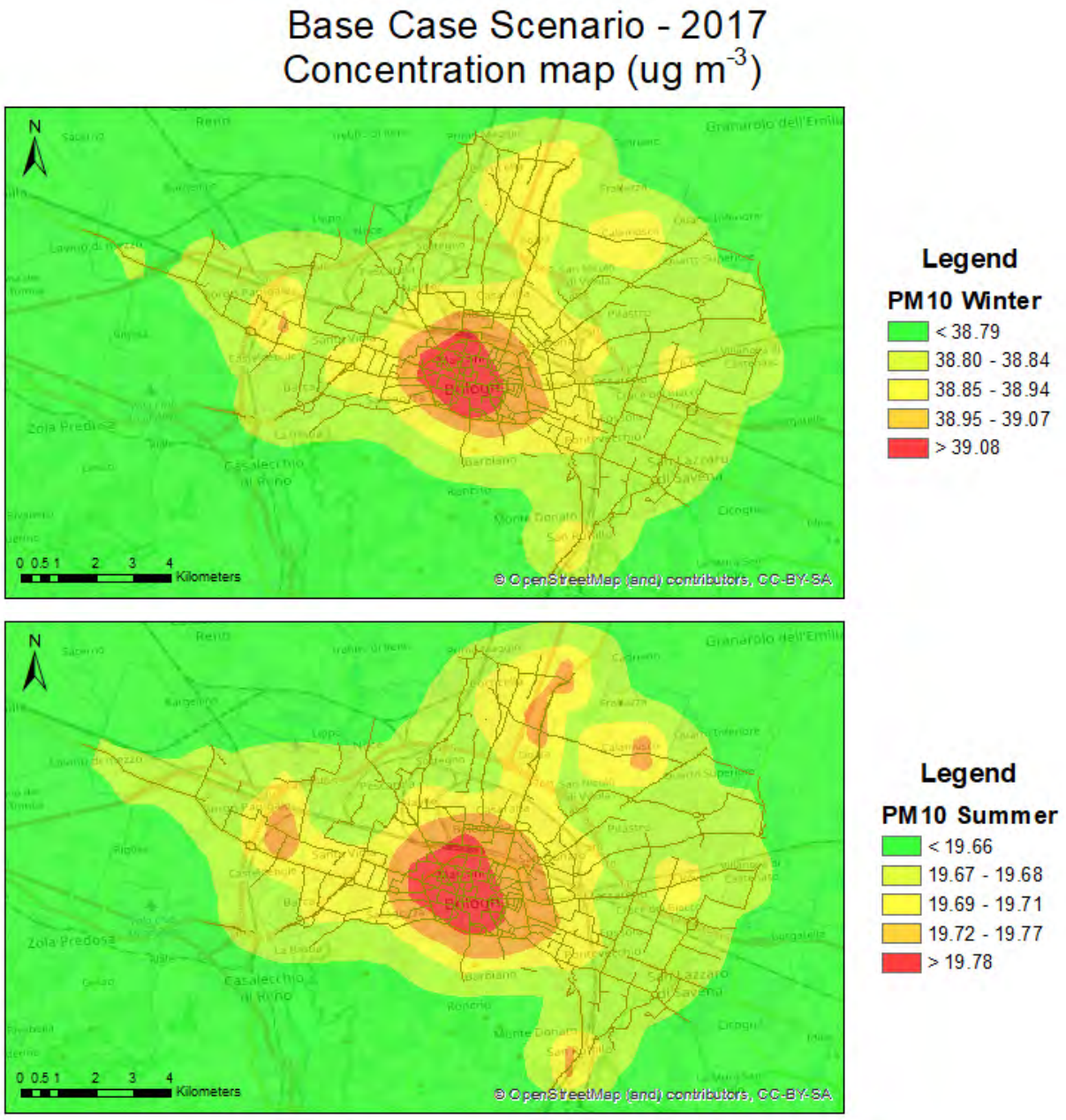

Figure 46. Concentration maps for PM_{10} (top: winter, bottom: summer) in the 2017BC scenario for Bologna. The maps represent concentration values averaged over the period considered.

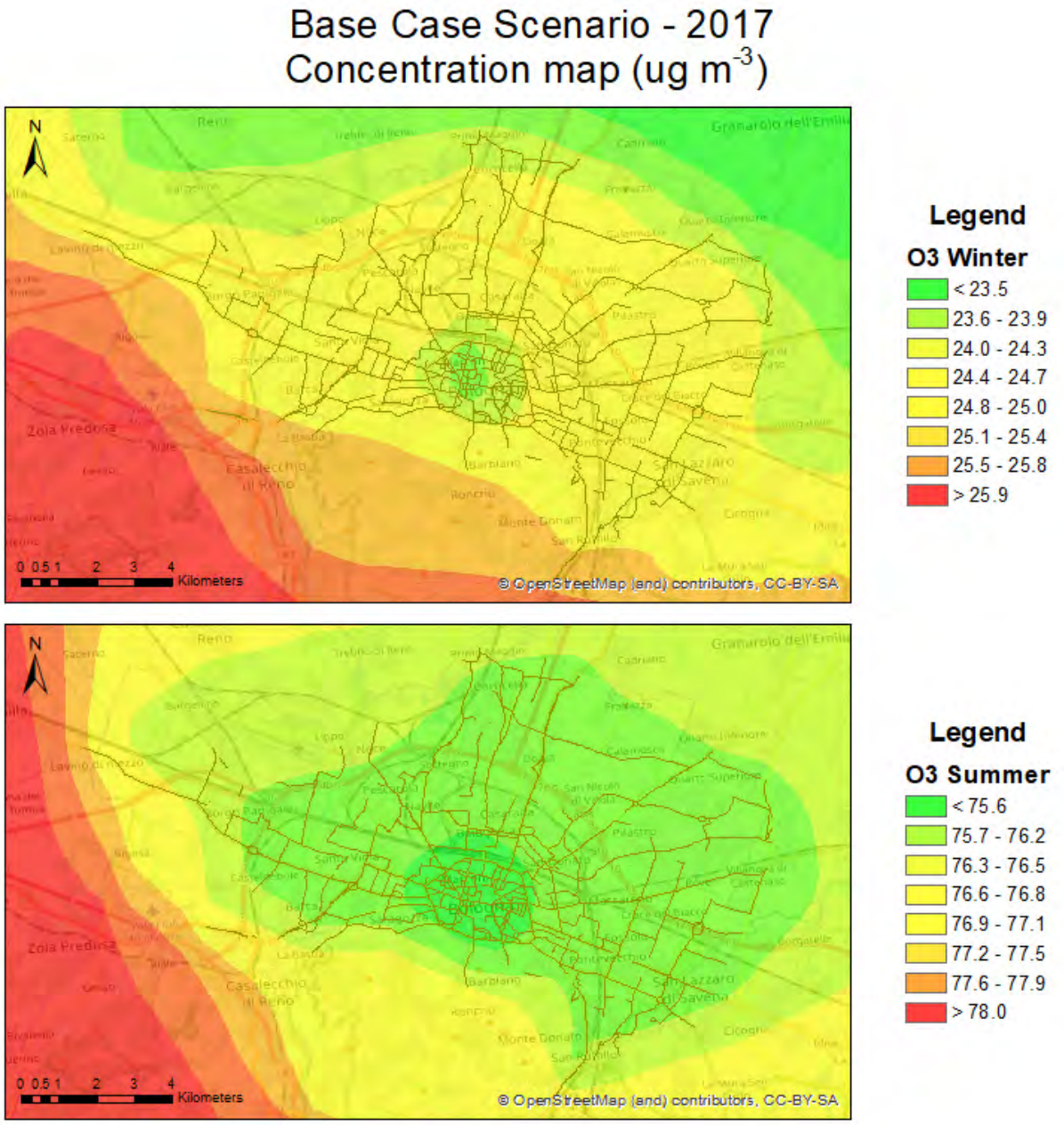

Figure 47. Concentration maps for O_3 (top: winter, bottom: summer) in the 2017BC scenario for Bologna. The maps represent concentration values averaged over the period considered.

This pattern is due to the titration effects of O_3 by NO. The high NO_2 concentrations, typical of urban areas, tend to produce O_3 from NO_2 reaction under warm and sunny conditions. The winds transport the O_3 produced in urban areas to the country and mountain areas, where the reduced NO concentrations inhibit O_3 degradation and allow its accumulation.

The highest concentration values of O_3 are found in both seasons in the southwest area of the city. The wind roses in Figure 48 show the wind directions and speeds with their relative frequencies in the two periods considered in Bologna.

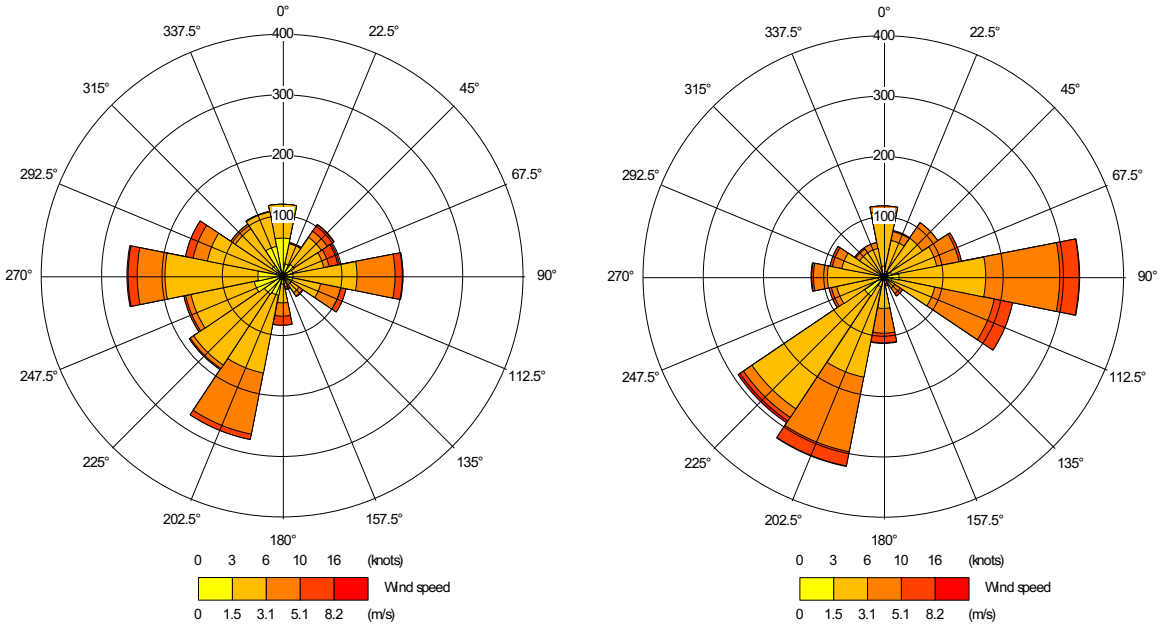

Figure 48. Wind rose for base reference case in Bologna, winter (left) and summer (right) 2017. Data from LIPE meteorological station.

In general, this simulation shows that the centre of Bologna is the main pollution hot spot for all pollutants. The comparison of the average values at the receptors (point corresponding to the ARPAE control units, used in the simulations to model the dispersion at that point), highlights how winter represents a critical period (Table 14).

Season	Receptor name	NO_x ($\mu g\ m^{-3}$)	NO_2 ($\mu g\ m^{-3}$)	CO ($mg\ m^{-3}$)	O_3 ($\mu g\ m^{-3}$)	PM_{10} ($\mu g\ m^{-3}$)
Winter	V. Chiarini	64.8	41.4	0.82	24.8	38.8
Winter	Porta S. Felice	166.0	60.6	0.85	18.4	43.15
Winter	Giardini Margherita	66.2	41.83	0.82	24.7	38.9
Summer	V. Chiarini	15.8	12.1	0.47	76.2	19.7
Summer	Porta S. Felice	60.8	30.2	0.48	63.3	21.6
Summer	Giardini Margherita	16.2	12.3	0.47	76.0	19.7

Table 14. Average concentration values to receptors in winter and summer for the 2017BC scenario in Bologna.

4.2.1.2 Policy 1: Electric Centre

As reported in section 3, the policy 1 that we tested on the territory of Bologna is a traffic limitation for the entire area inside the inner ring road. Light and heavy vehicles are forbidden in the internal ring road, while only electric vehicles are allowed to enter and circulate in this area.

The comparison of the average values of receptors in Electric Centre scenario (2017P1EC scenario) for the two periods (Table 15), shows that the winter is still a critical period. However, the average concentrations are lower than in the 2017BC scenario for all pollutants, except for ozone.

Season	Receptor name	NO_x ($\mu g\ m^{-3}$)	NO_2 ($\mu g\ m^{-3}$)	CO ($mg\ m^{-3}$)	O_3 ($\mu g\ m^{-3}$)	PM_{10} ($\mu g\ m^{-3}$)
Winter	V. Chiarini	64.7	41.4	0.82	24.8	38.8
Winter	Porta S. Felice	65.3	41.5	0.83	24.8	39.3
Winter	Giardini Margherita	64.7	41.3	0.82	24.9	38.8
Summer	V. Chiarini	15.7	12.0	0.47	76.3	19.7
Summer	Porta S. Felice	15.9	12.1	0.47	76.2	19.9
Summer	Giardini Margherita	15.7	12.0	0.47	76.3	19.7

Table 15. Average concentration values to receptors in winter and summer for 2017P1EC scenario in Bologna

Figure 49 and Figure 50 (winter case, summer case not shown) show the concentration maps for NO_x and PM_{10} pollutants in 2017P1EC scenario for comparison with the 2017BC scenario. As a result of the policy, it can be noted that:

1) the maximum values have decreased compared to the base case, especially for NO_x;

2) also the spatial pattern has changed, in fact the hot spot located over the centre of Bologna is no more present, but it is possible to recognize different less intense hot spots distributed on the territory, near the busiest streets.

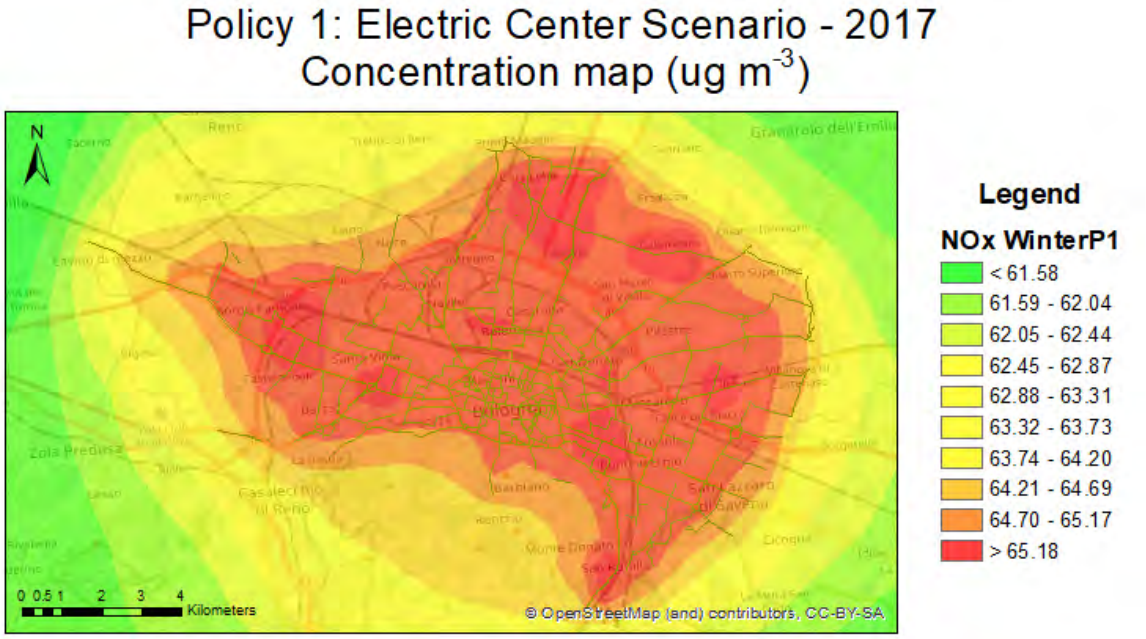

Figure 49. Concentration maps for NO_x in the 2017P1EC scenario for Bologna. The maps represent concentration values averaged over winter 2017.

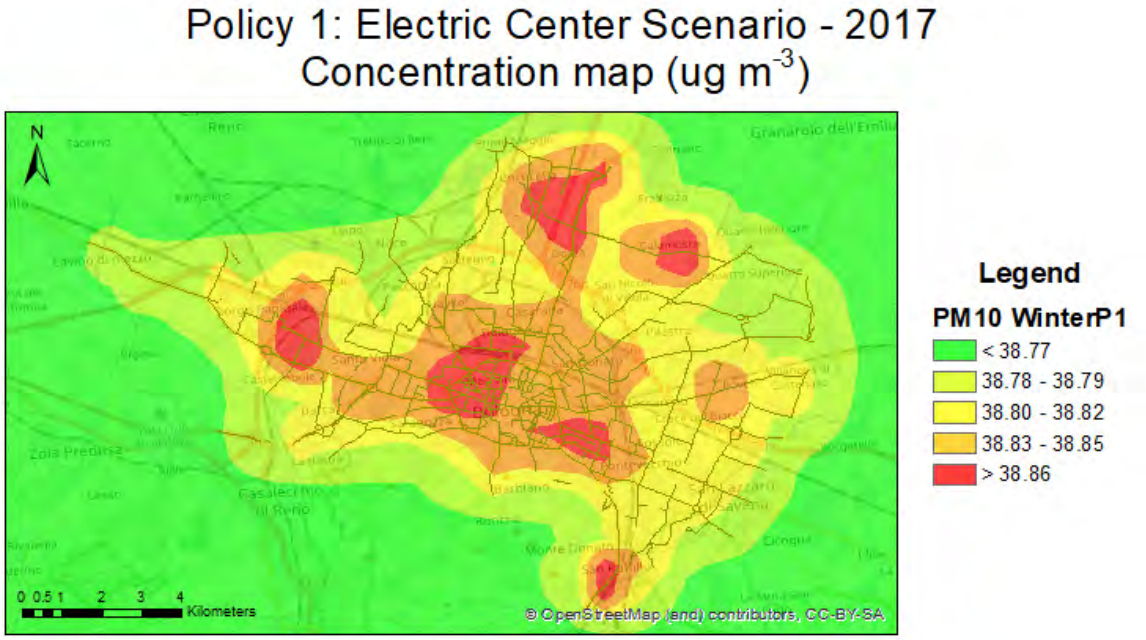

Figure 50. Concentration maps for PM_{10} in the 2017P1EC scenario for Bologna. The maps represent concentration values averaged over winter 2017.

Maps of concentration differences between the two scenarios are presented to highlight more clearly the effect of the policy in terms of increase and decrease in concentrations. Below, the maps for NO_x and PM_{10} are presented, while the concentration maps for O_3, NO_2, and CO are not shown.

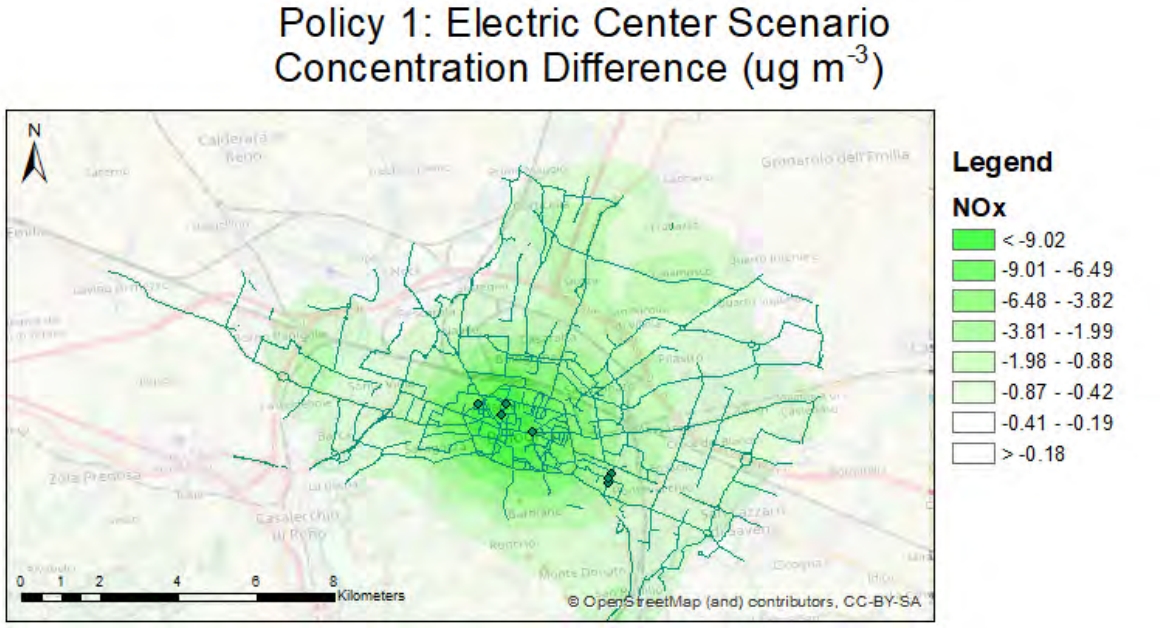

Figure 51. Maps of concentration differences for NO_x for winter 2017. The differences are calculated between 2017P1EC scenario and 2017BC scenario.

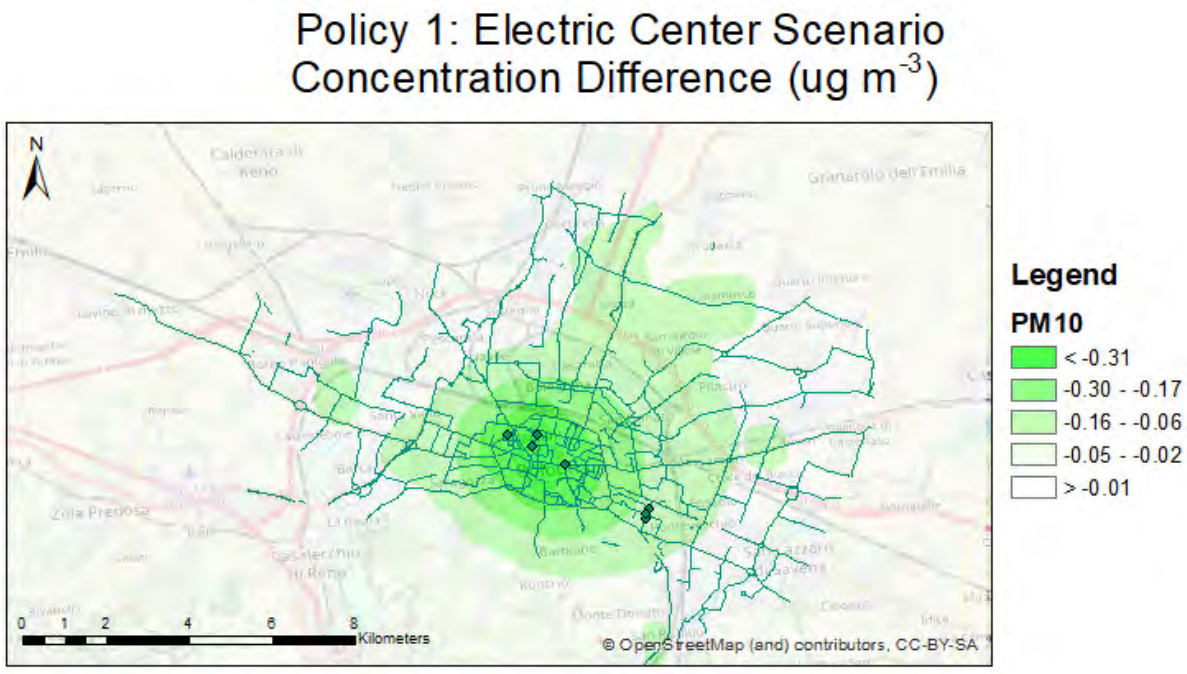

Figure 52. Maps of concentration differences for PM_{10} for winter 2017. The differences are calculated between 2017P1EC scenario and 2017BC scenario.

Figure 51 and Figure 52 show a decrease in concentrations over the city centre. Therefore, the effect of the policy can be considered satisfactory, as shown by the percentages of reduction/increase in concentration, compared to the base case (Table 16, calculated for all the receptor sites).

Policy	Season	Receptor name	NO_x	NO_2	CO	O_3	PM_{10}
1	Winter	V. Chiarini	-0.2%	-0.2%	0.0%	0.1%	0.0%
1	Winter	Porta S. Felice	-61%	-32%	-2%	35%	-9%
1	Winter	Giardini Margherita	-2%	-1%	-0.1%	1%	-0.2%
1	Summer	V. Chiarini	-1%	-1%	0.0%	0.1%	0.0%
1	Summer	Porta S. Felice	-74%	-60%	-2%	20%	-8%
1	Summer	Giardini Margherita	-3%	-3%	0.0%	0.3%	-0.1%

Table 16. Percentages of reduction/increase in concentration in the policy 1 scenario compared to the base case (calculated for all the receptor sites).

4.2.1.3 Policy 2: Electric Buses

The second policy implemented in Bologna concerns the conversion of the entire urban buses fleet to electric. Furthermore, we also considered that the city centre (the area inside the internal ring road) will be affected by an increase in bus frequency and a ban on all non-electric vehicles.

The comparison of the average values of receptors in Electric Buses scenario (2017P2EB scenario) for the two periods shows that the winter is still a critical period (Table 17). However, averages are lower than the 2017BC scenario for all pollutants, with the exception of ozone and PM_{10}.

Season	Receptor name	NO_x ($\mu g\ m^{-3}$)	NO_2 ($\mu g\ m^{-3}$)	CO ($mg\ m^{-3}$)	O_3 ($\mu g\ m^{-3}$)	PM_{10} ($\mu g\ m^{-3}$)
Winter	V. Chiarini	64.8	41.4	0.82	24.8	38.8
Winter	Porta S. Felice	65.8	41.6	0.83	24.7	44.7
Winter	Giardini Margherita	64.7	41.3	0.82	24.9	38.9
Summer	V. Chiarini	15.8	12.0	0.47	76.2	19.7
Summer	Porta S. Felice	16.1	12.2	0.47	76.0	22.2
Summer	Giardini Margherita	15.8	12.0	0.47	76.2	19.7

Table 17. Average concentration values to receptors in winter and summer for 2017P2EB scenario in Bologna.

Figure 53 and Figure 54 (winter case, summer case not shown) show the concentration maps for the NO_x and PM_{10} pollutants (concentration maps for O_3, NO_2, and CO have been evaluated but are not shown) in the 2017P2EB scenario for the comparison with the 2017BC scenario. Compared to the base case, this policy also results in a decrease in the maximum values, especially for NO_x. Regarding the spatial pattern, NO_x concentrations present several hot spots, less intense and distributed throughout the territory, close to the most trafficked roads, while the PM_{10} concentrations still show a hot spot in the

centre of Bologna. This could be caused by non-exhaust emissions due to increased frequency in electric buses.

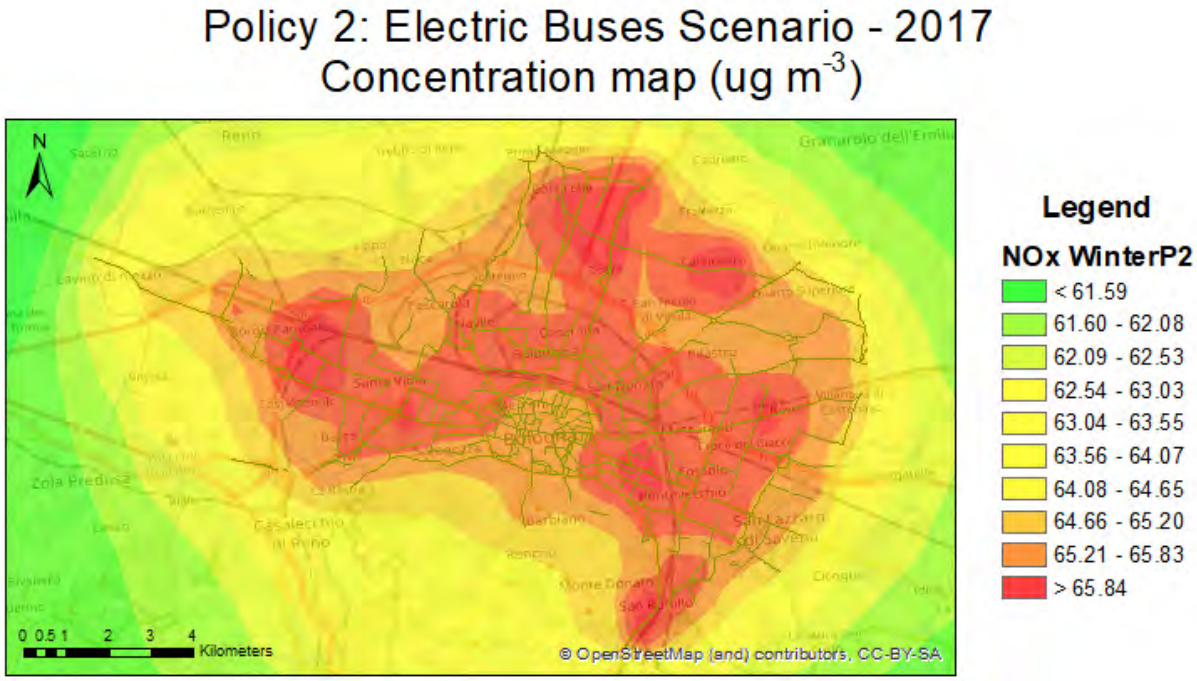

Figure 53. Concentration maps of NO_x in the 2017P2EB for Bologna. The maps represent concentration values averaged over winter 2017.

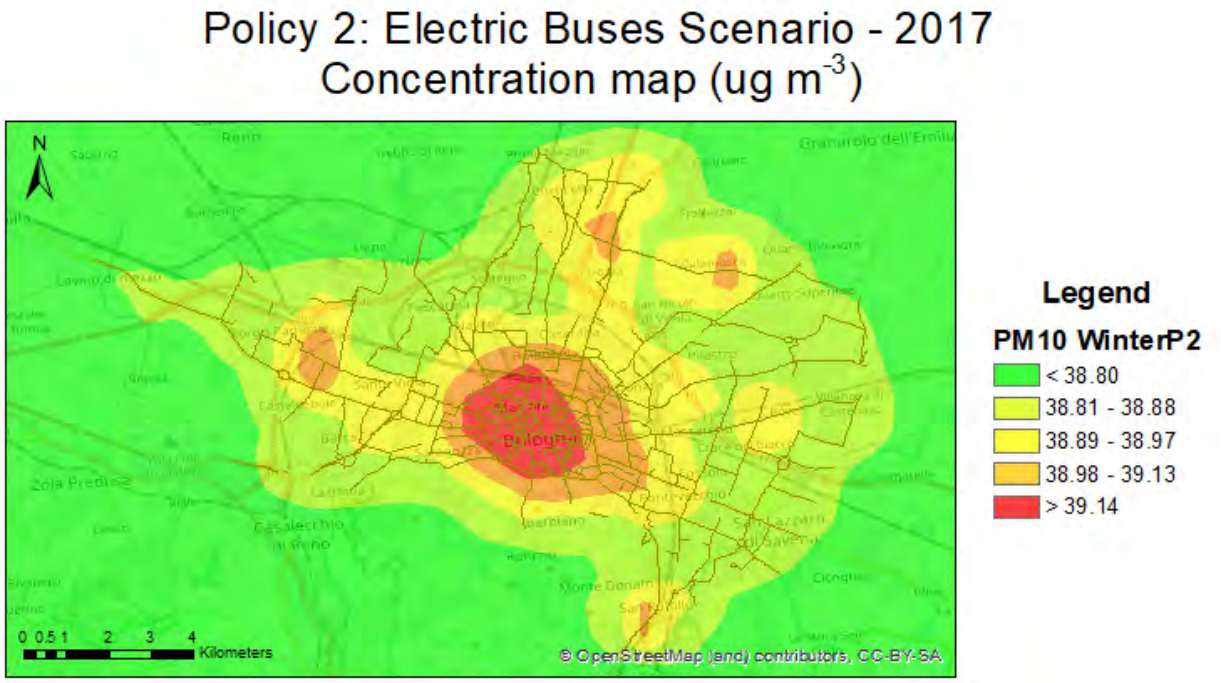

Figure 54. Concentration maps of PM_{10} in the 2017P2EB for Bologna. The maps represent concentration values averaged over winter 2017.

For the comparative analysis with the 2017BC scenario, also in this case maps of concentration differences are presented. Figure 55 and Figure 56 show maps of concentration differences for NO_x and PM_{10} (for O_3, NO_2, and CO are not shown).

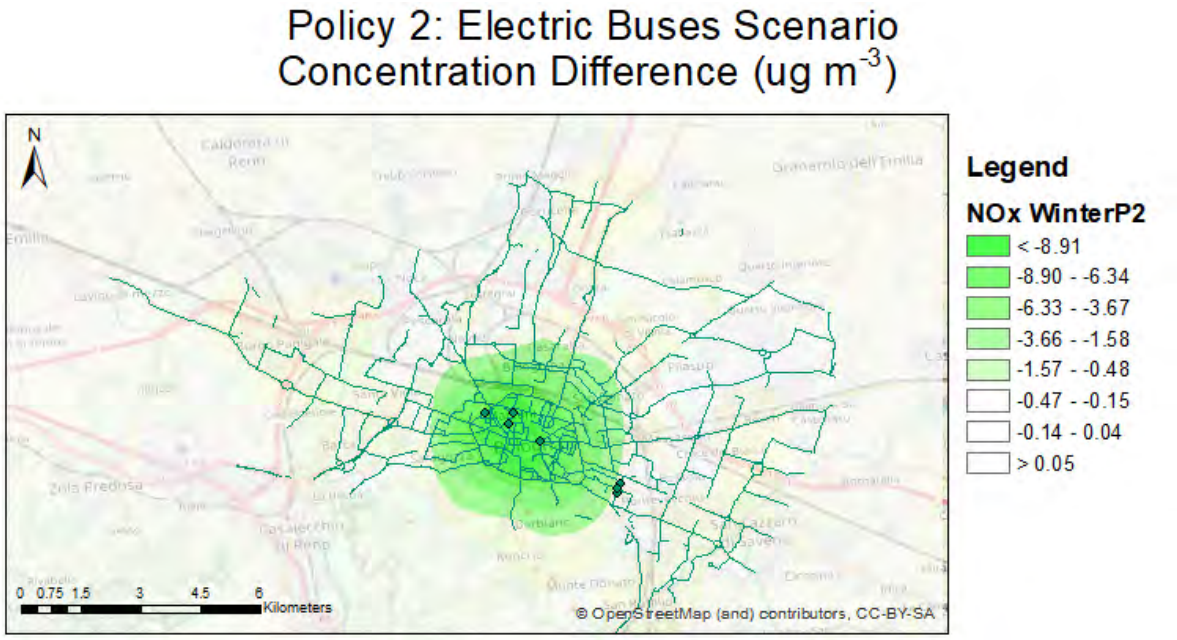

Figure 55. Maps of concentration differences for NO_x for winter 2017. The differences are calculated between 2017P2EB scenario and 2017BC scenario.

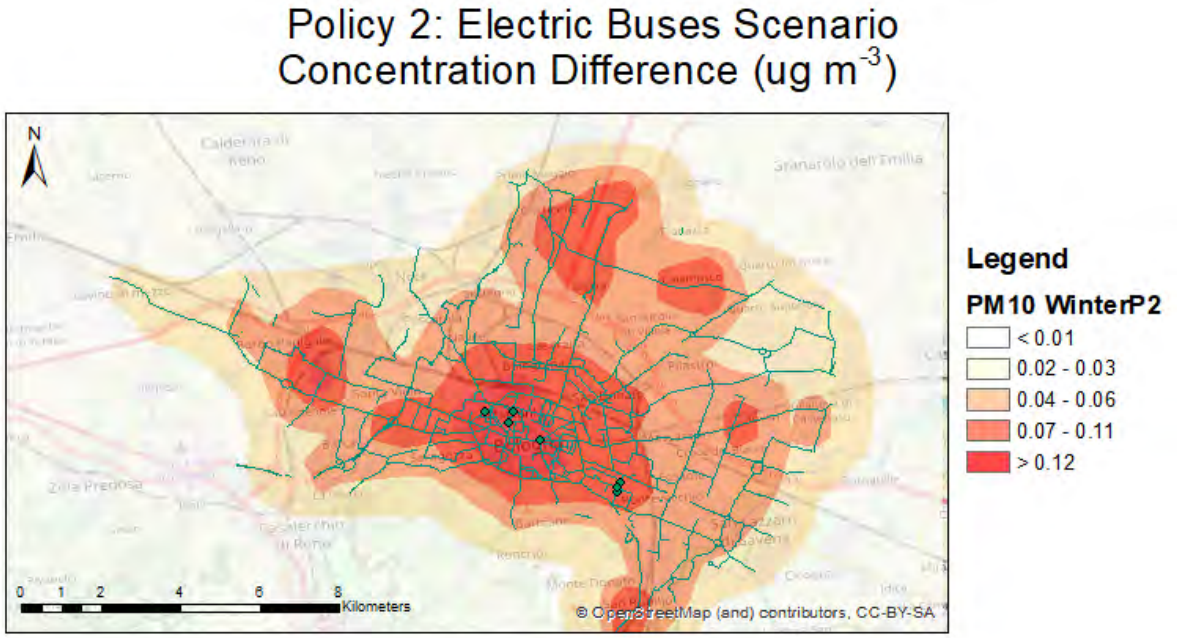

Figure 56. Maps of concentration differences for PM_{10} for winter 2017. The differences are calculated between 2017P2EB scenario and 2017BC scenario.

Also in the 2017P1EC scenario NO_x concentrations have decreased. In particular, it can be noted that there is no decrease for PM_{10}, which can be attributed to the non-exhaust emission due to the increased frequency of electric buses.

The effect of the policy can be considered satisfactory, as shown by the percentages of reduction/increase in concentration compared to the base case (Table 18, calculated for all receptor).

Policy	Season	Receptor name	NO_x	NO_2	CO	O_3	PM_{10}
2	Winter	V. Chiarini	-0.1%	-0.1%	0.0%	0.0%	0.1%
2	Winter	Porta S. Felice	-60.4%	-31.4%	-2.3%	34.7%	3.5%
2	Winter	Giardini Margherita	-2.2%	-1.2%	-0.1%	0.8%	0.1%
2	Summer	V. Chiarini	-0.3%	-0.3%	0.0%	0.0%	0.0%
2	Summer	Porta S. Felice	-73.4%	-59.6%	-1.8%	20.2%	2.8%
2	Summer	Giardini Margherita	-2.6%	-2.3%	0.0%	0.3%	0.1%

Table 18. Percentages of reduction/increase in concentration compared to the base case (calculated for all receptor).

The percentages of reduction are comparable with the policy 1 regarding the receptor positioned at Porta San Felice. The results obtained for the receptor of Giardini Margherita, located outside the centre of Bologna, can be used to evaluate the impact of this policy in more external areas. In these areas the reductions are smaller, which could be due to a lower impact of the policy. The percentages of increase of PM_{10}, as already discussed above, are due to the non-exhaust emissions due to the electric buses. This increase, however, is very limited, with a maximum of 3.5% (on the Porta San Felice receptor in winter) which corresponds to 1.5 $\mu g/m^3$ increase compared to the base case.

4.2.2 Hasselt

Since the performance of the model proved more satisfactory during the January month, in the following maps results from the present scenario (base reference case) and applying two selected policies in the current (baseline) scenario are presented only for that month. In addition, since the model presented a somewhat large NO_x overestimation, only maps of NO_2 and particulate matter in the form of PM_{10} are presented for all the cases. The evaluation of the policies is performed comparing the concentration maps obtained applying those policies to the traffic sources without altering the other input data (meteorological data, background concentrations, emissions of residential heating). Maps present the long-term averages considering the selected period (i.e. in this case, monthly).

4.2.2.1 Present scenario

Figure 57 and Figure 58 present the concentration maps for NO_2 and PM_{10} obtained considering the present scenario both for emissions and for meteorology (January 2016).

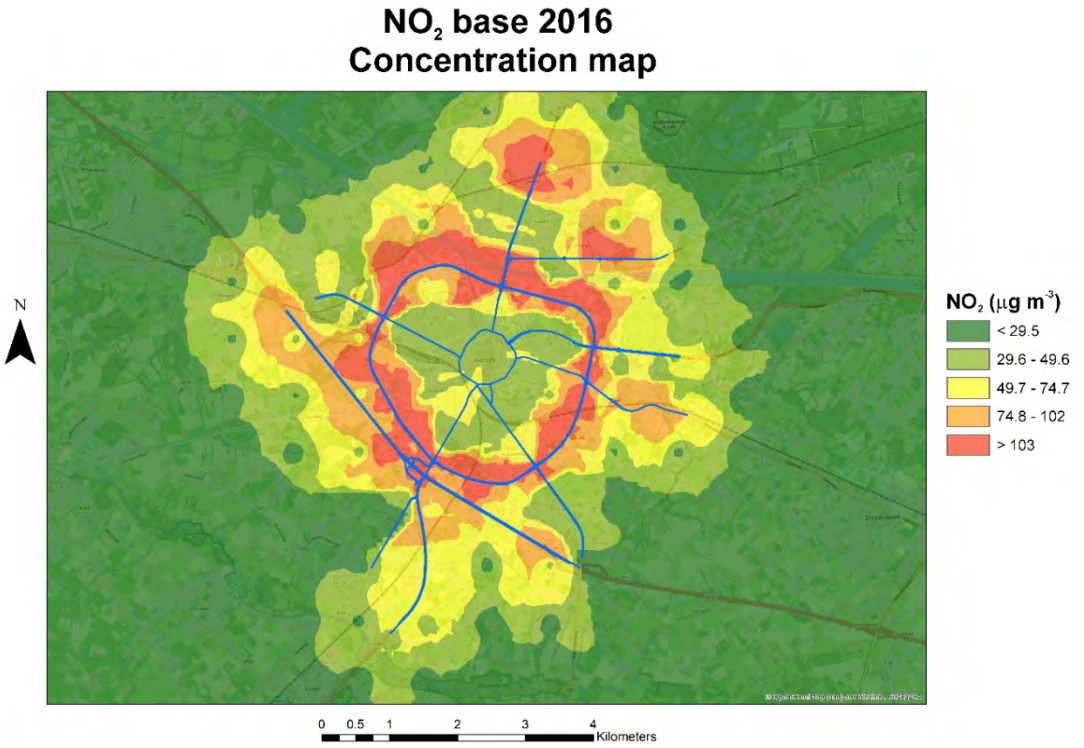

Figure 57. NO_2 concentration map for the Hasselt present scenario (January 2016 mean). Also shown are the major roads considered in the simulations. The map represents the average concentration for January 2016.

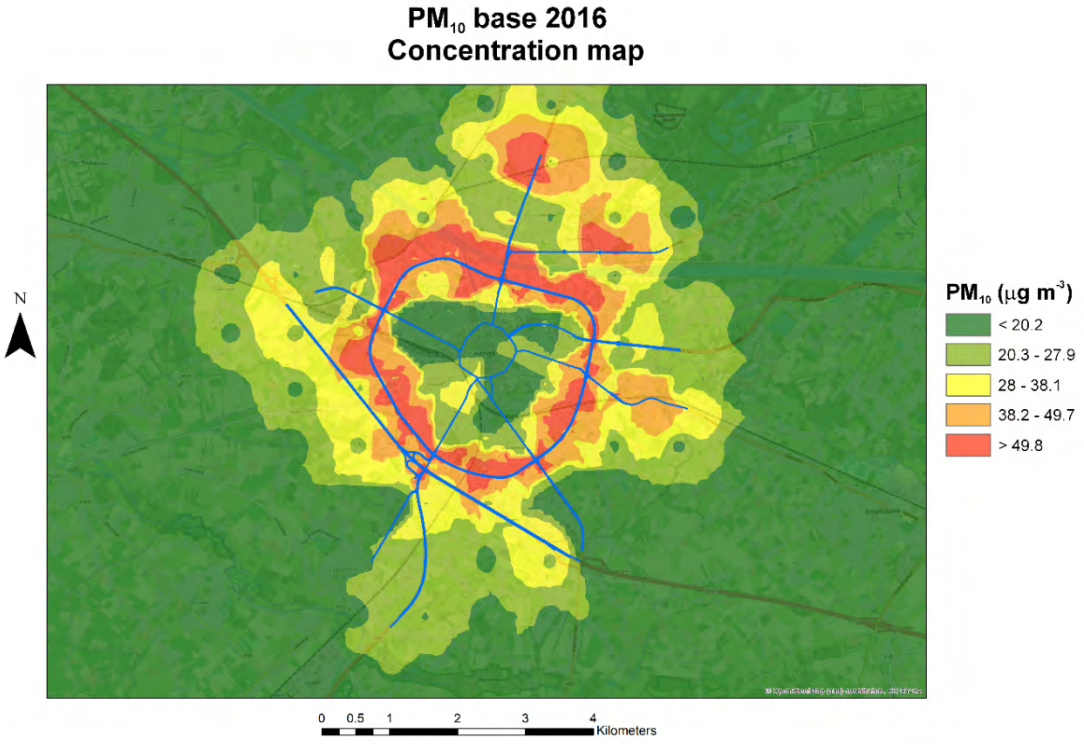

Figure 58. PM_{10} concentration map for the Hasselt present scenario (January 2016 mean). Also shown are the major roads considered in the simulations. The map represents the average concentration for January 2016.

Both Figures show a typical pattern with locally enhanced concentrations in the vicinity of major roads and especially of the outer ring. However, local hotspots are evidenced also in proximity of junctions, and especially one in the north of Hasselt close to the outer ring. This result, besides depending on local emissions, might depend also on the wind rose of the period, as the northern part of the city was always located upwind the major emitting sources (Figure 59). The inner ring, though also formed by major roads, is instead relatively lower impacted by traffic and other emitting sources, which seems to depend on the lower traffic counts (cf. emissions) as presented in the emission inventory (Section 3).

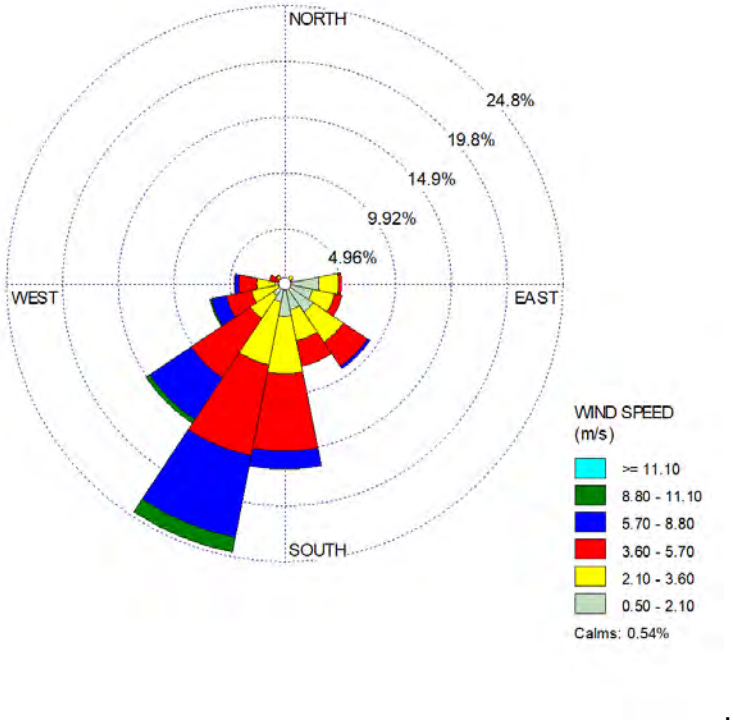

Figure 59. Wind rose for the January 2016 base reference case in Hasselt.

4.2.2.2 Policy 1: Closure of the inner ring

As reported in Section 3, the first policy implemented in Hasselt consisted in the complete closure of the Hasselt inner ring and of roads within it. As such, by construction this policy is expected to provide major changes in the emissions in the vicinity of the city centre, which should be reduced even though not zero because of the absence of change in residential heating largely impacting in the very populated city centre, as presented in Section 3.

Figure 60 and Figure 61 present the results in terms of concentration maps for NO_2 and PM_{10} pollutants previously considered in the base case scenario, for comparison. Although the concentration pattern is the same, as impacted and driven by the same meteorology, and in particular wind speeds and directions, it can be noted that minimum and maximum values are decreased with respect to the base case.

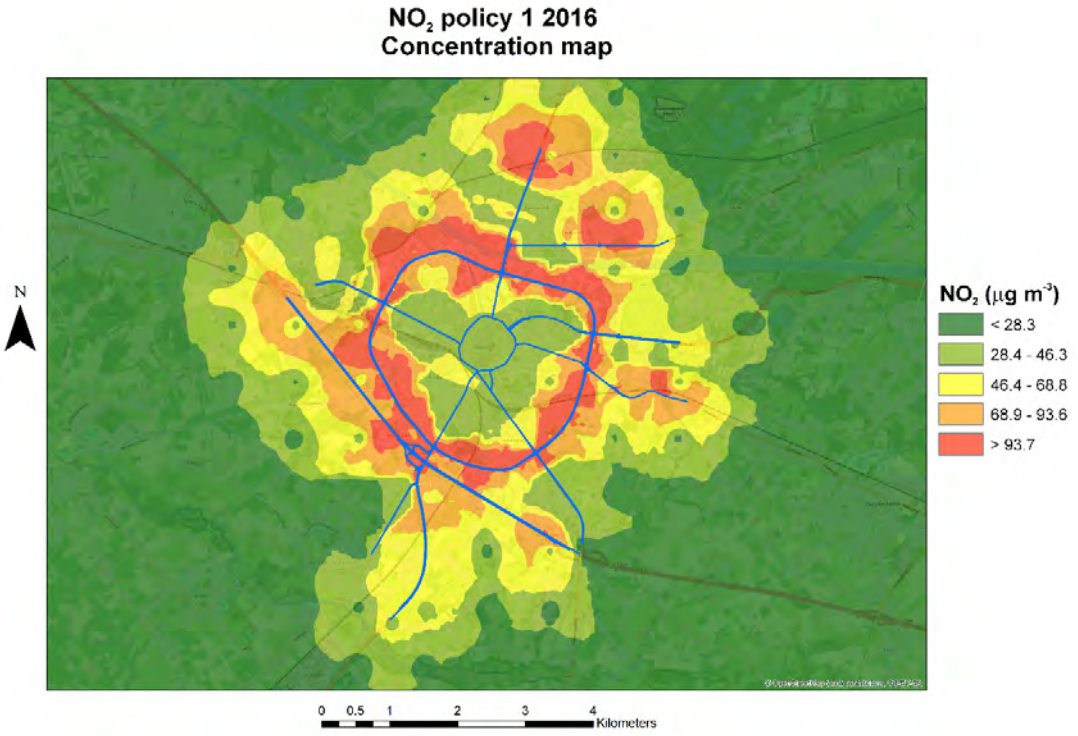

Figure 60. NO_2 concentration map for the implementation of the policy 1 for Hasselt case in the present (January 2016) scenario.

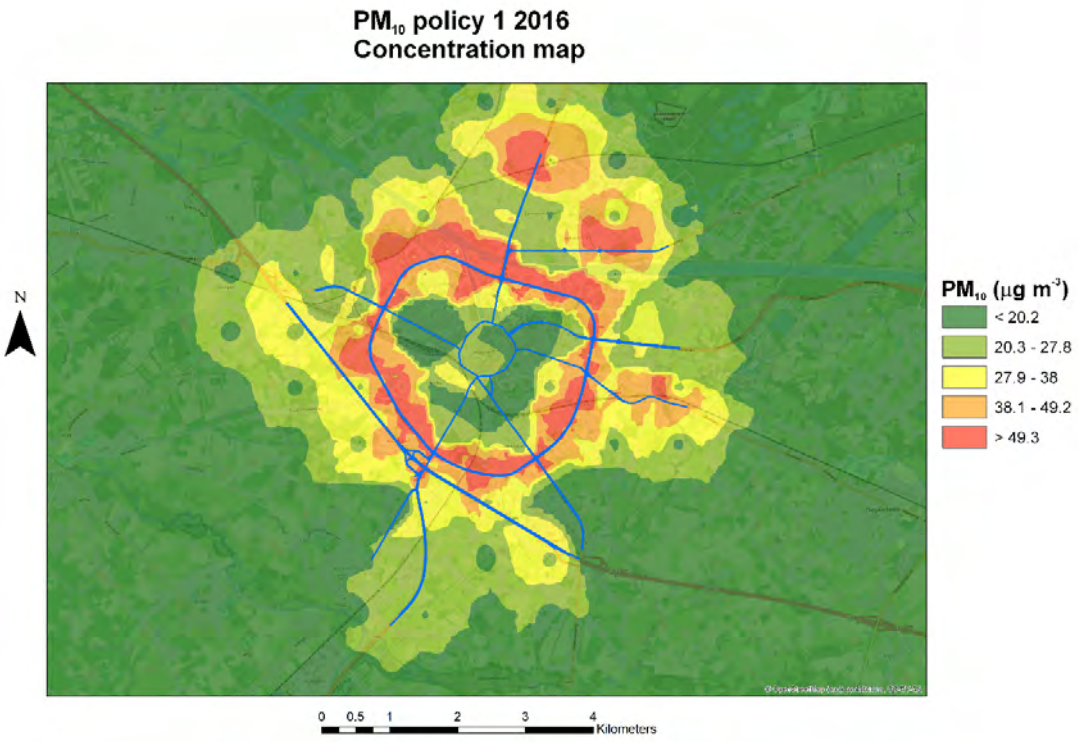

Figure 61. PM_{10} concentration map for the implementation of the policy 1 for Hasselt case in the present (January 2016) scenario.

The comparison is also presented in terms of maps of concentration differences between the scenario with the implementation of the policy 1 and the base case (Figure 62 and Figure 63). The Figures highlight more clearly the presence of large areas of reduced NO_2 and PM_{10} concentrations, even though in both cases also a few areas of increased concentrations emerge. These can possibly result from the increasing car traffic in other areas where the policy was not implemented and where cars that cannot enter the inner ring look for parking. Due to its complexity and the need of information for other variables to implement this policy in the behavioral simulation model, the precise position of such areas could be not totally correct. In general, however, the impact of this policy seems overall beneficial in the surroundings of the city centre where the policy is implemented and in the surroundings of the outer ring. In particular, this policy exhibits more potential in reducing NO_2 than PM_{10}, even though also increases are larger for NO_2 than for PM_{10}.

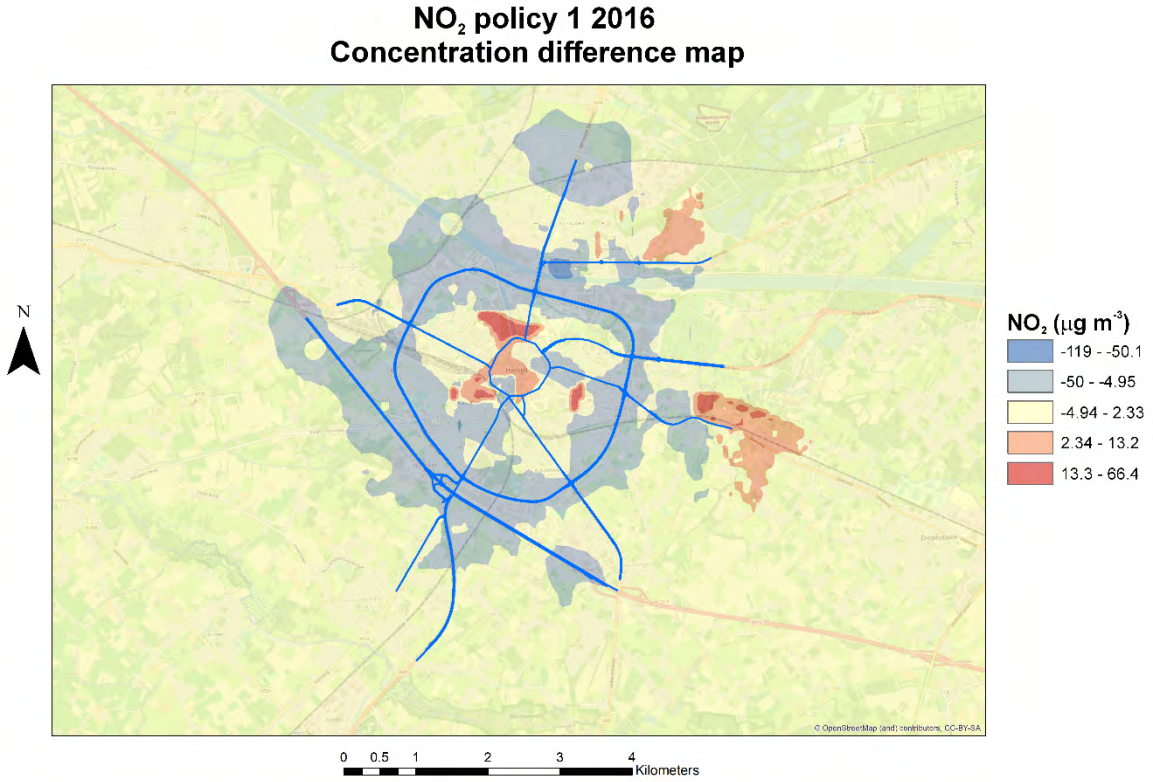

Figure 62. Map of differences in NO_2 concentration between the policy 1 scenario and the base case in Hasselt.

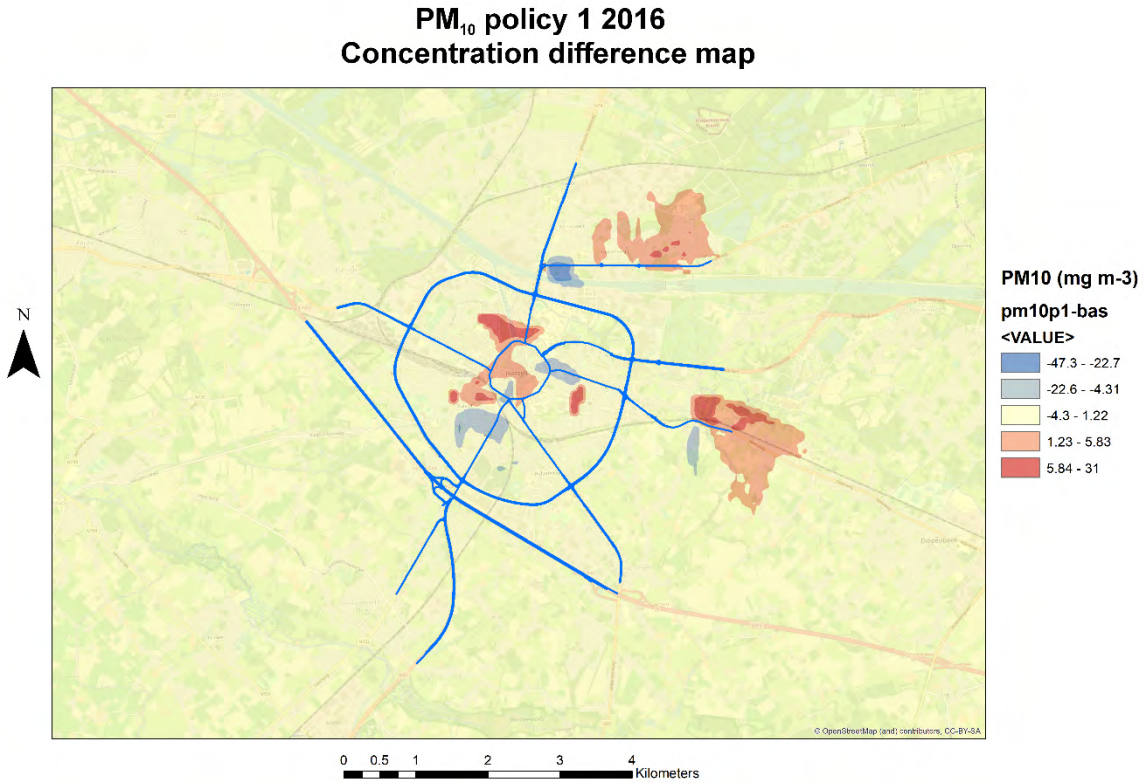

Figure 63. Map of differences in PM_{10} concentration between the policy 1 scenario and the base case in Hasselt.

Finally, we provide the maps of observed NO_2 and PM_{10} reductions in the scenario when the policy is implemented (Figure 64 and Figure 65), calculated as the ratio of the concentration differences previously presented (Figure 62 and Figure 63) and the concentration observed in the base case.

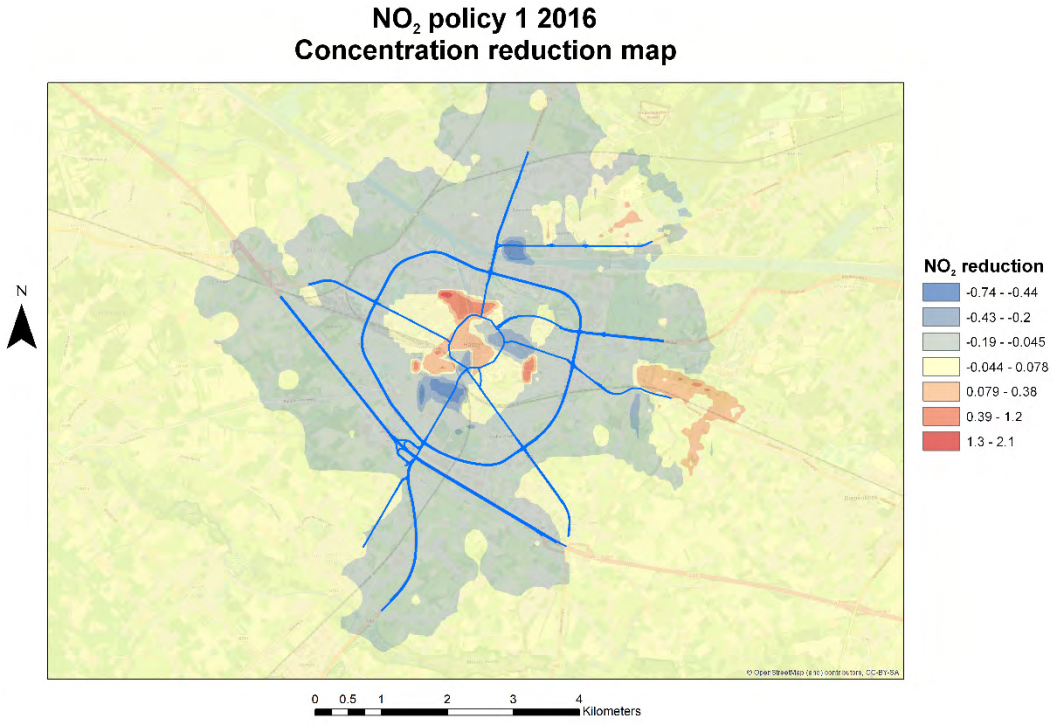

Figure 64. NO_2 reduction in the policy 1 scenario in Hasselt, evaluated as concentration ratio between the concentration difference previously evaluated (Figure 62) and the concentration observed in the base case (Figure 57).

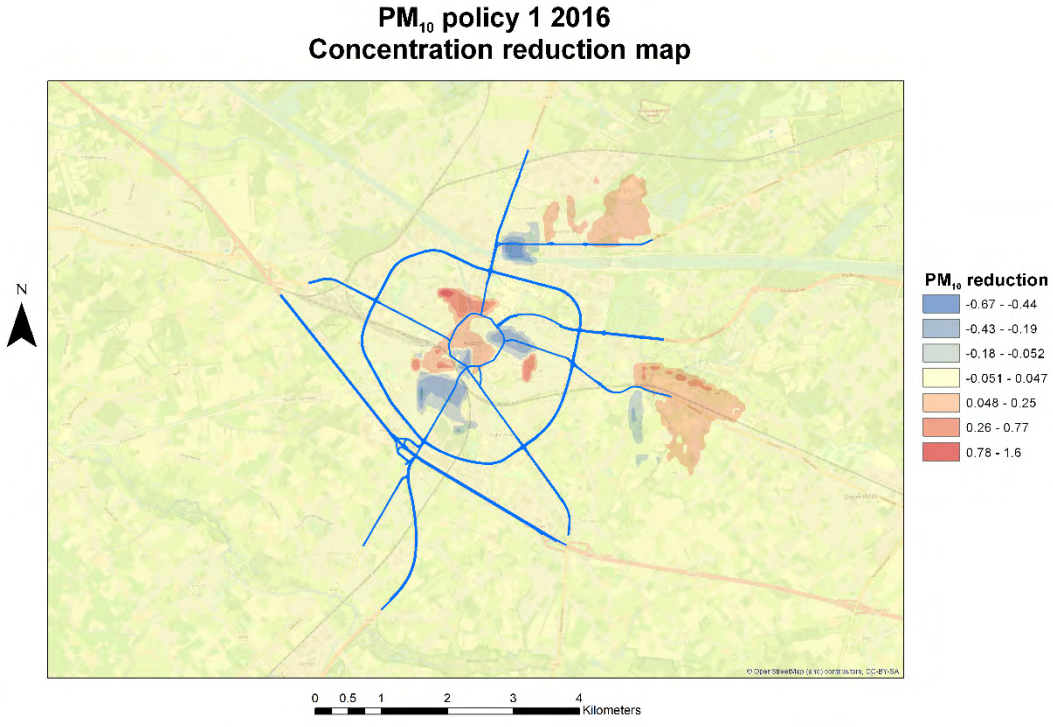

Figure 65. PM_{10} reduction in the policy 1 scenario in Hasselt, evaluated as concentration ratio between the concentration difference previously evaluated (Figure 63) and the concentration observed in the base case (Figure 58).

Maps of reductions indicate clearly that the policy effectively reduces NO_2 over a widespread area in the outer ring and its surroundings, while PM_{10} reductions, even though also significant (44-67%), are sparse and concentrated over limited areas. However, the implementation of this policy in the current (baseline) case may lead to reductions of NO_2 in the 44%-74% range over some areas in the surroundings of the inner ring and of 20-43% in the outer ring, which is clearly potentially beneficial to the health of Hasselt's citizens.

4.2.2.3 Policy 2: Increase in the frequency of buses

Results for the implementation of the policy 2 are presented in the same way of the results for policy 1, i.e. as concentration maps for this case and then as maps of concentration differences between the base case and the case with the policy. Here we must remember that in the second policy, the impact on air quality of increasing the frequency of buses in Hasselt, thus increasing the number of buses but decreasing the number of vehicles for private transport (i.e., light vehicles), was tested. Even in this case, minimum and maximum values are reduced with respect to the base case (Figure 66 and Figure 67).

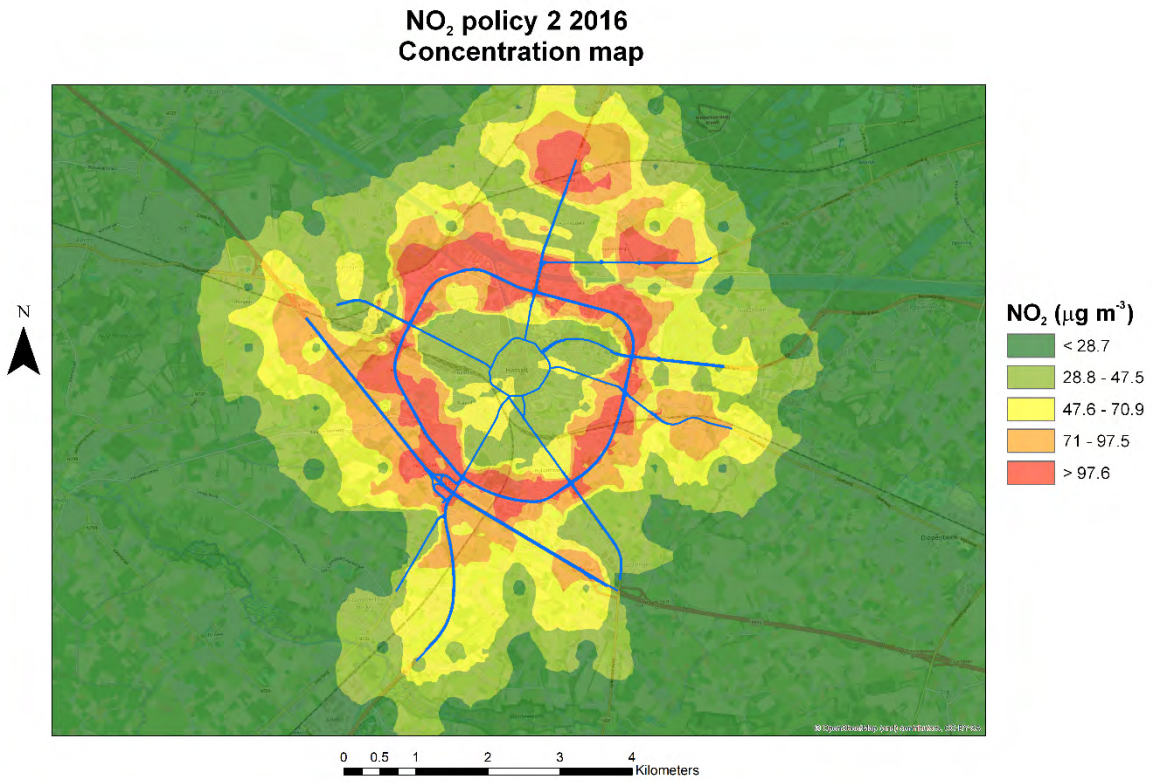

Figure 66. NO_2 concentration map for the implementation of the policy 2 for Hasselt case in the present (January 2016) scenario.

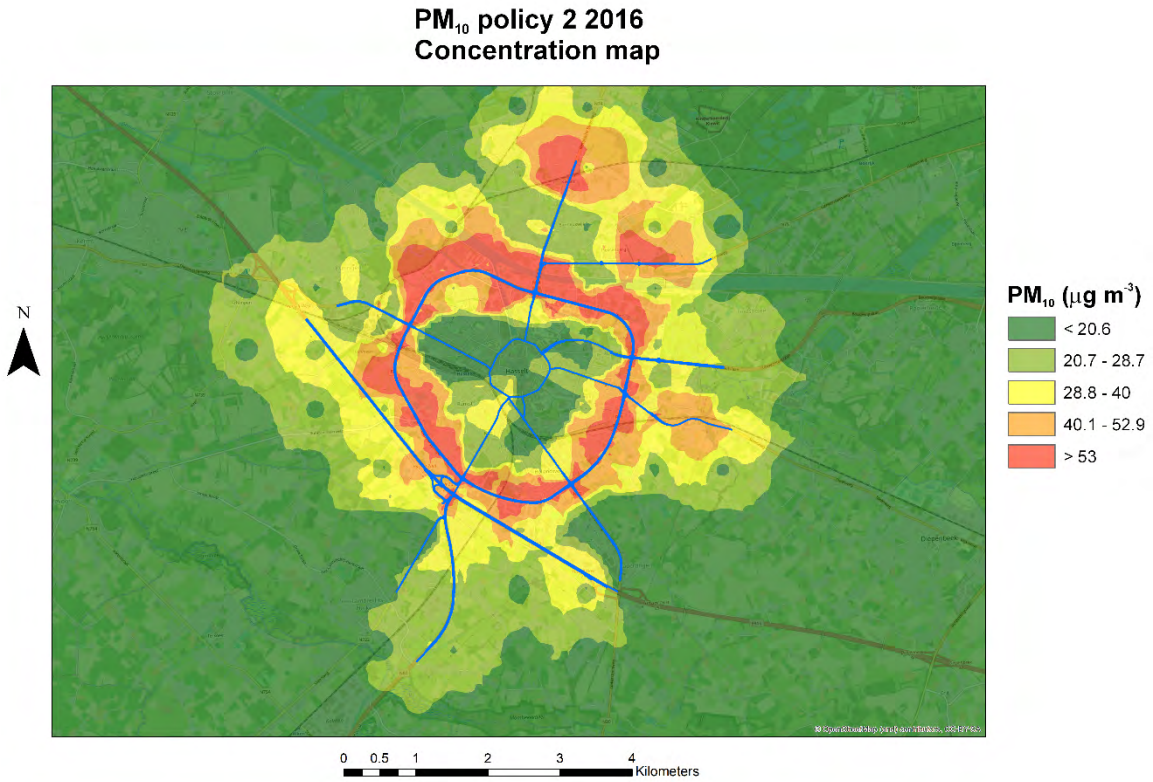

Figure 67. PM_{10} concentration map for the implementation of the policy 2 for Hasselt case in the present (January 2016) scenario.

.

The evaluation of maps of concentration differences (Figure 68 and Figure 69) between the scenario in which the policy 2 is implemented and the base case highlights no relevant change or even slight increases for NO_2 over the majority of the domain, but reductions are observed in the outer ring and its surroundings. These reductions can be attributed to the reduction of traffic due to the change of transport mode from private cars to public transport, which seems particularly important and effective over pollution hotspots. On the contrary, PM_{10} concentrations tend to increase in particular close to the city centre and major roads of the outer ring. The reason of the PM_{10} increase may be linked to the increase in the buses and to its effect on non-exhaust emissions, i.e. those produced by abrasion on mechanical parts (tires, brakes) due to their large load weight, far higher than that of light vehicles. Finally, this policy seems more impacting on air quality in the city than the first one, as partially expected due to the very local change implemented over an already largely pedestrian area in the first case.

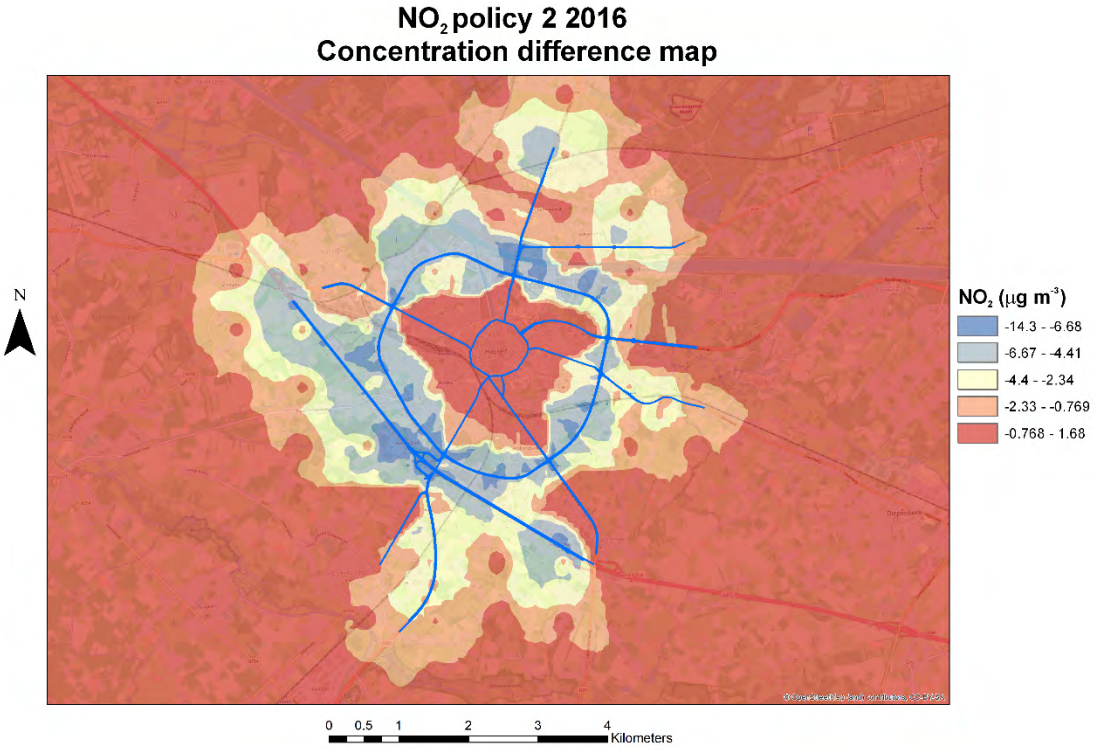

Figure 68. Map of difference in NO_2 concentration between the base case and the policy 2 case in Hasselt.

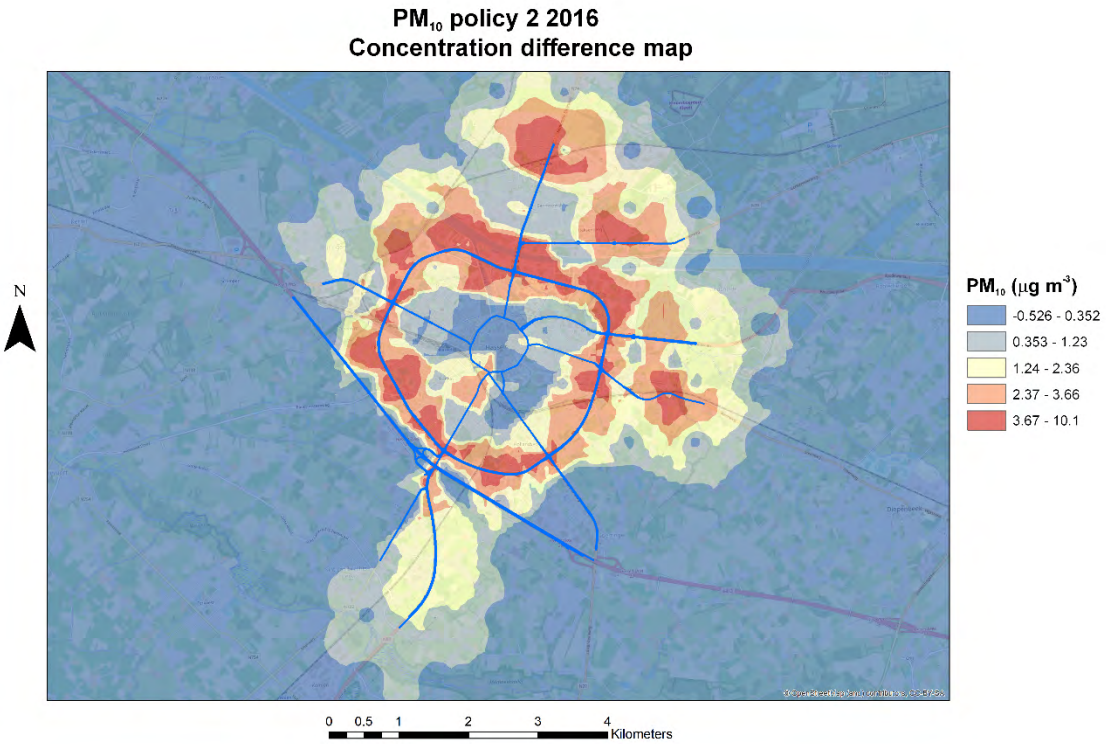

Figure 69. Map of difference in PM_{10} concentration between the base case and the policy 2 case in Hasselt.

Again, as done in the policy 1 scenario, we then present the maps of reductions observed in the policy 2 scenario with respect to the base case. As previously noted, the two maps reveal clearly that the policy does not provide significant reductions for NO_2. For PM_{10}, areas of strong increases are also observed, which can be due to the high PM_{10} emissions generated by mechanical wear of all the parts of vehicles, which are especially important for buses due to their large weight load. In this case, reductions are more limited both for NO_2 as well as for PM_{10}, with maxima reductions of 6-8% and 0.8-1.3% for NO_2 and PM_{10}, respectively.

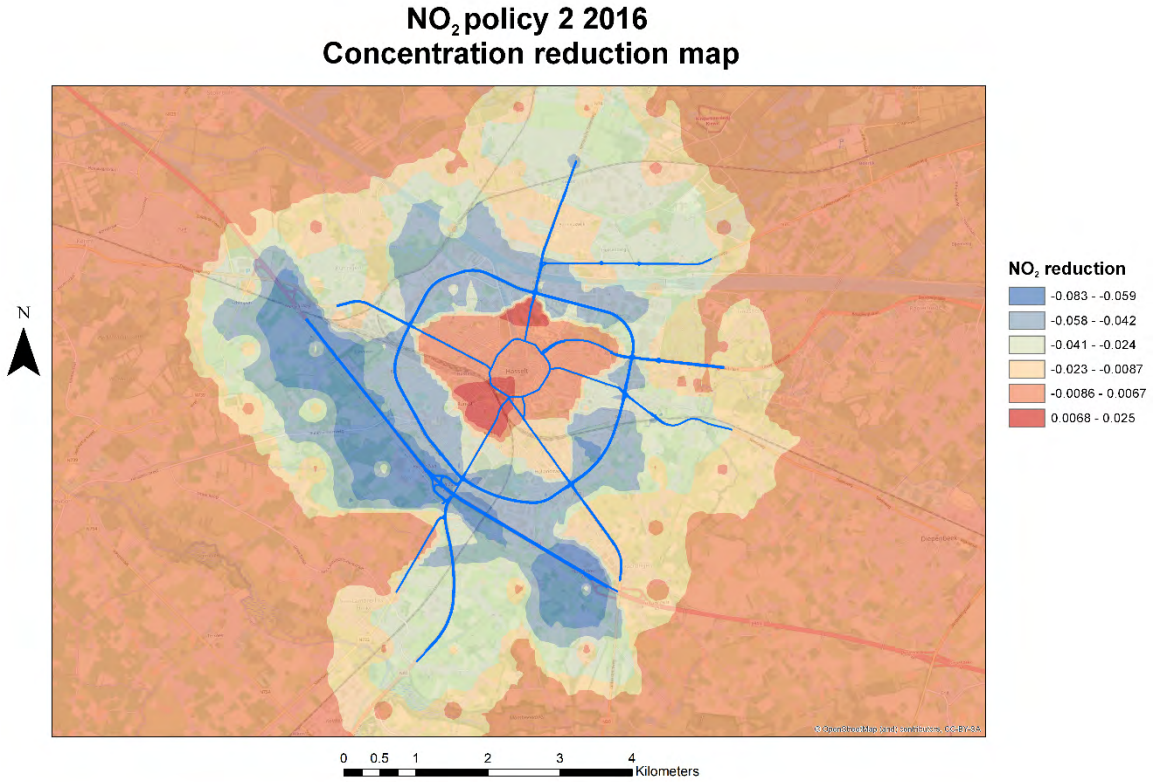

Figure 70. NO_2 reduction in the policy 2 scenario in Hasselt, evaluated as concentration ratio between the concentration difference previously evaluated (Figure 68) and the concentration observed in the base case (Figure 57).

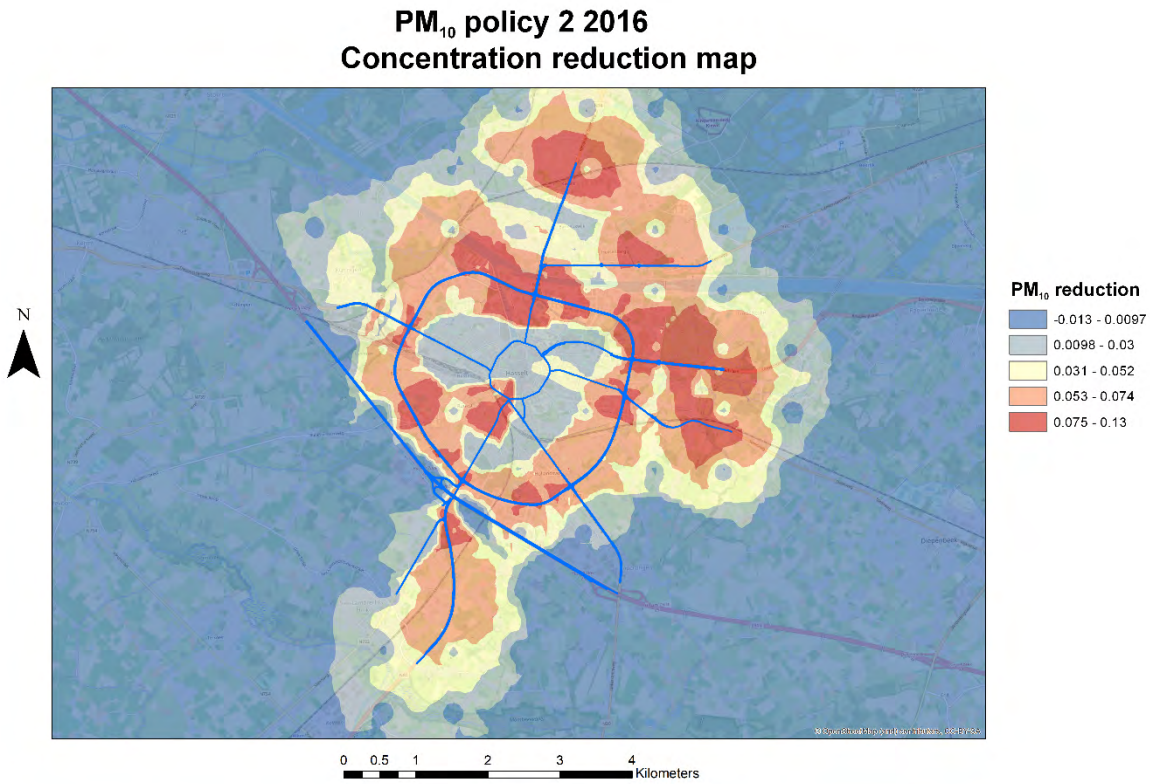

Figure 71. PM_{10} reduction in the policy 2 scenario in Hasselt, evaluated as concentration ratio between the concentration difference previously evaluated (Figure 69) and the concentration observed in the base case (Figure 58).

4.2.3 Vantaa

The model performance for Vantaa was evaluated comparing simulated NO2 and PM2.5 concentrations with observed concentrations of the same pollutants at three air quality stations during the January 2017 month. In the following, therefore, results obtained in the present reference scenario and applying one policy in the reference scenario will be presented only for NO2 and PM2.5 concentrations for the month of January 2017. As done previously for Hasselt, the evaluation of the policy is performed comparing the concentration maps obtained applying the policy to the traffic sources without altering the other input data (meteorological data, background concentrations, emissions of residential heating). Maps present the long-term averages considering the selected period (i.e. in this case, monthly).

4.2.3.1 Present scenario

Figure 72 and Figure 73 present the concentration maps for NO_2 and PM_{10} obtained considering the present scenario both for emissions and for meteorology (January 2017).

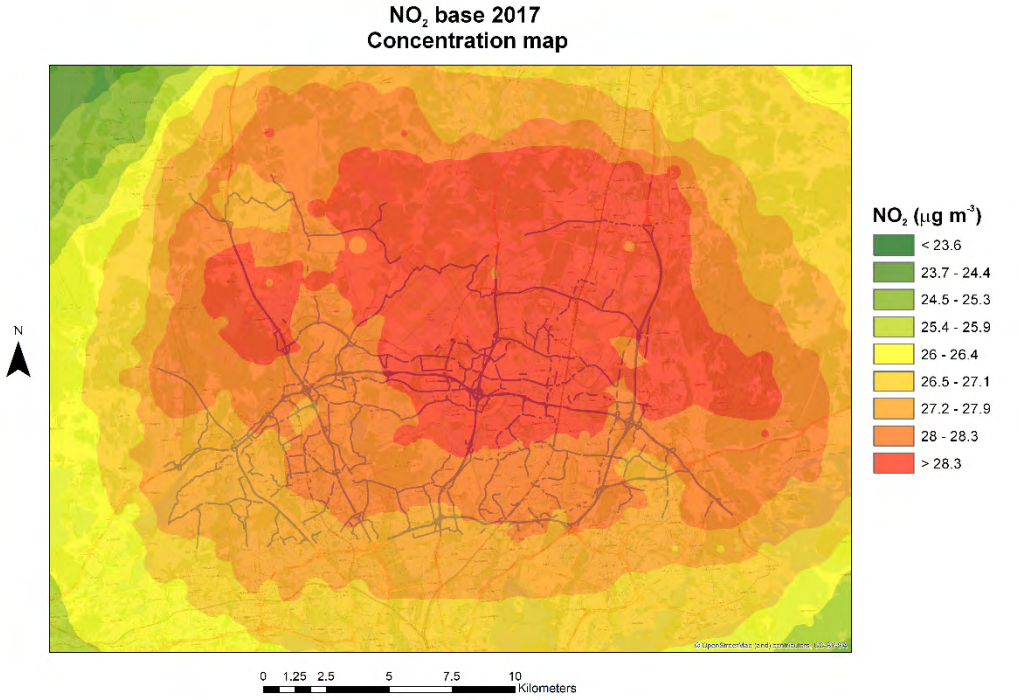

Figure 72. NO_2 concentration map for the Vantaa present scenario (January 2017 mean). Also shown are the major roads considered in the simulations. The map represents the average concentration for January 2017.

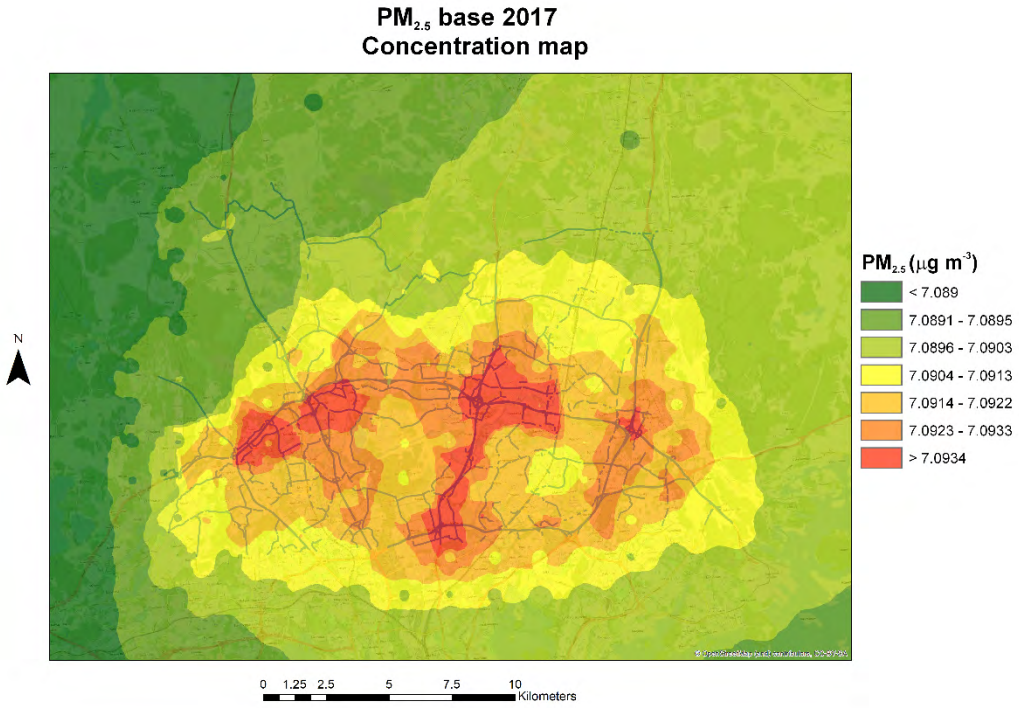

Figure 73. $PM_{2.5}$ concentration map for the Vantaa present scenario (January 2017 mean). Also shown are the major roads considered in the simulations. The map represents the average concentration for January 2017.

Both Figures show a typical pattern with generally low concentrations as compared to those observed in Bologna and Hasselt, with one only major pollution enhancement in proximity of major roads, especially for $PM_{2.5}$. The "concentration hotspot" zone roughly corresponds to the city centre, and concentrations decrease towards the borders of the simulation domain. This result clearly depends on the spread in pollutants' emissions previously evidenced in Vantaa, and on local increases in emissions in proximity of junctions and very trafficked streets. Major roads to the north-west of the domain seem less impacted, a result that can depend not only on reduced traffic volumes as previously reported in Section 3.2.3 (Figure 30 and Figure 31), but also on the wind rose of the period, mainly impacted by winds from W and SW (Figure 74).

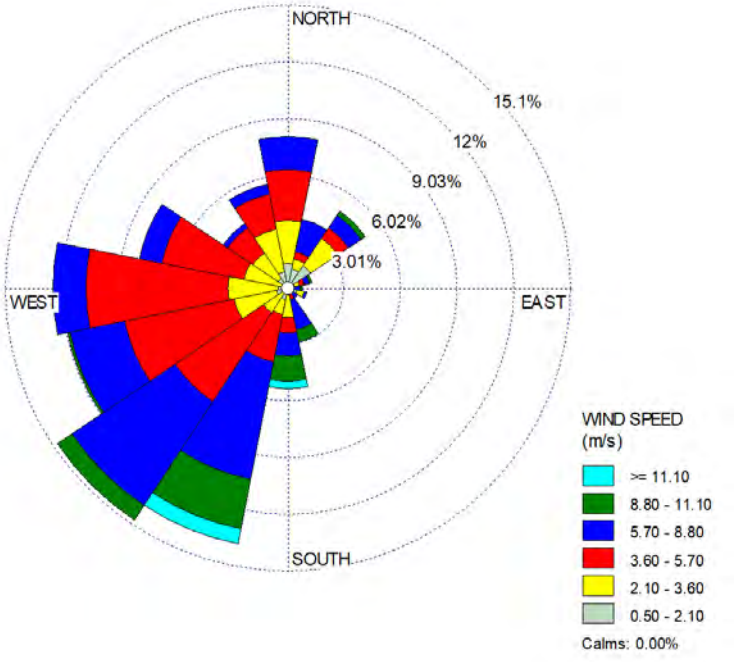

Figure 74. Wind rose for the January 2017 base reference case in Vantaa.

4.2.3.2 Policy 1: Closure of the inner ring

As reported in Section 3, in Vantaa we tested the impact of a policy similar to the first one implemented in Hasselt, i.e. closing completely one area to the traffic. The implementation of this policy was meant to evaluate the efficacy in a city where the spatial distribution of pollutants' emissions, and the resulting pollutants' concentrations, was completely different from that observed in Hasselt.

The area of the implementation of this policy is located to the east of the simulation domain, and is small compared to it (see Figure 33). As such, this policy is expected to present a local impact, in the vicinity of the area where it is implemented

Figure 75 and Figure 76 present the results in terms of concentration maps for NO_2 and $PM_{2.5}$ pollutants previously considered in the base case scenario, for comparison. It can be noted that in the scenario not only the concentration pattern is the same as that observed in the base case, which depends by the influence of the same meteorology, and in particular wind speeds and directions, but also minimum and maximum values in this case remain the same, with only a minor decrease in $PM_{2.5}$ maximum.

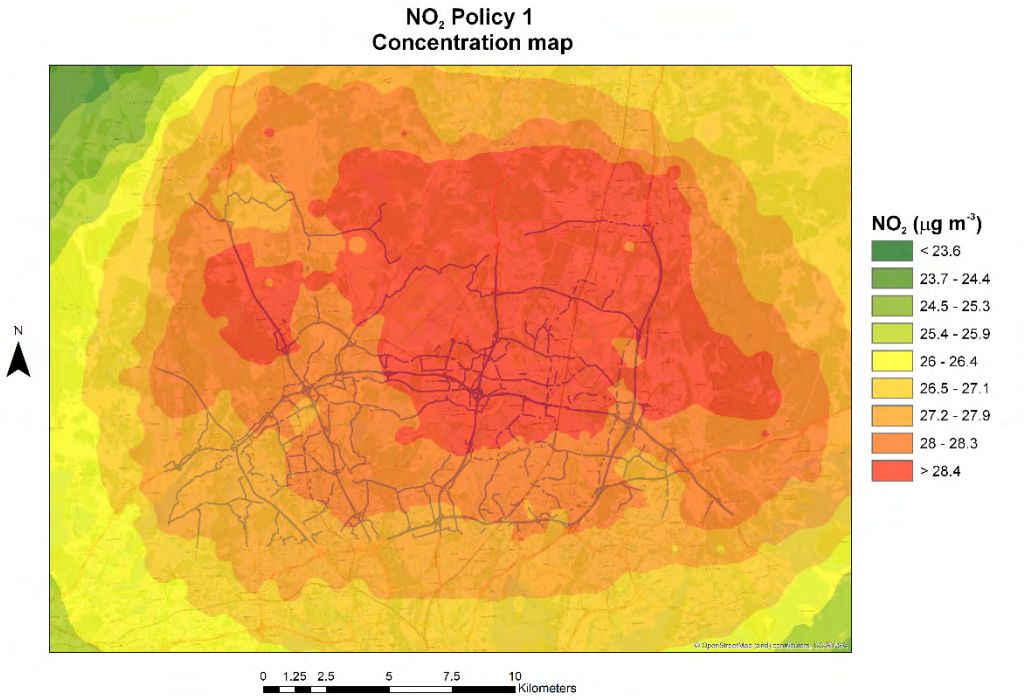

Figure 75. NO_2 concentration map for the implementation of the policy 1 for Vantaa case in the present (January 2017) scenario.

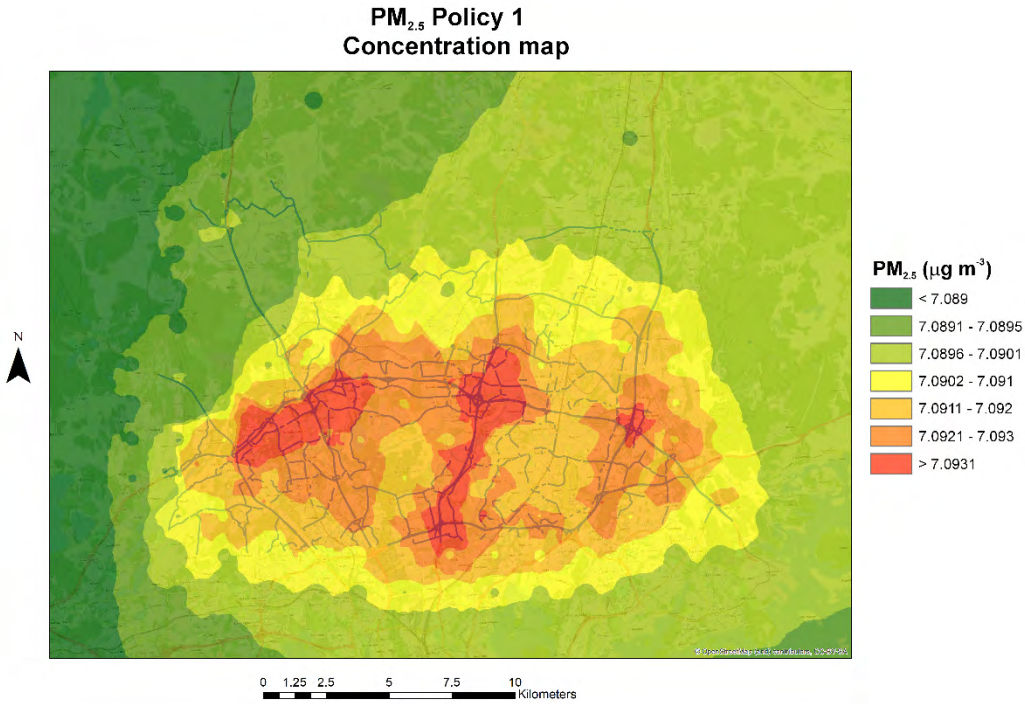

Figure 76. $PM_{2.5}$ concentration map for the implementation of the policy 1 for Vantaa case in the present (January 2017) scenario.

As previously done for Hasselt, the comparison is also presented in terms of maps of concentration differences between the scenario with the implementation of the policy 1 and the base case (Figure 77 and Figure 78). The Figures highlight that in general the impact of this policy in Vantaa is very small, both due to the limited area chosen for the intervention as well as to the low concentrations observed in the base case scenario. In general, however, NO_2 concentrations seem impacted more in areas different than that of the intervention, where instead a small enhancement is observed, while $PM_{2.5}$ on the contrary is impacted exactly in the area of the intervention. Similar to what previously observed, the impact of this policy is slightly higher for NO_2 than for PM concentrations.

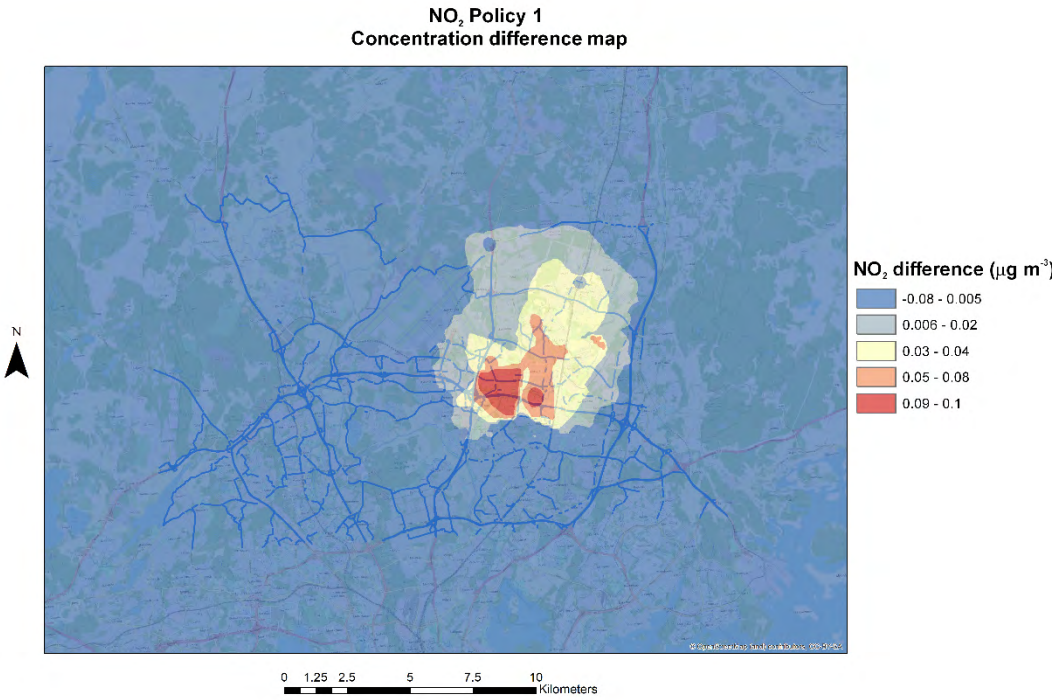

Figure 77. Map of differences in NO_2 concentration between the policy 1 scenario and the base case in Vantaa.

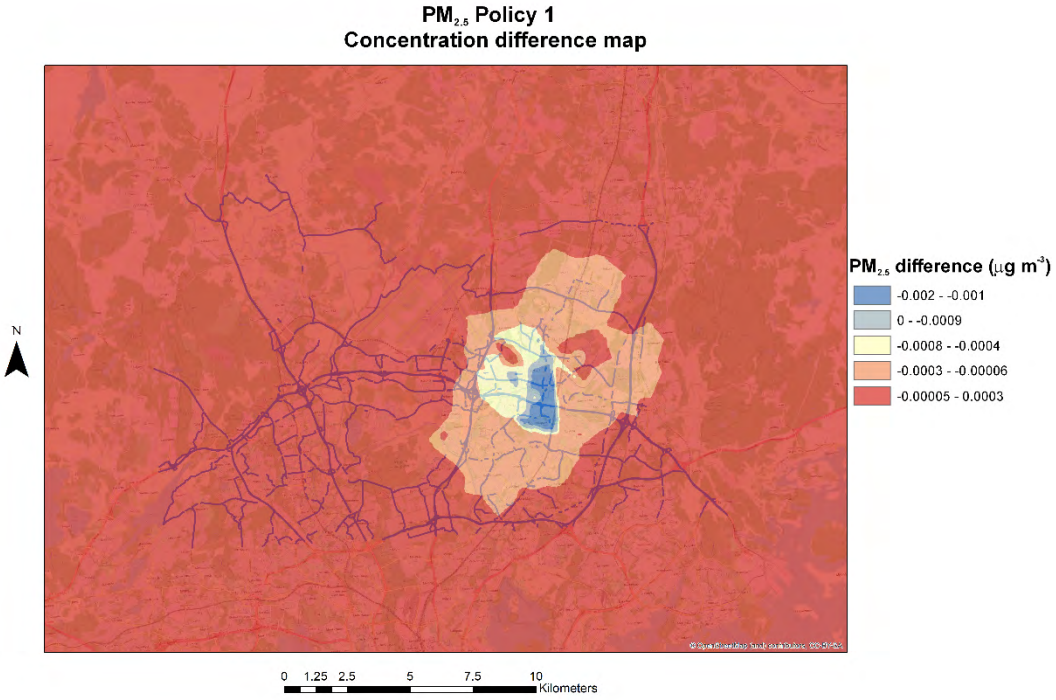

Figure 78. Map of differences in $PM_{2.5}$ concentration between the policy 1 scenario and the base case in Vantaa.

Finally, we provide the maps of observed NO_2 and $PM_{2.5}$ reductions in the scenario when the policy is implemented (Figure 79 and Figure 80), calculated as the ratio of the concentration differences previously presented (Figure 77 and Figure 78) and the concentration observed in the base case.

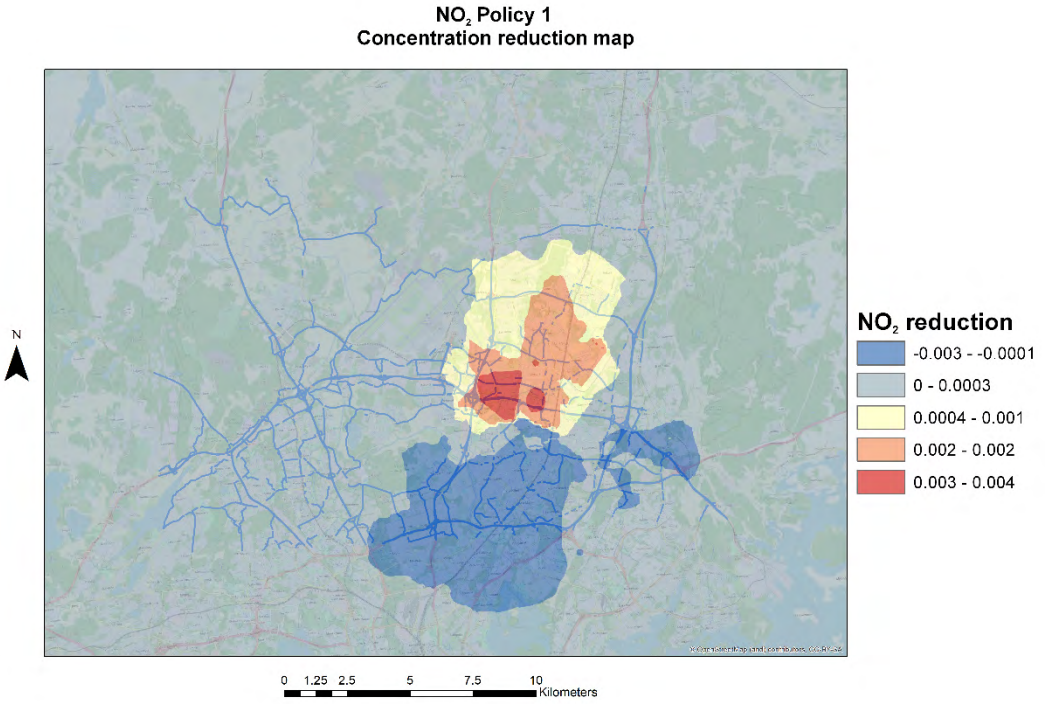

Figure 79. NO_2 reduction in the policy 1 scenario in Vantaa, evaluated as concentration ratio between the concentration difference previously evaluated (Figure 77) and the concentration observed in the base case (Figure 72).

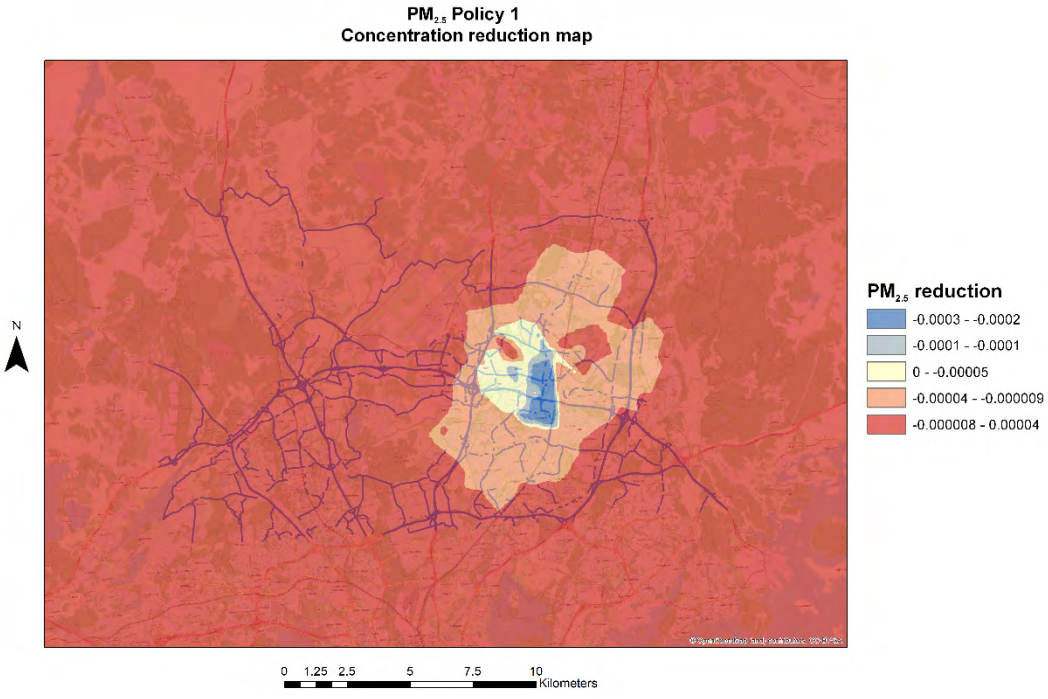

Figure 80. $PM_{2.5}$ reduction in the policy 1 scenario in Vantaa, evaluated as concentration ratio between the concentration difference previously evaluated (Figure 78) and the concentration observed in the base case (Figure 73).

Maps of reductions indicate clearly that the impact of this policy is overly small both for NO_2 and $PM_{2.5}$ concentrations, with slightly higher reductions for NO_2. The impact of the policy is spread outside the area of the intervention while for $PM_{2.5}$ small reductions are observed over the area where the policy is implemented. Overall, however, the efficacy of this policy in Vantaa where the pollutants' emissions are spread and the intervention was tested over a small area compared to the simulation domain, is limited. To analyse the local impact of the policy, we also present the reductions observed at the three receptor sites (Table 19). The Table confirms the overall small impact of the policy in Vantaa, with slight or null reductions for $PM_{2.5}$ and with slight increases of NO_2 at the three receptor sites.

Policy	Period	Receptor name	NO_2 (%)	$PM_{2.5}$ (%)
1	Jan-17	Tikkurila	0.16	-0.01
1	Jan-17	Rekola	0.03	0.00
1	Jan-17	Airport	0.02	0.00

Table 19. Percentages of reduction/increase in concentrations in the case of implementation of the policy 1 in Vantaa compared to the base case (calculated for all receptor).

5 Methodology for AQ simulations in future scenarios

In this section, the methodology adopted to carry out AQ simulations in future scenarios in the three cities is presented. First of all, the methodology adopted to carry out simulations of future climate projections is briefly presented, and the general results in terms of change in the main meteorological variables are discussed. After that, we present the methodology adopted to perform dispersion modeling simulations in future scenarios in the three cities.

5.1 Future climate projections

Besides emissions of air pollutants, future air quality is affected by meteorological conditions. The magnitude of future climate change in the iSCAPE cities (and elsewhere), in turn, strongly depends on the evolution of global anthropogenic greenhouse gas emissions (GHGs) and thereby on socioeconomic and technical developments, as well as on decisions and current (baseline) effectiveness of human behavioral changes. In this report, climate projections for the cities of Bologna, Hasselt and Vantaa are based on two alternative global scenarios for GHGs and aerosols: RCP8.5 and RCP4.5 (RCP=representative concentration pathways; Taylor et al. 2012; Van Vuuren et al. 2011). For the sake of simplicity, these could be denoted as high-emission and moderate-emission scenarios, respectively. Various shared socioeconomic pathways (SSPs) could be consistent with RCP4.5, although the costs associated with policy and impacts would vary (van Vuuren et al., 2014). For RCP8.5, however, a socioeconomic pathway (SSP1), illustrated by a narrative description (storyline) of sustainability - taking the green road (O'Neill et al., 2017) could not be consistent (van Vuuren et al., 2014). Under the RCP4.5 scenario, the global mean temperature would increase by 1.4 (0.9-2.0) °C between the periods 1986-2005 and 2046-2065, while under the RCP8.5 scenario the projected global warming would be 2.0 (1.4-

2.6) °C (IPCC, 2013). Neither of the RCP scenarios considered here would meet the goal of maintaining the global warming well below 2°C above pre-industrial levels and pursuing efforts to limit the temperature increase to 1.5 °C, as agreed at the 21st Conference of the Parties of the UNFCCC in Paris in 2015.

5.1.1 Bologna

The future climate change projections for Bologna are based on four grid points, centred over the city centre (44.76694, 10.94859; 44.76694, 11.79886; 44.16897, 11.79886; 44.16897, 10.94859) on a large ensemble of state-of-the-art global climate model simulations, CMIP5 GCMs (Taylor et al., 2012). Details about the GCMs and methods used to post-process the model data are given by Ruosteenoja et al. (2016), who also provided the data used to generate the projections for Bologna (and for Hasselt in Sec. 5.1.2). The main emphasis is given to the projections under the RCP8.5 scenario. The climatological variables of highest relevance for air quality and considered below are: surface temperature; precipitation; solar radiation; wind speed and direction, being linked to sea level pressure patterns.

The number of CMIP5 GCMs used to construct the multi-model projections was 28 for daily mean temperature, precipitation, solar radiation and air pressure, 25 for daily minimum and maximum temperature and the diurnal temperature range, 24 for wind speed, and 21 for geostrophic and current (baseline) wind directions. The names and origins of the GCMs will be reported in a thorough report on climate change projections of the iSCAPE project (D6.4 under preparation). In calculating the multi-model means and standard deviations for the simulated changes, all the GCMs were weighted equally. For a fixed RCP scenario, the spread of future changes results from modelling uncertainty and internal natural variability. Using the standard deviations and the normality approximation, 90% uncertainty intervals for the change were calculated.

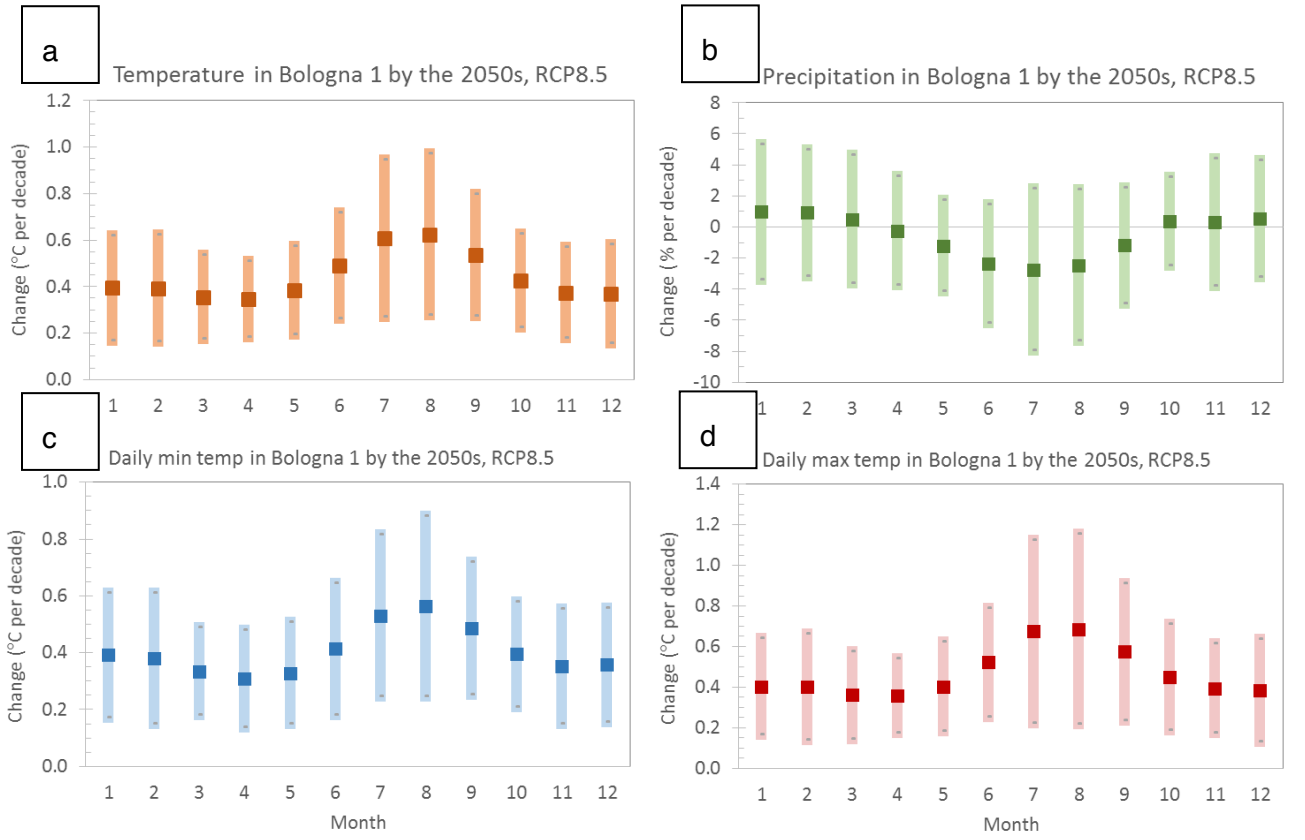

Figure 81. Projected trends in (a) monthly mean air temperature, (b) monthly precipitation total, (c) monthly mean of daily minimum temperature, and (d) monthly mean of daily maximum temperature between the periods 1981-2010 and 2040-2069 in Bologna (grid point 1) under the RCP8.5 scenario. The multi-model mean projections for each calendar month (1 = January, 12 = December) are denoted by symbols. Shading shows the 90% uncertainty intervals for the change.

The projected increases in monthly mean temperature in Bologna by the 2050s are largest in summer and smallest in spring (Figure 81a). Under the RCP8.5 scenario, the multi-model mean estimates (the 90% uncertainty intervals in parenthesis) range from 0.35 (0.19–0.51) °C per decade in April, to 0.62 (0.28–0.97) °C per decade in August. Under the RCP4.5 scenario, the projected warming rate is about 30% smaller. The differences between the four grid points in the Bologna area are minor, from 0 to 4 % depending on the calendar month and grid point.

While all the models agree about a general warming trend in all seasons, for precipitation the projected climate change signal is less clear and the spread across the models is rather wide (Figure 81b). Based on the multi-model mean estimates, little changes can be expected from October to April. In July the best-estimate trend is -3 % per decade and almost the same in June and August. As reported previously in D1.4, Bologna belongs to a wide area in southern and central Europe where more than 75% of the models agreed on a decrease in summer precipitation. The decreasing rainfall in summer contributes to the rapid warming in that season. Less precipitation means drier soil, less evapotranspiration, reducing latent heat energy and thereby increasing the share of sensible heat.

The increases in temperature manifest themselves as higher daily maximum temperatures in all seasons, and in particular during summer (Figure 81d). The projected trends in summertime daily minimum temperatures are somewhat weaker (Figure 81c). Consequently, the diurnal temperature range is projected to increase by about 0.1°C per decade in summer (Figure 82a). In other seasons the trends for daily minimum and maximum temperatures are close to each other and the diurnal temperature range is projected to remain almost unaltered.

Incident solar radiation is projected to increase by about 1% per decade from May to November, most strongly in early autumn (Figure 82b). Even in winter the multi-model mean estimates suggest slightly more solar radiation by the 2050s. Because clouds reduce incident solar radiation, it can be inferred that daytime cloudiness is likely to decrease rather than increase. In summer the interpretation of less cloudiness is supported by the growth of the diurnal temperature range (Figure 82a) and decreases in precipitation amounts (Figure 81b). On the other hand, the model results suggest that standard deviations of daily mean temperatures will slightly increase in summer, implying more day-to-day temperature fluctuations in the future (Figure 82c).

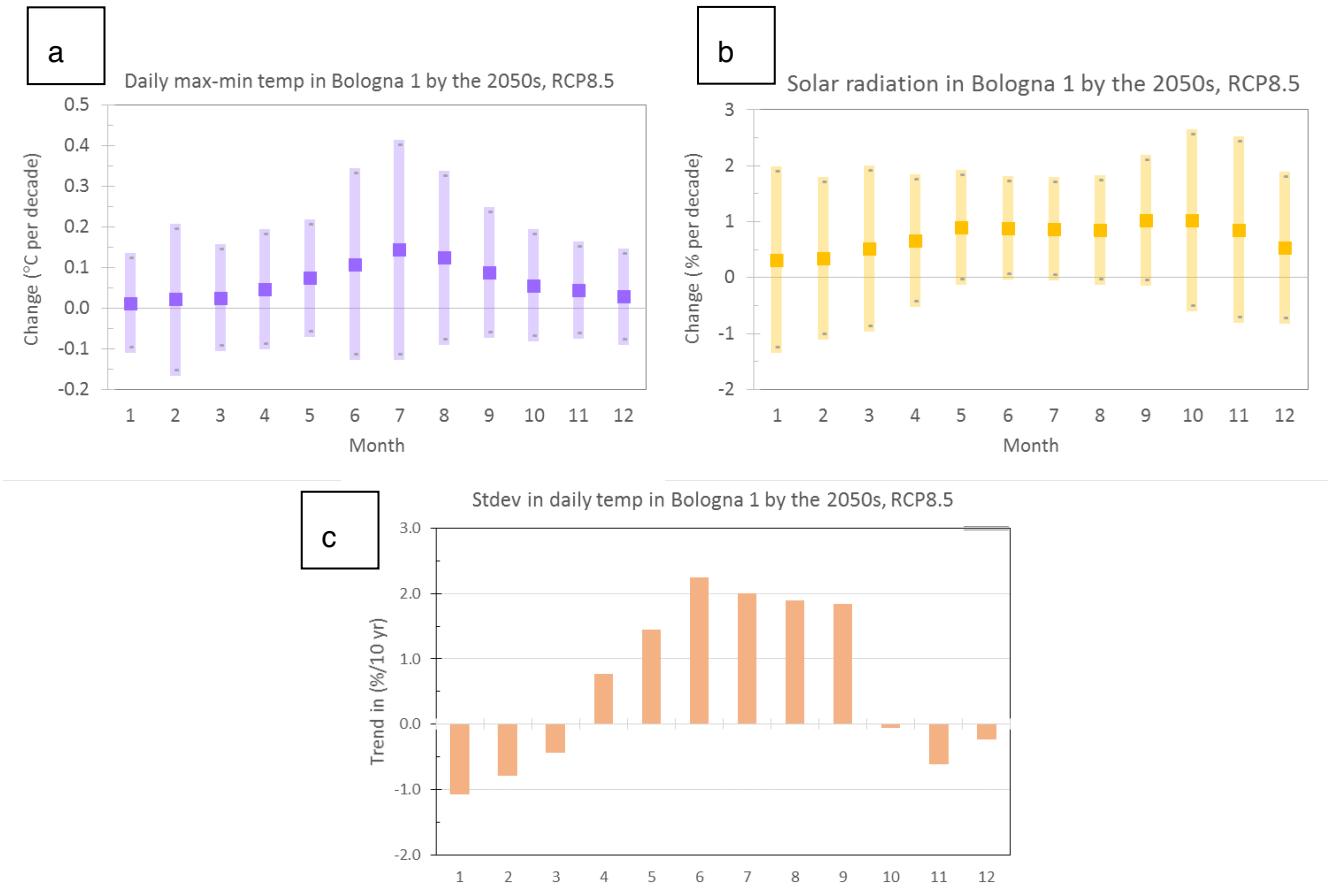

Figure 82. Projected trends in (a) monthly mean diurnal temperature range, (b) monthly mean incident solar radiation and (c) monthly standard deviation of daily mean temperature (in % per decade, bottom) by the period 2040–2069 in Bologna under the RCP8.5 scenario. The baseline period is 1981-2010 (top) or 1971-2000 (bottom). For further information, see caption of Figure 81.

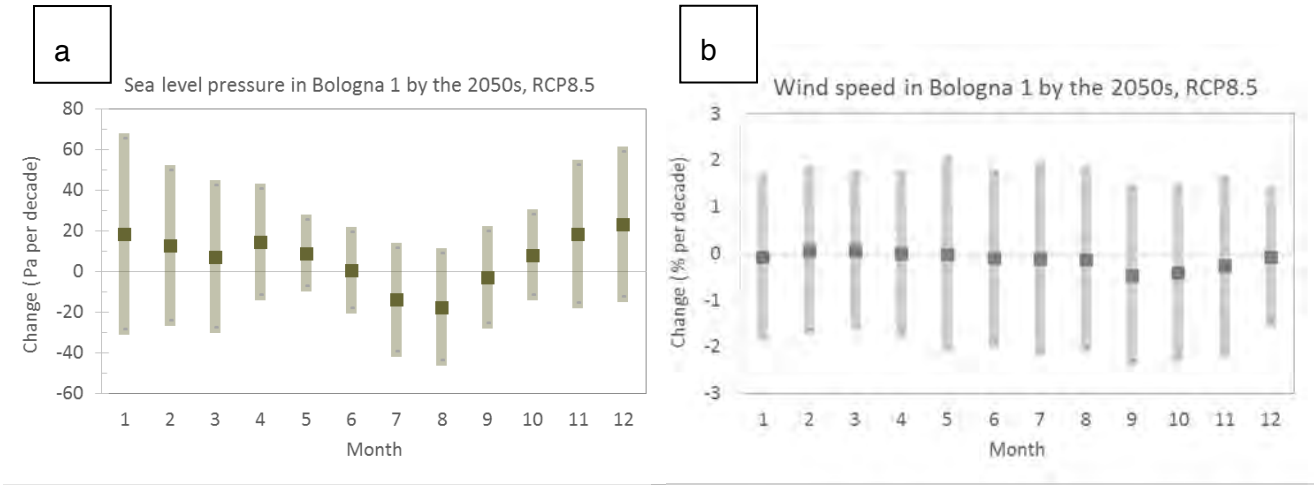

Figure 83. Projected trends in (a) monthly mean surface air pressure and (b) wind speed between the periods 1981-2010 and 2040-2069 in Bologna under the RCP8.5 scenario. For further information, see caption of Figure 81.

According to the multi-model mean climate projections, sea level air pressure in Bologna will decrease in July and August but increase or remain practically unaltered during the rest of the year (Figure 83a). The inter-model differences are large for monthly mean wind speed, the multi-model mean projections suggesting slight reductions (in autumn) or negligible changes.

Although the projected changes in monthly mean wind speed are minor, wind directions might be affected. Based on Figure 84, the frequency of southerly and westerly winds would increase by 1-1.5 percentage points in winter by the 2050s, compared to the 1980s. In summer, in contrast, the frequency of northerly and northeasterly wind would increase at the expense of southerly and westerly winds.

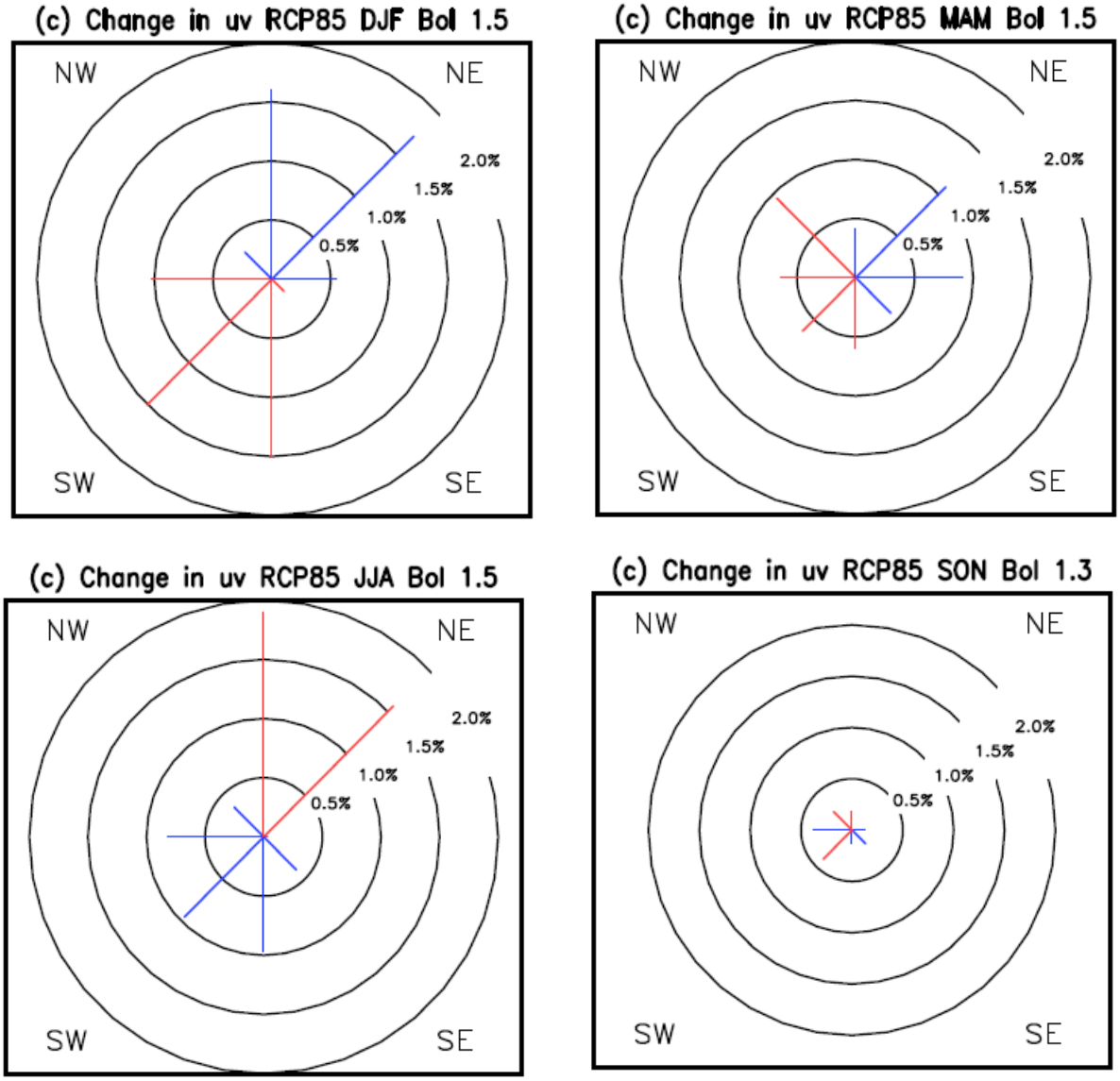

Figure 84. Projected changes in frequency distributions of simulated wind directions in winter (DJF), spring (MAM), summer (JJA) and autumn between the periods 1971-2000 and 2040-2069 in Bologna based on simulations with 21 GCMs under the RCP8.5 scenario. The unit is percentage points, with red bars depicting an increase and blue bars a decrease. The circles indicate the changes for each cardinal and intercardinal direction with an interval of 0.5%.

5.1.2Hasselt

The climate projections for Hasselt resemble those for Bologna. There is a general trend towards higher temperatures, particularly in summer, reductions of summer precipitation, increase in solar radiation, little changes in mean wind speed, but some small changes in wind directions.

In more detail, the monthly mean temperature is projected to increase in Hasselt with a rate of 0.30 (range: 0.14–0.46) °C per decade in April and 0.49 (range: 0.21–0.77) °C per decade in August under

the RPC8.5 scenario (Figure 85) and with a 25-30% slower rate under RCP4.5. Similar to what done for Bologna, the future climate change projections for Hasselt are based on four grid points centred over the Hasselt city centre, which differ on average by 1-3 %.

For monthly mean precipitation totals, the multi-model mean estimates indicate decreases of 2.2% per decade in July, but increases of 1.5% per decade in December, January and February (Figure 85b). Decreasing precipitation in summer can be expected to result in reduced soil moisture and evapotranspiration. This increases the portion of energy that is transmitted into the atmosphere in the form of sensible heat rather than latent heat, and thereby adds to the enhanced summertime warming.

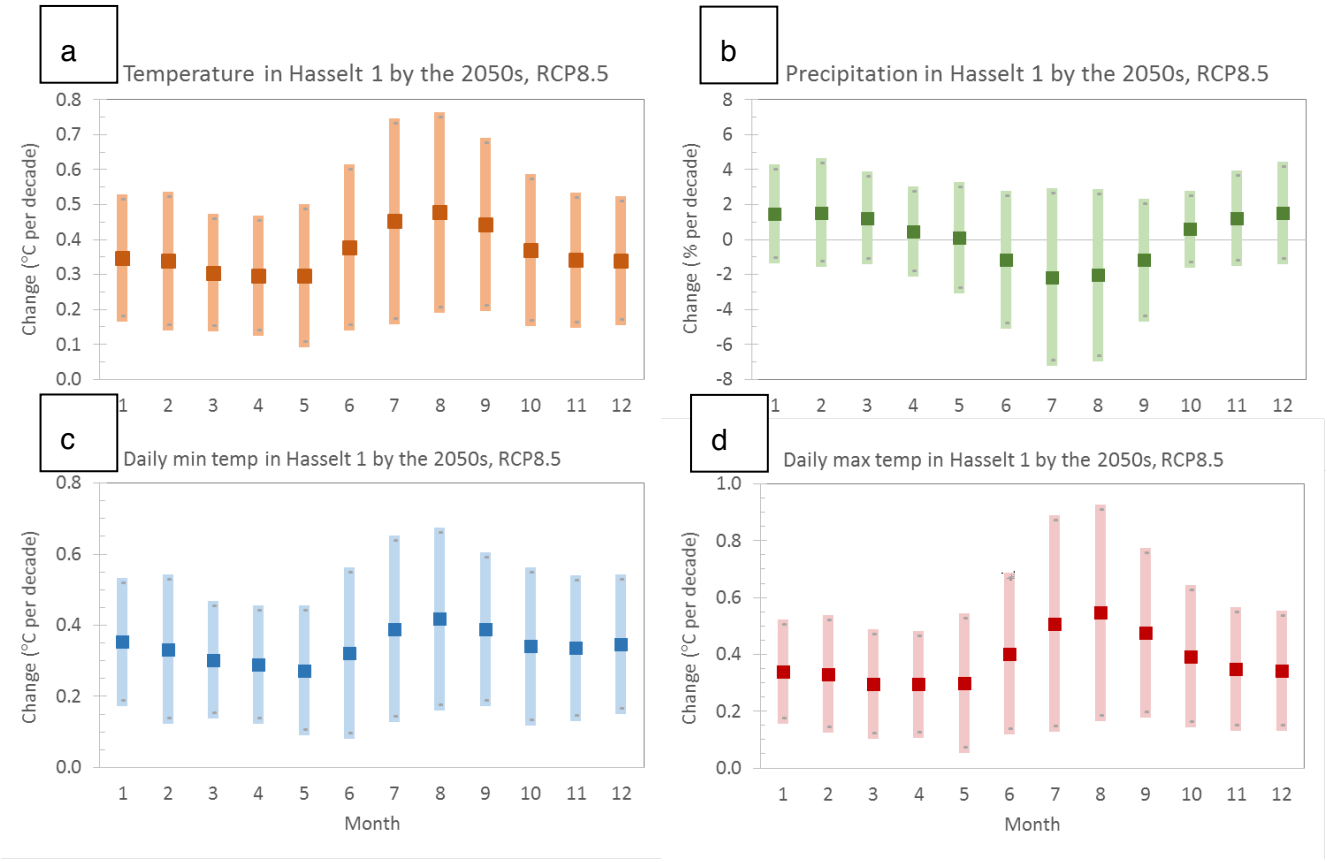

Figure 85. Projected trends in (a) monthly mean air temperature, (b) monthly precipitation total, (c) monthly mean of daily minimum temperature, and (d) monthly mean of daily maximum temperature between the periods 1981-2010 and 2040-2069 in Hasselt under the RCP8.5 scenario. The multi-model mean projections for each calendar month (1 = January, 12 = December) are denoted by squares. Shading shows the 90 % uncertainty intervals for the change.

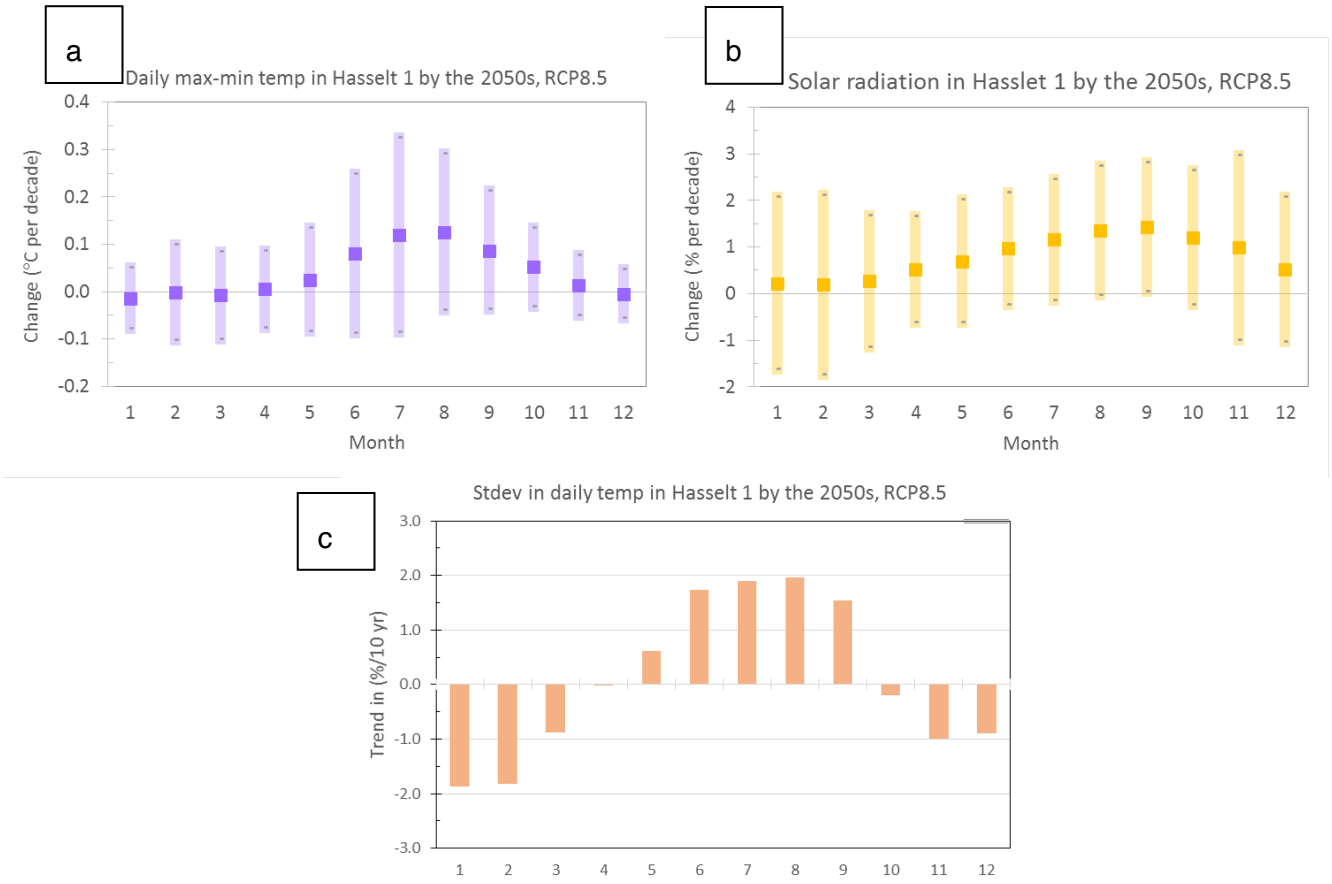

Figure 86. Projected trends in (a) monthly mean incident solar radiation, (b) monthly mean diurnal temperature range, and (c) monthly standard deviation of daily mean temperature by the period 2040–2069 in Hasselt under the RCP8.5 scenario. The baseline period is 1981-2010 (top) or 1971-2000 (bottom). For further information, see the caption of Figure 85.

In Hasselt in November-April, the projected increases in daily minimum temperatures are similar to or slightly higher than the increases in daily maximum temperatures (Figures Figure 85c-d), implying a narrower diurnal temperature range (Figure 86a). In addition, the day-to-day temperature fluctuations are projected to diminish in the future during those months (Figure 86c). The opposite is true from May to September or October. The projected increases in incident solar radiation are more robust in August and September: 1.5 (0-2.9) % per decade (Figure 86b).

The multi-model mean projections show mainly slight increases in sea level air pressure in Hasselt, apart from July and August (Figure 87a) and little changes in monthly mean wind speeds (Figure 87b). In winter, the portion of southwesterly winds is projected to increase by about 3 percentage points in seven decades (Figure 88). In summer, by contrast, southwesterly and also southerly winds will become slightly less common, according to the climate model results.

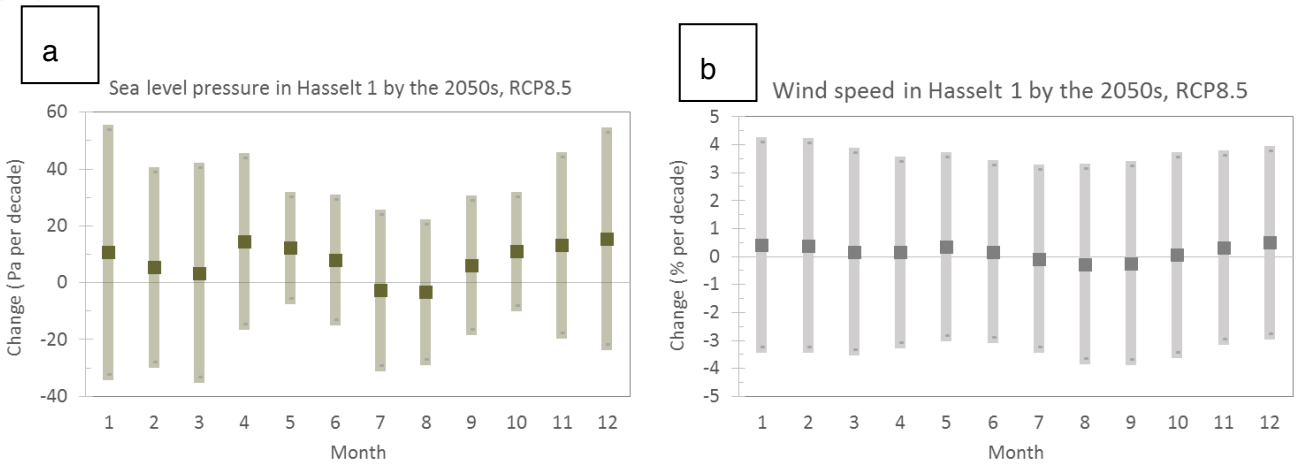

Figure 87. Projected trends in monthly mean surface air pressure (in hPa per decade, left) and wind speed (in % per decade, right) between the periods 1981-2010 and 2040-2069 in Hasselt under the RCP8.5 scenario. For further information, see caption of Figure 85.

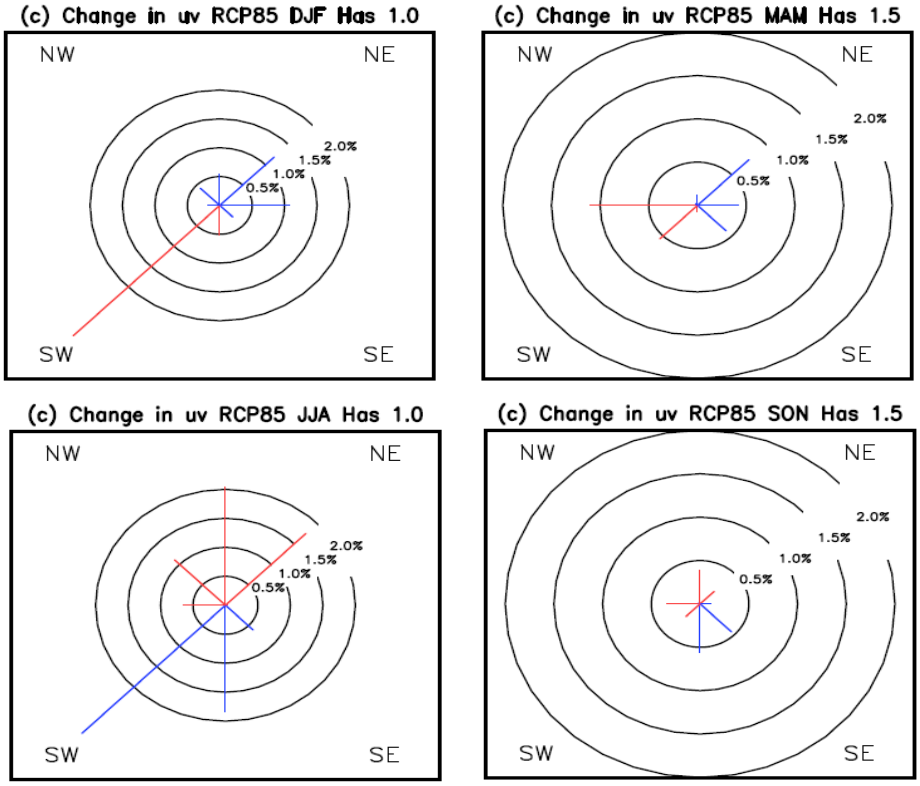

Figure 88. Projected changes in the frequency distributions of simulated current (baseline) wind directions in winter (DJF), spring (MAM), summer (JJA) and autumn between the periods 1971-2000 and 2040-2069 in Hasselt based on simulations with 21 GCMs under the RCP8.5 scenario. The changes are given in percentage points, with red bars depicting an increase and blue bars a decrease in the frequency. The circles indicate the changes for each cardinal and intercardinal direction with an interval of 0.5%.

5.1.3 Vantaa

Based on climate model projections, future changes in Vantaa deviate from those for Bologna and Hasselt. There is a general trend towards higher temperatures, but opposite to what observed at the two other cities, the trend is stronger in winter than in summer. Also, the projected changes in precipitation and solar radiation are more pronounced in winter than in summer. Similar to Bologna and Hasselt, little changes are expected in mean wind speed, but some minor changes in wind directions are apparent.

Under the RPC8.5 scenario, the projected rates of warming in Vantaa range from 0.44 (0.18–0.68) °C per decade in May and June to 0.74 (0.38–1.1) °C per decade in January (Figure 89a). Under RCP4.5, the trends in monthly mean temperatures are 20-30% smaller.

The multi-model mean estimates indicate increases in precipitation in all seasons but summer (Figure 89b). Almost all models agree on a tendency towards higher precipitation amounts in November to January, with the highest rate, 2.9 (0.16-5.6) % per decade, in January. In the summer months, the multi-model mean estimates suggest little changes but the uncertainty intervals are wide.

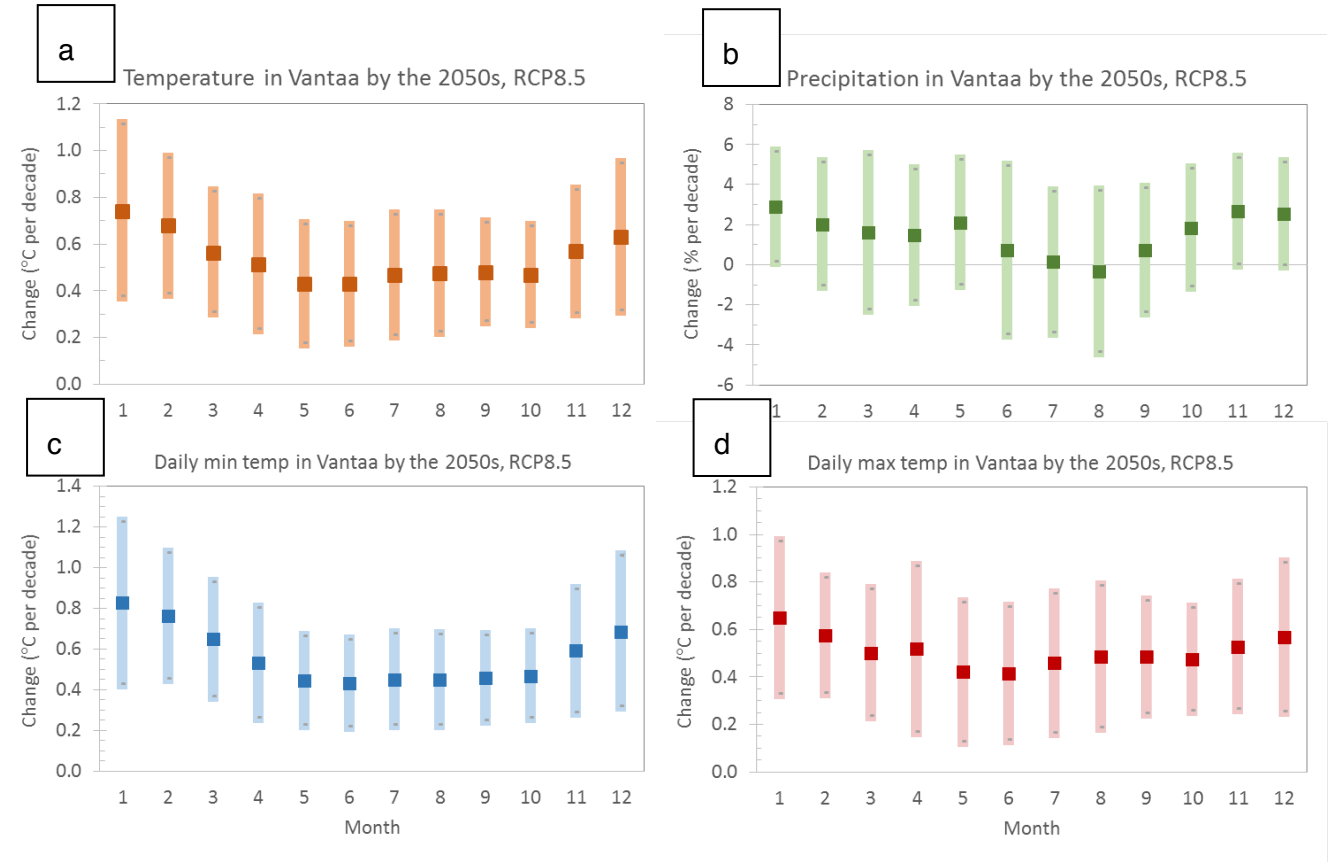

Figure 89. Projected trends in (a) monthly mean air temperature, (b) monthly precipitation total, (c) monthly mean of daily minimum temperature, and (d) monthly mean of daily maximum temperature between the periods 1981-2010 and 2040-2069 in Vantaa under the RCP8.5 scenario. The multi-model mean projections for each calendar month (1 = January, 12 = December) are denoted by squares. Shading shows the 90 % uncertainty intervals for the change.

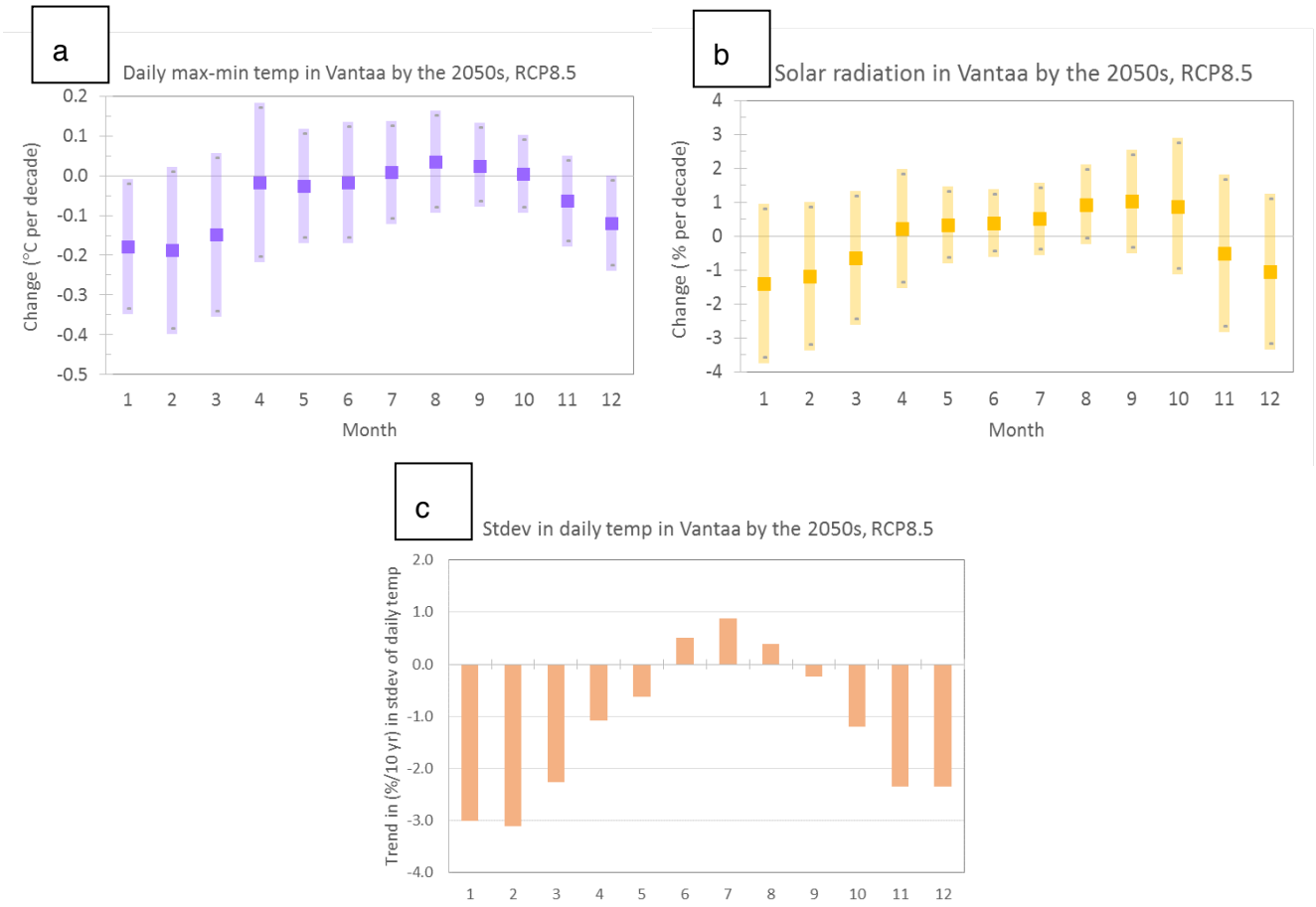

Figure 90. Projected trends in (a) monthly mean diurnal temperature range, (b) monthly mean incident solar radiation, and (c) monthly standard deviation of the temporal variability of daily mean temperature by the period 2040–2069 in Vantaa under the RCP8.5 scenario. The baseline period is 1981-2010 (top) or 1971-2000 (bottom). For further information, see the caption for Figure 89.

In Vantaa in November-March, the projected increases in daily minimum temperatures are higher than the increases in daily maxima (Figure 89c-d). In January and February, the difference in the trends is almost 0.2 °C per decade. Accordingly, the diurnal temperature range is projected to decrease in winter (Figure 90a). The day-to-day temperature fluctuations are projected to attenuate in the future not only during those months but also in April, May and October (Figure 90c) when little changes are expected in the diurnal temperature range. Only in August do the multi-model estimates show small increases both in day-to-day temperature fluctuations and the diurnal temperature range.

The projected changes in incident solar radiation (Figure 90b) resemble those for the diurnal temperature range. Both quantities are tightly linked with clouds. Increasing cloudiness reduce incident solar radiation as well as nocturnal infrared cooling, thereby cutting down the differences between the day- and night-time temperatures. The opposite is true for decreasing cloudiness. We can thus deduce that future winters in Vantaa will be even cloudier (and wetter; see Figure 89b) but early autumns will be slightly sunnier than in the recent past.

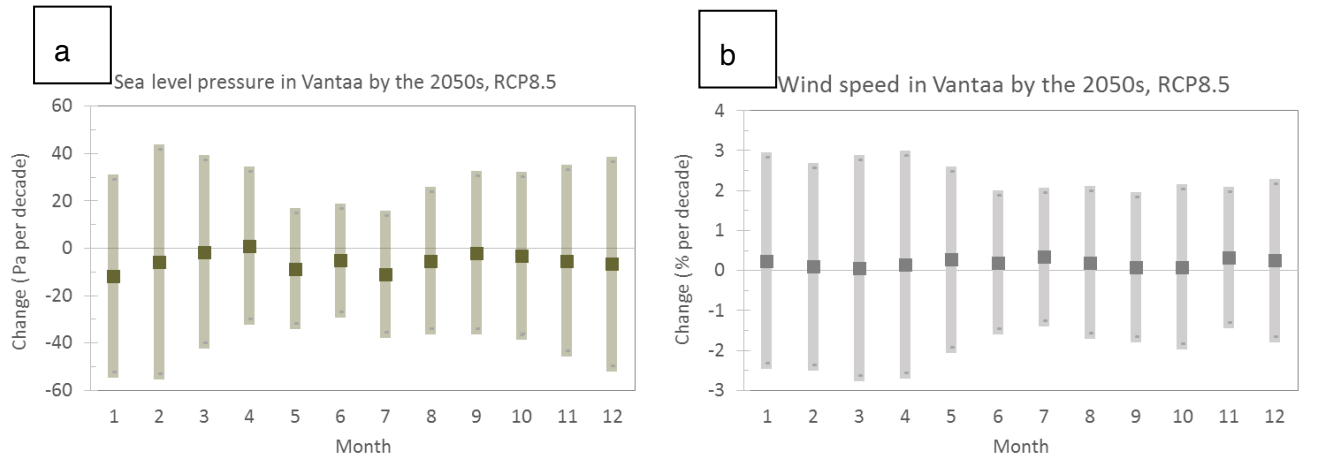

Figure 91. Projected trends in a) monthly mean surface air pressure and b) wind speed between the periods 1981-2010 and 2040-2069 in Vantaa under the RCP8.5 scenario. For further information, see caption for Figure 89.

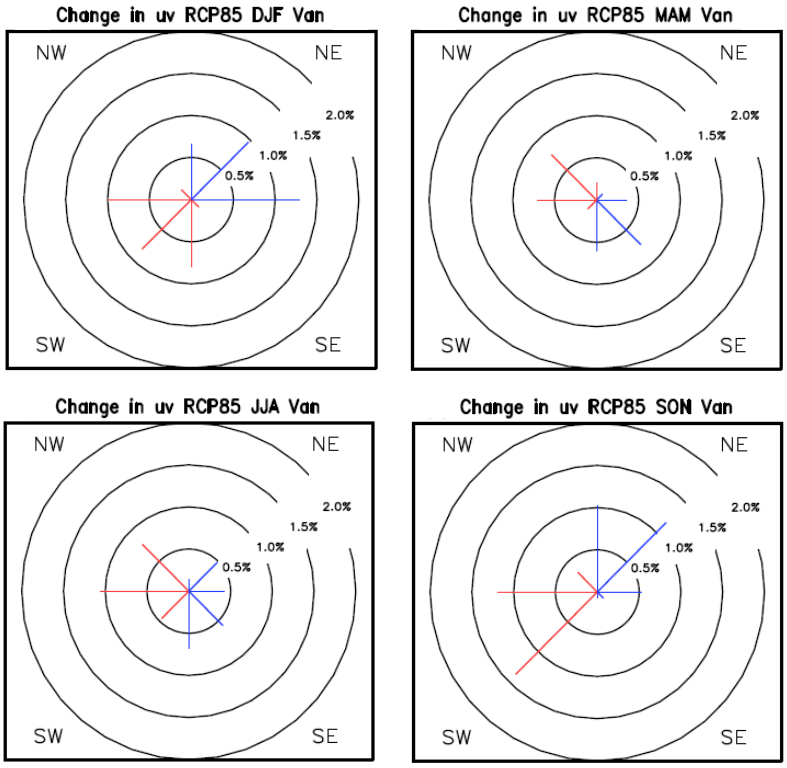

Figure 92. Projected changes in the frequency distributions of simulated wind directions in winter (DJF), spring (MAM), summer (JJA) and autumn between the periods 1971-2000 and 2040-2069 in Vantaa based on simulations with 21 GCMs under the RCP8.5 scenario. The changes are given in percentage points, with red bars depicting an increase and blue bars a decrease in the frequency. The circles indicate the changes for each cardinal and intercardinal direction with an interval of 0.5%.

The multi-model mean projections mainly show slight decreases in monthly mean sea level air pressure in Vantaa (Figure 91a) and little changes in monthly mean wind speeds (Figure 91b). In all seasons, the portion of westerly winds is projected to slightly increase (Figure 92). The largest change in the frequency distributions of the simulated wind directions is projected to occur in autumn, when the share of southwesterly winds would increase by about 1.5 percentage points within seven decades.

5.2 Dispersion modeling

In this section, we provide a description of the methodology used to perform the dispersion modeling simulations in the two cities in the future scenarios.

The emission inventory previously created for the base case (2016) was used to extract information on the future emissions. Here, the previously presented NAEI 2014 urban road type emission factors for 2030 (maximum year for which data are available) are used. In this case, the use of the 2030 emissions may be considered as a precautionary limit, where 2055 emissions should be consistently lower than 2030. For residential heating, even though variations in population and due to the effect of changing meteorology should be taken into account, we considered only changes in emissions due to the effect of cleaner technologies. Therefore we used the same methodology adopted to extract the emissions in the base case, considering emissions for 2050 instead that those for 2016/2017. From the previously presented climate change projections for the three iSCAPE cities, hourly future meteorological variables were extracted, using the methodology of Jyhlä et al. (2015) adequately adapted. Below we provide the equation for estimating future hourly temperature data using data from the climate change simulations and the current situation:

$$T_{TRY2055}(t) = T_{TRYactual}(t) + \Delta\bar{T} + \left(\frac{\sigma_{T2040-2069}}{\sigma_{Tactual}} - 1\right)(T_{TRYactual}(t) - \bar{T}_{TRYactual})$$

where $T_{TRYactual}$ denotes the hourly temperature value in the current reference year (i.e., 2017 for Bologna and Vantaa, and 2016 for Hasselt), $\Delta\bar{T}$ is the projected change (°C) in the 30-year average monthly mean temperature from the current to the future time period, $\sigma_{T2040-2069}$ and $\sigma_{Tactual}$ are the standard deviations of monthly temperatures in the climate model simulations for the thirty year period centred over 2055 and in the meteorological data in the current reference year, and $\bar{T}_{TRYactual}$is the monthly mean in the current (baseline) reference period. We considered the RCP8.5 scenario for greenhouse gas, i.e. considering high population and relatively slow income growth with modest rates of technological change and energy intensity improvements, which in the long term will lead to high energy demand and GHG emissions, if no climate change policy is adopted (Riahi et al., 2011). This is somehow consistent to considering 2030 emissions for traffic.

Applying such transformation method to solar radiation, wind speed and precipitation can produce logic errors, including negative data. To avoid this issue, similar to Soga (2018), these three meteorological parameters were transformed by expansion or contraction based on the rate of future change in the monthly means. In particular, hourly data for the future period were generated with the following equation:

$$P_{TRY2055}(t) = 1 + \frac{\Delta\bar{P}}{\bar{P}_{TRYactual}} * P_{TRYactual}(t)$$

Where P is the meteorological parameter for which we want to extract the hourly future value (alternatively, wind speed, precipitation, and solar radiation), $\Delta\bar{P}$ is the projected change (m s^{-1}, mm, or W m^{-2}) in the 30-year average monthly mean of the parameter from the current to the future time period, $\bar{P}_{TRYactual}$is the monthly mean (accumulated rainfall for precipitation) in the current (baseline) reference period and $P_{TRYactual}$ denotes the hourly parameter value in the current reference year.

For wind direction, since no relevant change in frequencies of the directions was predicted from the climate change simulations in the two cities of Bologna and Hasselt, the hourly values similar to the reference period were inserted there; in Vantaa, instead, the wind directions were adjusted to take into account the frequency changes previously highlighted. Finally, as it was not possible to extract information on cloud cover from the future climate change simulations, and given that it is possible to estimate only daily average cloud cover from solar radiation and extraterrestrial solar radiation values using the Hargreaves model (Hargreaves et al., 1985) proposed by Supit and Van Kappel (1988), here it was chosen to derive hourly sensible heat fluxes. In particular, sensible heat fluxes were estimated from future hourly temperature data applying the methodology developed by de Rooy & Holtslag (1998) starting from the equation proposed by van Ulden and Holtslag (1985), and the following simple approximation:

$$G = -A_G(T_r - T_0)$$

Where G is the soil heat flux, A_G is an empirical coefficient for soil heat transfer, T_R is the reference temperature, and T_0 is the temperature at radiation level. Following Rooy & Holtslag (1998), T_R was defined as the average 24-h mean of the observed 2-m temperature as estimated with the previous equation, which reflects the time history of the atmosphere acting on the soil at the specific location and T_0 is the hourly mean temperature previously determined.

No changes were instead applied to the background concentrations. Even though of course changes in emissions will imply changes also in the background concentrations, the idea of leaving the background concentrations unchanged is to consider only the changes directly applied to the meteorology and the emission sources.

Similar to what previously done in the present scenario, described in Section 3, derived emissions and meteorological variables were used to feed the dispersion model ADMS-Urban 4.1.1. Here we have performed and compared the results of dispersion simulations obtained considering the following various cases:

1) the unique changes in meteorology;

2) changes in meteorology and changes in emissions due to the effect of the adoption of cleaner technologies in the future (for example, due to changes in fleet composition and cleaner fuel);

3) changes in meteorology and implementation of the policies previously selected and implemented in the base case scenario in the two cities.

5.2.1 Bologna

The methodology described above was applied to estimate the hourly meteorological variables (wind speed, wind direction, air temperature, solar radiation, and sensible heat flux) for winter and summer 2055 in Bologna.

5.2.2Hasselt

In the case of Hasselt, the methodology outlined above was applied to estimate the hourly meteorological variables (wind speed, wind direction, air temperature, solar radiation, and sensible heat flux) for January 2055, to be directly compared with the results obtained for January 2016.

5.2.3 Vantaa

In the case of Vantaa, the methodology outlined above was applied to estimate the hourly meteorological variables (wind speed, wind direction, air temperature, solar radiation, and sensible heat flux) for January 2055, to be directly compared with the results obtained for January 2017.

6 AQ simulation in future scenarios

As anticipated in Section 5, here we present the results of dispersion modeling simulations obtained in the future scenarios considering various steps of changes in more variables. Firstly, the effect of only changes in meteorology was taken into account performing simulations with exactly the same emission sources as in the base case scenario and changing only the meteorological variables. We then applied changes in emissions, considering the effect of cleaner technologies reducing the emissions of traffic and domestic heating. Finally, we conducted the simulations in the event the policies previously implemented in the base case scenario were successively implemented in the future scenario. Below we present the results of the dispersion simulations performed in these cases for the two cities previously taken into consideration in the base case scenario.

6.1 Results

Here we will present the results of the dispersion simulations conducted in the future scenarios in the three cities with changes in meteorology as well as considering the implementation of the policies previously presented. Results are presented in the form of concentration maps for considered pollutants, obtained as output of long-term simulations of the ADMS-Urban 4 dispersion model. In addition, the policies scenarios are presented with maps of concentration differences between the scenario when the policy is implemented and the current (baseline) case. Finally, reductions are evaluated in terms of concentration ratios between these concentration differences and the concentrations observed in the base case.

6.1.1Bologna

In this section we will present and discuss NO_x, O_3 and PM_{10} concentration maps obtained for the winter and summer 2055, comparing the results obtained in the future CC (Climate Change) scenario with the one in the present (presented in Section 4).

6.1.1.1 Meteorology in future CC

The CC projections predict that in Bologna it will be relatively warmer, windier and less rainy than in the current scenario, while wind directions are not predicted to change relevantly in the future.

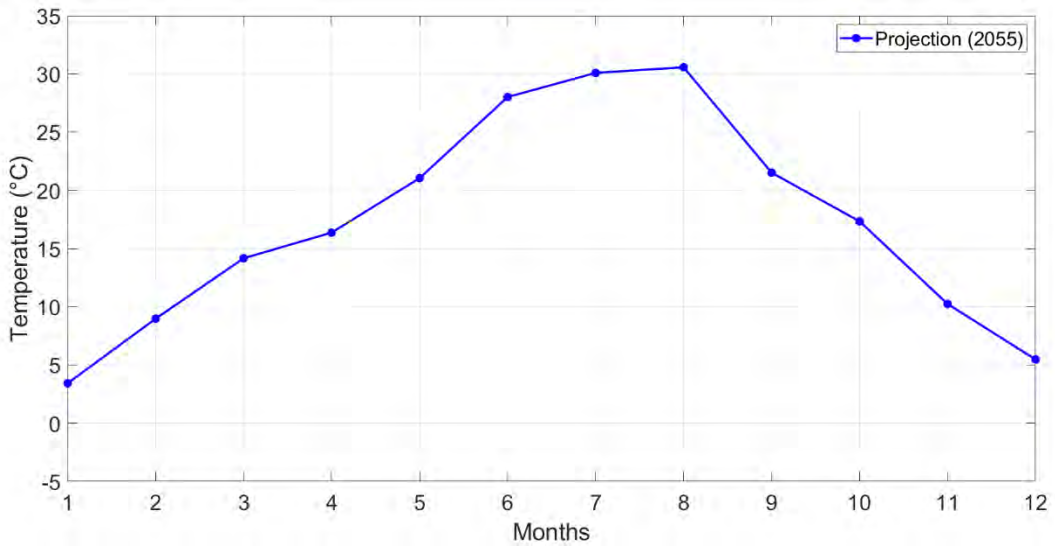

Figure 93. Monthly mean temperature as estimated by the CC projections (RCP8.5) for Bologna.

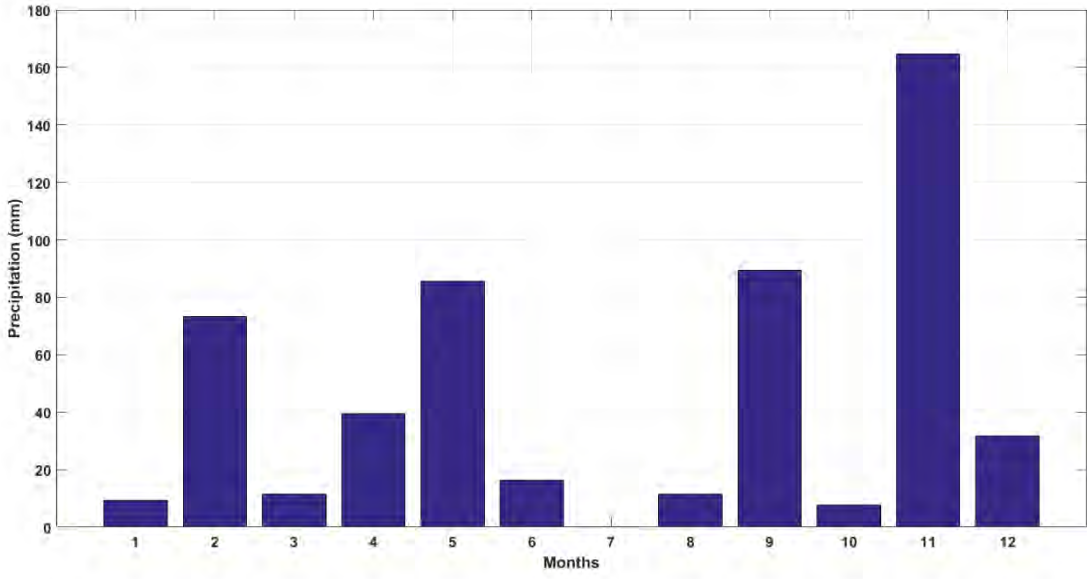

Figure 94. Monthly accumulated rainfall as estimated by the CC projections (RCP8.5) for Bologna.

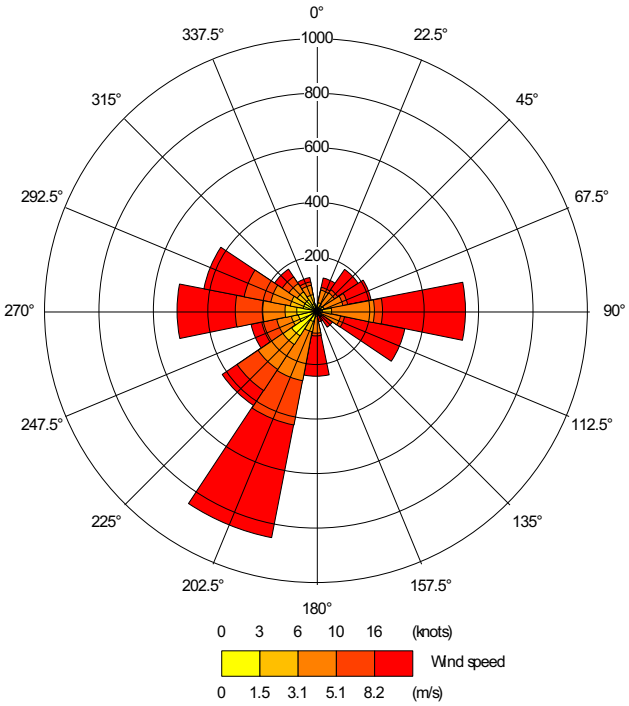

Figure 95. Wind rose of yearly wind frequencies as estimated by CC projections for Bologna.

Since wind directions in the future should not change significantly in Bologna, the pattern of air quality dispersion will not change significantly. Pollutants show the same hot spots, with only small expected reductions, due to the increase in wind speed.

6.1.1.2 Base Case in future CC

In the base case in the future CC (2055BC) for Bologna, only the effect of changes in meteorological variables was taken into consideration, i.e. with the same emission sources as those considered in the base scenario and modifying only the meteorological variables.

The following figures show the spatial distribution of the concentration of pollutants in the 2055BC scenario, averaged over the period considered. Figure 96 and Figure 97 (winter case, summer case not shown) show the concentration maps for NO_2 and PM_{10} pollutants (NO_2, O_3 and CO are not shown) in 2055BC scenario.

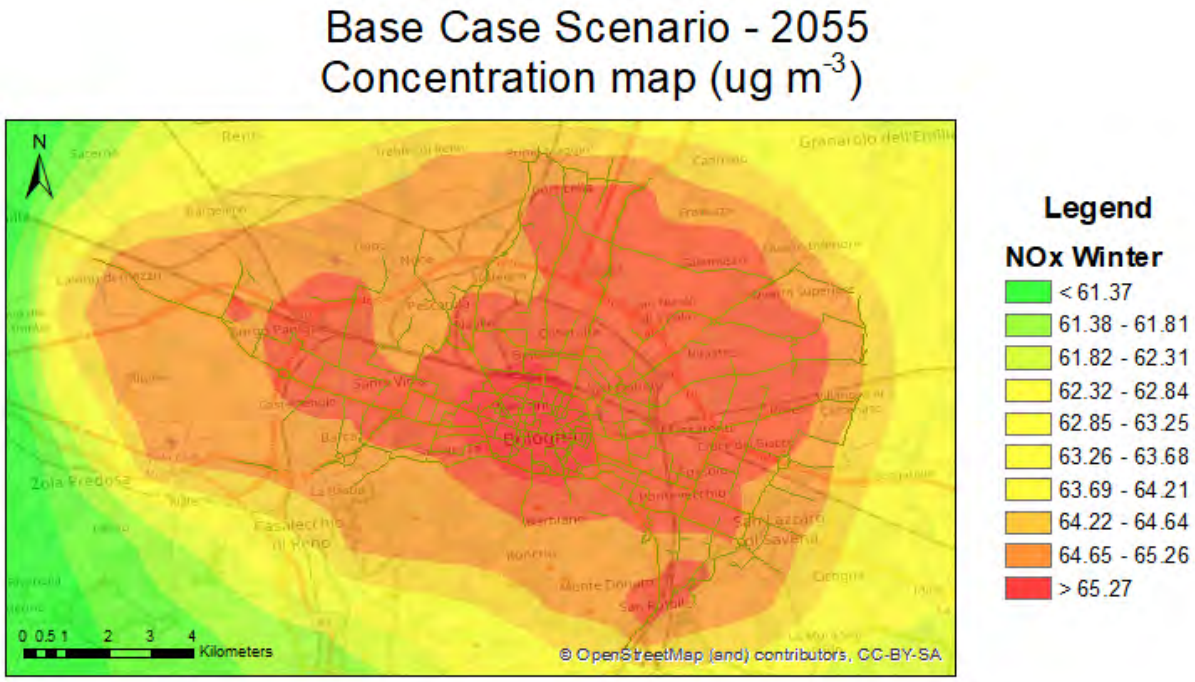

Figure 96. Concentration maps for NO_x in the 2055BC scenario for Bologna. The maps represent concentration values averaged over winter 2055.

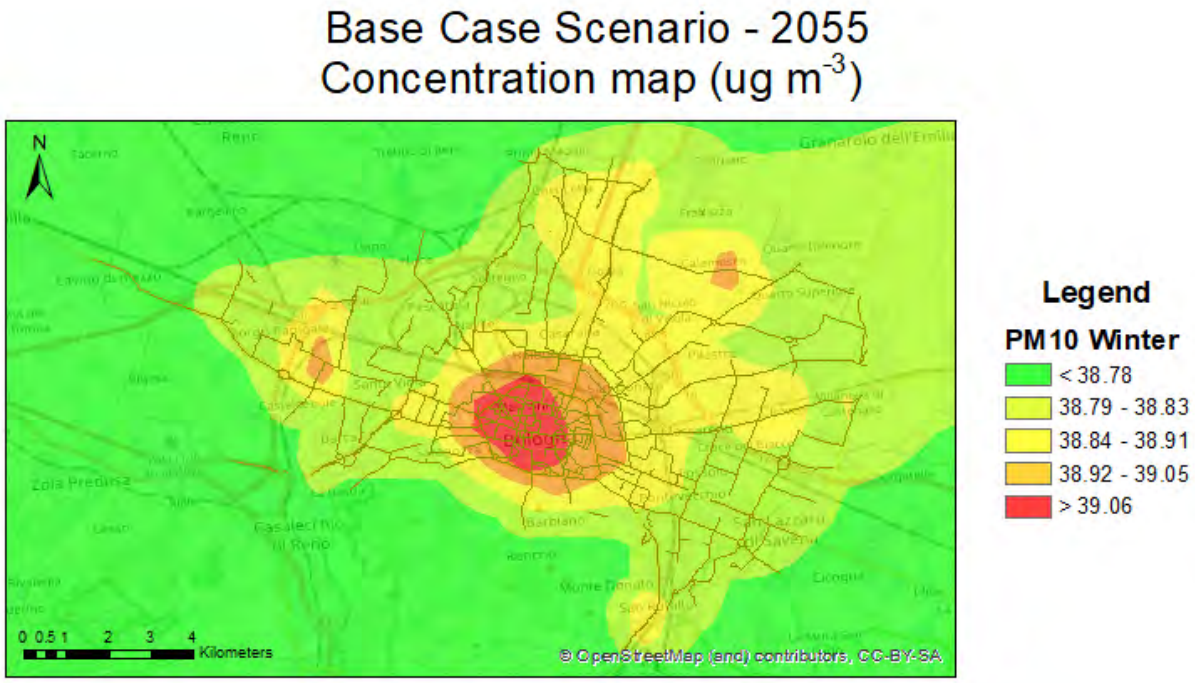

Figure 97. Concentration maps for PM_{10} in the 2055BC scenario for Bologna. The maps represent concentration values averaged over winter 2055.

As previously discussed, wind directions are not predicted to change relevantly in the future in Bologna. For this reason, the pattern of air quality dispersion will not significantly change in future (Figure 96 and Figure 97). Both pollutants show the same hotspots as in the base case scenario for 2017, due to the absence of changes in wind direction, while only small reductions are predicted due to the increases in wind speeds.

The comparison of the average values at the receptors for winter and summer (Table 20) highlights that winter is always a critical period.

Season	Receptor name	NO_x ($\mu g\ m^{-3}$)	NO_2 ($\mu g\ m^{-3}$)	CO ($mg\ m^{-3}$)	O_3 ($\mu g\ m^{-3}$)	PM_{10} ($\mu g\ m^{-3}$)
Winter	V. Chiarini	64.7	38.2	0.82	28.1	38.8
Winter	Porta S. Felice	196.1	63.9	0.86	18.8	44.5
Winter	Giardini Margherita	65.4	38.4	0.82	28.0	38.8
Summer	V. Chiarini	15.9	10.9	0.47	77.5	19.7
Summer	Porta S. Felice	64.9	27.4	0.48	66.8	21.8
Summer	Giardini Margherita	16.0	11.0	0.47	77.4	19.7

Table 20. Average concentration values to receptors in winter and summer for the 2055BC scenario in Bologna.

Considering a future scenario where only the climatic conditions vary, without considering other variables (for example population growth), current policies would lead to an overall increase in pollutant concentrations in the air.

6.1.1.3 Policy 1 in future CC

The first policy implemented in Bologna concerns a traffic limitation in the city centre. Only electric vehicles are allowed in this area, and in addition the bus frequency was also increased. The comparison of the average values of receptors in Electric Buses scenario (2055P1EC scenario) for winter and summer (Table 21), shows that the winter is still a critical period. However, average concentrations are lower than in the 2055BC scenario for all pollutants, with the exception of ozone and PM_{10}.

Season	Receptor name	NO_x ($\mu g\ m^{-3}$)	NO_2 ($\mu g\ m^{-3}$)	CO ($mg\ m^{-3}$)	O_3 ($\mu g\ m^{-3}$)	PM_{10} ($\mu g\ m^{-3}$)
Winter	V. Chiarini	64.6	38.1	0.82	28.1	38.8
Winter	Porta S. Felice	65.5	38.5	0.84	27.9	39.4
Winter	Giardini Margherita	64.6	38.1	0.82	28.1	38.8
Summer	V. Chiarini	15.7	10.8	0.47	77.6	19.7
Summer	Porta S. Felice	15.9	10.9	0.47	77.5	19.9
Summer	Giardini Margherita	15.7	10.8	0.47	77.6	19.7

Table 21. Average concentration values to receptors in winter and summer for 2055P1EC scenario in Bologna.

Figure 98 and Figure 99 show the concentration maps for NO_x and PM_{10} pollutants in the 2055P1EC scenario for comparison with the 2055BC scenario. As a result of the implementation of this policy, it can be noted that:

1) the maximum values have decreased compared to the base case, especially for NO_x;

2) also the spatial pattern has changed, in fact the hot spot located over the centre of Bologna is no more present, but it is possible to recognize different less intense hot spots distributed on the territory, near the busiest streets.

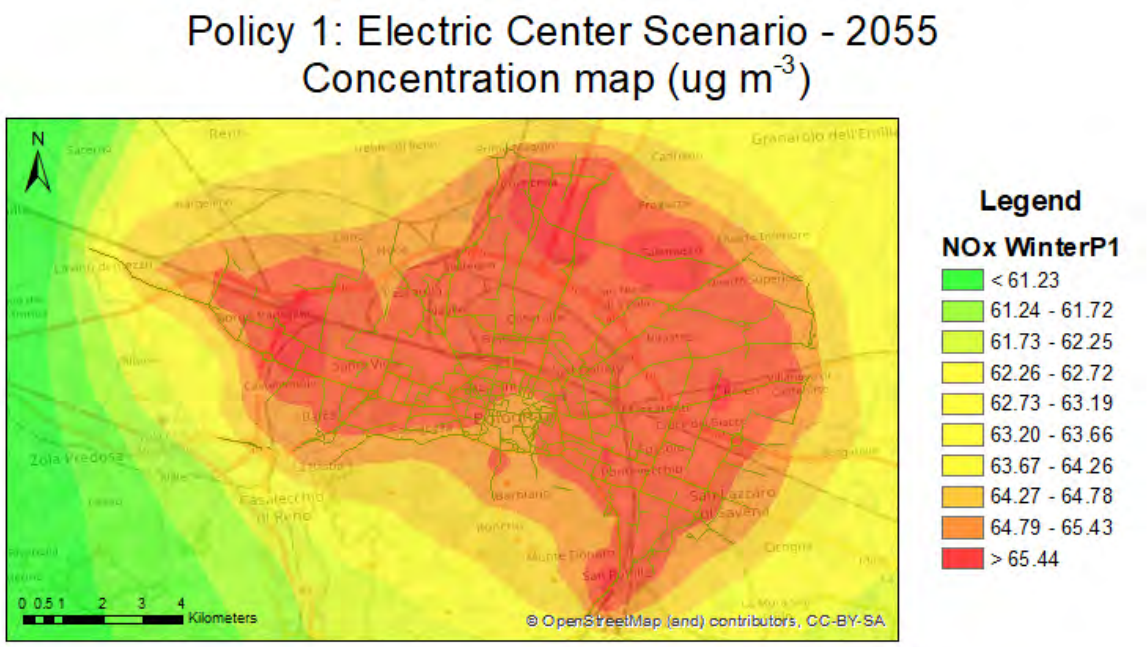

Figure 98. Concentration maps of NO_x in the 2055P1EC for Bologna. The maps represent concentration values averaged over winter 2055.

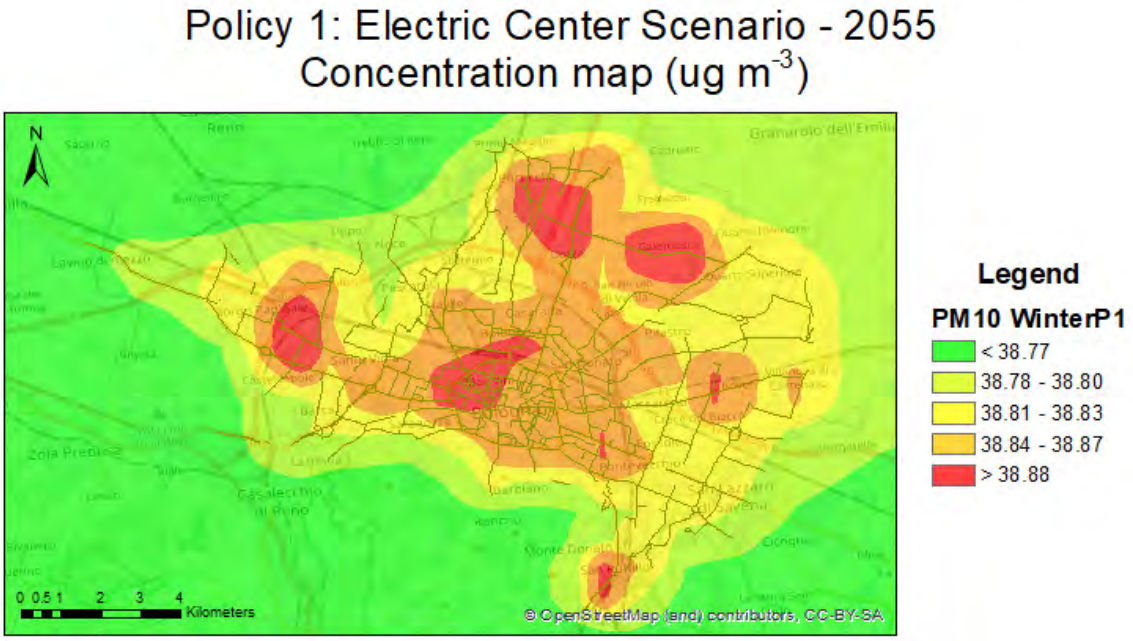

Figure 99. Concentration maps of PM_{10} in the 2055P1EC for Bologna. The maps represent concentration values averaged over winter 2055.

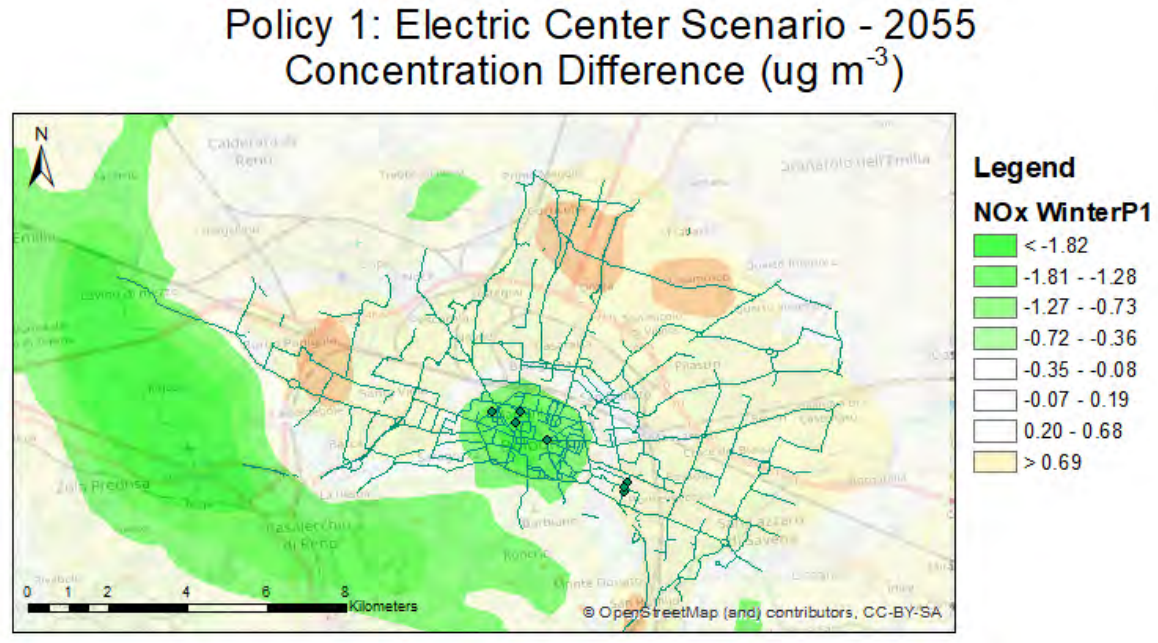

Figure 100. Maps of concentration differences for NO_x for winter 2055. The differences are calculated between 2055P1EC scenario and 2055BC scenario.

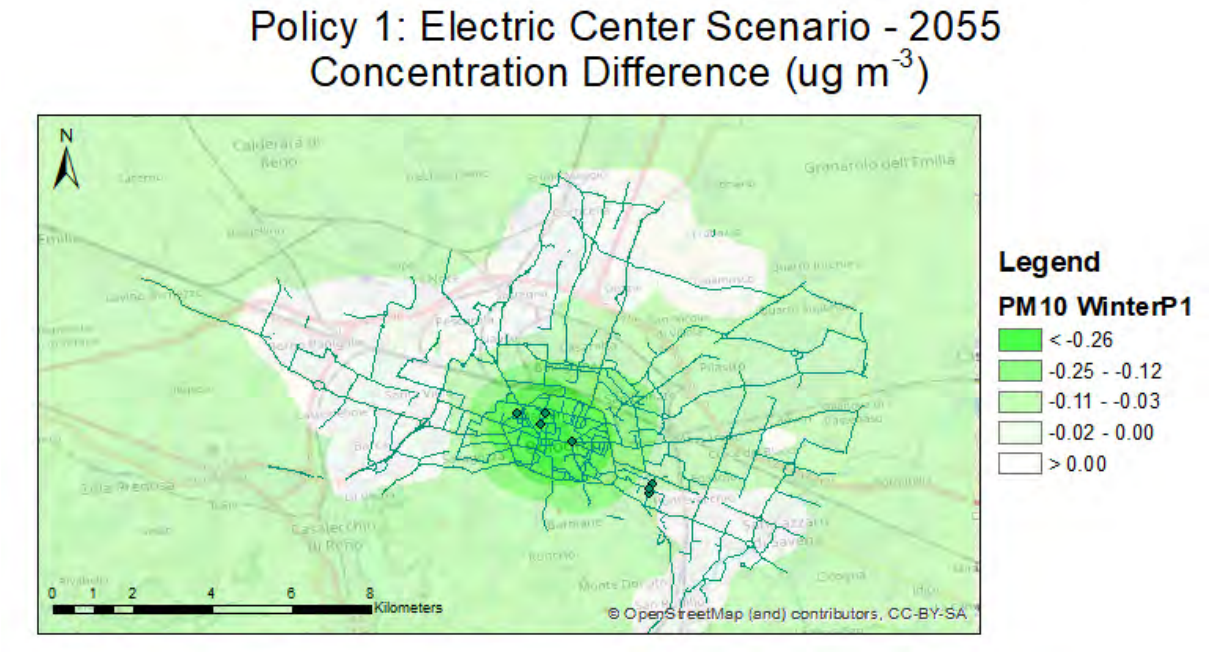

Figure 101. Maps of concentration differences for PM_{10} for winter 2055. The differences are calculated between 2055P1EC scenario and 2055BC scenario.

Comparing this scenario with the 2055BC scenario, the map of NO_x concentration differences shows a decrease in concentrations in the centre of Bologna, while in the outskirts there is a little increase in NO_x concentrations, however the increase is so low that it has no impact on the overall effect. Table 22 shows the percentages of reduction/increase in concentration evaluated at the receptors.

Policy	Season	Receptor name	NO_x	NO_2	CO	O_3	PM_{10}
1	Winter	V. Chiarini	-0.1%	-0.1%	0.0%	0.0%	0.0%
1	Winter	Porta S. Felice	-66.6%	-39.8%	-2.9%	48.2%	-11.3%
1	Winter	Giardini Margherita	-1.2%	-0.8%	-0.1%	0.5%	-0.1%
1	Summer	V. Chiarini	-0.9%	-1.0%	0.0%	0.1%	0.0%
1	Summer	Porta S. Felice	-75.5%	-60.3%	-1.9%	16.1%	-8.7%
2	Summer	Giardini Margherita	-2.1%	-2.1%	0.0%	0.2%	-0.1%

Table 22. Percentages of reduction/increase in concentration compared to the base case (calculated for all receptor).

At the Porta San Felice receptor, NO_x concentrations present a significant decrease, while at the Giardini Margherita receptor, reductions are smaller. Therefore, the effect of the policy can be considered satisfactory, as shown by the percentages of reduction/increase in concentration compared to the base case.

6.1.1.4 Policy 2 in future CC

The second policy implemented in Bologna concerns the conversion of the entire urban buses fleet to electric. Furthermore, we also considered that the city centre (the area inside the internal ring road) will be affected by an increase in bus frequency and a ban of all non-electric vehicles.

The comparison of the average values of receptors in Electric Buses scenario (2055P2EB scenario) for winter and summer (Table 23), shows that the winter is still a critical period. However, averages are lower than the 2055BC scenario for all pollutants, with the exception of ozone and PM_{10}.

Season	Receptor name	NO_x ($\mu g\ m^{-3}$)	NO_2 ($\mu g\ m^{-3}$)	CO ($mg\ m^{-3}$)	O_3 ($\mu g\ m^{-3}$)	PM_{10} ($\mu g\ m^{-3}$)
Winter	V. Chiarini	64.7	41.4	0.82	24.8	38.8
Winter	Porta S. Felice	65.3	41.5	0.83	24.8	39.3
Winter	Giardini Margherita	64.7	41.3	0.82	24.9	38.8
Summer	V. Chiarini	15.7	12.0	0.47	76.2	19.7
Summer	Porta S. Felice	15.9	12.1	0.47	76.2	19.9
Summer	Giardini Margherita	15.7	12.0	0.47	76.3	19.7

Table 23. Average concentration values to receptors in winter and summer for 2055P2EB scenario in Bologna.

Figure 102 and Figure 103 (winter case, summer case not shown) show the concentration maps for NO_x and PM_{10} pollutants (concentration maps for O_3, NO_2, and CO are not shown) in the 2055P2EB scenario for the comparison with the 2055BC scenario. Compared to the base CC case, this policy also causes a decrease in the maximum values, particularly for NO_x. Regarding the spatial pattern, NO_x concentrations present several hot spots (less intense) distributed throughout the territory, close to the most trafficked roads, while the PM_{10} concentrations still show a hot spot in the centre of Bologna, which could be due to non-exhaust emissions due to the increased frequency of electric buses.

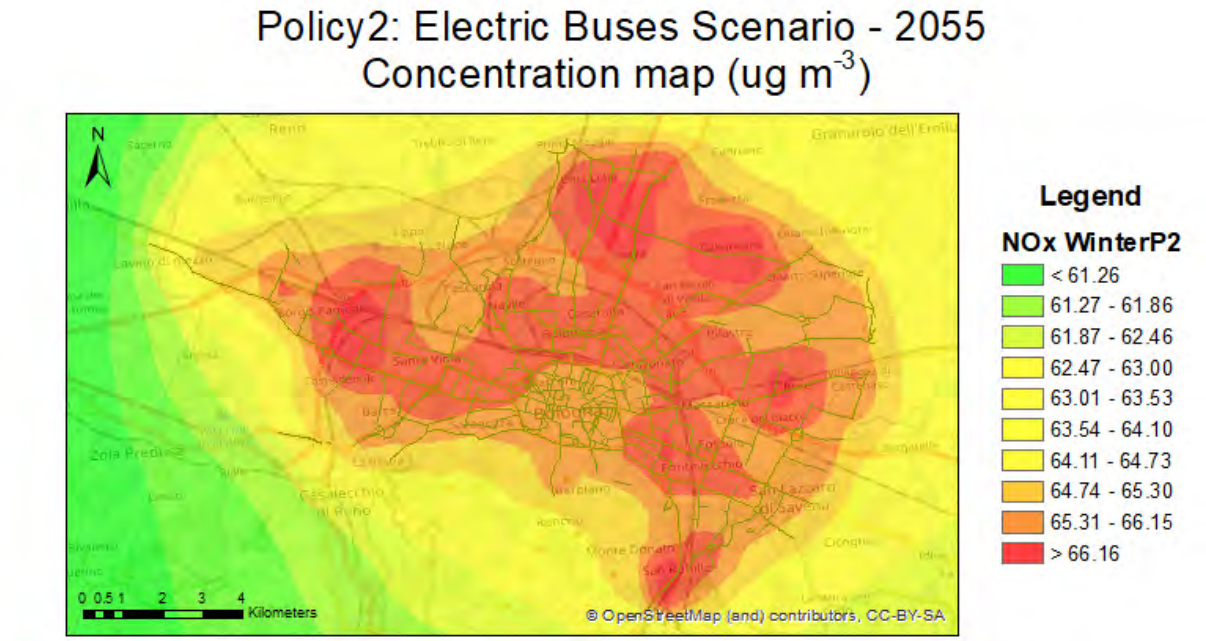

Figure 102. Concentration maps of NO_x in the 2055P2EB for Bologna. The maps represent concentration values averaged over winter 2055.

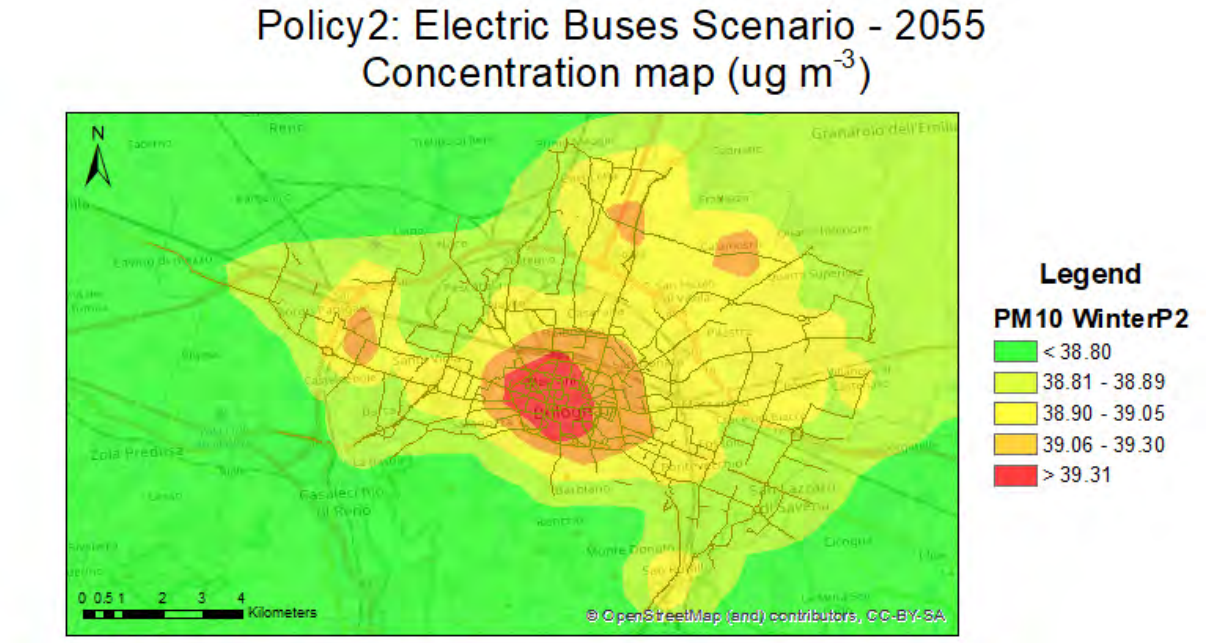

Figure 103. Concentration maps of PM_{10} in the 2055P2EB for Bologna. The maps represent concentration values averaged over winter 2055.

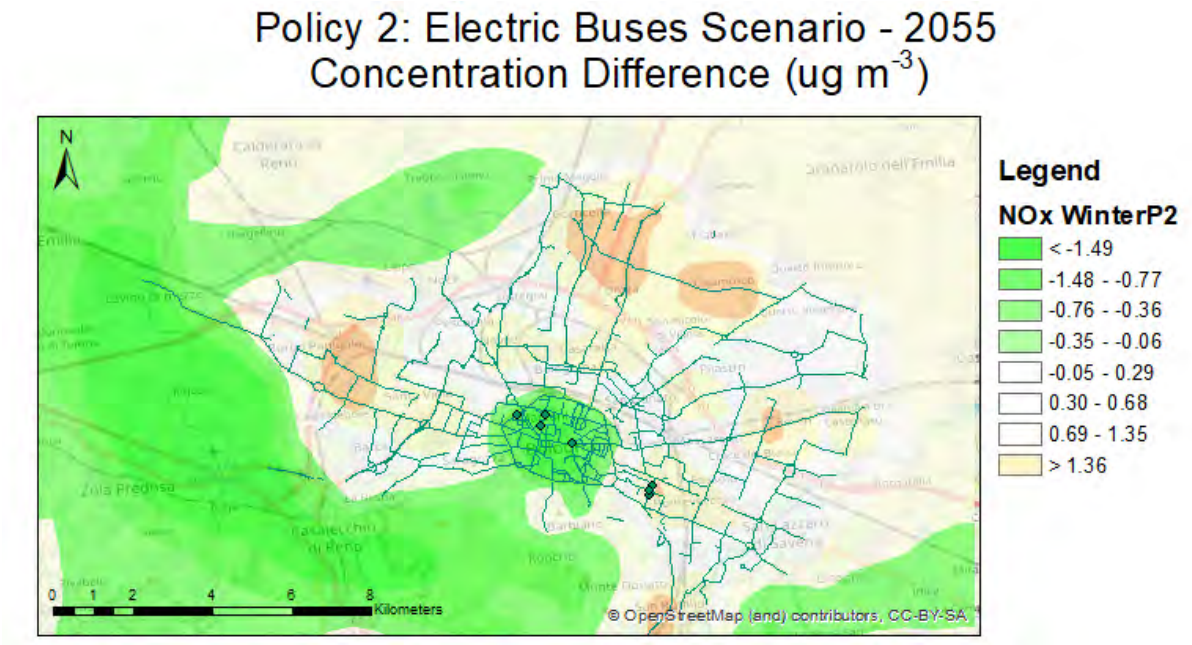

Figure 104. Maps of concentration differences for NO_x for winter 2055. The differences are calculated between 2055P2EB scenario and 2055BC scenario.

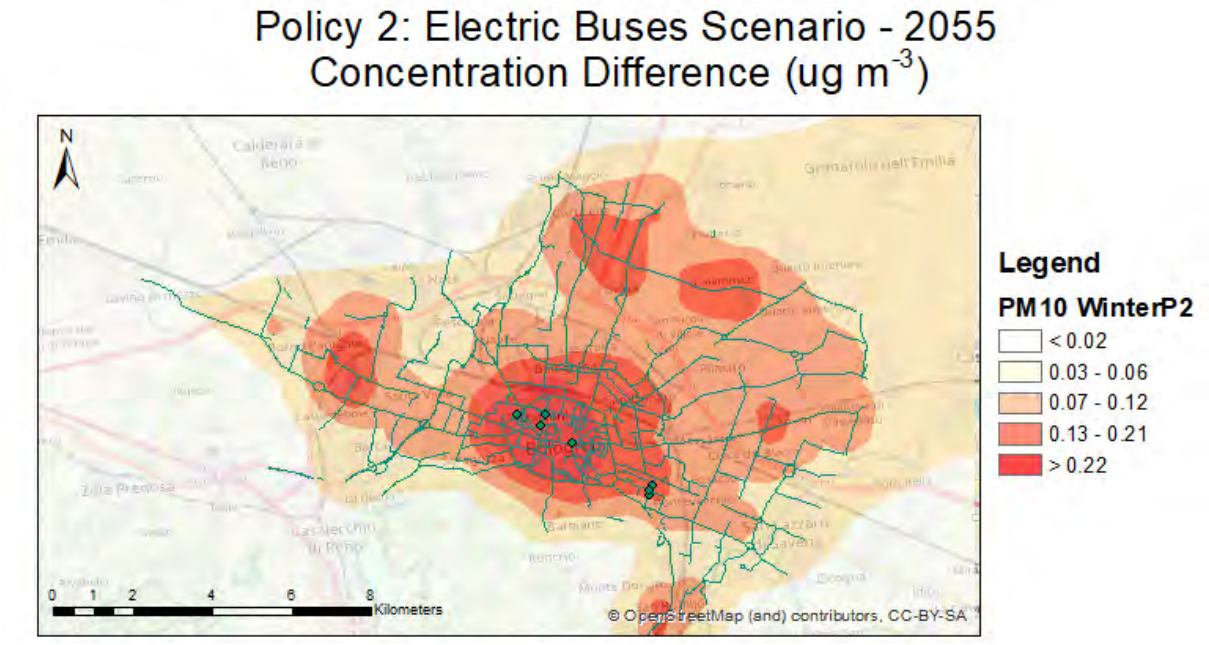

Figure 105. Maps of concentration differences for PM_{10} for winter 2055. The differences are calculated between 2055P2EB scenario and 2055BC scenario.

Comparing this scenario with the 2055BC scenario, the NO_x concentration difference map shows a decrease in concentrations in the centre of Bologna, while in the outskirts there is an increase in concentrations. However, the increases in NO_x concentrations in the outskirts are so low that they do

not have an impact on the overall effect. PM_{10} concentrations instead do not present any reductions, which is due to non-exhaust emissions deriving from the increased frequency electric buses.

Table 24 shows the percentages of reduction/increase in the concentrations evaluated at the receptors. At the Porta San Felice receptor, NO_x concentrations present a significant decrease, while at the Giardini Margherita receptor, reductions are smaller. As for PM_{10}, the percentages show a little increased compared to the base case. As already discussed above, this increase is due to the buses non-exhaust emissions. This increase, however, is very limited, with a maximum of 5.2% (on the Porta San Felice receptor in winter) that corresponds to 2.3 µg/m³ increase compared to the base case.

Policy	Season	Receptor name	NO_x	NO_2	CO	O_3	PM_{10}
2	Winter	V. Chiarini	0.0%	0.0%	0.0%	0.0%	0.0%
2	Winter	Porta S. Felice	-66.3%	-39.5%	-2.9%	47.4%	5.2%
2	Winter	Giardini Margherita	-1.1%	-0.8%	-0.1%	0.4%	0.1%
2	Summer	V. Chiarini	-0.5%	-0.5%	0.0%	0.0%	0.1%
2	Summer	Porta S. Felice	-75.1%	-60.0%	-1.9%	15.9%	3.3%
2	Summer	Giardini Margherita	-1.7%	-1.8%	0.0%	0.2%	0.1%

Table 24. Percentages of reduction/increase in concentration compared to the base case (calculated for all receptor).

The percentages of reduction/increase in concentration compared to the base CC case, show that the effect of the policy can be considered satisfactory.

6.1.2Hasselt

As done for the results presented in Section 4, for Hasselt we will present and discuss NO_2 and PM_{10} concentration maps obtained for the month of January 2055, due to our previous choice to consider these two pollutants in the current scenario (January 2016), with which we need to compare the results obtained for the future CC.

6.1.2.1 Meteorology in future CC

Under the effect of CC, the CC projections predict that in Hasselt it will be relatively warmer, windier and rainier than in the current scenario (Figure 106 and Figure 107).

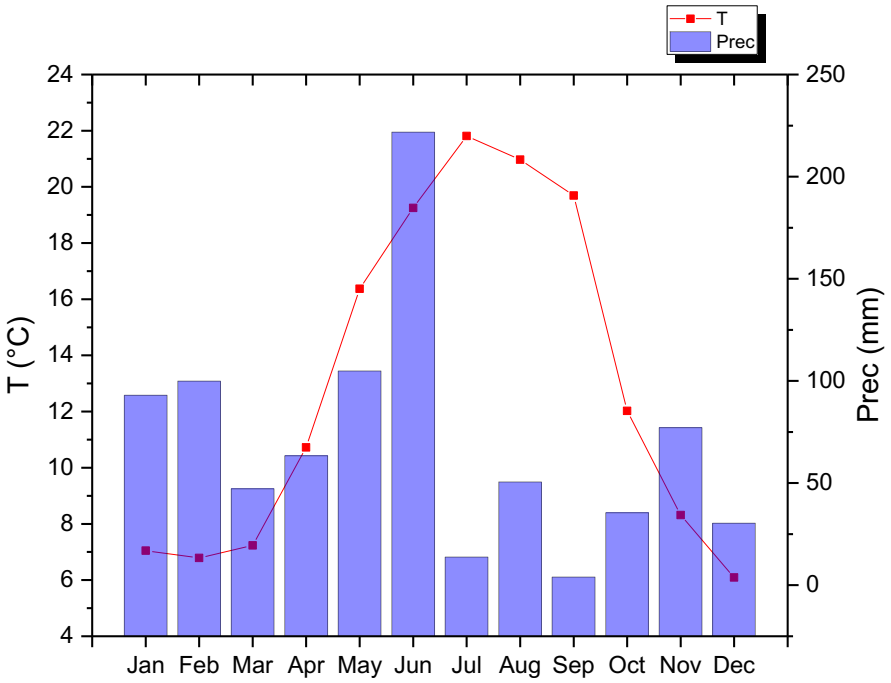

Figure 106. Monthly mean temperature and accumulated rainfall as estimated by the CC projections for Hasselt.

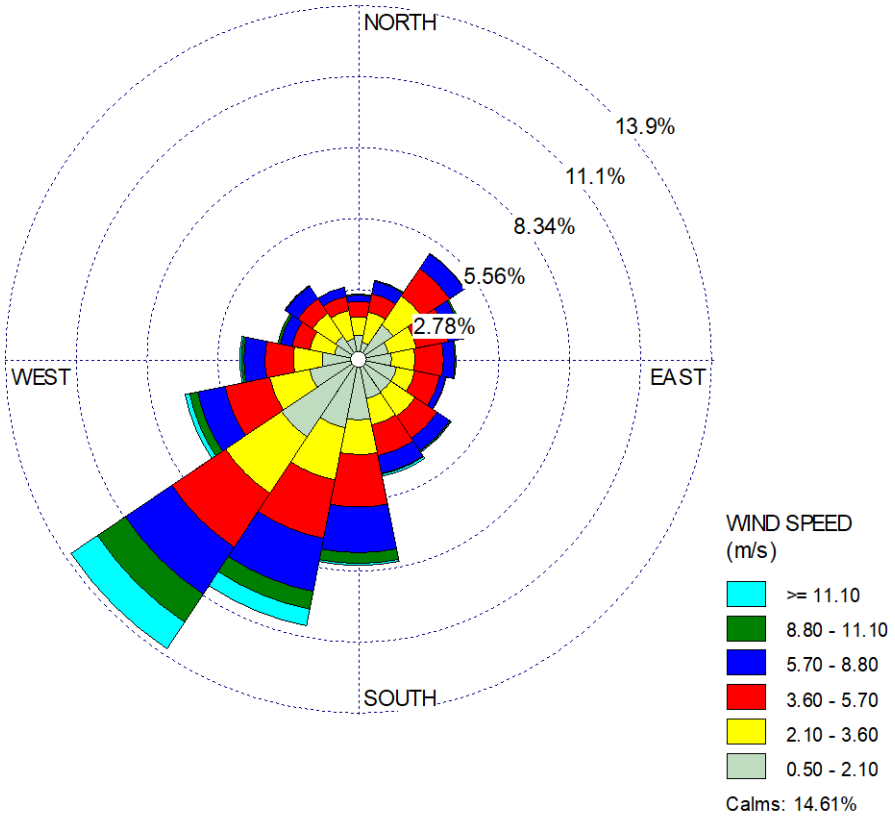

Figure 107. Wind rose of yearly wind frequencies as estimated by CC projections for Hasselt.

Wind directions are not predicted to change relevantly in the future in Hasselt. For this reason, the pattern of air quality dispersion will not significantly change as resulting of meteorology only (Figure 108 and Figure 109). In particular, both pollutants show the same hotspots as in the base case scenario, due to the absence of changes in wind direction and in the traffic policies. The same junctions are connected to local increases in air pollution, and only small reductions are predicted due to the increases in wind speeds. However, these reductions are really too limited to be considered significant.

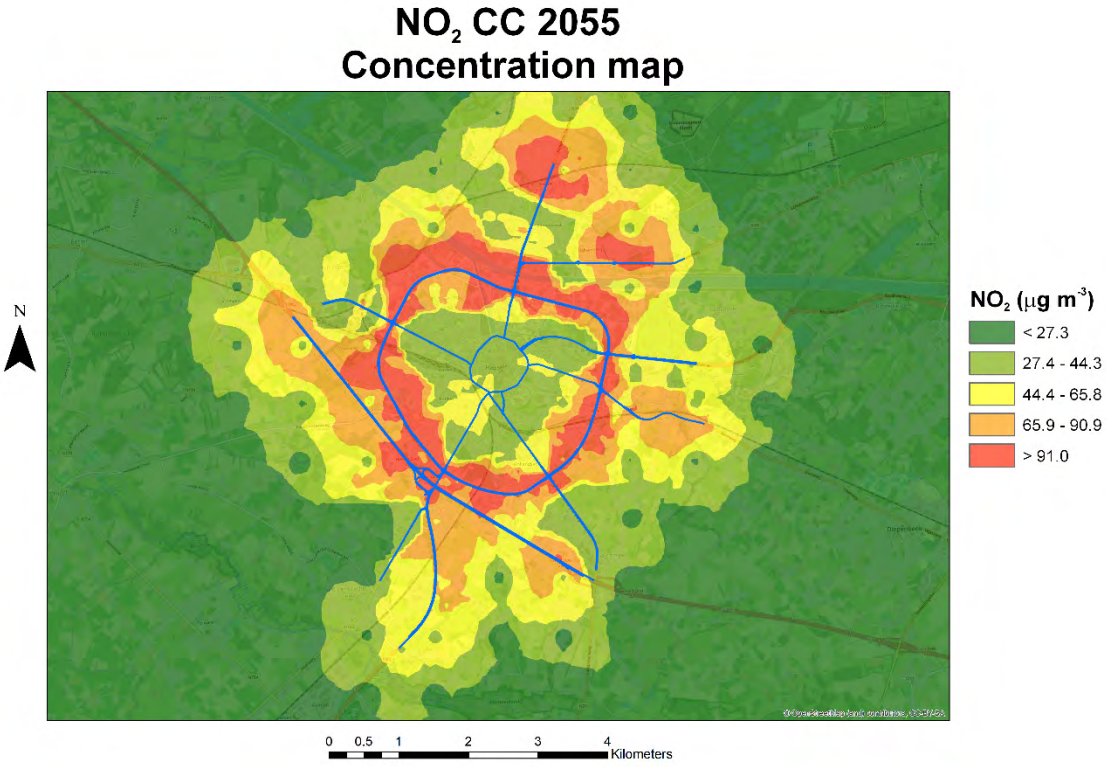

Figure 108. NO_2 concentration map in Hasselt in January 2055, as resulting from changes in meteorology only.

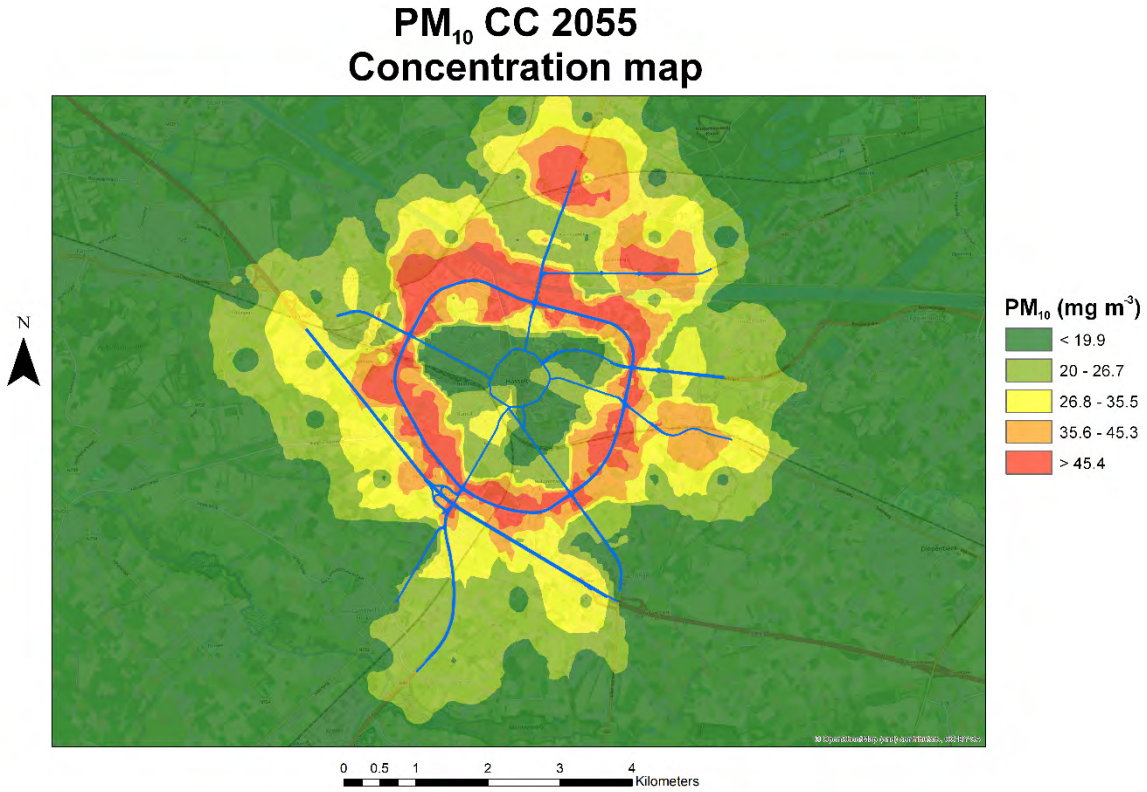

Figure 109. PM_{10} concentration map in Hasselt in January 2055, as resulting from changes in meteorology only.

6.1.2.2 Meteorology in future CC and future emissions

Besides changes in meteorology, here we also considered changes in emissions associated to the adoption of cleaner technologies in the future. Such reductions can be visualized comparing the emissions calculated in this case for road traffic (Figure 110 and Figure 111) and residential heating (Figure 112), with those previously presented in the base case for Hasselt.

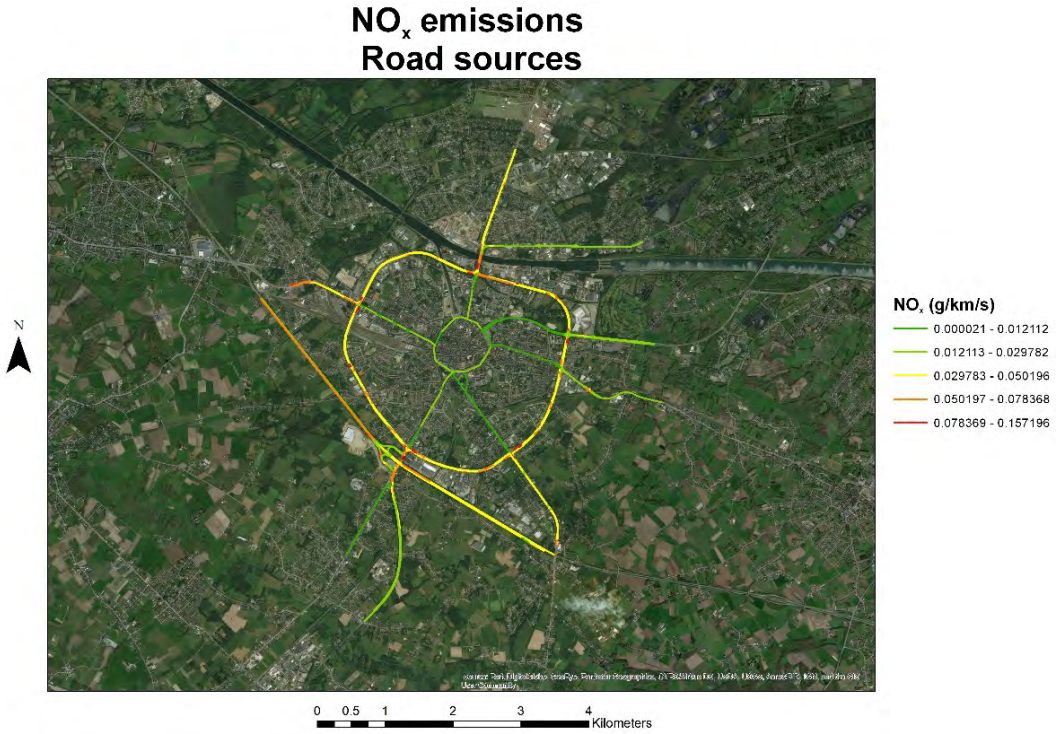

Figure 110. NO_x emissions (in g/km/s) for road sources considered as major roads in Hasselt in 2030 as estimated from the adoption of cleaner technologies and changes in fleet composition in the future.

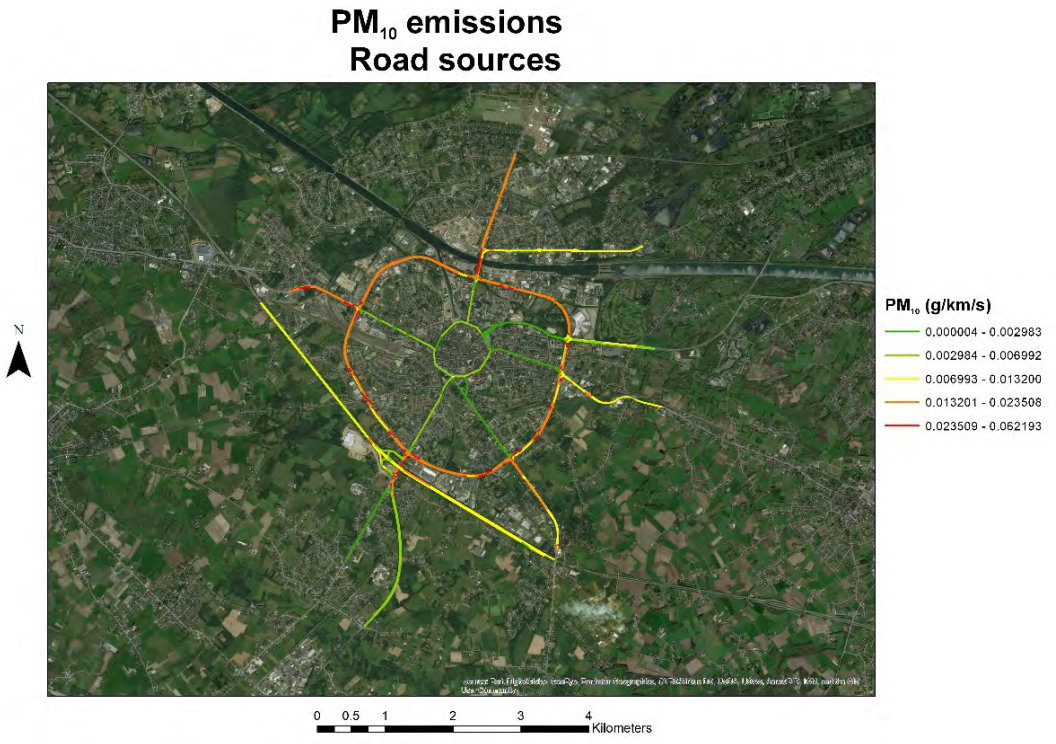

Figure 111. PM_{10} emissions (in g/km/s) for road sources considered as major roads in Hasselt in 2030 as estimated from the adoption of cleaner technologies and changes in fleet composition in the future.

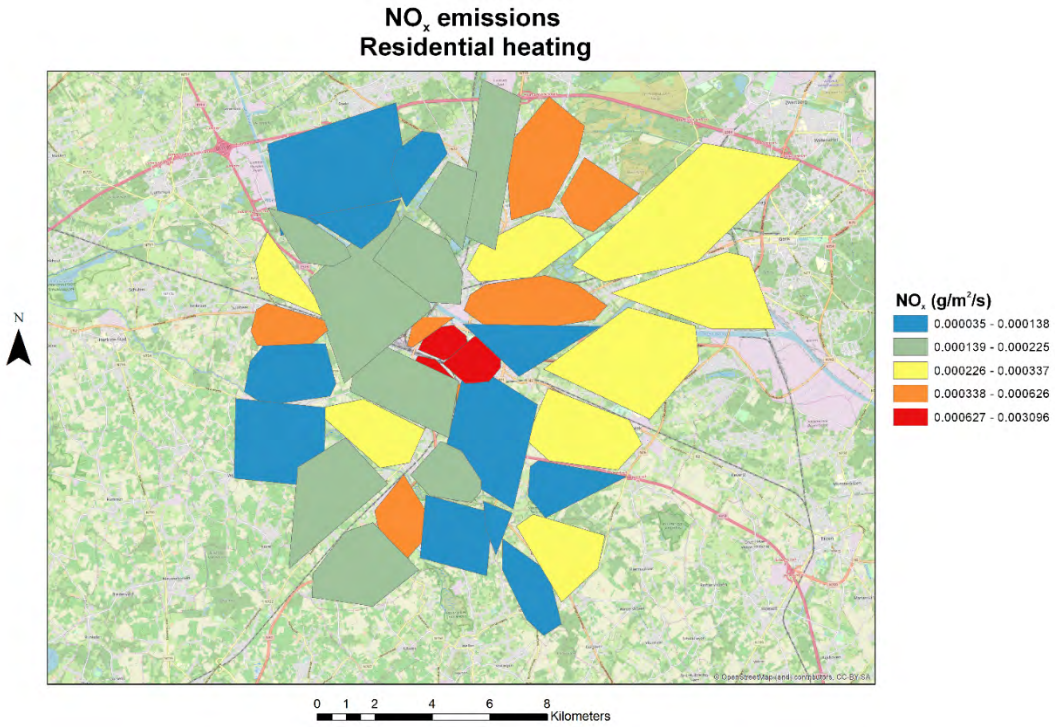

Figure 112. NO_x emissions ($g/m^2/s$) from residential heating in Hasselt in 2050 as estimated from the adoption of cleaner technologies.

As expected, the adoption of cleaner technologies (cleaner fuels, changes in engines) and the changes in fleet composition for road traffic cause relevant decreases in emissions for road sources, while for residential heating reductions are more limited. However, the effect of decreasing emissions seems indeed more relevant than the effect of the changes in meteorology presented above. However, as we applied any changes neither in the position of the sources (no changes in local population) nor in the position of roads, by construction the relative position of the hotspots is not predicted to change in our simulations.

In fact, as observed from Figure 110 and Figure 111, NO_2 and PM_{10} emissions will decrease strongly as a result of the adoption of cleaner technologies. In particular, reductions in concentrations appear strongly linked to the reductions in emissions more than to the changes in meteorology. This observation is partially in agreement with the results of Barmpadimos et al. (2011, 2012), and Colette et al. (2011) who observed a PM_{10} drop in the period late '90s-2010 in Europe, attributed mostly to a decrease in anthropogenic emissions even though with a contribution also of meteorological processes. Again, however, we might note that the concentration patterns for the two pollutants show no relevant changes and the pollution hotspots in Hasselt remain located in the same position as in the base case.

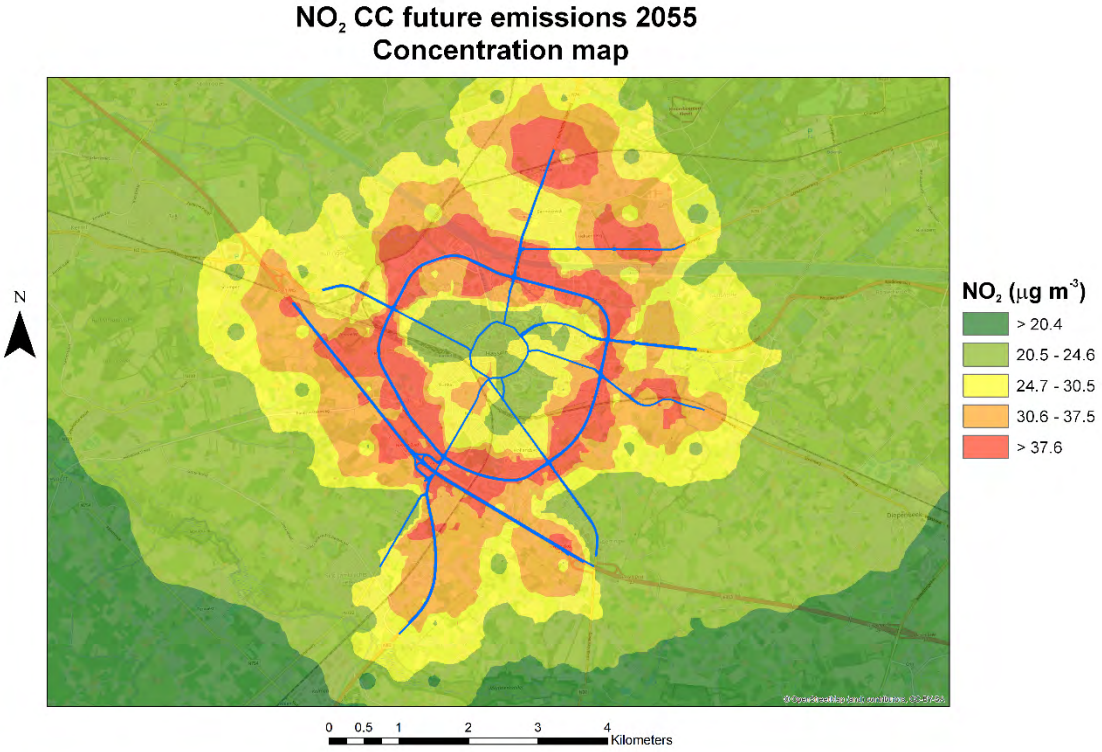

Figure 113. NO_2 concentration map in Hasselt in January 2055, as resulting from changes in meteorology and reduction emissions due to the effect of cleaner technologies.

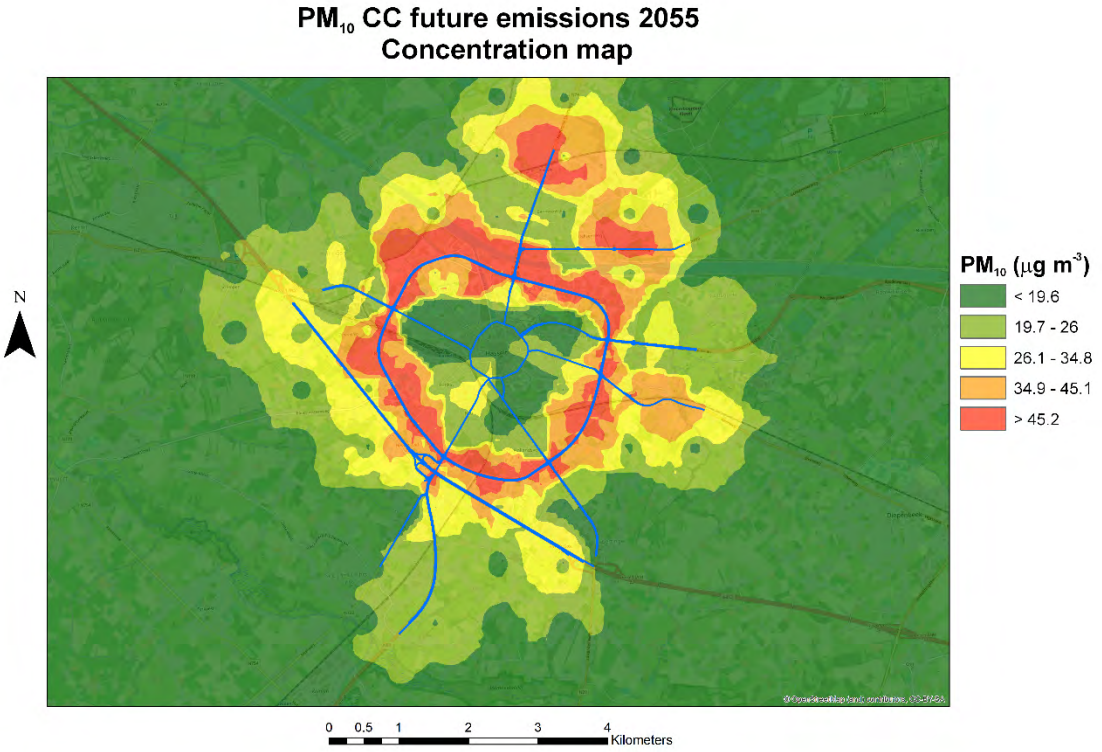

Figure 114. PM_{10} concentration map in Hasselt in January 2055, as resulting from changes in meteorology and reduction emissions due to the effect of cleaner technologies.

6.1.2.3 Policy 1 in future CC

In this subsection we provide the results for the long-term simulations in the event that policy 1 (closure of the inner ring) were implemented in the CC scenario with the changes in meteorology outlined in previous subsection 6.1.2.1.

Figure 115 and Figure 116 report the NO_2 and PM_{10} concentration maps resulting as an output from long-term dispersion simulations in January 2055 with the CC change scenario previously discussed and in case of implementation of the policy 1 of closure of roads of and within the inner ring.

In general, the minimum and maximum concentrations are only slightly decreased with respect to the case that the policy is not implemented (Figure 108 and Figure 109) while concentrations are only slightly higher with respect to the case of reductions in emissions all over the domain (Figure 113 and Figure 114).

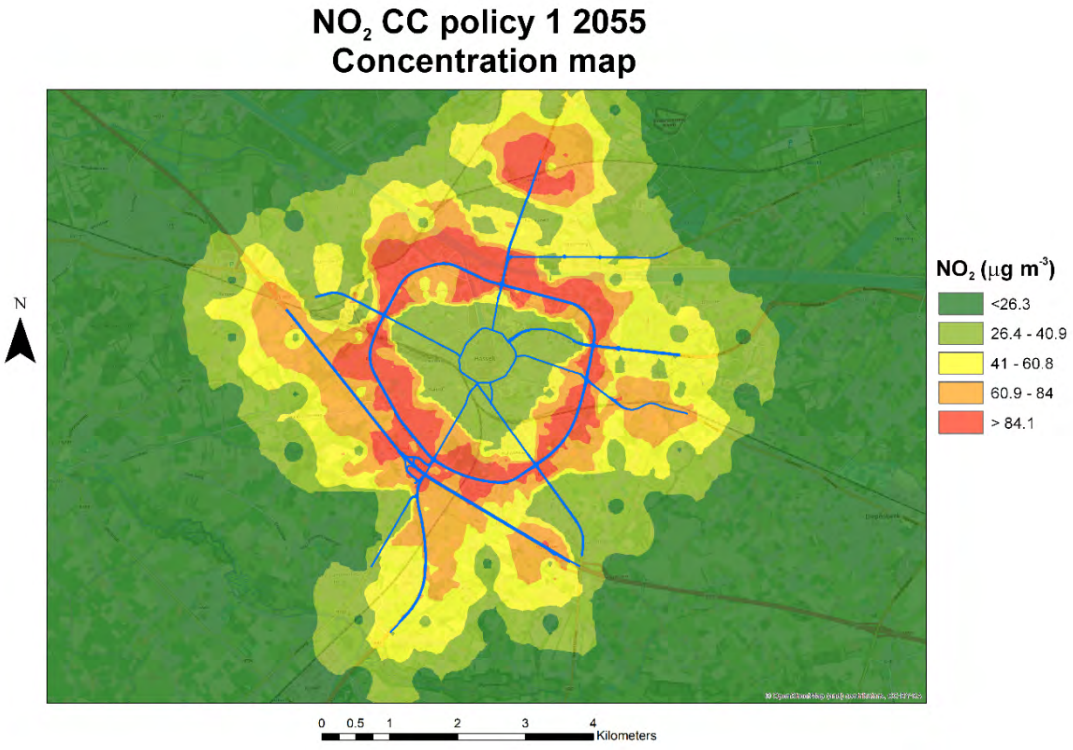

Figure 115. NO_2 concentration map in Hasselt in January 2055, as resulting from climate changes in meteorology and with the implementation of the policy 1, i.e. closing the inner ring road to the traffic.

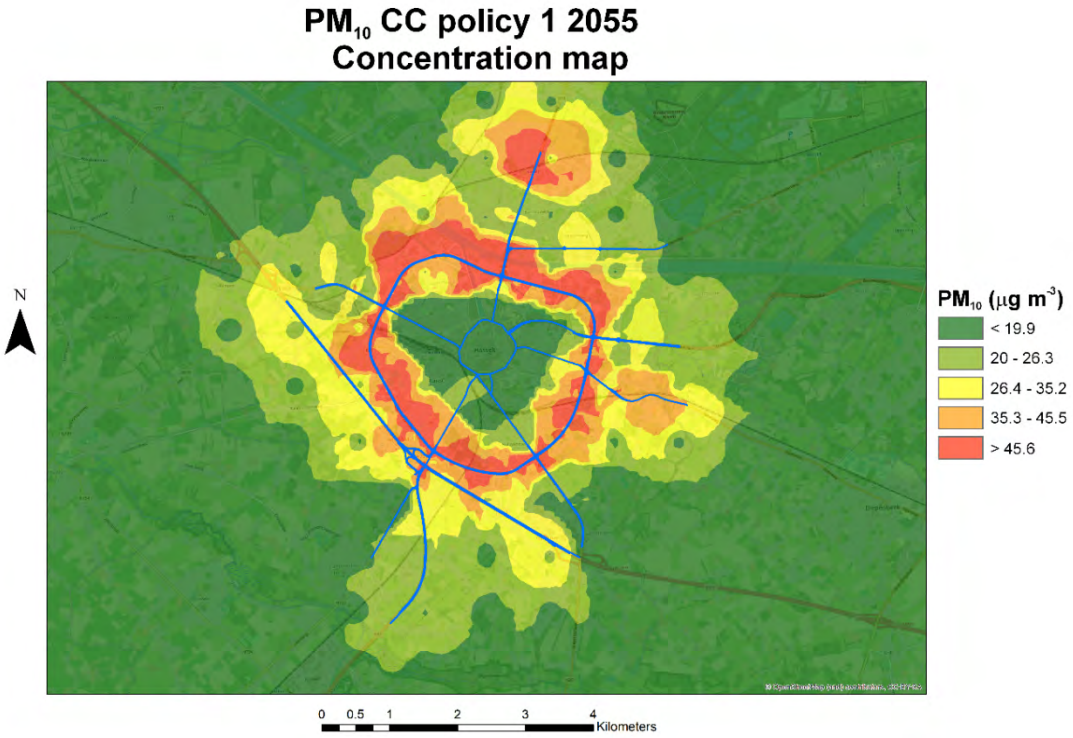

Figure 116. PM_{10} concentration map in Hasselt in January 2055, as resulting from climate changes in meteorology and with the implementation of the policy 1, i.e. closing the inner ring road to the traffic.

Figure 117 and Figure 118 depict the maps of NO_2 and PM_{10} concentration differences between the CC scenario when the policy is implemented and without implementation of the policy. The Figures offer the possibility to get a clearer picture of the results of the implementation of the policy in future CC in terms of NO_2 and PM_{10} concentrations. In particular, similar to what observed in the current (baseline) case, we can observe that the policy affects only a very small portion of the domain, due to the limited area where it was implemented. So, the largest portion of the domain presents reduced or no changes with respect to the case without the policy. NO_2 and PM_{10} reductions are observed close to the area where the policy is implemented, but also in the vicinity of the outer ring, probably because of the reduced number of cars going to the city centre because of the closure operated there. Areas of increased concentrations can be observed, which can derive from the effect of increased congestion in some roads where the people look for a parking close to the banned area. Overall, the result is similar for both air pollutants, with comparatively higher reductions for NO_2 than for PM_{10}.

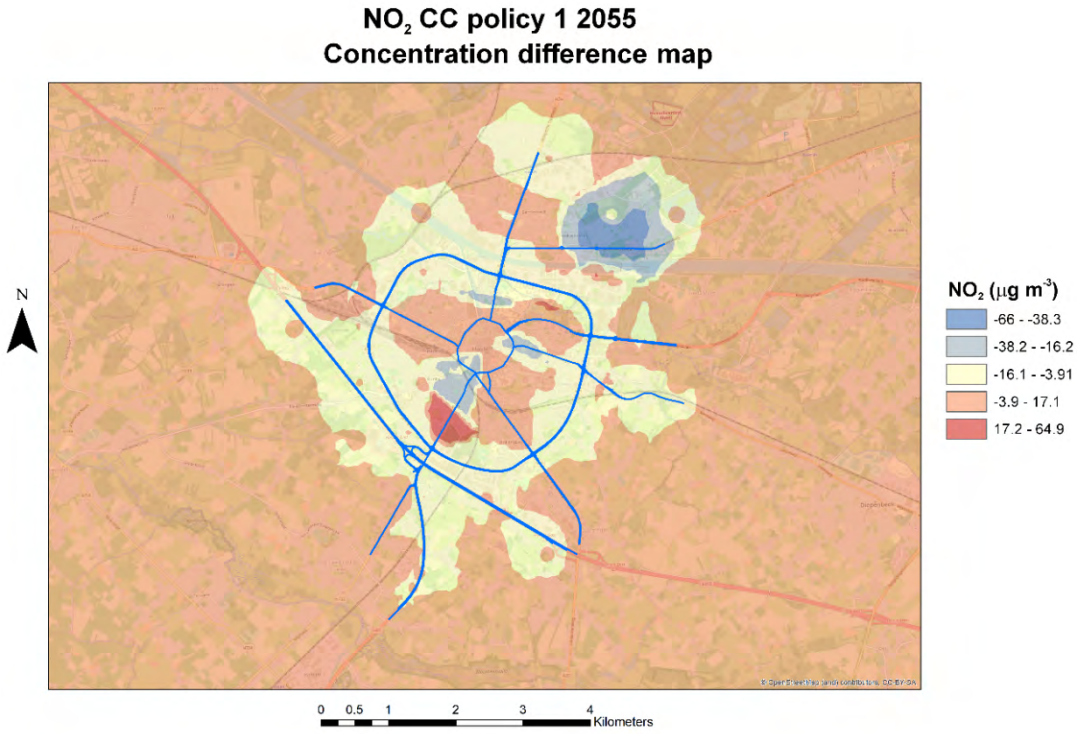

Figure 117. Map of differences in NO_2 concentration between the climate change scenario with reduction in emissions and the same scenario but in case of implementation of policy 1 in Hasselt.

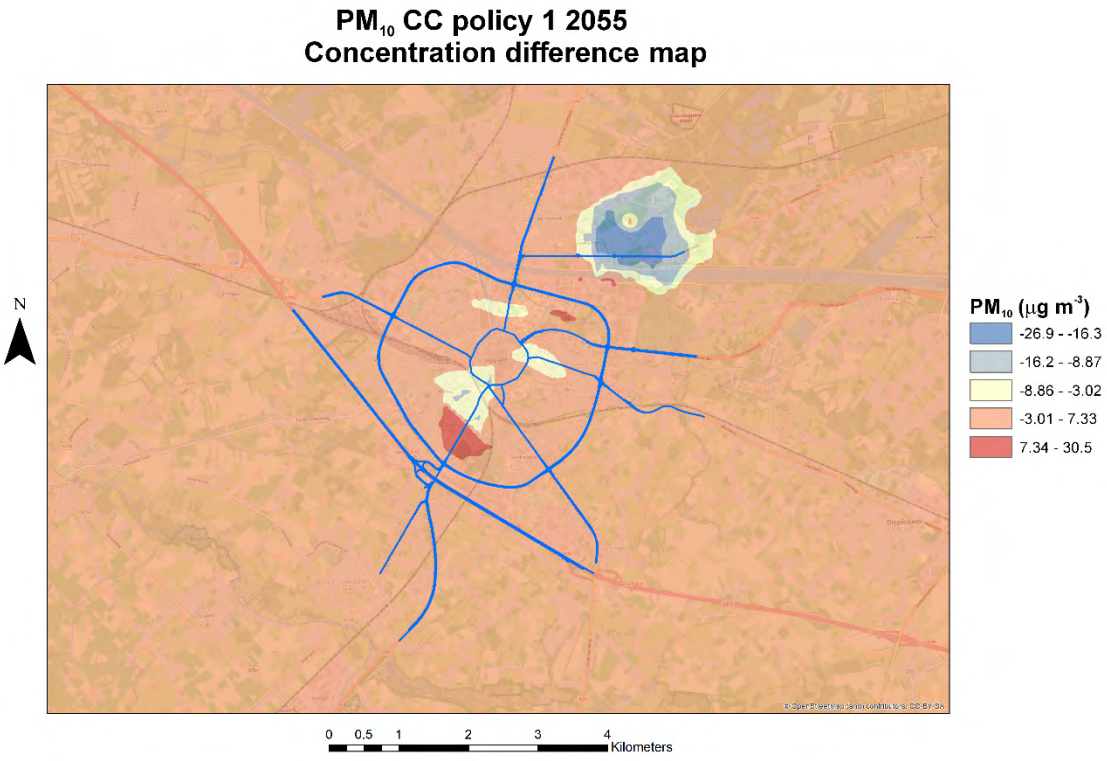

Figure 118. Map of differences in PM_{10} concentration between the climate change scenario with reduction in emissions and the same scenario but in case of implementation of policy 1 in Hasselt.

Similar to what done in the scenario with the implementation of the policy in the current (baseline) case, we also evaluated the NO_2 and PM_{10} reductions as ratio between the calculated differences and the concentration simulated in the CC scenario. Significant NO_2 reductions are observed in two areas up to 40-63% (Figure 119), while the outer ring is characterized by lower reductions although still relevant. Increases in NO_2 concentrations are observed only over some small areas. Reductions in PM_{10} connected with the implementation of the closure of the inner ring policy are instead more limited in terms of their spatial extension (Figure 120), though being also significant (34-53%).

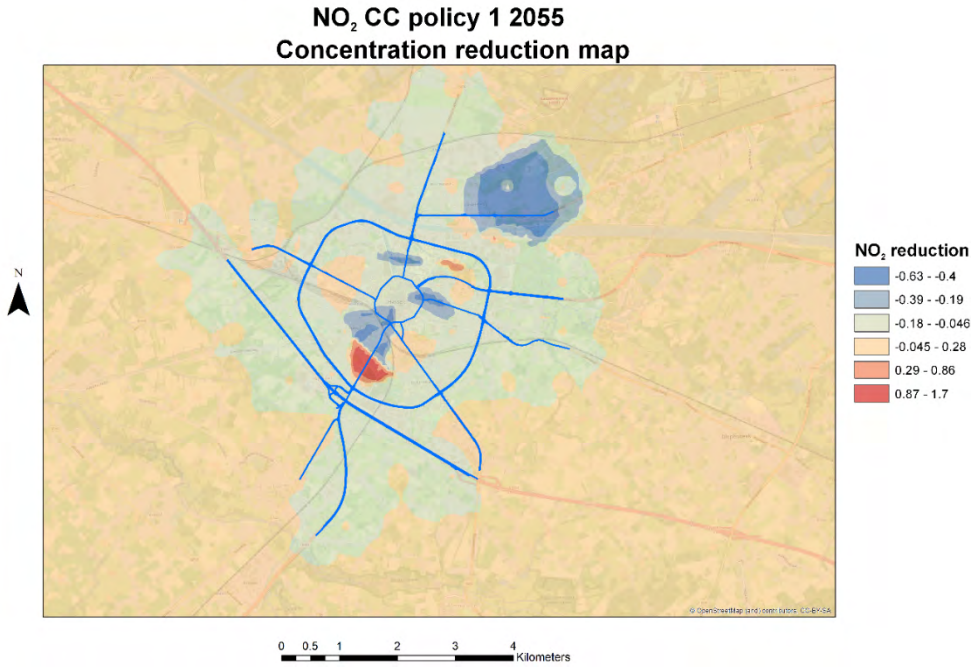

Figure 119. NO_2 reduction in case of implementation of policy 1 in CC scenario in Hasselt, evaluated as concentration ratio between the concentration difference previously evaluated (Figure 117) and the concentration observed in the CC scenario (Figure 113).

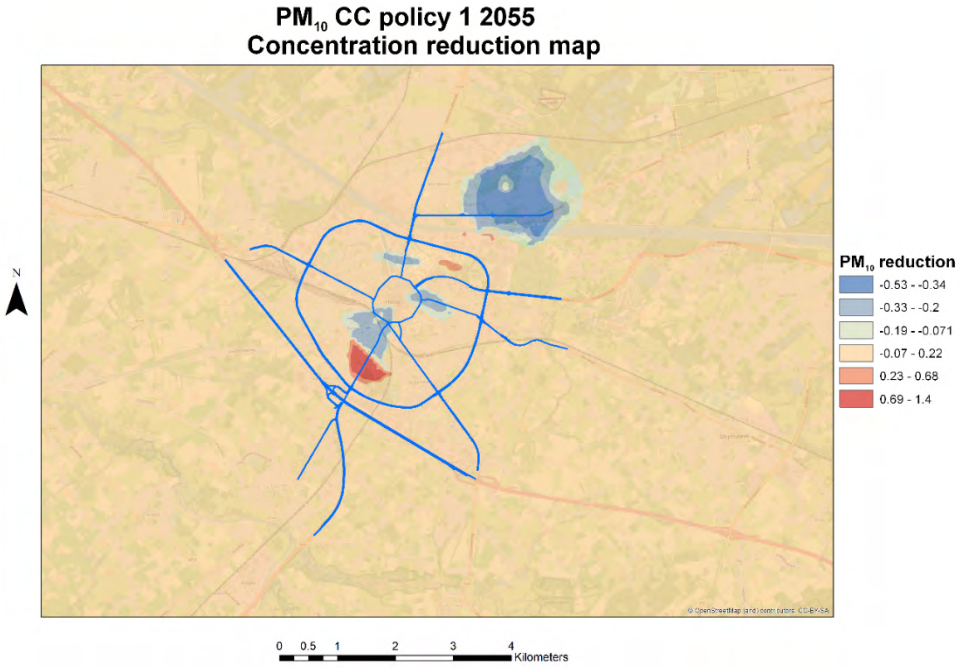

Figure 120. PM_{10} reduction in case of implementation of policy 1 in CC scenario in Hasselt, evaluated as concentration ratio between the concentration difference previously evaluated (Figure 118) and the concentration observed in the CC scenario (Figure 114).

6.1.2.4 Policy 2 in future CC

In the following, we provide the results for the long-term simulations in the event of implementation of policy 2 (increase in bus frequency) in the CC scenario with the changes in meteorology and emissions reduced as outlined above.

As per Figure 121 and Figure 122, and as previously noted in the base case scenario, the policy does not change dramatically the concentration patterns of air quality pollutants with respect to the case in which the policy was not implemented. However, and again similar to the base case, reductions in both NO_2 and PM_{10} concentrations are observed.

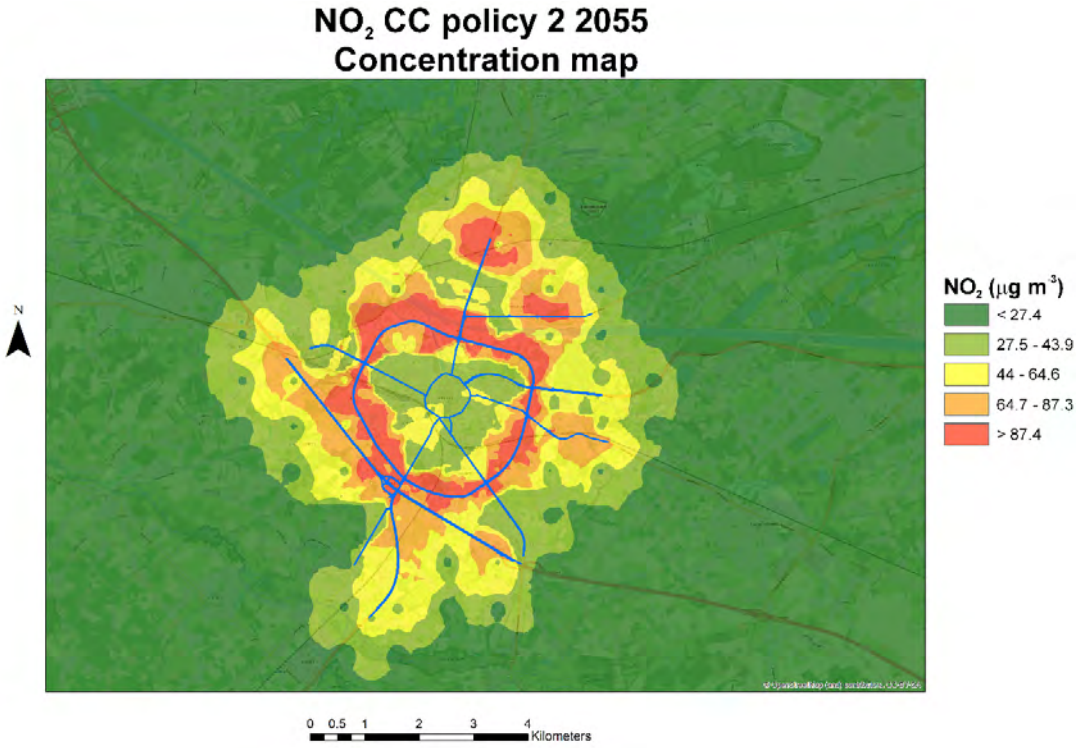

Figure 121. NO_2 concentration map in Hasselt in January 2055, as resulting from changes in meteorology and with the implementation of the policy 2 i.e. with an increase in the bus frequencies.

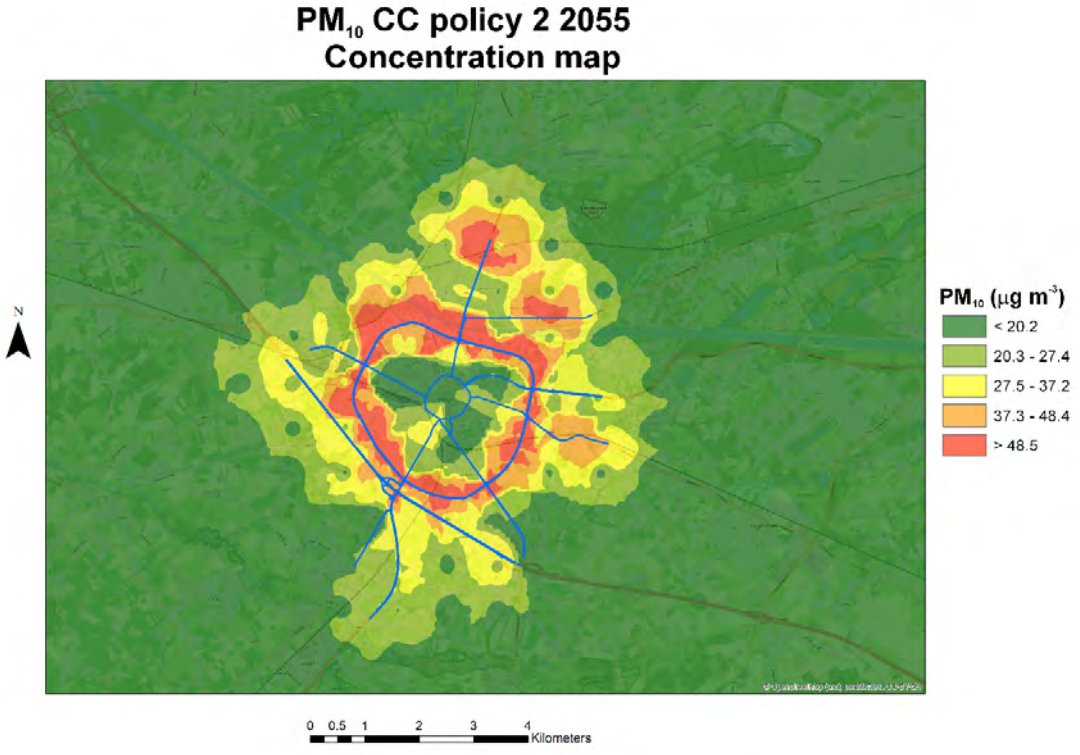

Figure 122. PM_{10} concentration map in Hasselt in January 2055, as resulting from changes in meteorology and with the implementation of the policy 2 i.e. with an increase in the bus frequencies.

Reductions with respect to the case without the implementation are even clearer when looking at maps of concentration differences. Again, we may observe that while reductions in NO_2 are limited mostly to the outer ring (Figure 123), reductions in PM_{10} extend over larger areas (Figure 124). Areas of PM_{10} increases are also observed, which are due to the increase of PM_{10} mechanically produced by wear on mechanical parts.

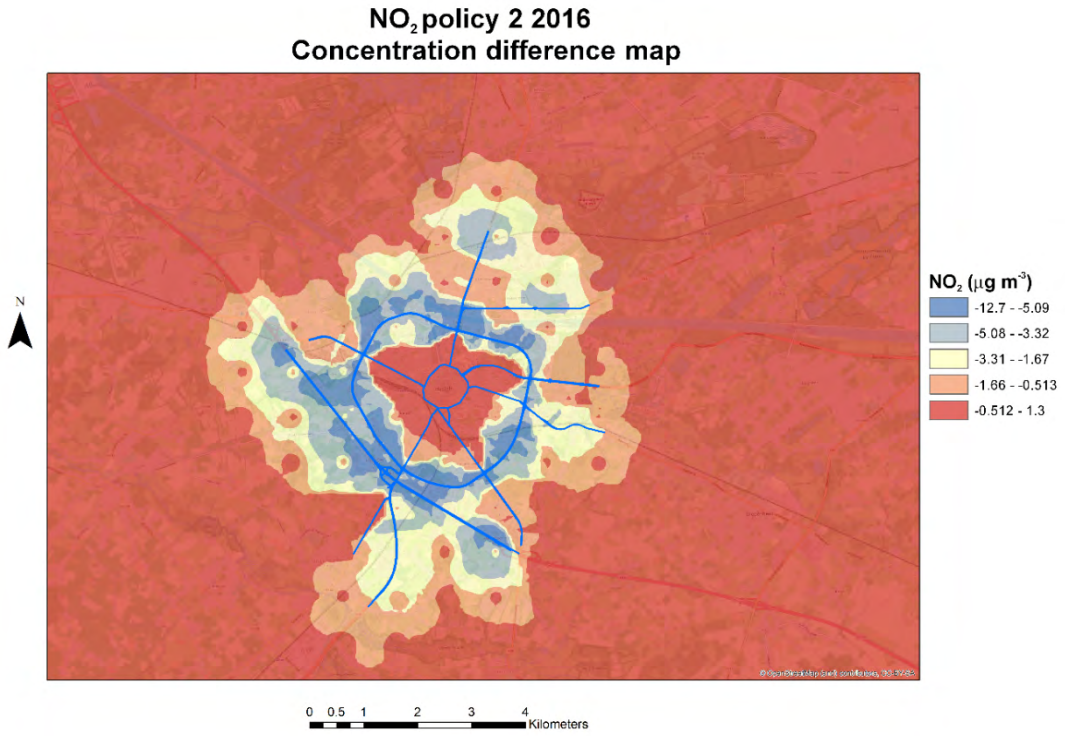

Figure 123. Map of differences in NO_2 concentration between the climate change scenario with reduction in emissions and the same scenario but in case of implementation of policy 2 in Hasselt.

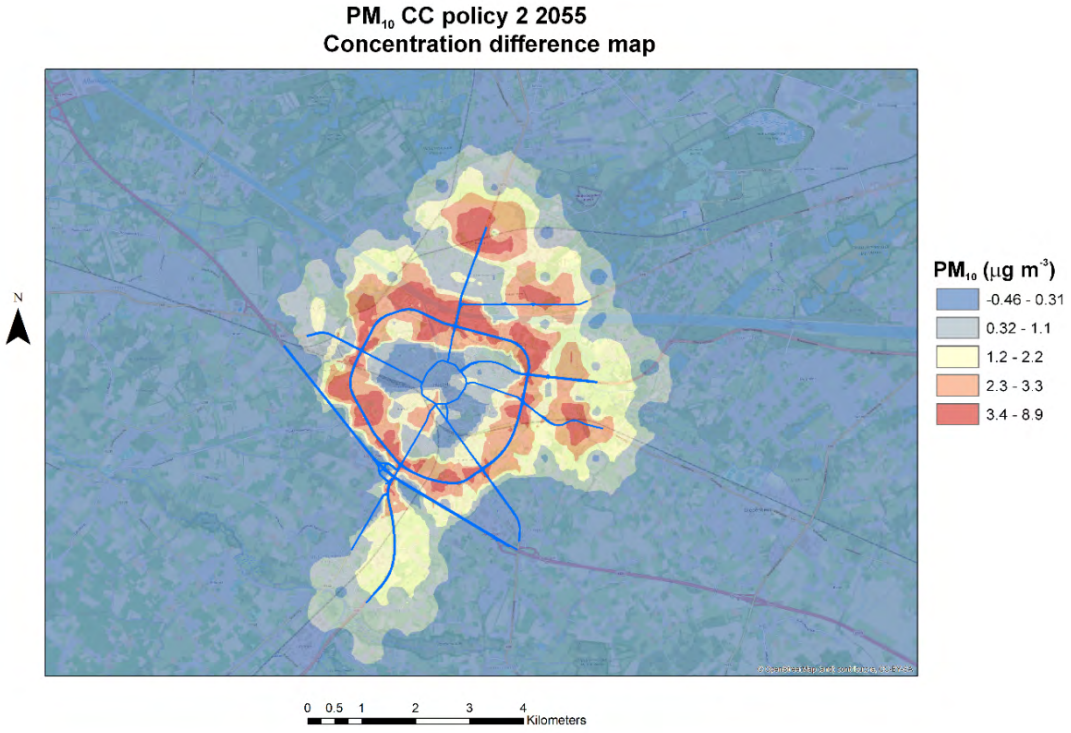

Figure 124. Map of differences in PM_{10} concentration between the climate change scenario with reduction in emissions and the same scenario but in case of implementation of policy 2 in Hasselt.

We then evaluated the reductions for the CC scenario with the implementation of this policy. The results (Figure 125 and Figure 126) indicate that NO_2 and PM_{10} reductions are more limited (only 0.5-0.8% and 0.8-1.2% for NO_2 and PM_{10}, respectively), similar to what observed in the base case. As such, the impact of the implementation of this policy in the CC scenario seems very limited.

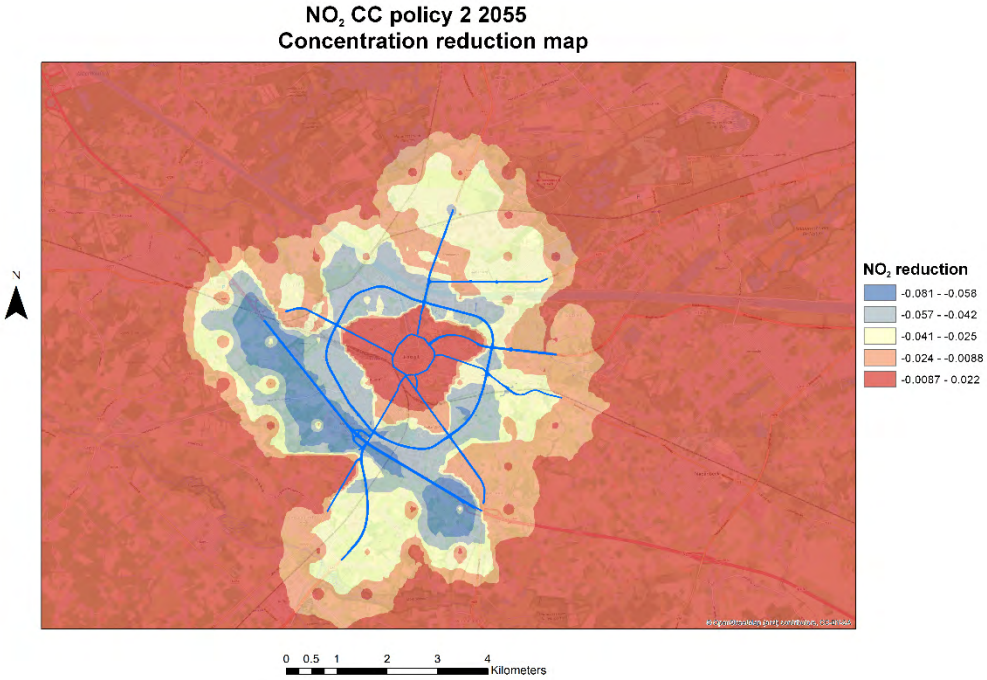

Figure 125. NO_2 reduction in case of implementation of policy 2 in CC scenario in Hasselt, evaluated as concentration ratio between the concentration difference previously evaluated (Figure 123) and the concentration observed in the CC scenario (Figure 113).

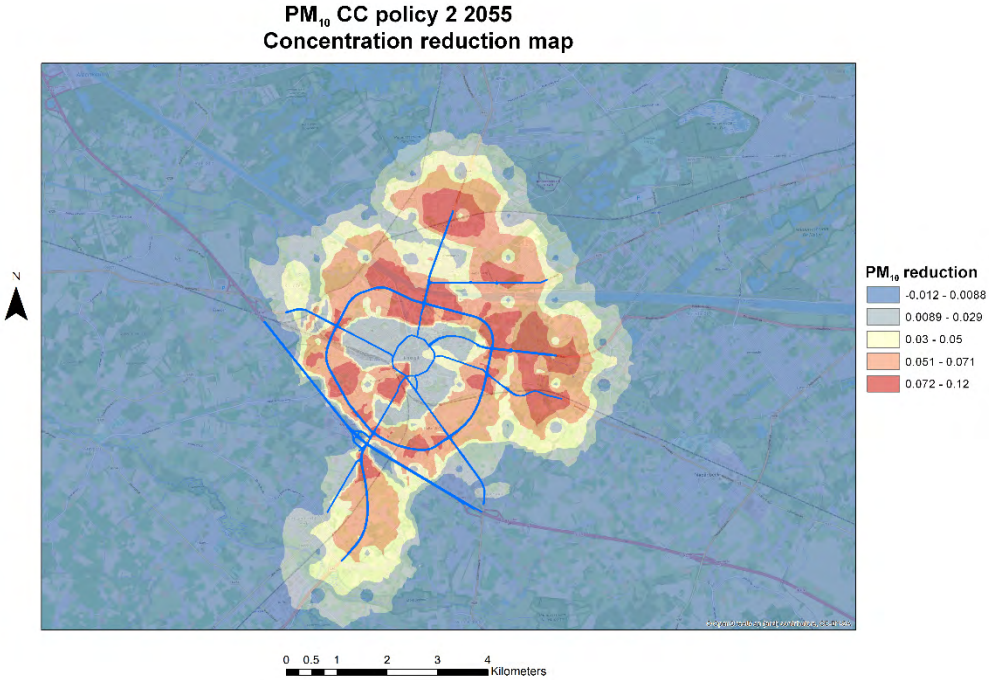

Figure 126. PM_{10} reduction in case of implementation of policy 2 in CC scenario in Hasselt, evaluated as concentration ratio between the concentration difference previously evaluated (Figure 124) and the concentration observed in the CC scenario (Figure 114).

6.1.3 Vantaa

Similar to Section 4, and to what previously presented for Hasselt, in Vantaa we will present and discuss NO_2 and $PM_{2.5}$ concentration maps obtained for the month of January 2055, due to our previous choice to consider these two pollutants in the current scenario (January 2017), with which we need to compare the results obtained for the future CC.

6.1.3.1 Meteorology in future CC

Under the effect of CC, the CC projections predict that in Vantaa in January 2055 it will be relatively warmer and rainier than in January 2017, while wind speeds will not change significantly and the frequency changes in wind directions are not readily observed in the annual wind rose (Figure 127 and Figure 128).

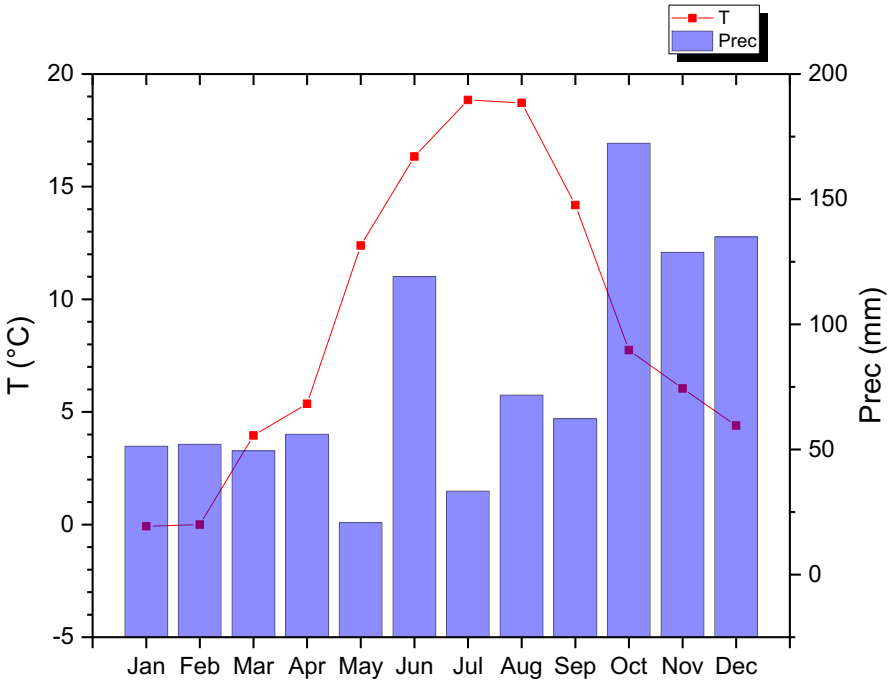

Figure 127. Monthly mean temperature and accumulate rainfall as estimated by the CC projections for Vantaa.

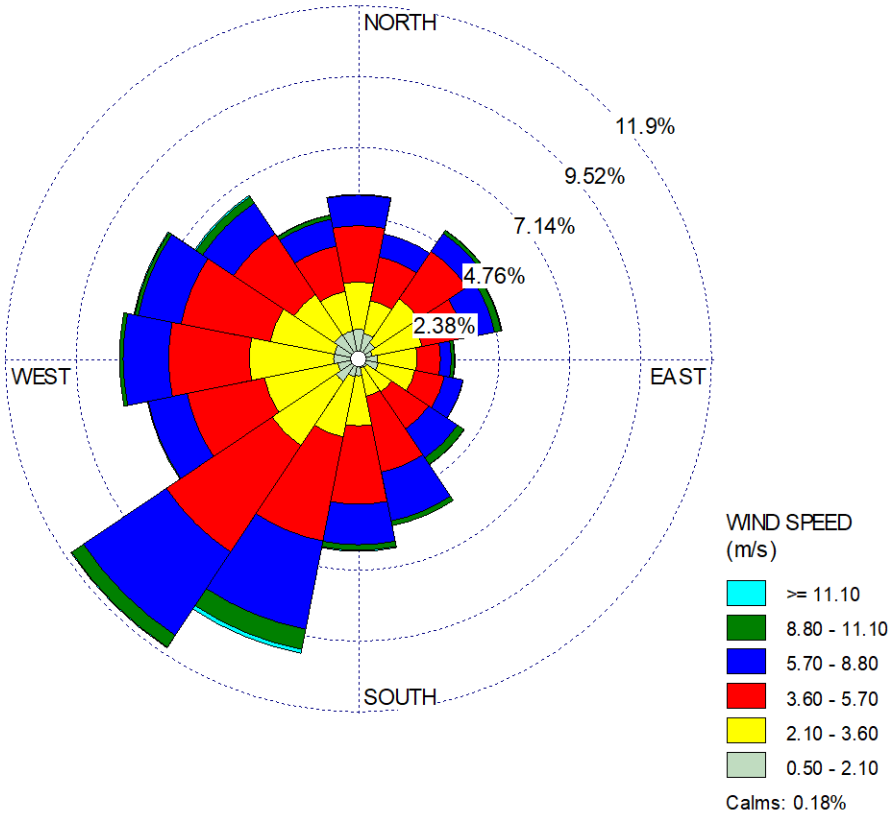

Figure 128. Wind rose of yearly wind frequencies as estimated by CC projections for Vantaa.

The small changes in wind directions will have limited impact on the pattern of air quality dispersion, which will not significantly change as resulting of meteorology only (Figure 129 and Figure 130). In particular, both pollutants show similar hotspots as in the base case scenario, but with slight decreases of minimum values for both NO_2 and $PM_{2.5}$, and only for $PM_{2.5}$ in case of maximum values.

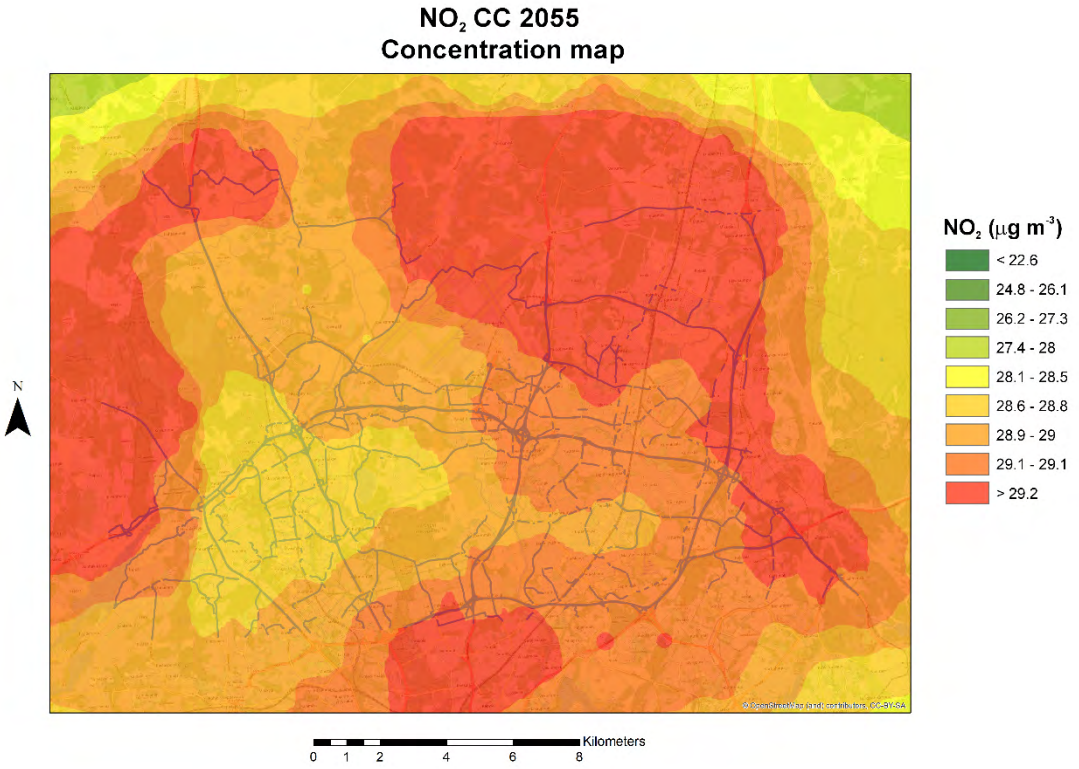

Figure 129. NO_2 concentration map in Vantaa in January 2055, as resulting from changes in meteorology only.

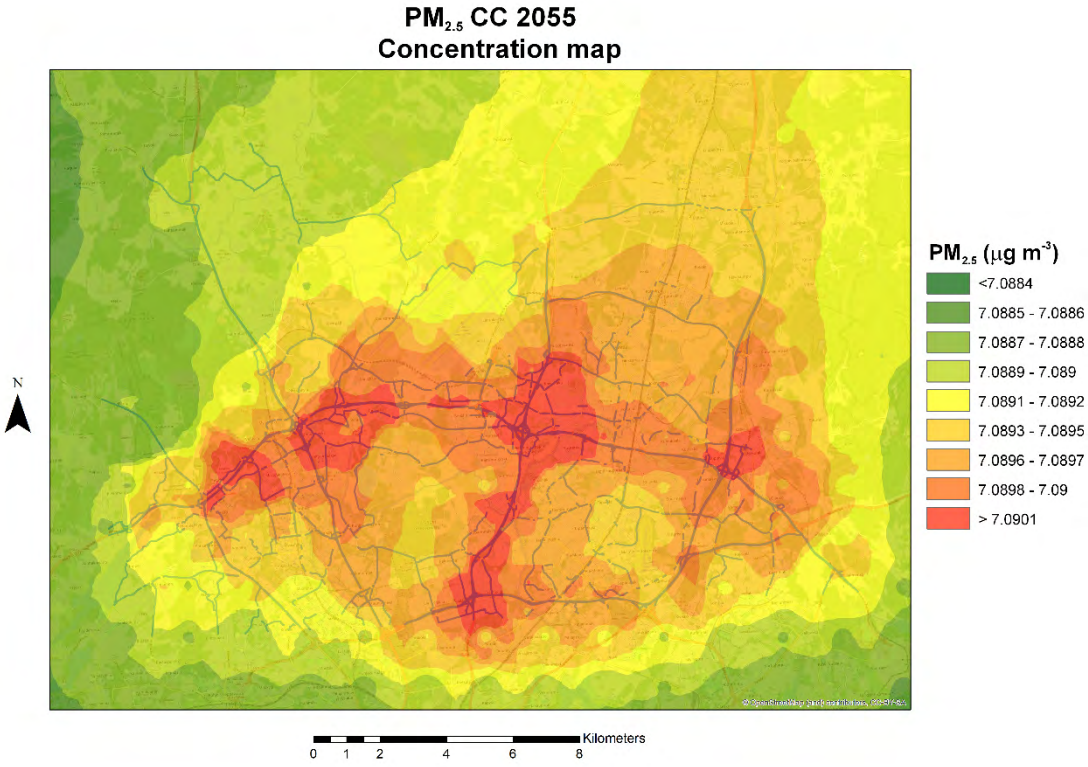

Figure 130. $PM_{2.5}$ concentration map in Vantaa in January 2055, as resulting from changes in meteorology only.

6.1.3.2 Policy 1 in future CC

In this subsection we provide the results for the long-term simulations in the event that policy 1 (complete closure of an area to the traffic, see Figure 33) were implemented in the CC scenario with the changes in meteorology outlined in previous subsection 6.1.3.1.

Figure 131 and Figure 132 report the NO_2 and PM_{10} concentration maps resulting as an output from long-term dispersion simulations in January 2055 with the CC change scenario previously discussed and in case of implementation of the policy 1 of closure of roads in the area previously illustrated.

In general, as in the present scenario, the impact of the intervention is very reduced for Vantaa: in particular $PM_{2.5}$ concentrations will not show any change with respect to the base case, while NO2 concentrations overall seem to present a pattern consistent with that observed in the base CC case but with slightly changed concentrations.

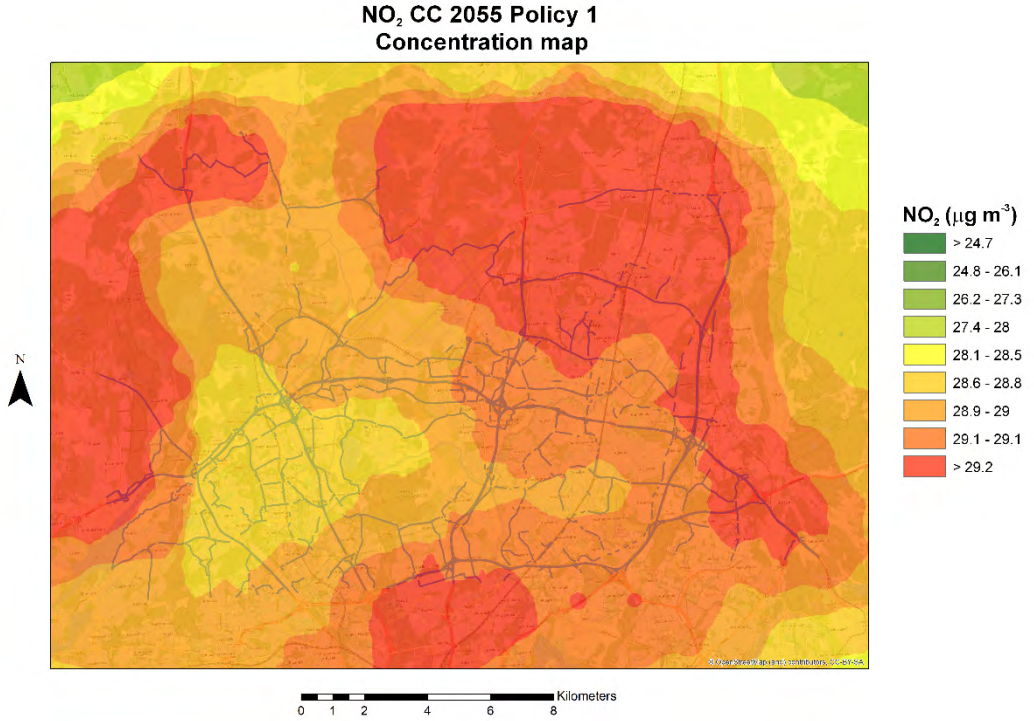

Figure 131. NO_2 concentration map in Vantaa in January 2055, as resulting from climate changes in meteorology and with the implementation of the policy 1, i.e. closing an area in the east of Vantaa to the traffic.

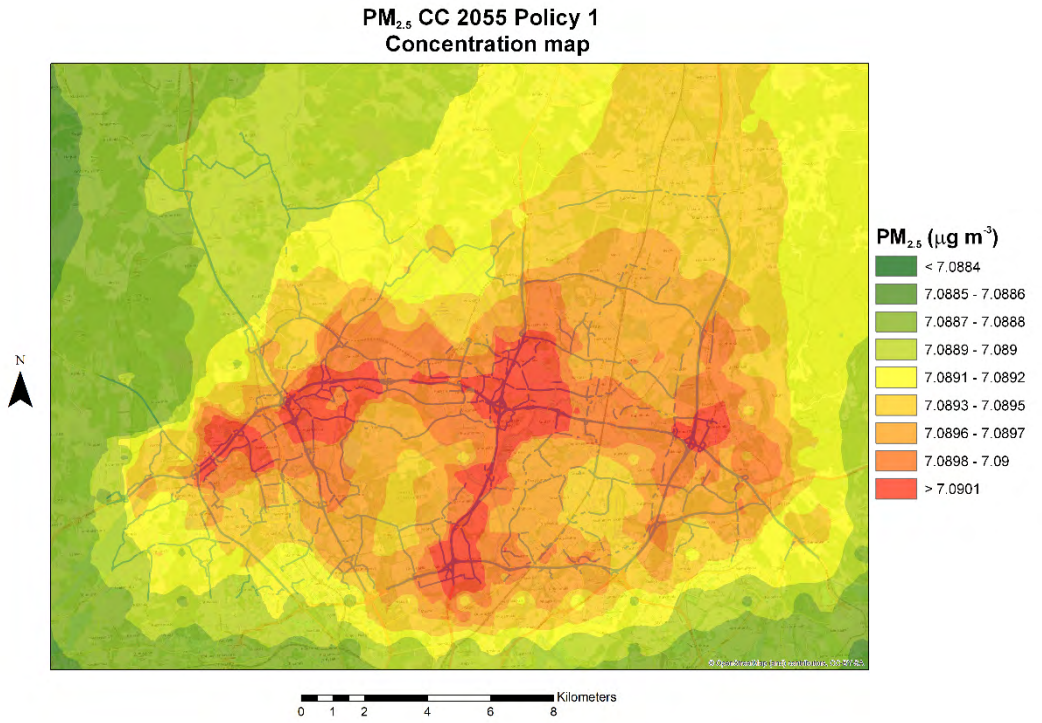

Figure 132. $PM_{2.5}$ concentration map in Vantaa in January 2055, as resulting from climate changes in meteorology and with the implementation of the policy 1, i.e. closing an area in the east of Vantaa to the traffic.

Figure 133 depicts the maps of NO_2 concentration differences between the CC scenario when the policy is implemented and without implementation of the policy. In case of $PM_{2.5}$, due to the absence of changes in the policy scenario, a similar Figure is not observed. The Figures offer the possibility to get a clearer picture of the results of the implementation of the policy in future CC in terms of NO_2 concentrations. In particular, we can observe that the policy affects limitedly NO_2 concentrations, both in terms of spatial extension and in terms of reductions. As noted in the base case, such small impact can be attributed both to the limited area where the intervention was implemented and to the spread of pollutants' emissions observed in Vantaa, differently than in the other two cities.

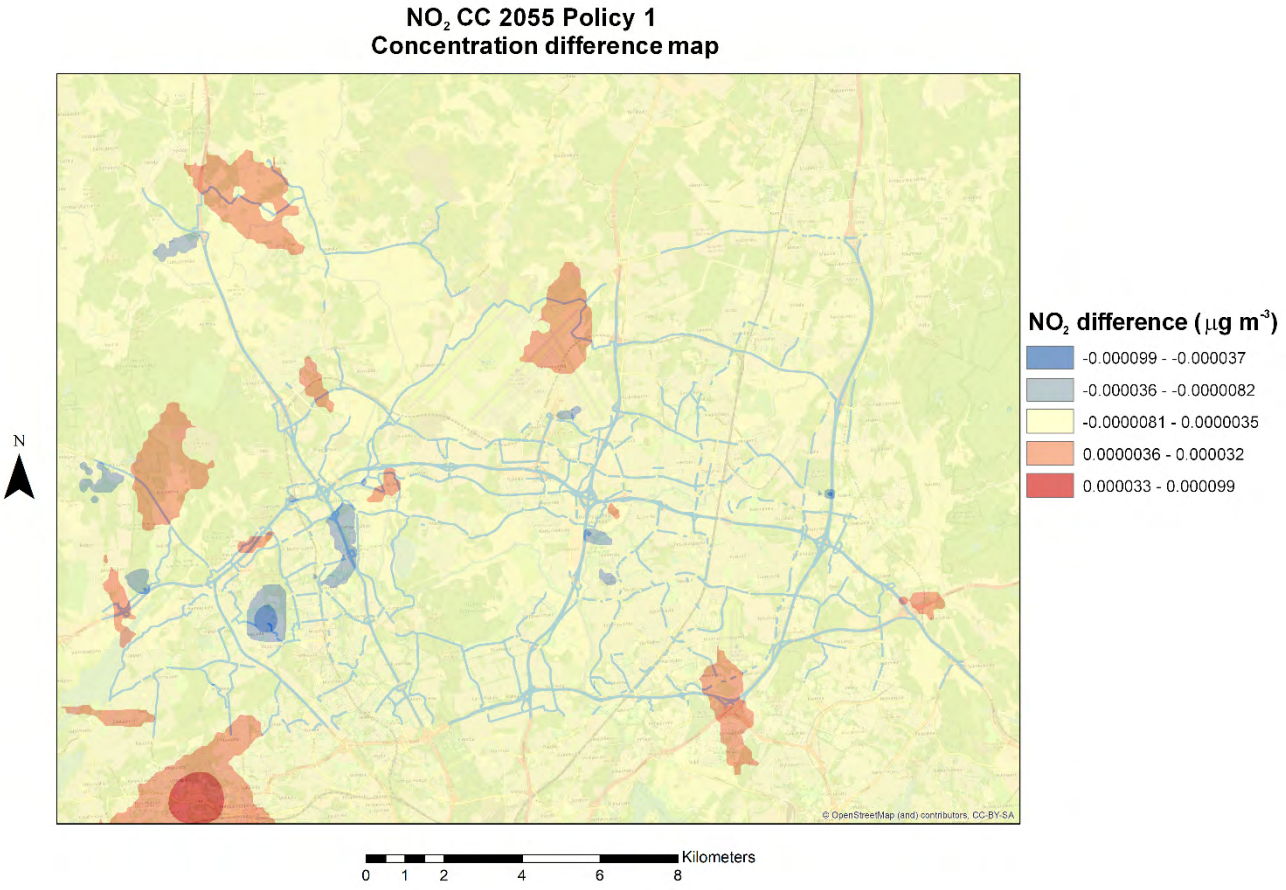

Figure 133. Map of differences in NO_2 concentration between the climate change scenario with reduction in emissions and the same scenario but in case of implementation of policy 1 in Vantaa.

Indeed, the evaluation of the concentration reductions calculated as ratios between the calculated differences and the concentrations simulated in the base case CC scenario shows limited non-significant reductions, that can be attributed to the reasons explained above.

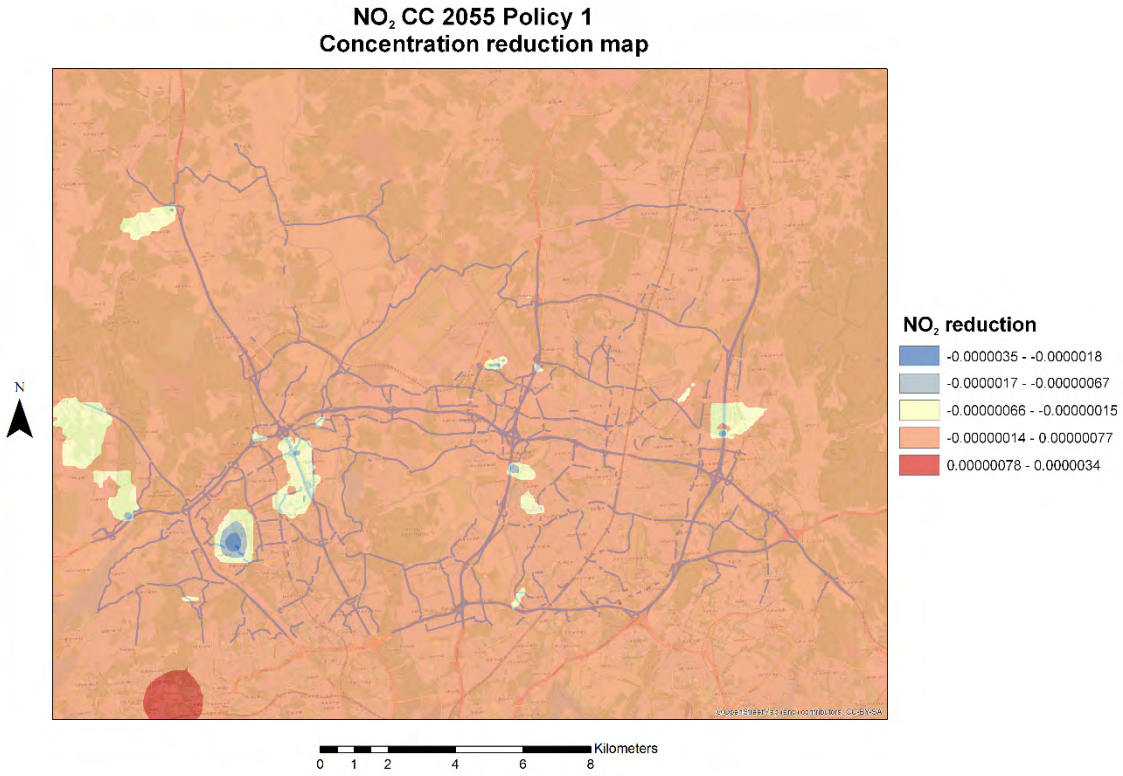

Figure 134. NO_2 reduction in case of implementation of policy 1 in CC scenario in Vantaa, evaluated as concentration ratio between the concentration difference previously evaluated (Figure 133) and the concentration observed in the CC scenario (Figure 129).

7 Conclusions

This report aims to describe and provide results about the effectiveness of behavioral changes related to mobility in contrasting air pollution both in present and in future scenarios in selected cities. Air quality dispersion model simulations were conducted in selected iSCAPE cities, namely Bologna in Italy, Hasselt in Belgium and Vantaa in Finland. Climate change scenarios have been estimated by the output of climate change projections downscaled at city level. The three cities were selected on the basis of the output of preceding tasks of the iSCAPE project and also to represent different latitudinal bands, i.e. Southern Europe, Central Europe and Northern Europe, differently impacted by climate change.

In all the three cities, the major pollution emitting sources are traffic and residential heating. Emission inventories to be provided as input to the dispersion models were built with different methodologies in the three cities: in Bologna, it was developed using data available from the Municipality of Bologna, while in Hasselt and Vantaa the emission inventory derived from the outputs of traffic simulations conducted at UH with an activity-based model, fine-tuned with the results of previous GPS-loggers campaigns carried out under iSCAPE Task 4.2.

In the three cities, the outputs of numerical simulations carried out in the current (baseline) case were verified against air quality concentrations measured by air quality stations in the three cities, providing satisfactory results as indicated by a number of statistical parameters and by time series and scatter plot graphs of simulated vs. observed concentrations. Though the inclusion of residential heating is of paramount importance for the correct evaluation and setup of the present scenario especially in the winter season, the work focuses especially on traffic source and on behavioral changes herein connected. In addition, the results of numerical simulations carried out in reference base case scenario served to provide insights on the pollution hotspots in the three cities. In particular, simulations indicated that while in Bologna the whole city centre represents a pollution hotspot, in Hasselt the outer ring road is significantly impacted by high concentrations of air quality pollutants. In Vantaa, differently than in the other two cities, air quality is generally better with lower concentrations of air quality pollutants; in addition, the fact that Vantaa is part of the Helsinki Metropolitan Area serving infrastructurally as its transport hub leads to a completely different pattern of emissions and therefore of air quality dispersion, with a large diffuse spread of higher concentrations in the vicinity of more trafficked roads and of the Vantaa city centre. The outputs of air dispersion simulations carried out in the policies scenarios were then compared with those obtained in the reference base case scenarios (current baseline and future) to evaluate the effectiveness of traffic management policies both in the present as well as in the future climate scenario. For each city, the impact of two traffic management schemes and subsequent behavioral changes was evaluated. Specifically, in Bologna, it was evaluated the effect of one “electric centre” policy, where only electric vehicles can enter the internal ring road, and one “electric buses” policy, where all the bus fleet is converted into electric with increase in their frequency, in addition to the banning of all non-electric vehicles from the internal ring road. In Hasselt and Vantaa, instead, the first policy scenario planned the complete closure of the inner ring road, while in the second one the frequency of buses was increased.

The results of this report suggest that in general traffic management policies can be very effective in improving air quality, provided that the major emission sources (in this case, roads) are identified and correctly envisaged into the policies.

In Bologna, where the centre was recognized as the major pollution hotspot for most air quality pollutants except ozone, both policies, produce significant reductions in air quality concentrations, both in the present as well as in the future scenarios, though accounting for measures focused on the city centre. The two policies provided NO_x reductions in the range of 20-43% and even 44-74% over some areas in the current (baseline) scenario. In the future scenario, when changes in meteorology are predicted to lead to increases in the concentrations of air pollutants, the implementation of the policies is predicted to lead to even higher reductions in NO_x concentrations, i.e. 66-75%.

In Hasselt, where the policies focused either over a limited area not significantly impacted by high emissions or widespread over the whole city domain, the impact of the two policies was smaller than in Bologna though still effective. For example, the closure of the inner ring provided NO_2 reductions in the range of 25-74% in the present case in the highly impacted outer ring, and in the range between 40 and 63% range in the future scenario. On the contrary the increase in the frequency of buses was less efficient and provided only reductions between 6 and 8%.

In Vantaa, instead, where the pollutants’ emissions were largely spread and not concentrated over particular areas as observed in the other two cities, the impact of the same traffic management policies implemented in Hasselt was tested, in order to prove the effectiveness of the policies in the presence

of a totally different spatial pattern of emissions and concentrations. The simulations showed that in the case of Vantaa, the impact of the policy of closure of the traffic in one area was significantly reduced with respect to what observed in Hasselt, both in present and climate change scenarios. This observation is attributed both to the limited area of the intervention and to the observed spread in emissions and consequently concentrations. However, in Vantaa, air quality concentrations do not present particular criticalities and as such the implementation of traffic management policies may not seem fundamental.

As a side observation, both policies planning an increase in the frequency of buses resulted in slight increases of PM_{10} concentrations in both cities, which suggests that the benefit provided by the change of transportation mode from private vehicle cars to buses is counteracted by the effect of PM non-exhaust emissions, especially important for heavy vehicles and buses.

It can be concluded that traffic management policies, are effective tools in contrasting air pollution in urban areas in short term (present scenario) and in long term considering climate change at city scale, once properly designed and planned on the basis of the best possible knowledge of emission sources and air pollution spatial distribution (high resolution maps).

These results, while on one side summarize the effect of behavioral changes related to mobility on air pollution both in the present and in the future climate change scenarios in selected European cities, establish the basis for WP7 to provide behavioral recommendations effective on AQ. The close link of this work with that carried out under WP6 related to simulations of CC and of interventions related to PCSs gives the possibility to widen the horizon including the effect of the policies also over a CC perspective and/or including the implementation of other urban planning strategies adequately planned.

As such, the report summarizes the effect of behavioral changes related to mobility on air quality both in the present and in the future scenarios in selected cities. The output of this task will provide the basis for the links between AQ and CC and for establishing behavioral recommendations in WP7. The following Figure presents in a schematic form the major connections and links of this task within the iSCAPE project.

8 References / Bibliography

Ahmed, S., Adnan, M., Janssens, D., Brattich, E., Yasar A.-u.-H., Kumar, P., Di Sabatino, S., & Shakshuki, E. M., 2018. Estimating pro-environmental potential for the development of mobility-based informational intervention: a data-driven algorithm. Personal and Ubiquitous Computing, doi:10.1007/s00779-018-1187-5

ARPAE, Rapporto Idrometeoclima Emilia-Romagna, 2018

ARPAE, Rete regionale di Monitoraggio e Valutazione della Qualità dell'aria Provincia di Bologna: Report dei dati 2017, 2018.

Barmpadimos, I., Hueglin, C., Keller, J., Henne, S., & Prévôt, A.S.H., 2011. Influence of meteorology on PM_{10} trends and variability in Switzerland from 1991 to 2008. Atmospheric Chemistry and Physics, 11, 1813-1835

Barmpadimos, I. Keller, J., Oderbolz, D., Hueglin, C., & Prévôt, A.S.H., 2012. One decade of parallel fine ($PM_{2.5}$) and coarse (PM_{10}-$PM_{2.5}$) particulate matter measurements in Europe: trends and variability. Atmospheric Chemistry and Physics, 12, 3189-3203.

Beevers, S.D., Westmoreland, E., de Jong, M.C., Williams, M.L., & Carslaw, D., 2012. Trends in NOx and NO2 emissions from road traffic in Great Britain. Atmospheric Environment, 54, 107-116.

Carruthers, D.J., Edmunds, H.A., Lester, A.E., McHugh, C.A., & Singles, R.J., 2000. Use and validation of ADMS-Urban in contrasting urban and industrial locations. International Journal of Environment and Pollution, 14, 363-374

CERC, 2011. ADMS-Urban User Guide. Version 3.1. Cambridge, UK, 324 pp., http://www.cerc.co.uk/environmental-software/assets/data/doc_userguides/CERC_ADMS-Urban4.1.1_User_Guide.pdf. *Accessed 16 Jan 2019*

CERC, 2015. EMIT Atmospheric Emissions Inventory Toolkit User Guide Version 3.4, Cambridge, UK, 390 pp, https://www.cerc.co.uk/environmental-software/assets/data/doc_userguides/CERC_EMIT3.4_User%20Guide.pdf Accessed 17 Jan 2019

Chang, J.C., & Hanna, S.R., 2004. Air quality model performance evaluation. Meteorology and Atmospheric Physics, 87, 167-196.

City of Vantaa, Centre for Environmental Affairs, 2012. State of the environment in Vantaa. Summary August 2012. Vantaan kaupungin paino, ISBN 978-952-443-392-1, 23 pp.

Colette, A., Granier, C., Hodnebrog, Ø., Jakobs, H., Maurizi, A., Nyiri, A., Bessagnet, B., D'Angiola, A., et al., 2011. Air quality trends in Europe over the past decade: a first multi-model assessment. Atmospheric Chemistry and Physics, 11, 11657-11678.

Comune di Bologna, Piano Urbano Della Mobilità Sostenibile (PUMS): Relazione, 2018

D'Amato, G., Bergmann, K.C., Cecchi, L., Annesi-Maesano, I., Sanduzzi, A., Liccardi, G., Vitale, C., Stanziola, A., & D'Amato, M., 2014. Climate change and air pollution. Effects on pollen allergy and other allergic respiratory diseases. Allergo Journal International, 23(1), 17-23.

Dėdelė, A. & Miškinytė, A., 2015. The statistical evaluation and comparison of ADMS-Urban model for the prediction of nitrogen dioxide with air quality monitoring network. Environmental Monitoring and Assessment 187:578

Degraeuwe, B., Thunis, P., Clappier, A., Weiss, M., Lefbvre, W., Janssen, S., & Vranck, S., 2017. Impact of passenger car NOx emissions on urban NO2 pollution – Scenario analysis for 8 European cities. Atmospheric Environment, 171, 330-337.

De Rooy, W.C., & Holtslag, A.A.M., 1998 Estimation of surface radiation and energy flux densities from single-level weather data. Journal of Applied Meteorology, 38, 526-540.

Di Sabatino, S., Buccolieri, R., Pulvirenti, B., & Britter, R.E., 2008. Flow and pollutant dispersion in street canyons using FLUENT and ADMS-Urban. Environmental Modeling and Assessment, 13(3),369-381.

EMEP, 2009. EMEP/EEA air pollutant emission inventory guidebook – 2009. Technical report No 9/2009: (September 2011). https://www.eea.europa.eu/publications/emep-eea-emission-inventory-guidebook-2009, accessed 21 Jan 2019

European Commission Directorate-General for Regional Policy, 2010. Survey on perception of quality of life in 75 European cities. Publications Office of the European Union, Luxembourg, http://ec.europa.eu/regional_policy/sources/docgener/studies/pdf/urban/survey2009_en.pdf, last accessed 28 Feb 2019

FEBIAC (Fédération belge et luxembourgeoise de l'automobile et du cycle), 2018. Datadigest 2018. http://www.febiac.be/public/statistics.aspx?FID=23&lang=FR accessed 18 Jan 2019

Goodess, C., Jacob, D., Déqué, M., Guttièrrez, J., Huth, R., Kendon, E., Leckebusch, G., Lorenz, P., and Pavan, V., 2009. Downscaling methods, data and tools for input to impacts assessment. In: ENSEMBLES: Climate Change and its Impacts: Summary of Research and Results from the ENSEMBLES project [van der Linden, P., and Mitchell, J.F.B. (eds.)]. Met Office Hadley Centre, Exeter, UK, pp.59-78.

Hanna, S.R., 1993. Uncertainties in air quality model predictions. Boundary-Layer Meteorology, 62, 3-20.

Hargreaves, G.L., Hargreaves, G.H., & Riley, P., 1985. Irrigation water requirement for the Senegal River Basin. J Irrig and Drain Engr, ASCE, 108(IR3), 223.230

Hood, C., MacKenzie, I., Stocker, J., Johnson, K., Carruthers, D., Vieno, M., and Doherty, R., 2018. Air quality simulations using a coupled regional-to-local modelling system. Atmospheric Chemistry and Physics, 18, 11221-11245

IPCC (Intergovernmental Panel on Climate Change), 2014. Contribution of Working Group III to the Fifth Assessment Report of the Intergovernmental Panel on Climate Change [Edenhofer, O., R. Pichs-Madruga, Y. Sokona, E. Farahani, S. Kadner, K. Seyboth, A. Adler, I. Baum, S. Brunner, P. Eickemeier, B. Kriemann, J. Savolainen, S. Schlömer, C. von Stechow, T. Zwickel and J.C. Minx (eds.)]. Cambridge University Press, Cambridge, United Kingdom and New York, NY, USA.

ISTAT, 2018 http://dati.istat.it/index.aspx?queryid=1602#

Jacob, D., Kotova, L., Teichmann, C., Sobolowski, S., Vautard, R., Donnelly, C., et al., 2018. Climate impacts in Europe under +1.5°C global warming. Earth's future, 6, 264-285.

Jyhlä, K., Ruosteenoja, K., Jokisalo, J., Pilli-Sivhola, K., Kalamees, T., Mäkelä, H., Hyvönen, R., &, Drebs, A., 2015. Hourly test reference weather data in the changing climate of Finland for building energy simulations. Data in Brief, 4, 162-169

Karppinen, A., Kukkonen, J., Elolähde, T., Konttinen, M., Koskentalo, T., & Rantakrans, E., 2000. A modelling system for predicting air pollution: model description and applications in the Helsinki metropolitan area. Atmospheric Environment, 34, 3723-3733.

Katsis, P., Ntziachristios, L., & Mellios, G., 2012. Description of new elements in COPERT 4 v10.0, EMISIA SA Report No.12.RE.012.V1

Kjellström E., Nikulin, G., Hansson, U., Strandberg, G., and Ullerstig, A., 2011. 21st century changes in the European climate: uncertainties derived from an ensemble of regional climate model simulations. Tellus A, Series A, 63A(1), 24-40.

Kota, S.H., Ying, Q., & Zhang, Y., 2013. Simulating near-road dispersion of gaseous air pollutants using three-dimensional eulerian model. Science of the Total Environment, 454-455, 348-357

Kovats, R.S., Valentini, R., Bouwer, L.M., Georgopoulou, E., Jacob, D., Martin, E., Rounsenvell, M., & Soussana, J.-F., Europe. In: Climate Change 2014: Impacts, Adaptation, and Vulnerability. Part B: Regional Aspects. Contribution of Working Group II to the Fifth Assessment Report of the Intergovernmental Panel on Climate Change [Barros, V.R., Field, C.B., Dokken, D.J., Mastrandrea, M.D., Mach, K.J., Bilir, T.E., Chatterjee, M., Ebi, K.L., Estrada, Y.O., Genova, R.C., Girma, B., Kissel, E.S., Levy, A.N., MacCracken, S., Mastrandrea, P.R., & White, L.L., (eds.)]. Cambridge University Press, Cambridge, United Kingdom and New York, NY, USA, pp. 1267-1326.

Khreis, H., & Nieuwenhuijsen, M.J., 2016. Car free cities: pathway to healthy urban living. Environment International, 94, 251-262.

Larsen, J.N., Anisimov, O.A., Constable, A., Hollowed, A.B., Maynard, N., Prestrud, P., Prowse, T.D., & Stone, J.M.R., 2014. Polar regions. In: Climate Change 2014: Impacts, Adaptation, and Vulnerability. Part B: Regional Aspects. Contribution of Working Group II to the Fifth Assessment Report of the Intergovernmental Panel on Climate Change [Barros, V.R., Field, C.B., Dokken, D.J., Mastrandrea, M.D., Mach, K.J., Bilir, T.E., Chatterjee, M., Ebi, K.L., Estrada, Y.O., Genova, R.C., Girma, B., Kissel, E.S., Levy, A.N., MacCracken, S., Mastrandrea, P.R., & White, L.L., (eds.)]. Cambridge University Press, Cambridge, United Kingdom and New York, NY, USA, pp. 1267-1326.

Lehtomäki, H., Kohronen, A., Asikainen, A., Karvosenoja, N., Kupiainen, K., et al., 2018. Health impacts of ambient air pollution in Finland. International Journal of Environmental Research and Public Health, 15(4), 736.

QGIS Project, 2017. QGIS User Guide, Release 2.14

Riahi, K., Rao, S., Krey, V., Cho, C., Chirkov, V., Fischer, G., Kindermann, G., Nakicenovic, N., & Rafaj, P., 2011. RCP 8.5 – A scenario of comparatively high greenhouse gas emissions. Climatic change, 109:33

Righi, S., Lucialli, P., Pollini, E.: Statistical and diagnostic evaluation of the ADMS-Urban model compared with an urban air quality monitoring network. Atmospheric Environment 43, 3850–3857, 2009.

Robine, J.M., Cheung, S.L., Le Roy, S., Van Oyen, H., Griffiths, C., Michel, J.P., et al., 2008. Death toll exceeded 70,000 in Europe during the summer of 2003. Compte Rendus Biologies, 331(2), 171-178.

Smith, S.E., Stocker, J., Seaton, M., & Carruthers, D., 2017. Model inter-comparison and validation study of ADMS plume chemistry schemes. International Journal of Environment and Pollution, 62, 395-406.

Soares J., Kousa A., Kukkonen J., Matilainen L., Kangas L., Kauhaniemi M., Riikonen K., Jalkanen J.-P., Rasila T., Hänninen O., Koskentalo T. & Karppinen A., 2014. Refinement of a model for evaluating the population exposure in an urban area. Geoscientific Model Development, 7, 1855–1872.

Soga, K., 2018. Development of future weather data using global warming projection: Research on future weather data for designing building and equipment which are adaptable to climate change. Japan Architectural Review, 1, 1, 175-190.

Soret, A., Jimenez-Guerrero, P., & Baldasano, J.M., 2011. Comprehensive air quality planning for the Barcelona Metropolitan Area through traffic management. Atmospheric Pollution and Research, 2, 255e266

Stocker, J., Hood, C., Carruthers, D., & McHugh, C., 2012. ADMS-Urban: developments in modelling dispersion from the city scale to the local scale. International Journal of Environment and Pollution, 50, 308-316.

Supit, I., & Van Kappel, R.R., 1998. A simple method to estimate solar radiation. Solar Energy, 63, 147-160

Tukiainen, M., 2011. Helsinki, Finland-Sunrise, sunset, dawn and dusk times around the World Gaisma. Retrieved 11 February 2011.

Vantaan kaupunki, 2012. Vantaan kaupungin tilastollinen vuosikirja 2011 (Statistical yearbook of the city of Vantaa 2011). Vantaan kaupunki, Tietopalveluysikkö, 130 pp.

van Ulden, A.P., & Holtslag, A.A.M., 1985. Estimation of atmospheric boundary layer parameters for diffusion applications. Climate Applied Meteorology, 24, 1196-1207.

VMM (Flanders Environment Agency), 2018. Annual air report-Flanders (Belgium). Emissions 2000-2016 and air quality in Flanders in 2017.

Wang, Y.J., Denbleyker, A., McDonald-Buller, E., Allen, D., & Zhang, K.M., 2011. Modeling the chemical evolution of nitrogen oxides near roadways. Atmospheric Environment 45, 43-52.

WHO (World Health Organization), 2014. Burden of disease from Household Air Pollution for 2012. www.who.int/phe/health_topics/outdoorair/databases/FINAL_HAP_AAP_BoD_24March2014.pdf?ua=1, last accessed 24 Jan 2019

WHO, 2016. Ambient air pollution database, www.who.int/airpollution/en, last accessed 22 Feb 2019

Zeng, A., Mao, X., Hu, T., Xing, Y., Gao, Y., Zhou, J., and Qian, Y., 2017. Regional co-control plan for local air pollutants and CO2 reduction: Method and practice. Journal of Cleaner Production, vol 140, Part 3, pp. 1226-1235

Zhou, X.N., Yang, G.J., Yang, K., Wang, X.H., Hong, Q.B., Sun, L.P., et al., 2008. Potential impact of climate change on schistosomiasis transmission in China. Am J Trop Hyg, 78(2), 188-194